AD-778 769

T53 AND T55 GAS TURBINE COMBUSTOR AND ENGINE EXHAUST EMISSION MEASUREMENTS

Philip M. Rubins, et al

Avco Lycoming Division

Prepared for:

Army Air Mobility Research and Development Laboratory

December 1973

DISCLAIMERS

The findings in this report are not to be construed as an official Department of the Army position unless so designated by other authorized documents.

When Government drawings, specifications, or other data are used for any purpose other than in connection with a definitely related Government procurement operation, the United States Government thereby incurs no responsibility nor any obligation whatsoever; and the fact that the Government may have formulated, furnished, or in any way supplied the said drawings, specifications, or other data is not to be regarded by implication or otherwise as in any manner licensing the holder or any other person or corporation, or conveying any rights or permission, to manufacture, use, or sell any patented invention that may in any way be related thereto.

Trade names cited in this report do not constitute an official endorsement or approval of the use of such commercial hardware or software.

DISPOSITION INSTRUCTIONS

Destroy this report when no longer needed. Do not return it to the originator.

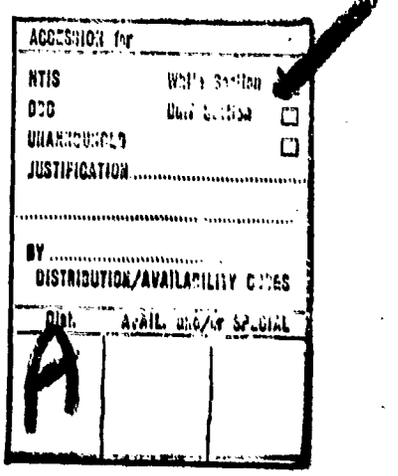

Unclassified
Security Classification

DOCUMENT CONTROL DATA - R & D

(Security classification of title, body of abstract and indexing annotation must be entered when the overall report is classified)

1. ORIGINATING ACTIVITY (Corporate author) Avco Corporation Avco Lycoming Division Stratford, Connecticut	2a. REPORT SECURITY CLASSIFICATION Unclassified 2b. GROUP

3. REPORT TITLE

T53 AND T55 GAS TURBINE COMBUSTOR AND ENGINE EXHAUST EMISSION MEASUREMENTS

4. DESCRIPTIVE NOTES (Type of report and inclusive dates)

Final Report, June 1972 through February 1973

5. AUTHOR(S) (First name, middle initial, last name)

Philip M. Rubins
Brian W. Doyle

6. REPORT DATE	7a. TOTAL NO. OF PAGES	7b. NO. OF REFS
December 1973	219	34

8a. CONTRACT OR GRANT NO.	9a. ORIGINATOR'S REPORT NUMBER(S)
DAAJ02-72-C-0102 b. PROJECT NO. c. Task 1G162207AA7102 d.	USAAMRDL Technical Report 73-47 9b. OTHER REPORT NO(S) (Any other numbers that may be assigned this report) LYC 73-8

10. DISTRIBUTION STATEMENT

Approved for public release; distribution unlimited.

11. SUPPLEMENTARY NOTES	12. SPONSORING MILITARY ACTIVITY
	Eustis Directorate, U. S. Army Air Mobility Research and Development Laboratory, Fort Eustis, Virginia

13. ABSTRACT

Extensive tests were made to determine the gaseous exhaust emission characteristics of T53-L-13A and T55-L-11A Lycoming gas turbine engines. In addition, the combustor for each engine was tested separately under laboratory conditions simulating engine operation. Data were analyzed for the full range of engine power operation for CO, hydrocarbons, NO, NO_x, and CO_2, and for smoke. Samples were taken with six-point traversing probes, a single-point traversing probe, and multiorifice averaging-type probes. Approximately 1500 data points were recorded. Results demonstrated that (1) laboratory emission measurements are representative of engine exhaust measurements; (2) all the three-probe sampling configurations produced similar results within 5 to 10 percent of each other; (3) results conformed to accuracy specified by SAE-ARP 1256; (4) emission characteristics of the engines show that neither engine produces visible smoke, except when there is an obvious oil seal failure. Comparisons with Navy test data on these engines show some differences. However, considering that the test differences included engine, instrumentation, time, place, and personnel, agreement is considered to be quite good. Extensive profile data were plotted. The "averaging" probe accuracy was found to be satisfactory and also has the advantage of a short-time sampling interval, as compared with lengthy single-point traverses. Several exhaust emission problems are analyzed and discussed.

DD FORM 1 NOV 68 1473 REPLACES DD FORM 1473, 1 JAN 68, WHICH IS OBSOLETE FOR ARMY USE.

Unclassified
Security Classification

Unclassified
Security Classification

14. KEY WORDS	LINK A		LINK B		LINK C	
	ROLE	WT	ROLE	WT	ROLE	WT
T53-L-13A Gas Turbine Engine						
T55-L-11A Gas Turbine Engine						
Exhaust Gas Compositon						
Exhaust Emissions						
Engine Performance						
Emissions in Gas Turbine Exhaust						
Smoke in Gas Turbine Exhaust						
Emission Measurement						
Laboratory Combustor vs Engine Emissions						
Laboratory Measurement To Prodict Engine Emissions						

16

Unclassified
Security Classification

12790-73

DEPARTMENT OF THE ARMY
U. S. ARMY AIR MOBILITY RESEARCH & DEVELOPMENT LABORATORY
EUSTIS DIRECTORATE
FORT EUSTIS, VIRGINIA 23604

The research described herein was conducted by Avco Lycoming Division under U.S. Army Contract DAAJ02-72-C-0102. The work was performed under the technical management of SP4 Charles R. Roehrig, Technology Applications Division, Eustis Directorate, U.S. Army Air Mobility Research and Development Laboratory.

The objective of this contractual effort was to obtain a sample of emission data on the T53-L-13A and the T55-L-11A engines. A prior emission characterization program was run with the Navy to measure the gaseous emissions of the T63, T53, and T55 engines; however, a second sample was deemed necessary due to the wide engine-to-engine variations that occur in emission levels for a particular engine model. Tests were also planned to establish the correlations between (1) component and engine emission data and (2) data taken with averaging and single-point probes. The effort performed here is part of an overall plan to establish the base-line emission levels of present high-inventory Army aircraft engines.

Appropriate technical personnel of this directorate have reviewed this report and concur with the conclusions contained herein.

The findings and recommendations outlined herein will be considered in planning future small gas turbine engines and combustor component development programs.

ic

Task 1G162207AA7102
Contract DAAJ02-72-C-0102
USAAMRDL Technical Report 73-47
December 1973

T53 AND T55 GAS TURBINE COMBUSTOR AND ENGINE EXHAUST EMISSION MEASUREMENTS

Final Report

Avco Lycoming Report LYC 73-8

By

Philip M. Rubins
Brian W. Doyle

Prepared by

Avco Lycoming Division
Stratford, Connecticut

for

EUSTIS DIRECTORATE
U.S. ARMY AIR MOBILITY RESEARCH
AND DEVELOPMENT LABORATORY
FORT EUSTIS, VIRGINIA

SUMMARY

This report is concerned with exhaust gas emission tests of Lycoming T53-L-13 and T55-L-11 engines and combustors. These engines were designed in the 1960's, and exhaust emission was not a design criterion at that time. The purpose of the present tests was to evaluate the engines and combustors from a pollutant standpoint and compare the results with the current state of the art. Extensive tests were made to determine the gaseous exhaust emission characteristics of both a T53-L-13A and a T55-L-11A Lycoming gas turbine engine. In addition, the combustor for each engine was tested separately under laboratory conditions simulating engine operation, with similar measurements of gaseous emissions. Engines were selected from those available which performed within the guaranteed range. Data were analyzed for the full range of engine power operation for CO, hydrocarbons, NO, NO_x, and CO_2, and for smoke. Samples were taken with six-point traversing probes, with a single-point traversing probe, and with multiorifice averaging-type probes. Approximately 1500 data points were recorded.

Results demonstrated that:

1. Laboratory emission measurements are representative of engine exhaust measurements.

2. Single-point probe, multiorifice probe, and single-point probe measurements in the same pattern configuration as the multiorifice probe produce similar results within 5 to 10 percent of each other.

3. By comparing the engine or test rig fuel-air ratio with the gas sample determined fuel-air ratio, we found the sample to be "representative" because the agreement was within 10 percent. This is within the accuracy recommended by SAE-ARP 1256 (specified 15 percent tolerance).

4. Emission characteristics of the engines show:

   a. Neither engine produces visible smoke, except when there is an obvious oil seal failure.

   b. Trends of emittants CO, hydrocarbons, NO, and NO_x are as expected. Comparisons with Navy test data on these

engines show some differences. However, considering that the test differences included engine, instrumentation, time, place, and personnel, agreement is considered to be quite good.

Extensive profile data plotted along diameters of the engine exhaust, around the circumference of the combustor exit plane, and as isopleth maps are presented.

Exhaust profiles for these engines were found to be uniform enough so that an averaging-type probe of cruciform configuration will ingest "representative" samples; that is, within 3 percent of the more detailed and extensive single-point probe average. The averaging probe also has the advantage of sampling over a short time interval, as compared with lengthy single-point traverses. Small variations over a long test period reduced some of the precision of multipoint sampling.

Although not a specific objective of this program, the measurements provide (1) an insight into the combustion processes and (2) indications of ways in which the exhaust emissions of the engine can be reduced.

FOREWORD

The work was performed by AVCO Lycoming for the Eustis Directorate, U.S. Army Air Mobility Research and Development Laboratory under Contract DAAJ02-72-C-0102, Task 1G162207AA7102, as a part of evaluation of emission properties of gas turbine engines used by the U.S. Army. The program monitor was Sp4 Charles R. Roehrig.

The authors acknowledge the significant contributions to this report made by the following members of Lycoming's Engineering Staff:

Messrs. J. Sweet and S. Osborn, who managed the test phase

Mr. J. Knight, who worked on the gas analyzer instrumentation

Mr. A. Myers, who performed the engine analysis work

Mr. G. Panas, who supervised the engine operation

TABLE OF CONTENTS

LIST OF ILLUSTRATIONS

LIST OF TABLES

LIST OF SYMBOLS

a	CO concentration term defined by Equation (2)
b	hydrocarbon ($CH_{m/n}$) concentration term defined by Equation (3)
C_nH_m	single carbon fuel composition molecule used as typical of unburned hydrocarbons
CO	chemical symbol for carbon monoxide
CO_2	chemical symbol for carbon dioxide
F/A	fuel-air mass ratio = W_f/W_a
HC	abbreviated chemical symbol for unburned hydrocarbon constituents
m	average number of hydrogen atoms per fuel molecule as determined by chemical analysis
n	average number of carbon atoms per fuel molecule as determined by chemical analysis
NO	chemical symbol for nitric oxide
NO_x	chemical symbol for total nitric oxide components, usually NO and NO_2
THC	total hydrocarbons measured by flame ionization detector (includes partially reacted and unreacted fuel components)
η_b	combustion efficiency
ϕ	equivalence ratio = $\frac{\text{actual F/A}}{\text{stoichiometric F/A}}$

INTRODUCTION

The control of exhaust gas emissions is a new requirement for aircraft powerplants. Although these pollutants can be classed in various ways, those which have been identified as important for gas turbines are carbon monoxide (CO), the nitric oxides (usually designated as NO_x), and the unburned hydrocarbons (C_nH_m). To assess the total pollutants produced from an engine and aircraft system, data is needed over the range of engine operation from idle to maximum power. Total cyclic emissions for an engine in one aircraft may be quite different from the total in another aircraft using that same engine.

An item requiring consideration is the designation of the "idle" power. This is important because the total emissions of a helicopter over a specified operational cycle are strongly a function of the time spent in a cycle at "idle". The "idle" power produces the largest quantity of unburned hydrocarbons (HC) and carbon monoxide (CO). In addition, "idle" power varies between aircraft, depending on the specific requirements for the aircraft. Because emissions are a function of the engine power output, it follows that "idle" is not a precisely defined term, but must be especially specified for each engine in each aircraft installation.

Part of the problem of measurements is the taking of exhaust gas samples that are representative of the average exhaust gas composition. Measurements in the JT 8D, reported in Reference 1, indicate that large numbers of data points are required in order to obtain representative sampling. Since these data were recorded for large fan engines, the obvious question is, do the same criteria apply to small turboshaft engines?

This report is concerned with exhaust gas emission measurements in the Lycoming T53 and T55 gas turbine engines (Figures 1 and 2). A single sample of exhaust emissions for the Lycoming T53-L-13A and T55-L-11A engines has been measured by the U.S. Naval Air Propulsion Test Center, and is reported in References 2 and 3. The tests described in this report were of similar nature, but included additional experimental and analytical evaluation, as discussed in the "Objectives" subsection.

OBJECTIVES

One of the principal objectives of the present work was to test T53 and T55 combustors under laboratory test conditions, with controlled

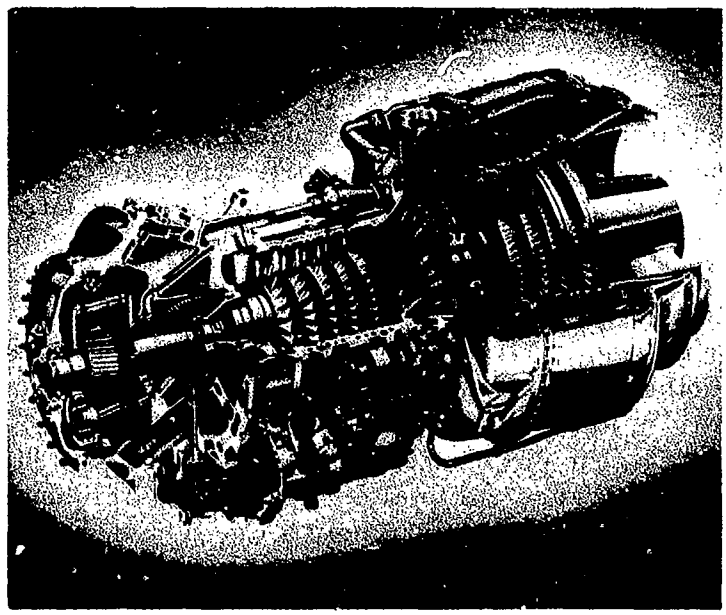

Figure 1. Lycoming T53-L-13A Engine Cutaway, Showing Combustor Arrangement.

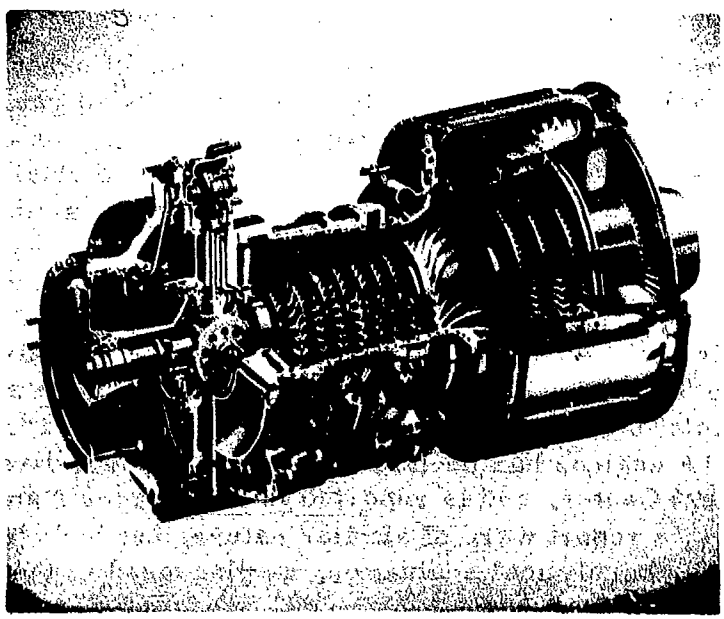

Figure 2. Lycoming T55-L-11A Engine Cutaway, Showing Combustor Arrangement.

air inlet pressure and temperature, and then to compare the results with data from these same combustors in their respective engines. A second important objective was to sample the exhaust of both engine and combustor at 60 single points and with averaging (manifolded) sample probes. An analysis of these data will be used to evaluate the effectiveness of the averaging probe. A third objective was to compare the emission measurement results with those obtained on the same model engines at the Naval Air Propulsion Test Center (References 2 and 3) and with results from other gas turbine engines reported in Reference 4.

TEST APPROACH

The concept of evaluating emissions in the engines and combustors was put into practice by:

1. Laboratory combustor tests under simulated engine operating conditions, with "average" sampling from multiorifice probes.

2. Laboratory combustor tests at the same engine-simulated operating conditions, during which time 60-point gas sample data were recorded.

3. Engine tests at a specified range of operating conditions, with "average" samples recorded with a cruciform probe. Smoke sampling was also recorded with an alternate cruciform probe.

4. Engine tests at specific operating conditions, during which time a single-point sampling probe was traversed to cover a predesignated sampling pattern.

The data points tested are shown in Table I. Note that combustor inlet pressure for some high-power engine test conditions could not be simulated in the laboratory tests. Therefore, temperature and fuel-air ratio simulation was correct, but not inlet pressure.

TABLE I. EMISSION MEASUREMENTS, SUMMARY OF TEST CONDITIONS

	Combustor Component Tests		Engine Tests		
	Gaseous Emissions		Gaseous Emissions		Smoke
	60-Point Traverse	Averaging Probe	60-Point Traverse	Averaging Probe	Averaging Probe
Idle	X	Y	X	Y	Y
1	-	-	-	Y	-
2	-	-	-	Y	-
30%	X	Y	X	Y	Y
60%	X	Y	X	Y	Y
75%	-	-	-	Y	Y
100%	X*	Y*	X	Y	Y

NOTES: X - Single test, repeated only if required.

Y - For this test, two separate runs were conducted to insure data repeatability. For each run, test data were measured ascending and descending the power range.

* - Test points were approximated as closely as facility and rig limitations permit. This included the 100 percent power point on the T53 and the 60 and 100 percent points on the T55.

Points 1 and 2 were selected to define the expected "knee" in the emissions data.

TABLE I - Continued

Actual Engine and Combustor Rig Test Conditions

T53-L-13A

Test Condition	Air Temp (°F) Engine	Air Temp (°F) Rig	Air Press. (psia) Engine	Air Press. (psia) Rig	Fuel Flow (lb/hr) Engine	Fuel Flow (lb/hr) Rig	F/A Engine Combustor	N_1 % Speed	SHP %	SHP
1	198	-	28.2	-	150	-	.0123	58	3	42
2	278	-	37.7	-	220	-	.0130	70	7	98
3	300	292	39	41	222	226	.0136	75	10	140
4	410	415	64.5	65	380	385	.0147	83	30	420
5	480	487	85.7	84	570	580	.0169	92	54	755
6	490	-	90.2	-	625	-	.0177	93.6	63	880
7	545	547	106	84	800	670	.0203	99.6	96	1340

T55-L-11A

Test Condition	Air Temp (°F) Engine	Air Temp (°F) Rig	Air Press. (psia) Engine	Air Press. (psia) Rig	Fuel Flow (lb/hr) Engine	Fuel Flow (lb/hr) Rig	F/A Engine Combustor	N_1 % Speed	SHP %	SHP
1	305	310	42.7	43	475	481	.0110	68	7	263
2	356	-	52.7	-	625	-	.0122	75	13	487
3	392	-	58.7	-	716	-	.0128	78	17	638
4	430	426	69	72	830	840	.0128	82.5	27	1013
5	500	498	91	82	1320	1170	.0166	90.8	56	2100
6	526	-	99.7	-	1545	-	.0183	93.0	70	2630
7	557	563	113.7	82	1960	1372	.0209	96.5	93	3490

Note: Operational and flight idle for the T53 is at Condition 2. Operational idle for the T55 is at Condition 4, approximately.

EXPECTED RESULTS

It was expected that several types of information could be obtained from the laboratory and engine tests:

1. The emission levels of each combustor independent of the engine

2. The emission level of the combustor installed in the engine

3. A comparison of the combustor laboratory and engine test results

4. Calculations of combustion efficiency for both engine and laboratory combustor

5. Determination of emission profiles, and a correlation between the combustor and the engine and between various probe position samples and the averaging probe

6. A comparison of the data with results from previous tests (References 2 and 3) and with other engine data (Reference 4)

7. A measure of any change in oil leakage from bearing seals by monitoring hydrocarbons in the engine exhaust

DESCRIPTION OF TEST EQUIPMENT

LABORATORY COMBUSTOR EQUIPMENT

The laboratory test equipment was installed in the Lycoming Building 19 complex, shown in Figure 3. A T55 compressor was used to produce airflow for the lower power conditions. A combination of two T55 compressors was used for pressure to simulate the higher power conditions. The compressor control panel is shown in Figure 4. As noted on Table I, pressure was not available for the peak power conditions, but fuel-air ratio and air temperature were correctly simulated.

The combustors for both the T53-L-13A and the T55-L-11A engines were production configurations used with these engines and contained no special modifications for these tests.

The combustor laboratory test rig for the T53 combustor consisted of the combustor liner, the engine housing, and the engine fuel manifold assembly. These parts were installed in the test way ducting with inlet and exhaust transition sections, as shown in Figure 5. Interior thermocouples and gas sampling, with the 360-degree rotating actuator mechanism, are shown in Figures 6 through 8. The arrangement of the probes in the annular exhaust is shown in Figure 9.

The T55 combustor test rig installed in the same test way is shown in Figure 10. This rig also consisted of a combustor liner, engine housing, and engine fuel manifold assembly, all installed with inlet and exhaust transition sections. Interior fixed probes are shown in Figure 11. The 360-degree rotating thermocouples and gas sampling probe installation are shown in Figure 12. The dimensional arrangement of the probes is shown in Figure 13.

The 360-degree rotating drum assembly containing the five thermocouples and the gas sampling probe was installed in the plane of the first turbine nozzle inlet for both T53 and T55 combustors. The five thermocouples were installed at different radii, so that, when the probe is rotated, a radial profile can be measured around the combustor exhaust annulus (Figures 9 and 13).

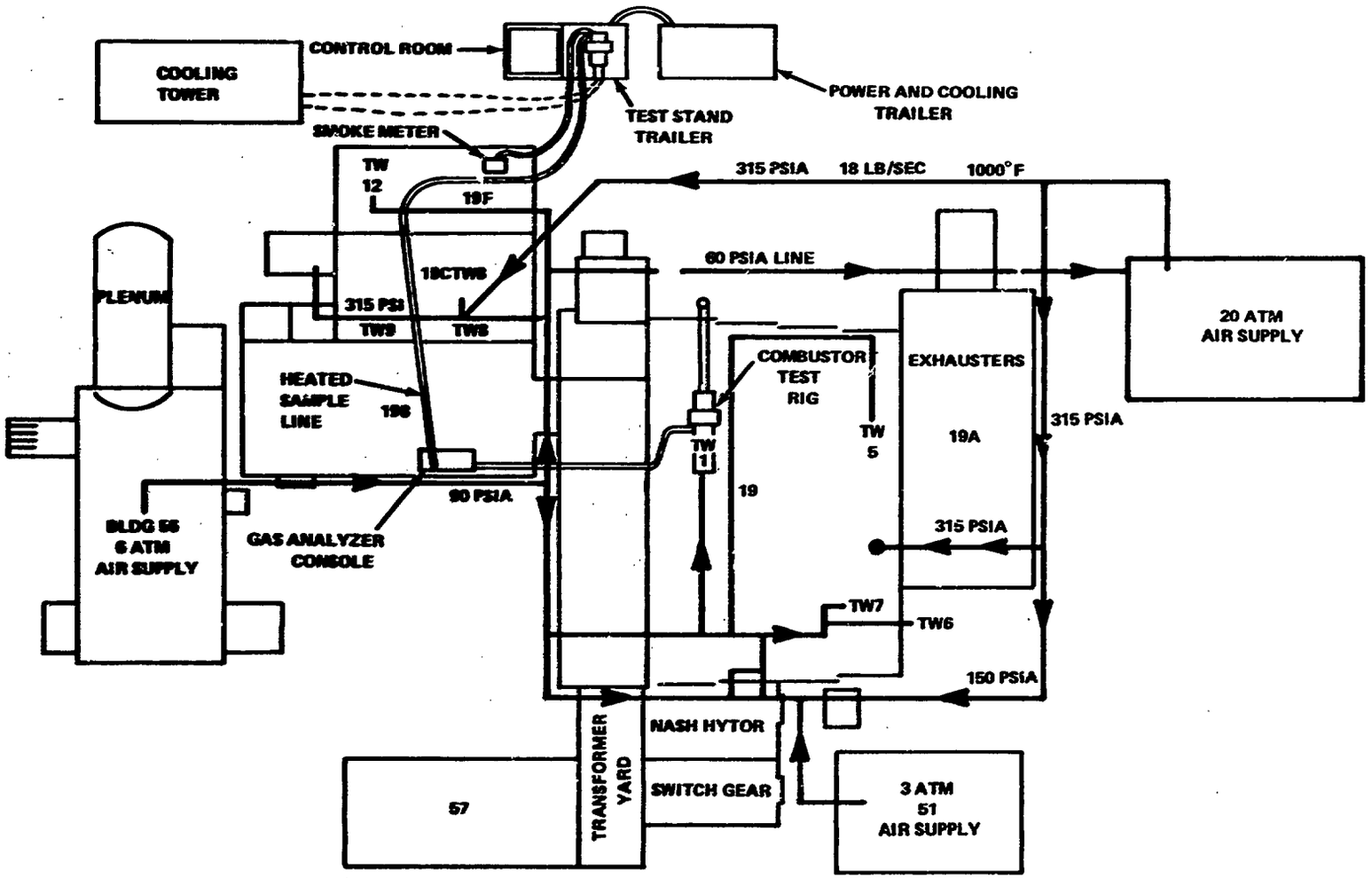

Figure 3. Combustor Laboratory Test Area, Showing Combustor Test Rig (Test Way 1) and Portable Engine Test Stand.

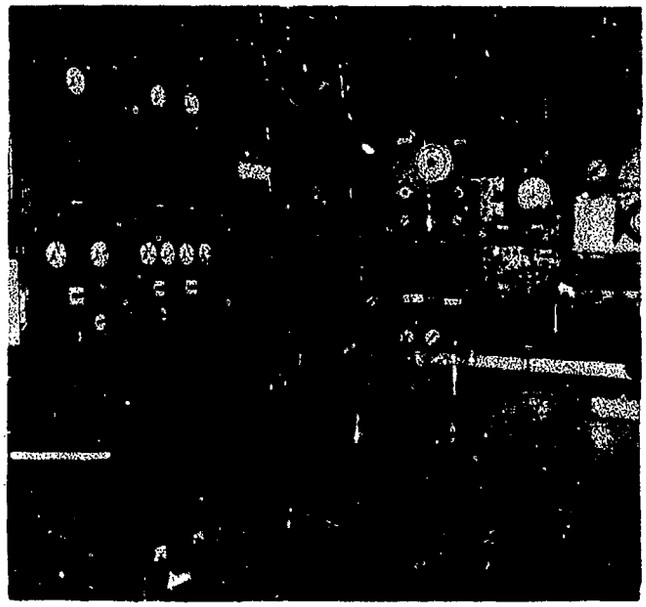

Figure 4. Compressor Control Panel.

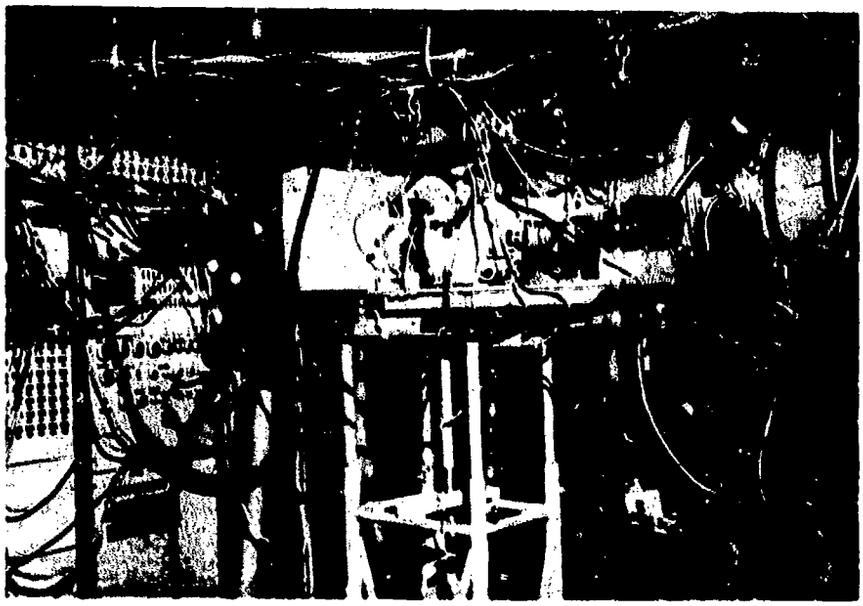

Figure 5. T53 Laboratory Combustor Test Rig in Test Way 1.

Figure 6. T53 Combustor Test Rig. Curl and Rotating Drum Assembly, Showing Thermocouple Leads and Flexible Gas Sampling Lines.

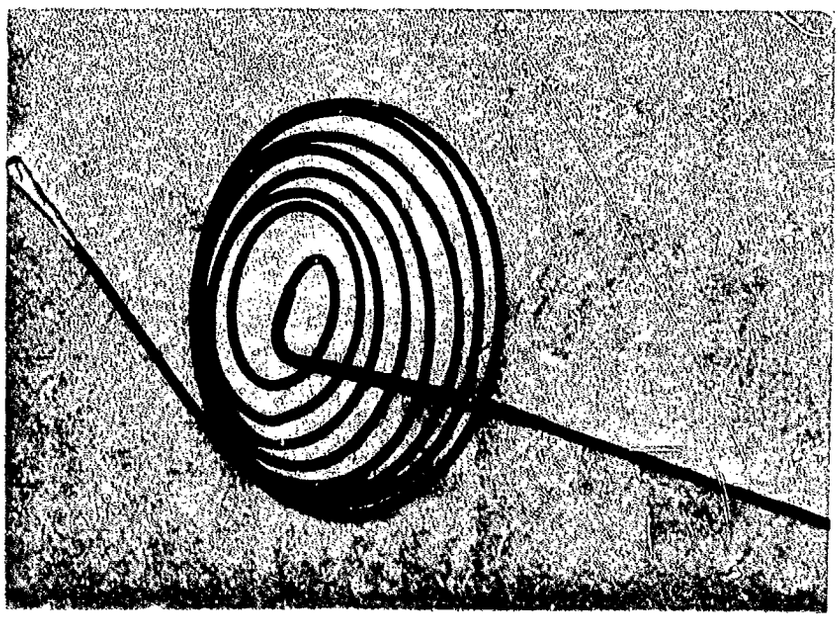

Figure 7. T53 Combustor Rig Gas Sampling Line for Rotating Probe.

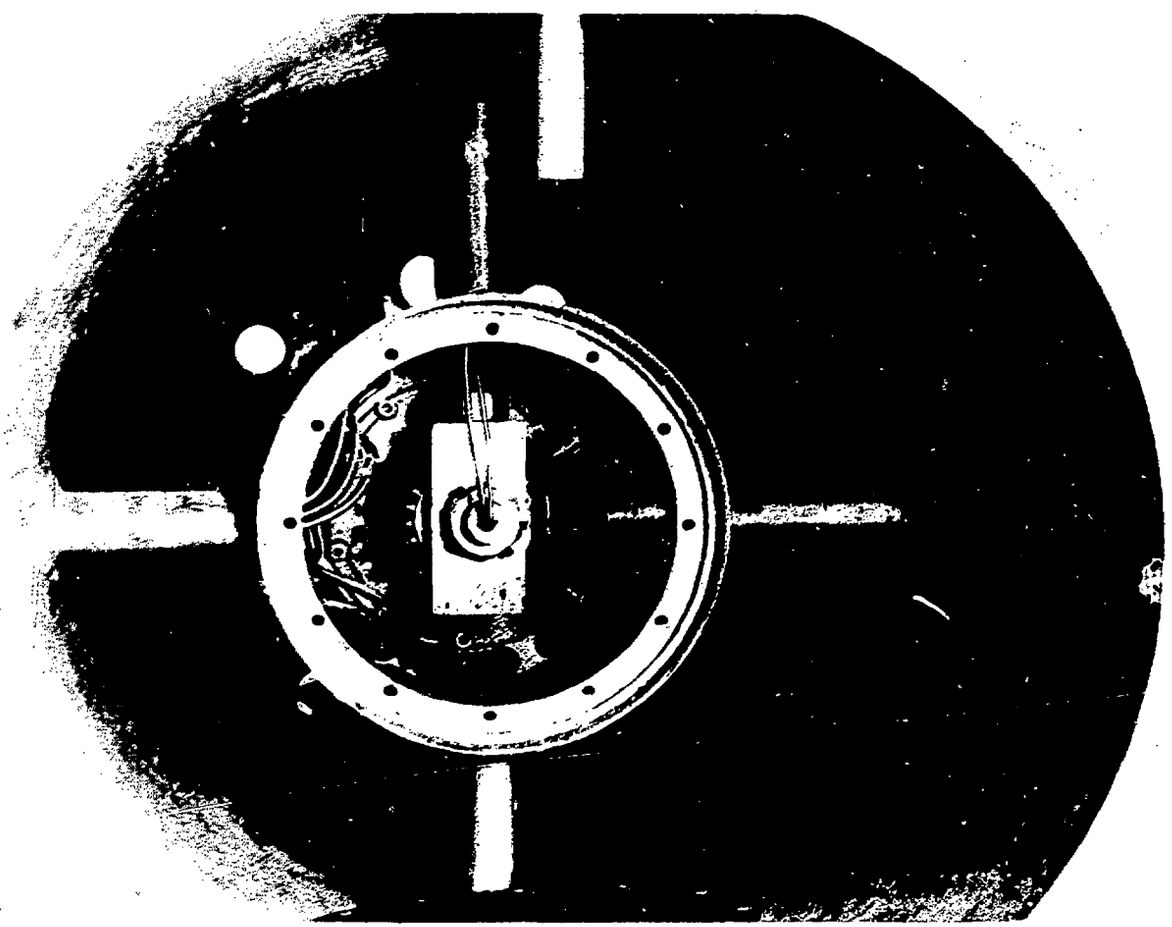

Figure 8. **T53 Combustor Rig, Showing Rotating Drum Drive Gears, Gas Sampling Lines, and Thermocouple Leads.**

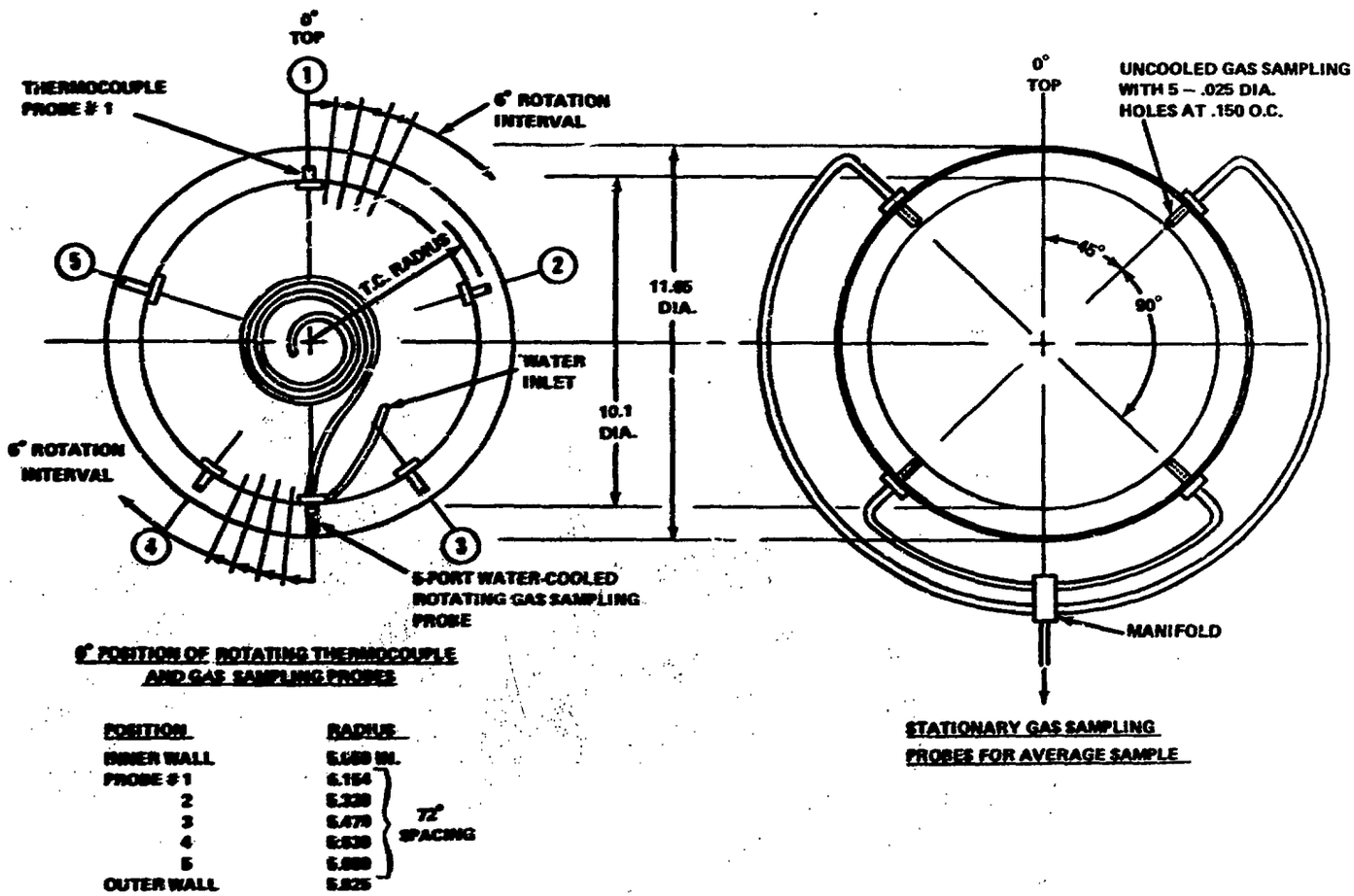

Figure 9. Installation of Thermocouple and Gas Sampling Probes for T53 Combustor Test.

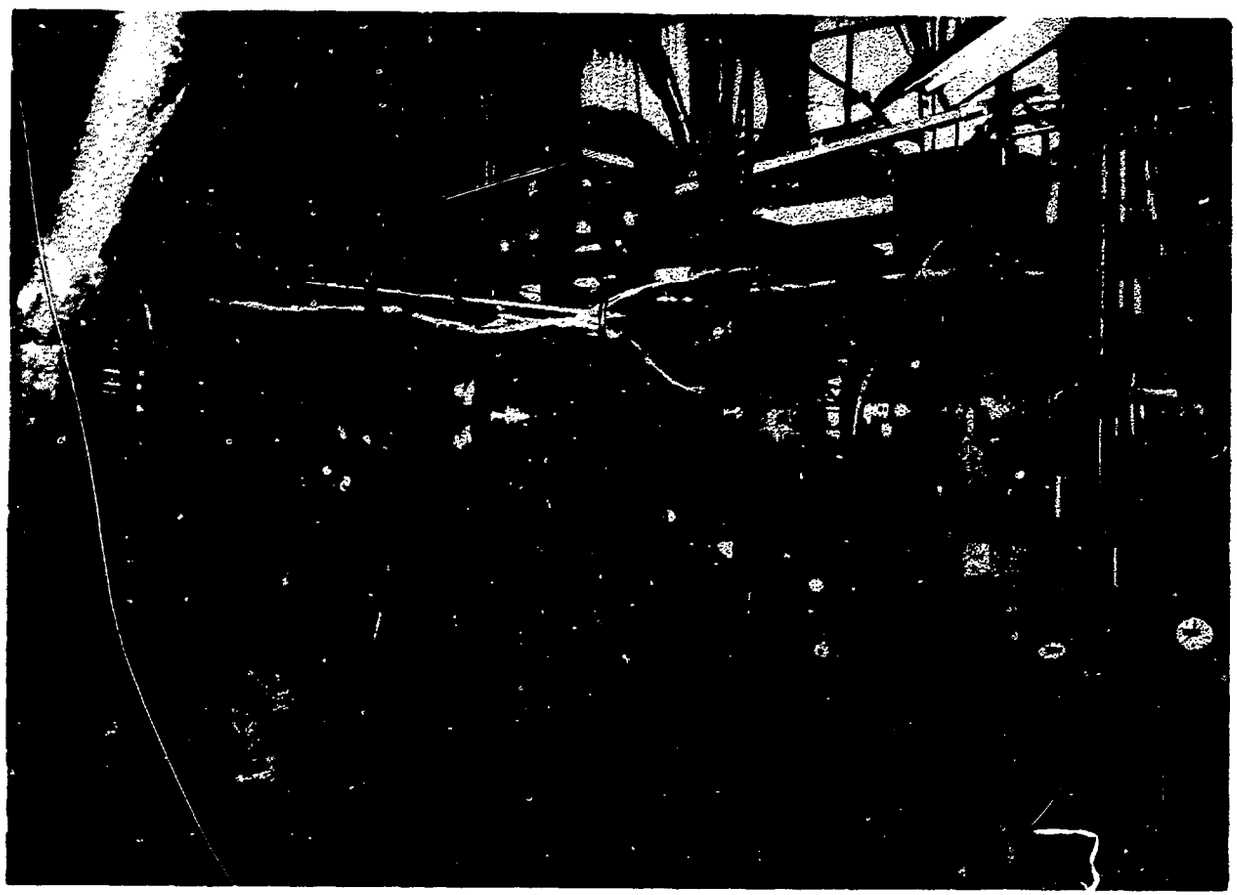

Figure 10. T55 Laboratory Combustor Test Rig in Test Way 1.

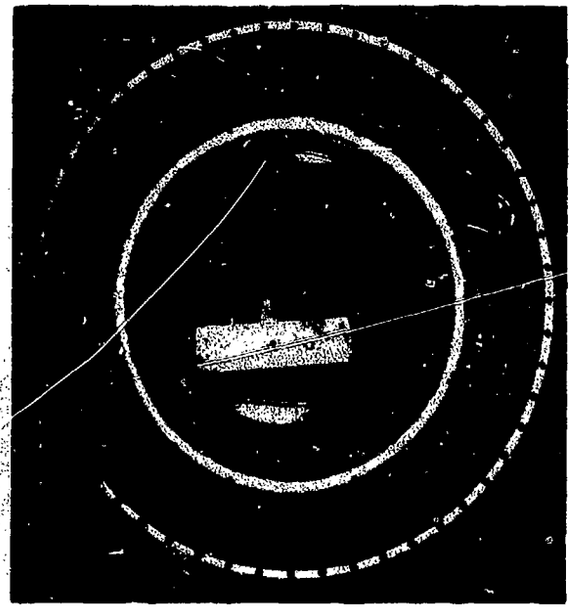

Figure 11. T55 Combustor Test Rig Hot End Assembly, Showing Curl, Combustor Exit Gas Sampling Probes, and Pressure Probes.

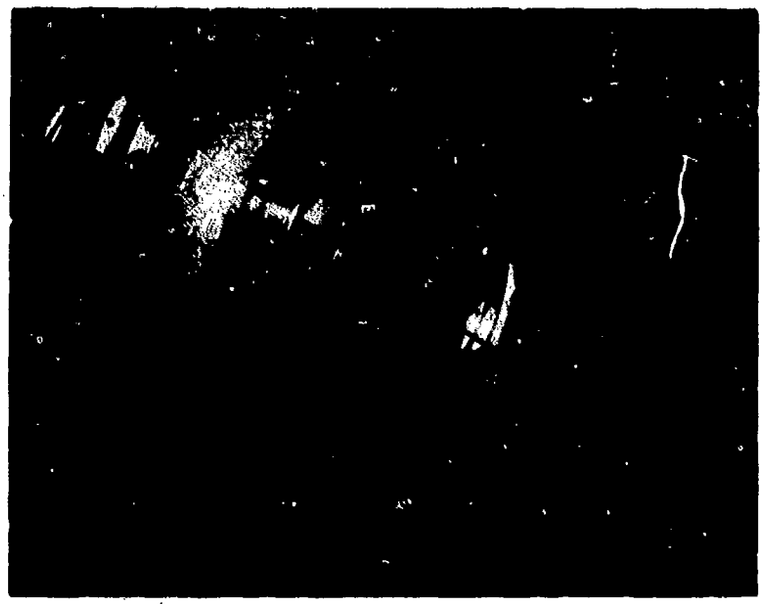

Figure 12. T55 Combustor Test Rig Curl and Rotating Drum Assembly, Showing Thermocouples and Flexible Gas Sampling Lines.

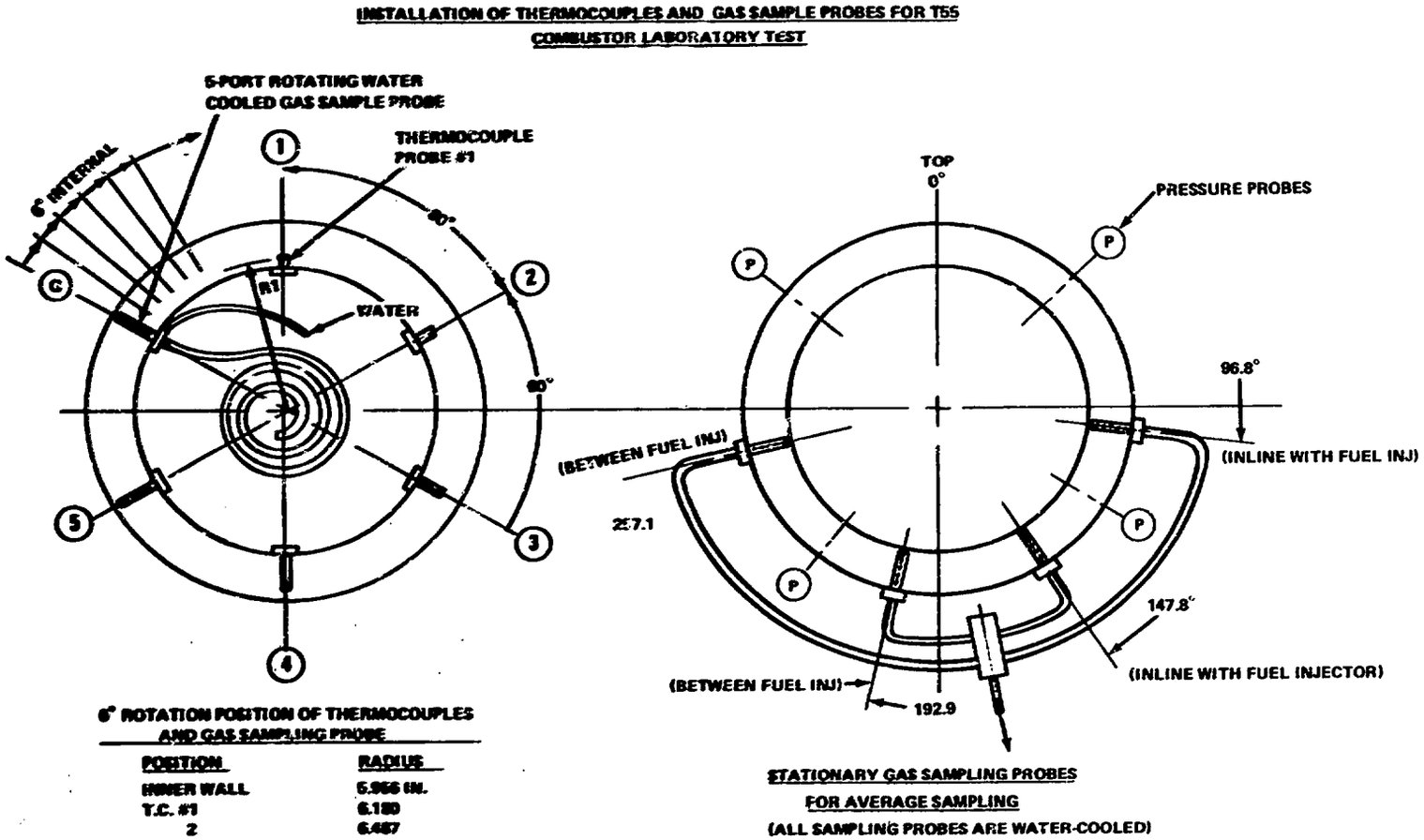

Figure 13. Installation of Thermocouples and Gas Sampling Probes for T55 Combustor Laboratory Test.

Additional instrumentation in the combustor rig measured combustor inlet air pressure and temperature, and exhaust pressure.

The 360-degree rotating mechanism five-port gas sampling probes for the T53 and T55 combustors were water-cooled (Figures 14 and 15). Water-cooling was specified because of the possibility of probe damage in the hot gases and to better ensure that the chemical reactions in the gases would be quenched on entering the probe. A coiled-tube method was used to allow the probe to be rotated without damaging the sampling line (Figures 6, 7, and 12).

The four fixed gas-sampling probes used in the T53 combustor test are shown in Figure 16. They were uncooled and were spaced as shown in Figure 9. They consist of five-port sampling which averages the gas sample at one circumferential position. The four probes were manifolded together.

Mounted near the T55 rig traversing probe were four fixed five-port averaging-type probes, water-cooled (Figure 17). The outlets of these probes were manifolded together for zone averaging. As seen in Figure 13, the probes are installed in the lower half of the combustor exit and are sloped slightly downward. Thus, if any fuel or water condensation occurs in the water-cooled section, it will run "downhill" until it reaches the heated section of the sample line. At this point, the temperature is high enough that the liquids will revaporize.

Gas samples are passed from the probe to an electrically heated "Dekoron" 3/8-inch stainless steel tube for transport to the detector console, DS-16A (Figures 4 and 18). An electric controller regulates the tube temperature at approximately $300^{\circ} \pm 10^{\circ}F$. A pressure drop across the sampling probe inlet was designed into the system to obtain an equal flow into each of the probe sampling ports.

Other instruments included temperature and pressure measurements to determine airflow and monitor the test rig, plus fuel meters. All measurements, except the gas analysis, were recorded on the DS-5 data system on punched tape (Figure 19). Tape was later converted to punched cards, and complete calculations were made on the central computer system (IBM 370/155).

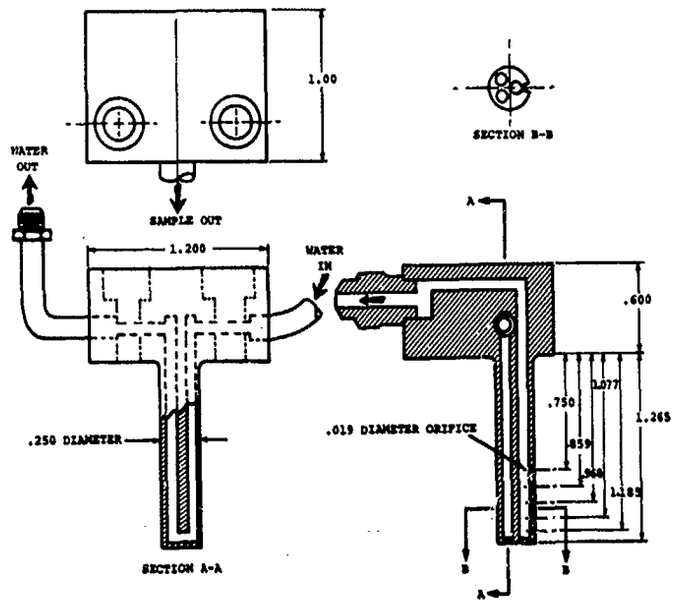

Figure 14. Water-Cooled Rotating Gas Sampling Probe for T53 Combustor Test.

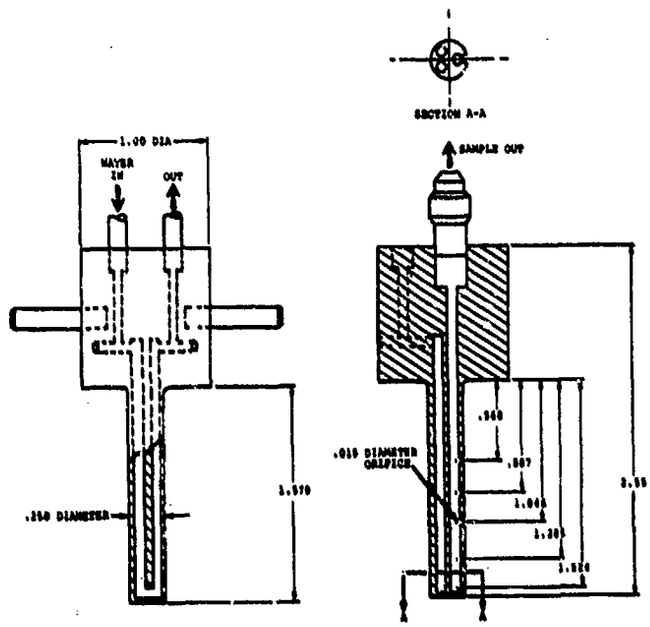

Figure 15. Water-Cooled Rotating Gas Sampling Probe for T55 Combustor Test.

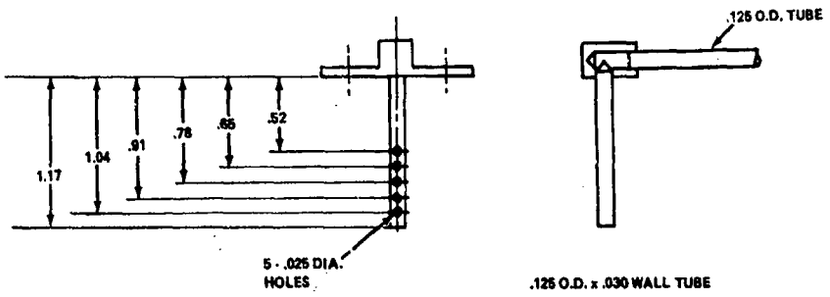

Figure 16. Fixed-Position Gas Sampling Probes (Uncooled) for T53 Combustor.

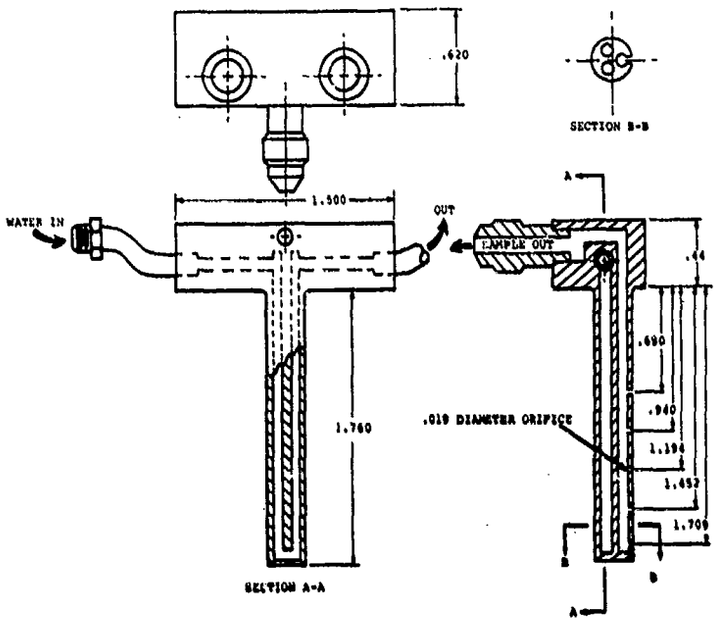

Figure 17. Water-Cooled Fixed Gas Sampling Probe for T55 Combustor Test.

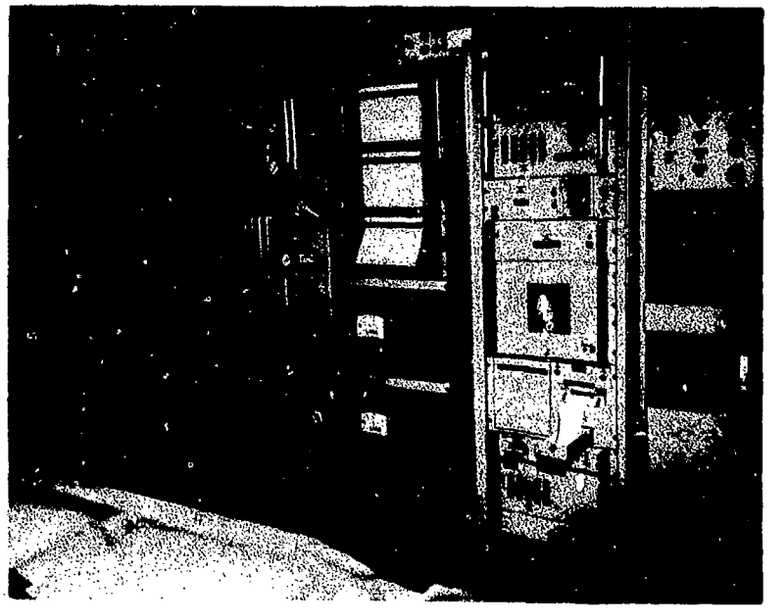

Figure 18. DS-16A Gas Analyzer Console in Combustion Laboratory and DS-8 Digital Recorder.

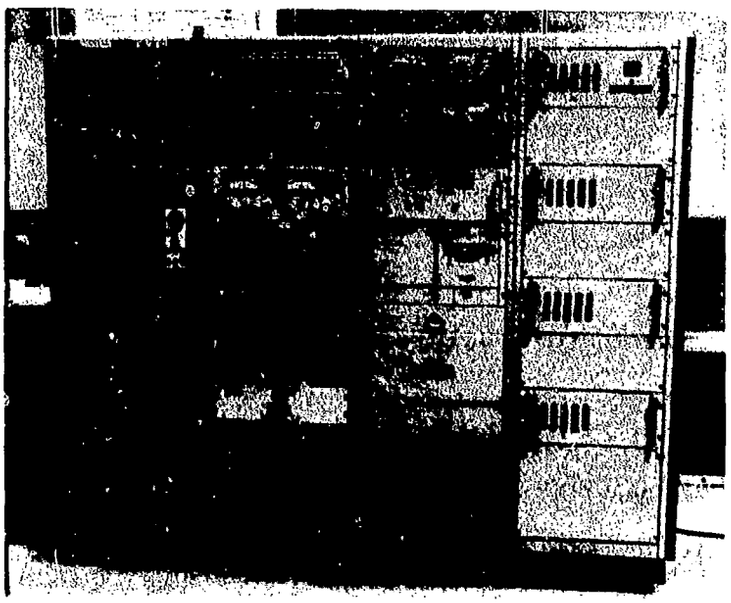

Figure 19. DS-5 Combustor Performance Digital Data Acquisition and Control System.

ENGINE TEST EQUIPMENT

To conduct exhaust gas analysis tests on T53-L-13A and T55-L-11A engines, an outdoor, mobile test stand was used in close proximity to the gas analysis equipment. The test stand with the necessary test equipment is shown in position in Figures 20 and 21. Control of the engine was maintained from the control room on the trailer. Further details of the installation are discussed in Reference 5.

Engine Instrumentation

For both the T53-L-13A and T55-L-11A engines, power was absorbed by a Lycoming water brake (Figures 20 and 21). A strain-gaged torque element mounted between the water brake and the engine inlet housing was used to measure output shaft torque in both instances.

Engine airflow was measured with a calibrated inlet bellmouth set consisting of an inner and outer bellmouth providing an inlet area of 95.16 square inches for the T53 and 141.20 square inches for the T55 engine. Static and total pressures in the bellmouth were used to determine referred engine airflow.

Compressor speed was measured by a Hewlett-Packard digital counter (Model No. 5214L), and power turbine speed was measured by a Standard Electric Time Tachometer (Model No. SG-6).

Fuel and oil flows were measured by the use of Cox turbine elements in conjunction with a Hewlett-Packard digital counter (Model No. 5214L).

Hydraulic and pneumatic pressures were measured by calibrated pressure gages.

Temperatures were measured with thermocouples in conjunction with self-balancing potentiometers.

Engine Exhaust Gas Measurements Equipment

Exhaust gas samples were acquired by both fixed and traversing probes positioned in the exhaust gas stream. The gas samples were fed directly to the analysis equipment in the control room through lines between the test stand and the building (Figure 3). The fixed

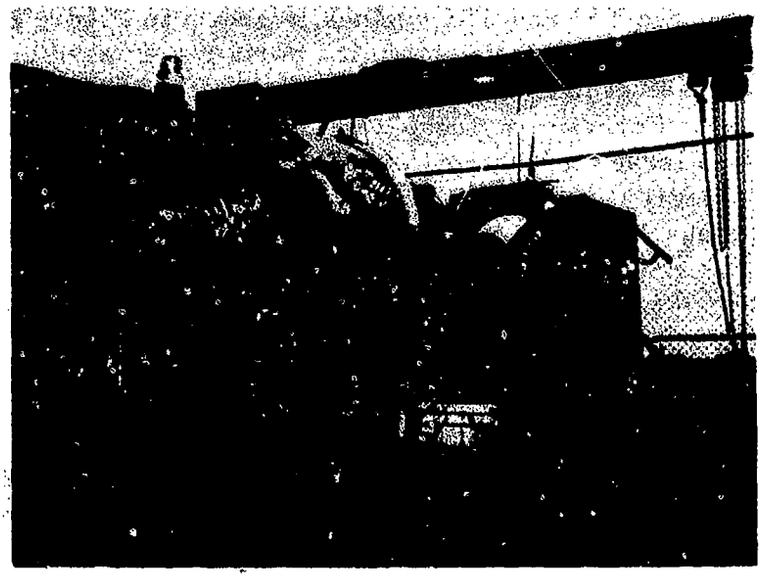

Figure 20. Intake End of T53-L-13A Engine Mounted on Portable Test Stand, Showing Water Brake and Control Room.

Figure 21. T55 Engine Installed on Portable Test Stand, Showing Inlet and Water Brake. (Power Supply Trailer Is in the Background.)

probe design for the T53 and T55 engines is shown in Figure 22. The dimensions of the tubes and sampling ports were based on a similar design used at the Naval Air Propulsion Test Center (References 2 and 3. A second cruciform probe was installed in tandem approximately 3 inches downstream of the gas sampler and at an angle of 45 degrees to it for taking smoke samples. The design dimensions for this probe are also shown in Figure 22.

A photograph of the T55 fixed probe is shown in Figure 23. Installation of this probe in the engine is shown in Figure 24, and the installation of a similar probe in the T53 engine is shown in Figure 25.

A second probe with actuator (Figure 26 and 27) was used in the engine exhaust to measure gas composition over a multipoint zone (Figure 28) during steady-state operation. This probe was designed in accordance with SAE-ARP 1179 specifications for smoke sampling (Reference 6). The probe position (angle and diameter location) was controlled from the engine trailer control room. The probe with actuator is shown installed in the T55 engine in Figure 27. The probe actuator installed in the T53 engine is shown in Figure 25.

A pattern for single-point gas analysis was developed to provide a large variety of data with a limitation of 60 sample points (Figure 28). The center point was added. The criteria for this pattern were:

1. Radial point location on "equal area" lines
2. Sufficient points for obtaining several diametric profiles
3. Circumferential points for a centroid traverse
4. In-between points for determining area concentration profiles

GAS ANALYSIS EQUIPMENT

The Lycoming on-line exhaust gas analysis system consists of detectors for measuring O_2, CO, CO_2, HC, and NO. In addition, an NO_x analyzer was added to this system. The oxygen analyzer was not used in these tests. The system schematically shown in

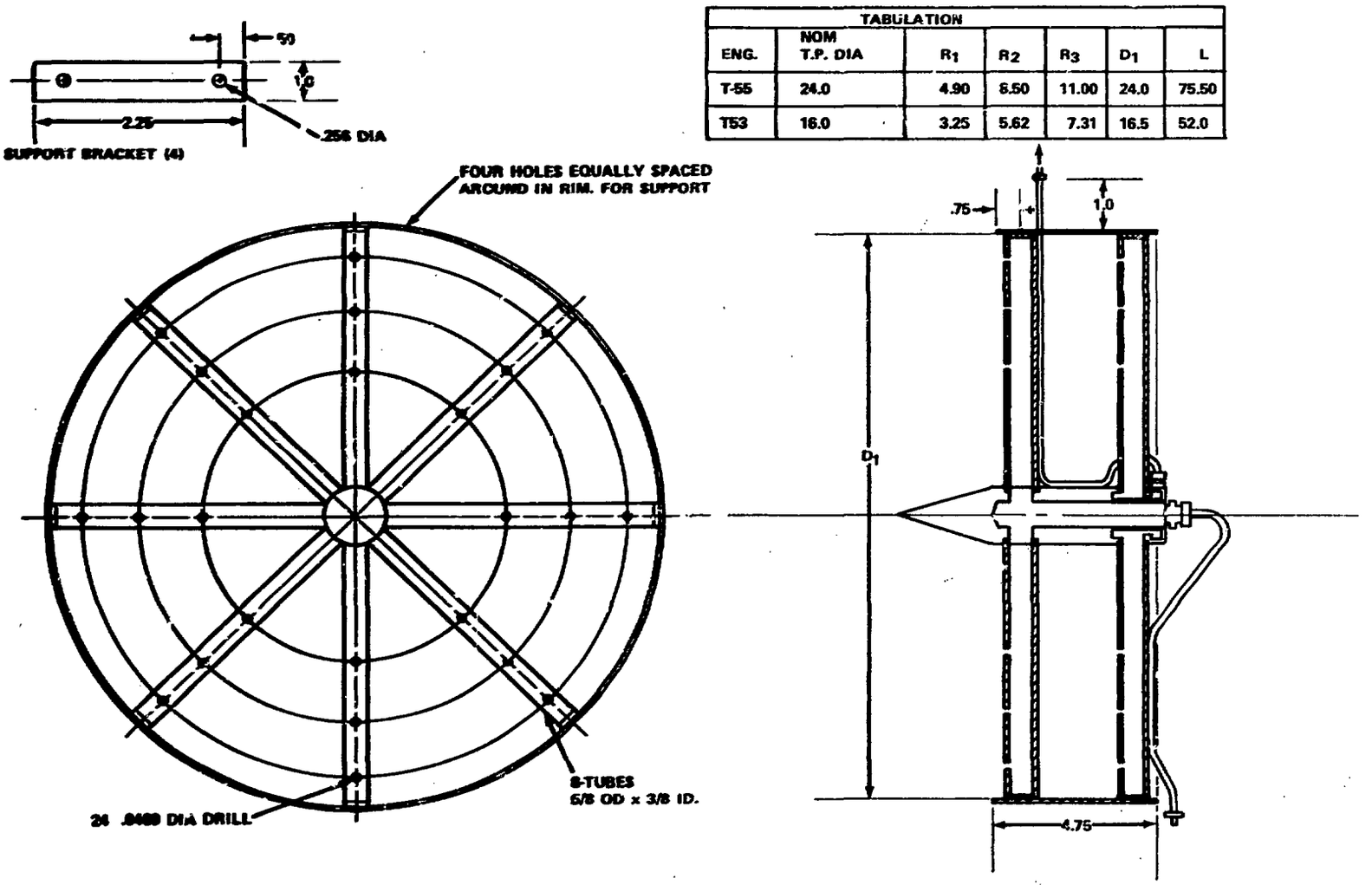

TABULATION						
ENG.	NOM T.P. DIA	R_1	R_2	R_3	D_1	L
T-55	24.0	4.90	6.50	11.00	24.0	75.50
T53	16.0	3.25	5.62	7.31	16.5	52.0

Figure 22. Dual Exhaust Averaging Gas Sampling Probe (Gas and Smoke) for T53 or T55 Engines.

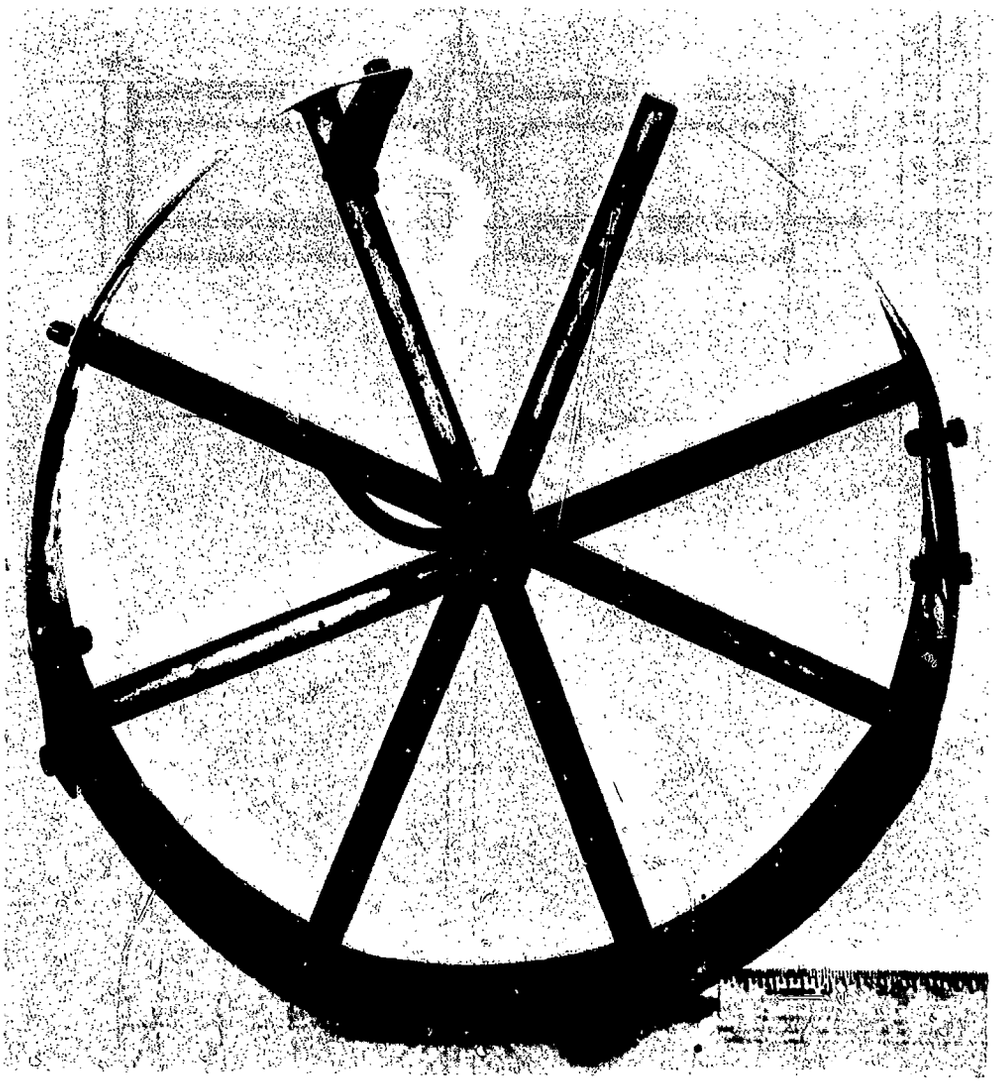

Figure 23. Dual Exhaust Averaging Gas Sampling Probe for T55 Engine.

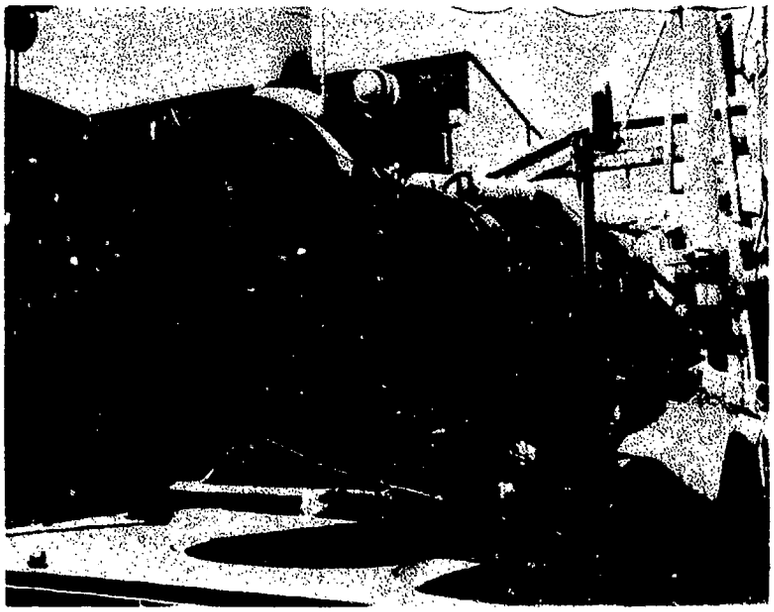

Figure 24. T55 Engine on Test Stand With Averaging Gas Sampling Probe in Place.

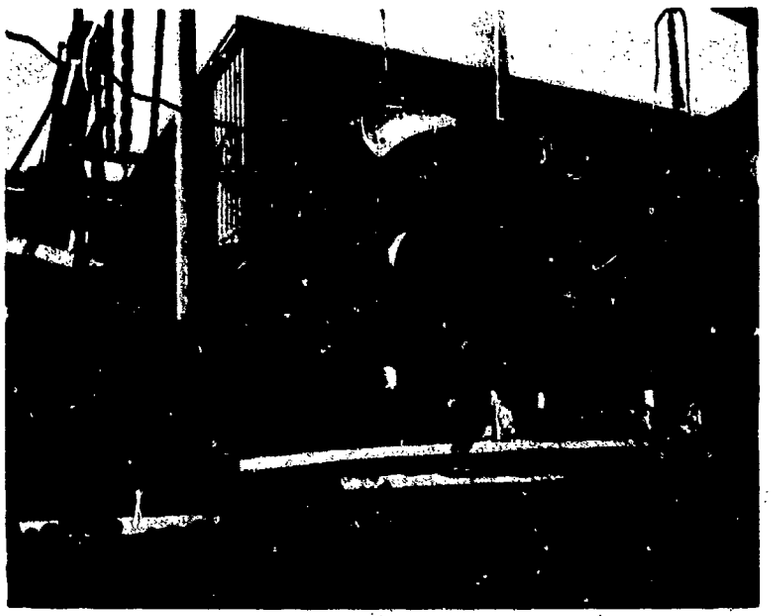

Figure 25. T53 Engine Installed on Portable Test Stand With Averaging Dual Gas Sampling Probe. (Actuator for Traversing Probe Is in Place.)

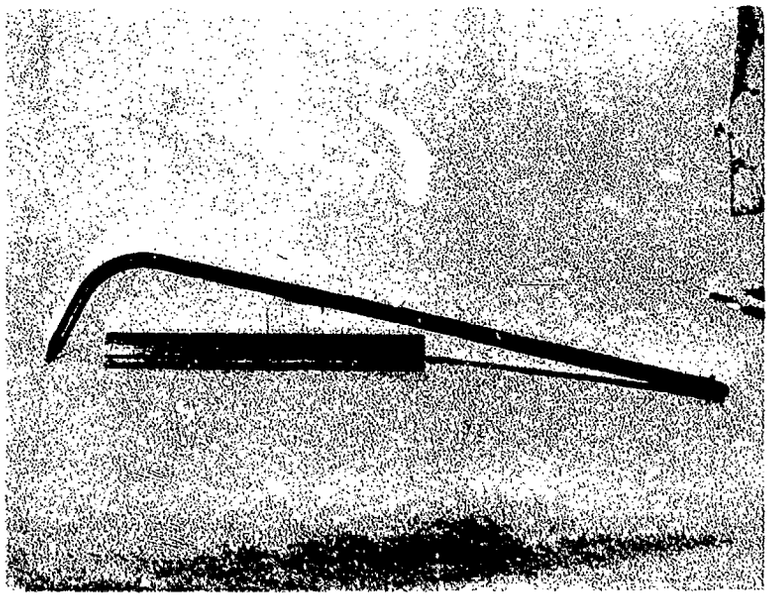

Figure 26. Single-Point Gas Sampling Probe Used With Traversing Mechanism for T53 and T55 Exhaust Sampling.

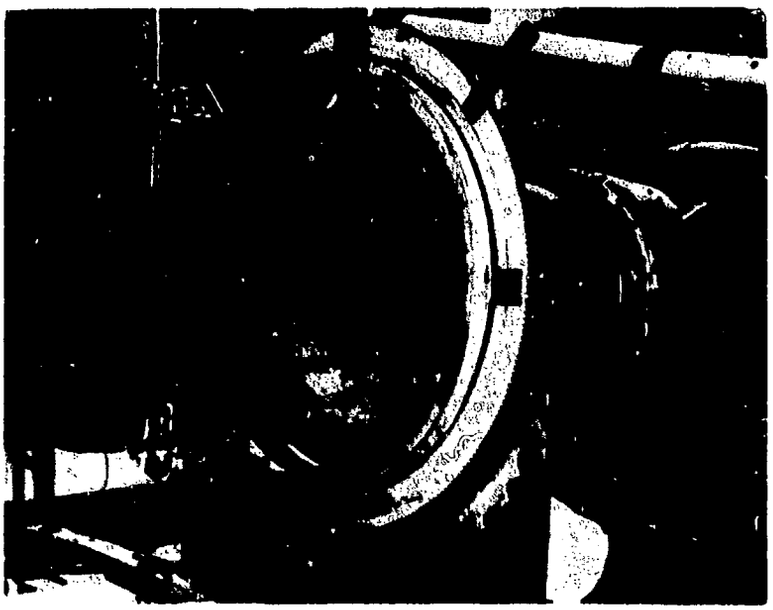

Figure 27. Single-Point Exhaust Gas Sampling Probe Installed on Actuator in T55 Engine Exhaust.

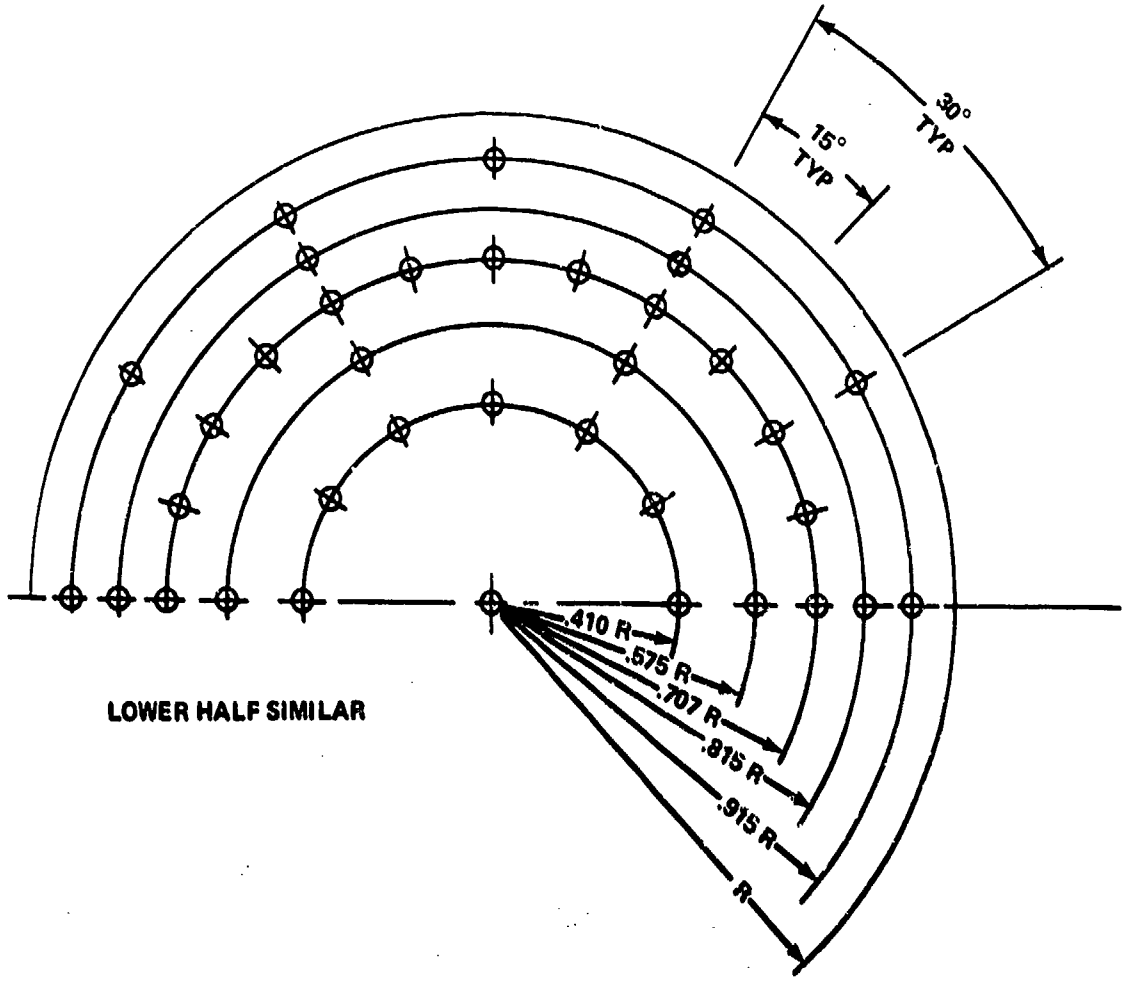

Figure 28. Location of Gas Sampling Points for T53 and T55 Engine Exhaust.

Figure 29 (Reference 7), consists of the following:

1. A high-speed pumping system to transport the sample from test rig to analyzer

2. A "hot" sampling leg for HC analysis, in order to prevent water and HC condensation

3. A "cold" sampling leg for the CO_2, CO, NO, and NO_x analyzers

4. Calibration valving for a wide range of gas compositions and ranges of measurement

Data are recorded both on strip chart recorders and on punched tape. The punched tape data are converted to cards, and these are used in a program to calculate all desirable parameters and plot some of the data.

Specific instruments in the system, their ranges, accuracy, and response time are listed in Table II. In addition, a TECO chemiluminescence NO-NO_x analyzer was used for two tests to check the various NO-NO_2-NO_x values.

A heated sample transport system is contained in the Lycoming Building 19 complex such that any test way can be connected to the gas analyzer console in a few minutes. Thus, one detector system can be used for several test rigs without moving it. The sample lines are made of 3/8-inch stainless steel tubing, electrically heated, and insulated with layers of fiberglass and asbestos wool. A controller is installed for 60 feet or less of heated sample line. Temperature control is set at about 300°F. A 60-foot heated extension section was run from test way 12 to the outdoor transportable engine test stand in order to connect to the gas analyzer console.

The velocity of gas in the sampling line was calculated to be 50 to 75 ft/sec under conditions of atmospheric inlet pressure, such as would be found with engine exhaust sampling. For this calculation, a 12-point sampling probe was used as shown in Figure 22. Sample pressure drop to the gas analysis console in this calculation was assumed to be 5 psi, which was the normal operating condition. The method of calculation included Fanno line calculations of compressible gas friction pressure drop in a .25-in. ID tube 150

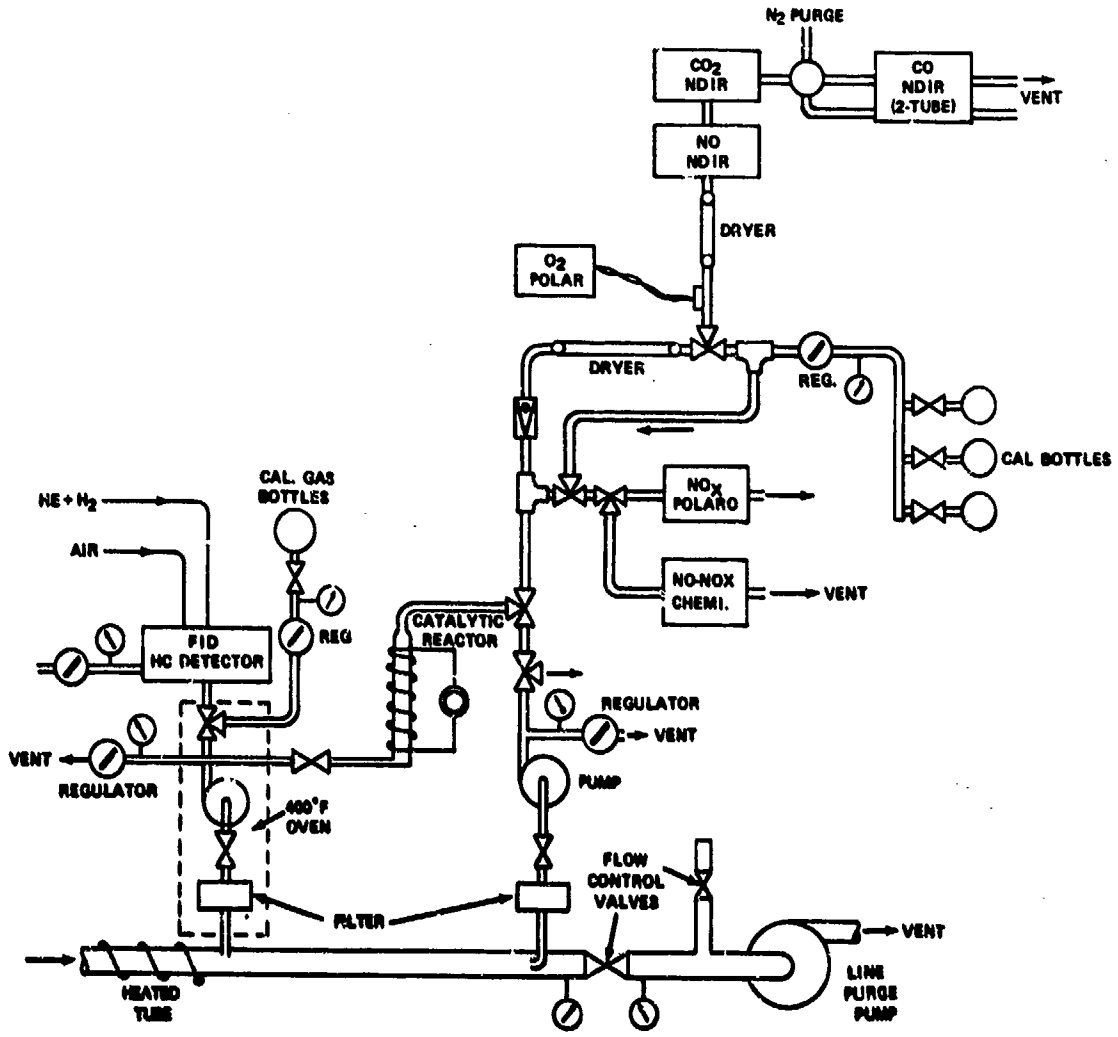

Figure 29. Schematic of the On-Line Gas Sampling System.

TABLE II. GAS ANALYSIS DETECTOR COMPONENTS

Gas	Model	Ranges	Full-Scale Accuracy*	Response Time*
Nitric Oxide (NO)	MSA-200S Infrared detector	0-300 ppm 0-1500 ppm	±1%	90% in 5 sec
Carbon Monoxide	MSA-200 Dual tube infrared detector	Tube No. 1 0-200 ppm 0-800 0-3200 Tube No. 2 0-5%	±1% ±1%	90% in 5 sec
Carbon Dioxide	MSA-300 Infrared detector	0-8% 0-40%	±1%	90% in 5 sec
Oxygen	Beckman 715 Polarographic detector	0-5% 0-25%	±1% (at constant temperature)	90% in 20 sec
Hydrocarbons	Varian 1400 Flame ionization detector	0-100 ppm to approx. 0-20,000 ppm	±2% in low range ±1% in high range	Approximately 90% in 10 sec
Nitrogen Oxides (NO_x)	EnviroMetrics NS-200	0-50 ppm to 0-10,000 ppm	±2%	90% in 5 to 10 sec

*Per manufacturer's specifications

feet long, with temperature held at 300°F (Reference 35).

SMOKE ANALYZER EQUIPMENT

The Lycoming smoke analyzer was designed to conform to SAE-ARP 1179 (Reference 6). It is shown in Figures 30 and 31. The analyzer consists of a pumping system which pulls a sample through heated lines, meters the flow, and passes the gas through a standardized filter paper. The sample lines are heated to prevent water condensation. The reflectance of the smoke deposit on the filter paper is measured with a McBeth model RD-400 reflection densitometer. ARP 1179 procedures are followed to determine the AIA smoke number.

The system was pressure-checked before each test to ensure that the sample lines did not leak.

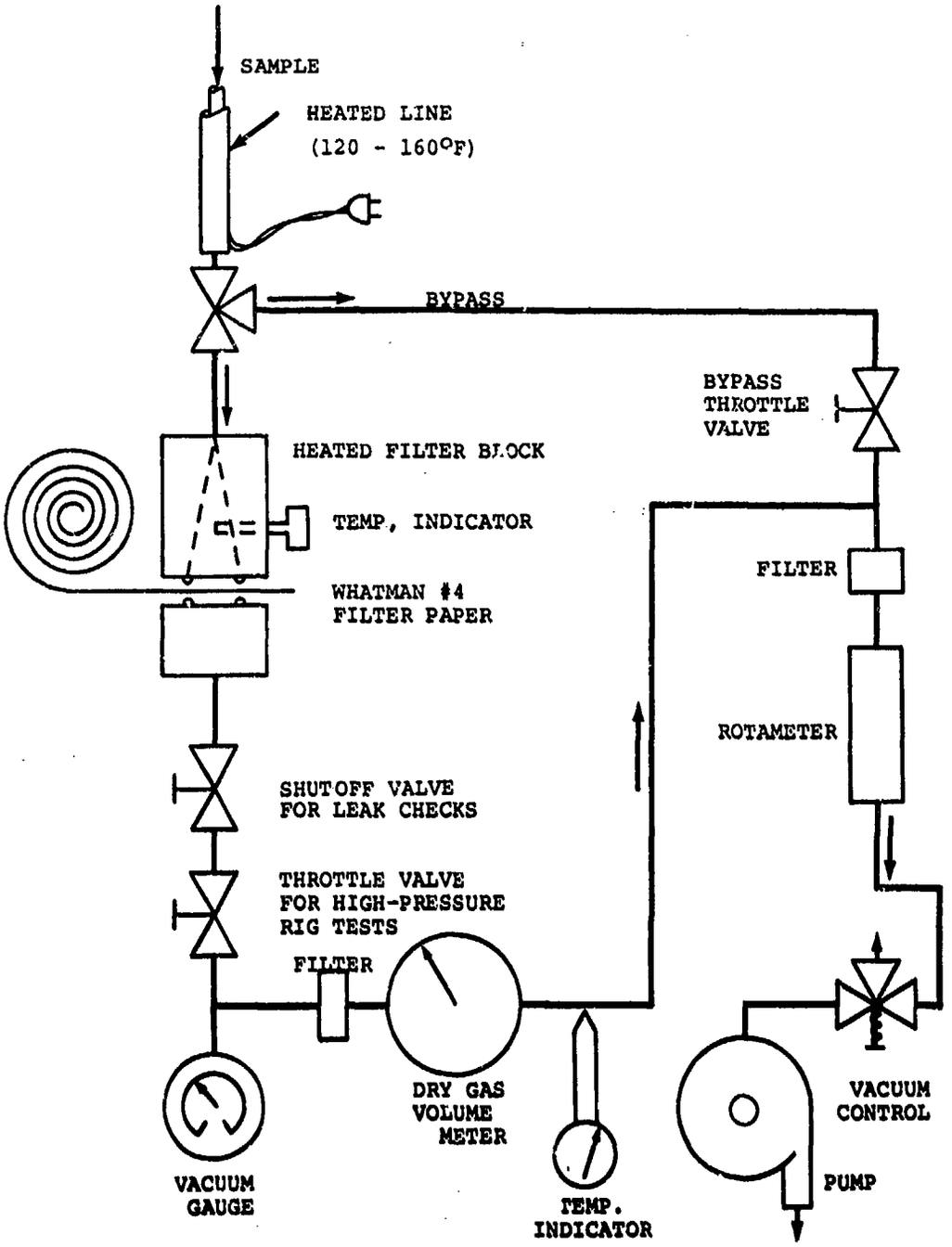

Figure 30. Schematic of the Lycoming Stained Filter Paper Smoke Analyzer.

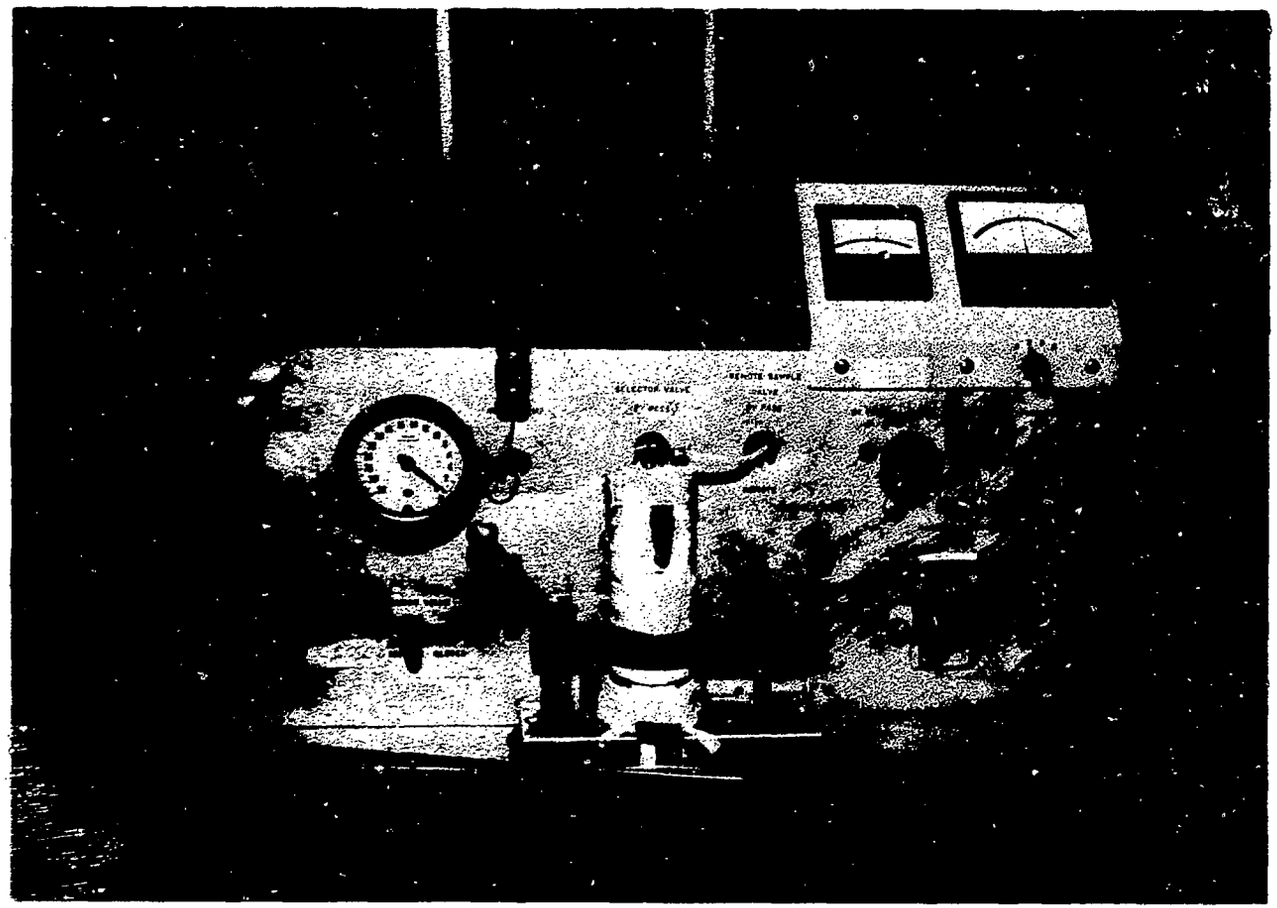

Figure 31. Lycoming Smoke Analyzer.

PROCEDURES

EXHAUST GAS ANALYSIS CHEMISTRY

The chemical reaction for a typical hydrocarbon fuel that is not completely reacted is assumed to be as follows (Reference 7):

$$\begin{aligned}
&\phi\, C_nH_m + (O_2 + 3.73\, N_2 + .04A)\,(n + m/4) \longrightarrow \\
&n\phi \left[(1 - a - b)\, CO_2 + aCO + bCH_{m/n}\right] + \phi\,(m/2)\,(1 - b)\, H_2O \\
&+ \left[(n + m/4) - \phi\,(n\left[1 - a/2 - b\right] + \left[m/4\right]\left[1 - b\right])\right] O_2 \\
&+ \left[.04A + 3.73\, N_2\right]\,(n + m/4) \qquad (1)
\end{aligned}$$

where

$$a = \frac{CO}{CO_2 + CO + CH_{m/n}} \qquad (2)$$

$$b = \frac{CH_{m/n}}{CO_2 + CO + CH_{m/n}} \qquad (3)$$

and CO, CO_2, and $CH_{m/n}$ are measured volume fractions on a dry basis.

The hydrocarbon product, $CH_{m/n}$, is used because the flame ionization detector measures effective carbon atoms.

It is assumed that unburned hydrocarbons remain as a combination of C-H atoms, and that the only other unburned component is CO. Smoke or carbon particles are not considered. Hydrogen is present in such small quantities at high combustion efficiency levels that its effect on combustion efficiency is assumed to be negligible (Reference 8).

The hydrocarbon component ($CH_{m/n}$) is actually measured within a heated gas stream in order to prevent condensation of hydrocarbons; hence the gas is not dried, and the measurement is on a "wet" basis. For a typical engine fuel rate at $\phi = .25$, the equilibrium water vapor is about 3.5 percent. Therefore, the maximum error by considering

$CH_{m/n}$ to be "dry" is about 3.5 percent. For a typical 10 ppmC at a high power point, 3.5 percent error is negligible. For a typical 100 ppmC at a low power point (F/A = .01), the possible error is 1 percent, also negligible. The effect on calculated equivalence ratio is negligible.

Point equivalence ratio can then be calculated from Equation (1) from a knowledge of the CO, CO_2, and unburned hydrocarbons ($CH_{m/n}$) on a dry basis:

$$\phi = \frac{4.77\ (1 + m/4n)}{1/(CO + CO_2 + CH_{m/n}) - a/2 - b\ (1 + m/4n) + m/4n} \qquad (4)$$

The stoichiometric F/A for any hydrocarbon fuel may be calculated from Equation (1):

$$(F/A)_{stoich.} \equiv (W_f/W_a)_{stoich.}$$

$$= \frac{(12)\ n + m}{(n + m/4)(32 + 3.73 \times 28 + .04 \times 40)} \qquad (5)$$

where

approximate molecular weights of C, O_2, N_2, and A are 12, 32, 28, and 40, respectively. For a JP-4 fuel used at Lycoming (Table IV), n = 7.24; m = 14.07; and $(F/A)_{stoich.}$ can be calculated to be 0.0679. For the JP-4R (referee grade) fuel used in these tests, with 15 percent aromatics, $(F/A)_{stoich.}$ is 0.0692, an appreciable difference. The atomic proportions of hydrogen and carbon are average values from an analysis of the fuel. The F/A can then be calculated from equivalence ratio:

$$F/A = (F/A)_{stoich.}\ \phi \qquad (6)$$

Combustion efficiency for fuel can be determined from equivalence ratio and a measure of the total unburned components, CO and $CH_{m/n}$. This equation is valid for all lean mixtures and rich mixtures at low values of η_b where some oxygen is still unused:

$$\eta_{b\ fuel} = 1 - \left[\frac{\left(W_{CH_{m/n}} + \left[\frac{\Delta H\ (CO)}{\Delta H\ (fuel)}\right] W_{CO}\right) \Big/ \left(W_a + W_f\right)}{W_f/(W_a + W_f)}\right] \qquad (7)$$

where

$\frac{W_{CH_{m/n}}}{W_a + W_f}$ = Mass concentration of unburned fuel in the exhaust gas

$\frac{\left[\frac{\Delta H(CO)}{\Delta H(fuel)}\right] W_{CO}}{W_a + W_f}$ = Mass CO equivalent to heating value of fuel in the exhaust gas

$W_f/(W_a + W_f)$ = Total fuel/gas ratio = $1/(W_a/W_f + 1)$

For the fuels used in these tests, a mean value of $\frac{\Delta H\ (CO)}{\Delta H\ (fuel)}$

$= \frac{4,343}{18,702} = .232.$

For best results, a fuel heating value determination should be made for the specific fuel used.

Carbon (n) and hydrogen (m) content and molecular weights are shown in Table I for a group of gas turbine fuels used at Lycoming.

For the data reduction used in the work reported here, Equation (4) was used to calculate equivalence ratio, Equations (5) and (6) to calculate F/A, and Equation (7) to calculate combustion efficiency. A chemical analysis was made of typical fuel samples to determine mean molecular weight and C-H ratio. Bomb calorimeter heat of combustion measurements were made to determine the fuel lower heating value used in Equation (7). The heat of combustion of CO was obtained from Reference 9.

CALCULATION PROGRAMS

Calculation programs were available for:

1. Laboratory combustor rig data, where data input into the DS-5 data system are converted to pressures, temperatures, fuel flow, and airflow. Also, temperature traverse data were programmed so that a plot of temperature profile can be made (Reference 10).

2. Engine data, where data recorded from instruments during the test are used to calculate fuel flow, airflow, and other engine parameters (Reference 11). Inlet bellmouth airflow was measured, and bleed flows were calculated to determine combustor airflow.

3. Gas analysis data, where instrument calibration and output signals are converted to ppm, lb/1000 lb fuel, F/A, and combustion efficiency (Reference 12). In addition, emission traverses were plotted with the "Calcomp" plotter.

CALIBRATION OF INSTRUMENTATION

Laboratory Instruments

All laboratory instrumentation outputs were fed to the DS-5 data system described in Reference 13. This system contains calibration standards. The calibration method complies with MIL-C-45662A (Reference 14).

Engine Test Instrument Calibrations

Instrumentation used to measure the engine performance was calibrated per "Measurements and Test Equipment Calibration Systems" standard (Reference 15). This standard operating procedure for instrument calibrations was also written to conform to MIL-45662-A (Reference 14).

Gas Analyzer Calibration

The Lycoming gas analyzer system is comprised of the detectors listed in Table II. Calibration curves were supplied by the manufacturer for the infrared analyzers (CO, CO_2, and NO). In this case, an initial check was made with various gas bottle calibration compositions as a check on the manufacturer's calibration curve. The checks were within the combined instrument accuracy and the guaranteed (2%) accuracy of the calibration gas sample. For each test, a calibration gas was used to set the electrical output for each instrument at a range convenient to read on the chart recorder.

The flame ionization detector (FID), used to measure total hydrocarbons, was calibrated on two ranges, a factor of 10 apart. The calibration curve of this instrument appears linear. Data in reports from the manufacturer also show linearity (Reference 16).

Because the FID flow quantity is a function of temperature and pressure at the metering orifice, it was deemed appropriate to control these two factors. Temperature was controlled by a very precise oven temperature control inside the instrument case through which the gas passed. Pressure was controlled by an exterior located precision "Wintec" back pressure regulator. In addition, the pressure was recorded to within 0.1 inch of water, and a calibration curve was made of pressure versus percent of "standard" reading (Figure 32). This correction was put into the computer program so that any pressure deviation from the standard value was compensated in the data calculations. The instrument operating standard pressure was set at 30 inches of water gage.

The polarographic NO_x detector was operated with an activated charcoal absorber in the sample train to absorb aldehydes, because the instrument is sensitive to aldehydes. However, the charcoal may also absorb some NO. Therefore, the calibration gas was set up to pass through the charcoal. It was assumed that the same fraction of NO is absorbed in the charcoal as during a test, so that the charcoal absorption of NO is effectively cancelled out. Most of the measurements were made in the range of 0 to 100 ppm, and the calibration gas was normally approximately 60 ppm. Linearity in this range was assumed.

A chemiluminescence analyzer (NO and NO_x) was used on one test as a check on the infrared and polarographic instruments. It was calibrated by using the same sample bottle mixture of NO and N_2 that was used on the other NO and NO_x instruments. The manufacturer (Thermal Electron Corporation) maintains that this instrument response is linear, and our tests did not indicate otherwise.

The calibration procedures recommended in ARP-1256 (Reference 17) were followed as closely as practicable.

Typical calibration curves are shown in Figure 33 for CO_2, in Figure 34 for NO (infrared) and hydrocarbons, in Figure 35 for CO, and in Figure 36 for NO_x (polarographic). Electrical noise levels are within the manufacturer's specifications.

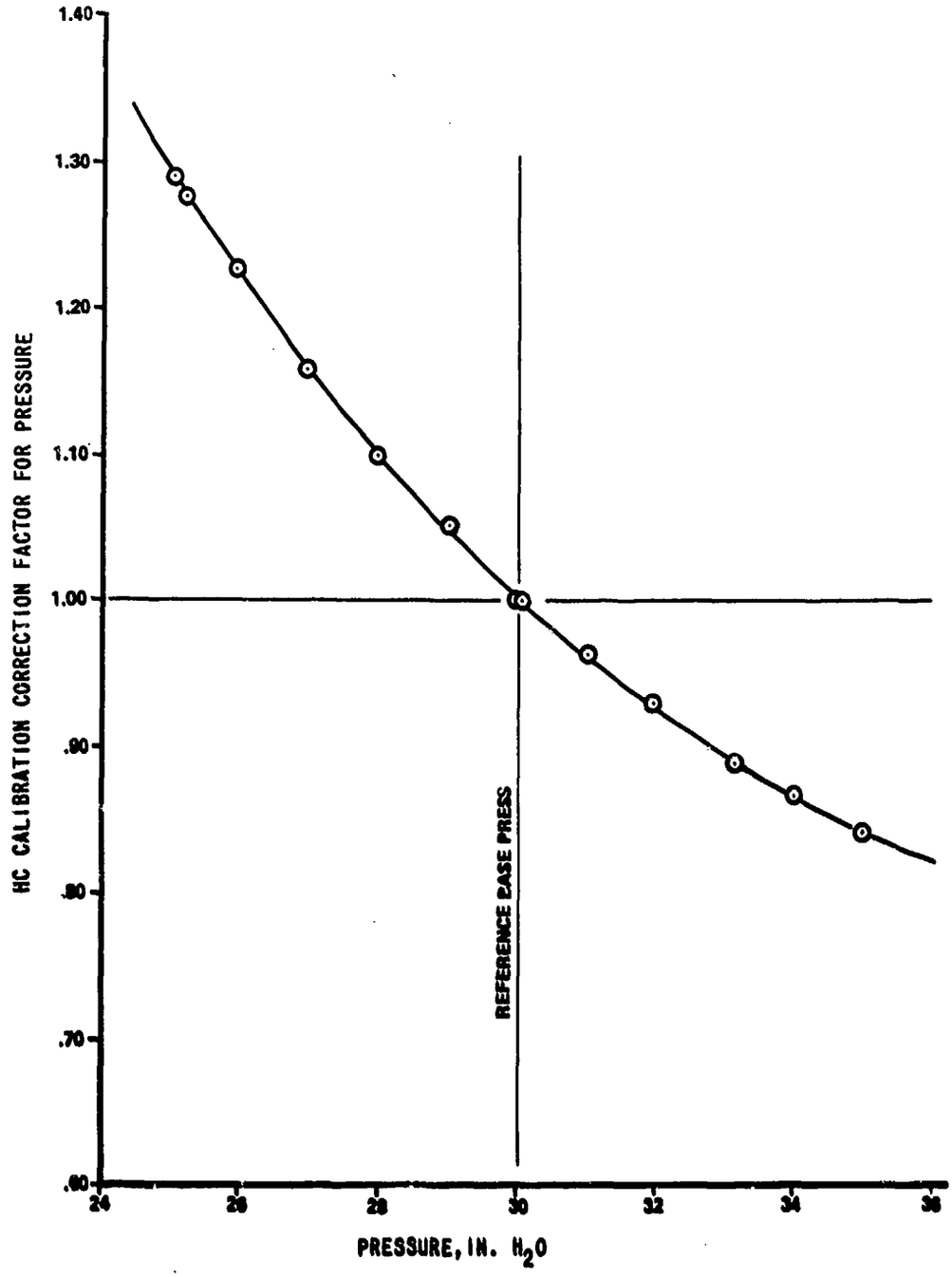

Figure 32. Hydrocarbon Calibration Correction Factor Versus Pressure for Flame Ionization Detector.

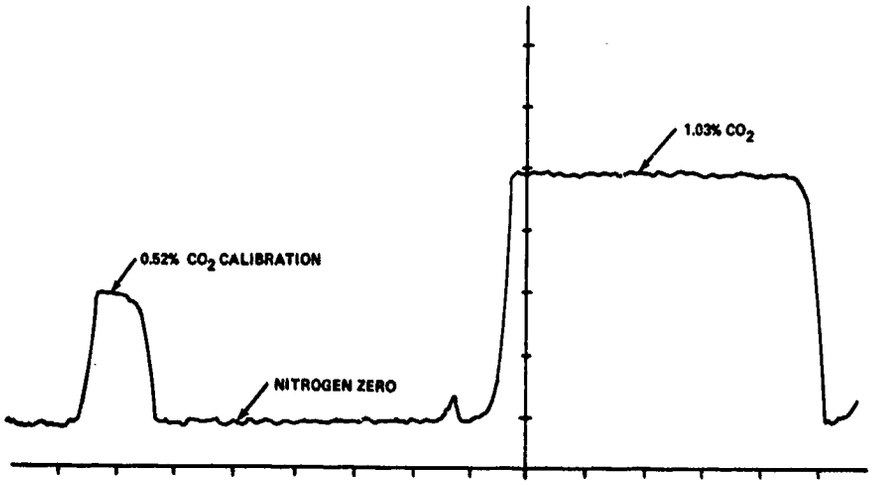

Figure 33. Typical Calibration Trace for NDIR CO_2 Analyzer.

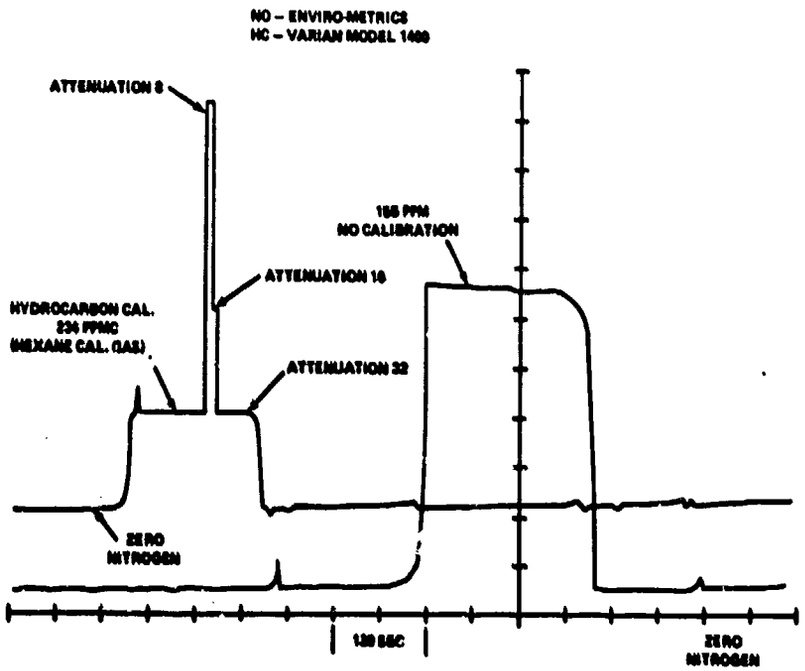

Figure 34. Typical Calibrations, NDIR NO Analyzer Hydrocarbon FID.

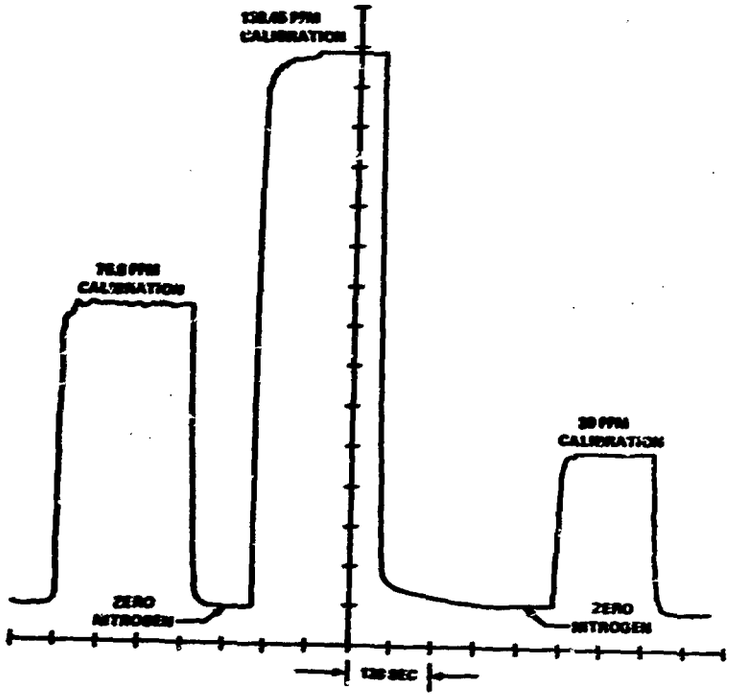

Figure 35. Typical Calibration Trace for NDIR CO Analyzer.

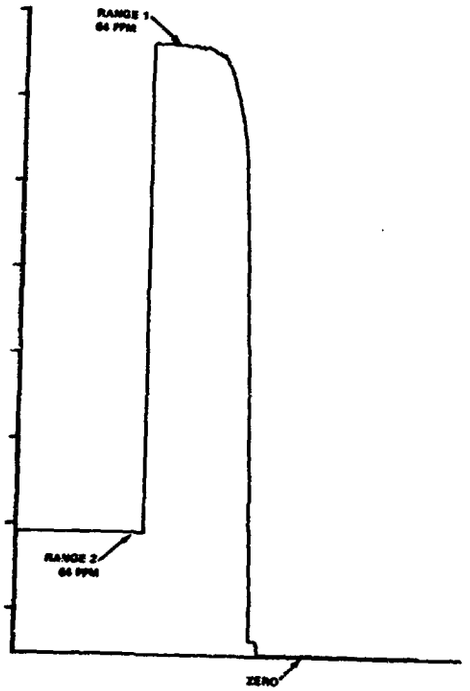

Figure 36. Typical Calibration Trace for Polarographic NO_x Analyzer.

COMBUSTOR TEST PROCEDURES

The combustor assembly, arbitrarily selected for both the T53-L-13A and T55-L-11A engine, could be tested in both an engine and the laboratory test rig. The test conditions included a specified idle power point, 30, 60, and 100 percent (Reference 18). Sixty-point traverses were run at idle, 30, 60, and 100 percent power (Table I). A sixty-first point was recorded as a check on the first point.

The conditions to simulate engine operation were taken from engine measurements and cycle calculations. The 100 percent power simulation pressure could not be met; therefore, the test was run at engine cycle specified temperature and F/A but not the specified pressure. The attainment of design pressure for the 60 percent power point for the T55 was also found to be marginal and was run at the highest attainable pressure, as shown in Table I.

The desired operating conditions of air pressure, airflow rate, air temperature, and fuel flow were controlled and allowed to stabilize before test data were recorded. Precautions were taken to maintain test conditions unchanged during the long single-point traverse. However, steady flow is only maintained in any system within some limit of both precision of control and precision of detecting any change. A check procedure was used to detect any appreciable changes in operating conditions, including:

1. For each 10 single-point samplings, an average sample was taken. Thus, if the overall conditions were changed, the average sample would show it.

2. For each 10 to 20 sample points, the gas analyzer was recalibrated.

3. Fuel-air ratio from the test rig data was used to check against F/A from the average gas sample. Disagreement larger than the expected experimental error would indicate either a leak, an error in measurement, or a nonrepresentative sample.

Traverse survey data points were recorded after moving the probe to the next position and allowing the sample line to purge. When the compositions reached a steady level on the recorder, the data were then electrically recorded and punched into the tape. Average time per data point was 2 minutes during traversing. Additional time was required for switching to the averaging probe, for recording the data, and for calibrating periodically.

At each point where the averaging probe was sampled, a thermocouple temperature profile traverse was also recorded in the combustor exit. These temperature data were used for comparison with exit profiles calculated from gas sampling, such as F/A. Adiabatic flame temperature can also be calculated from F/A and combustion efficiency (determined from gas analysis); however, this information was not considered to be needed for the analysis.

ENGINE TEST PROCEDURES

Initial engine tests were made for calibration purposes and to check out the installation and equipment.

For power performance tests, the engine was operated from the specified idle condition, increasing the power in steps up to full power, then back down to idle. This was repeated. Approximately 5 minutes was required to stabilize the engine operation at each power level before recording data. Both gas samples and smoke samples were recorded simultaneously on the double cruciform probe (Figure 22), as shown on Table I.

Gas samples were recorded when composition was observed to stabilize on the chart recorders. The punched tape system was used. Stable composition level was the signal to record the data. Two to four minutes were required per data point to move the probe, purge the lines, and obtain a stabilized reading. Calibration checks were recorded normally after 20 data points. The whole T53 traverse was done with one setting of the actuator position. Center points were repeated as each diameter was traversed as a check of operating stability; i.e., to determine if there were substantial changes in gas analysis determined F/A or any gas component with respect to time.

For the T55 engine, the exhaust traverse was performed in two halves of 40 points each. The center points were repeated on each diameter traverse, as with the T53, to check on stability and continuity of the engine operation. Also, the centerline diameter traverse was repeated on the second half of the traverse as a check of any change in operation from the first half.

DATA CALCULATION AND INITIAL DATA PLOTS

Laboratory test data were processed on an IBM 370/155 computer. The output of these computations include all the test rig conditions and flows of fuel and air, temperature (thermocouple) traverse data and plotted profiles, and gas analysis data, including F/A and combustion efficiency.

Engine operating data were manually recorded and processed for computer input. Gas analysis data from the engine employed the same system for readout and calculation as in laboratory combustor tests. Gas analysis profile data recorded in the engine exhaust were manually plotted.

GAS ANALYSIS PROBLEMS

Two problems in obtaining accurate gas analysis data were possibly significant, and sufficient information was not immediately available on them. These are the problems of (1) the required temperature of gas sampling lines to prevent hydrocarbon condensation and fouling of the sampling lines and (2) reliability of measurement of NO_x.

Hydrocarbon Condensation in Sampling Lines

Since we have been analyzing engine and combustor exhaust gases, there has been the problem of how hot the sampling line has to be to prevent unburned fuel condensation. The SAE-ARP-1256 (Reference 17) prescribes a sample line temperature of 302°F (150°C) as satisfactory. However, the 10 percent distillation point of a typical JP-4 fuel occurs at about 210°F and the 90 percent point at 410°F. For JP-4R, the initial point is less than 200°F and the 90 percent point is between 325° and 370°F. Does this mean that 302°F in the sampling

line is completely unsatisfactory if there are appreciable quantities of unburned fuel? What concentrations of fuel can be tolerated without problems? An analysis was made to find answers to these questions.

The factors influencing fuel condensation in the sampling lines are:

1. The molecular weight and vapor pressure of the heaviest molecular components of the fuel

2. The combustion efficiency, which determines approximately what fraction of raw and cracked fuel is present

3. The temperature of the sampling line

The mean molecular compositions of JP-4 and JP-4R fuels used at Lycoming are shown in Table III. Both higher and lower molecular weights are included in the average, but the exact range and concentrations are both unknown and quite variable within each fuel specification. A detailed analysis of all the components of the fuel would be costly, and probably worthless, because of the wide tolerable composition variability for each Military Specification. The original crude oil and the refining processes would also affect the type and concentration of the fuel components. Some indication of the range of component molecular weights was obtained at Lycoming through use of chromatographic analysis. The results of a JP-4 fuel analysis show components from C_5 to C_{15}, which was the highest weight detected (Figure 37).

Vapor pressure data (Reference 9) for various pure hydrocarbon compounds were plotted to determine the range of concentrations that might be expected in a sampling line at various line temperatures without getting condensation (Figure 38). However, the vapor pressure of mixtures is not the sum of vapor pressure of the components. Heavy molecules will reduce the vapor pressure of light molecules, and vice versa. In Figure 38, a range of possible saturated hydrocarbon fuel components is plotted against vapor pressure. The components were chosen to cover a range of molecular weights that might be found in the fuels, as noted in Table III and analyzed on Figure 37. This plot shows that a heavy fuel, such as Navy

TABLE III. AVERAGE COMPOSITIONS AND PROPERTIES OF FUELS ($C_n H_m$) USED

Fuel	JP-4	JP-5	Marine Diesel	JP-4 Ref: (15% Arom.)
Specific Gravity at 60°F	0.7796	0.8270	0.8358	.755
% C (Wt)	85.91	86.28	86.22	86.63
% H (Wt)	14.03	13.44	13.64	12.79
C/H Ratio (Wt)	6.12	6.42	6.32	6.78
Mean Molecular Unit	101.	160.	190.	108.5
n	7.24	11.54	13.67	7.82
m	14.07	21.39	25.75	13.76
m/n	1.942	1.852	1.885	1.760
ΔH (Lower Heating Value)				18,702

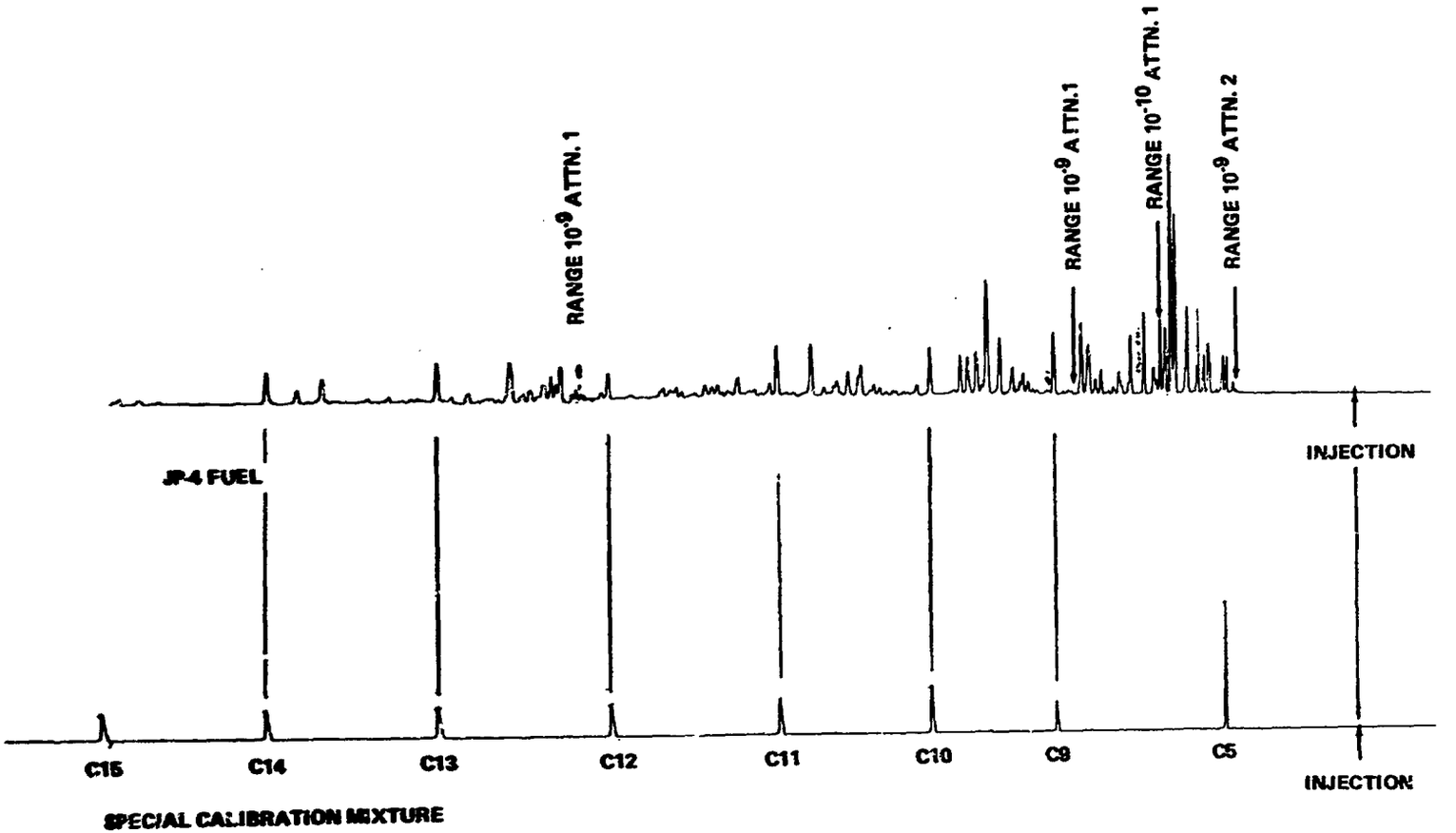

Figure 37. Typical Chromatograph of JP-4 Fuel Compared to Special Calibration Mixture, Showing Many Components and Approximate Carbon Content.

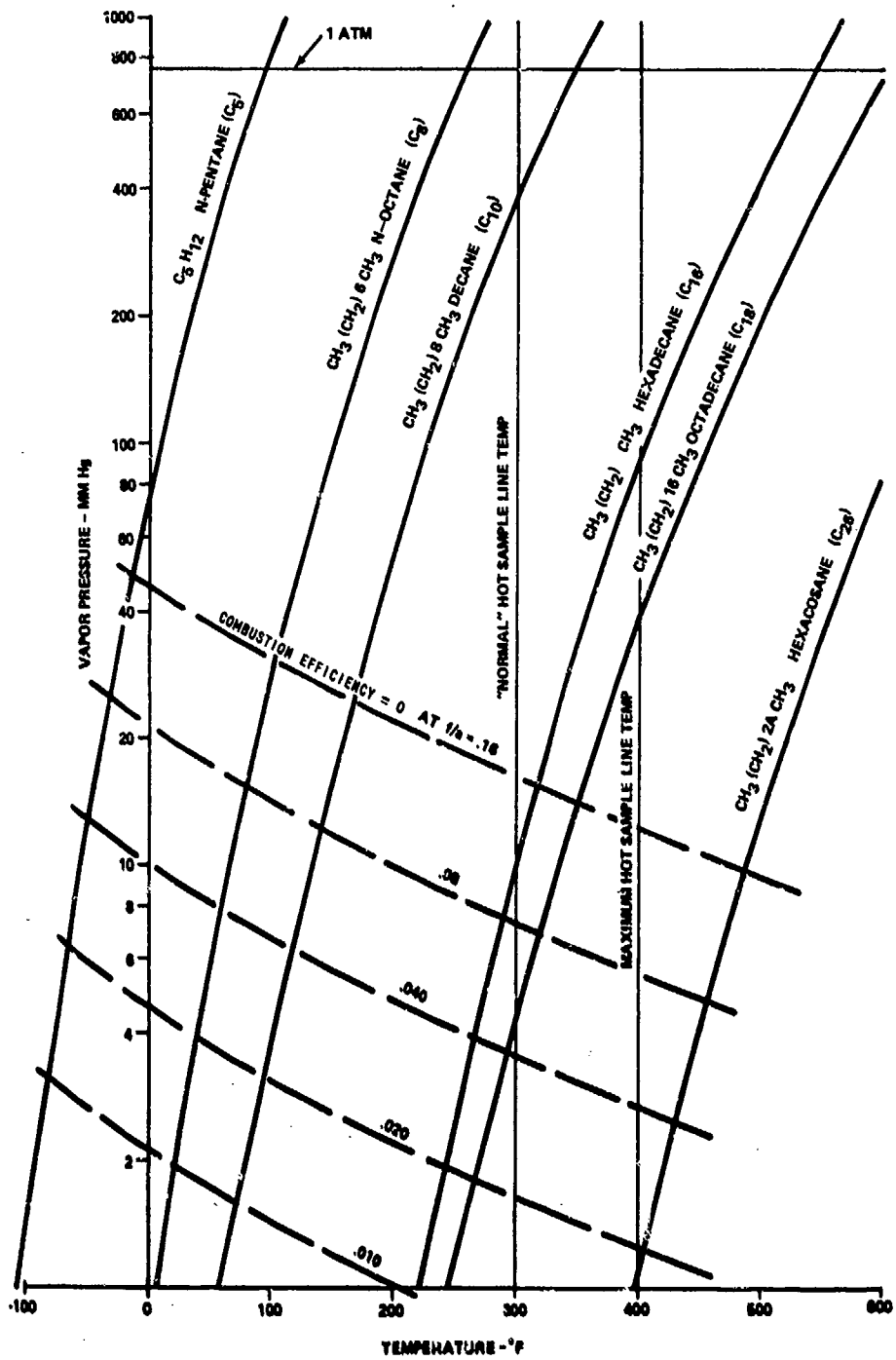

Figure 38. Vapor Pressure of Various Hydrocarbons Versus Temperature and Concentration.

distillate, may produce condensation that is a problem in the sampling lines if the 400°F temperature cannot be held, or if raw fuel of the order of .005 to .010 F/A is present even at 400°F. This assumes that some of the distillate components are C_{26} or heavier. The composition of JP-4R fuel contains fewer heavy molecules than Navy distillate, and has a high probability of remaining gaseous at 300° F.

In addition, "chromatographic" effect may be present. This effect is caused by absorption of components onto the wall for short periods as the sample moves down the sample line and is evidenced in the results by a longer period of time being required to purge the sample line than would normally be expected. This condition can be experienced even though the sample line is hot enough to keep all components in a vapor state, but does not present a serious problem. It only increases the time required to purge an old sample and obtain an equilibrium sample at a new test condition.

From an inspection of Figure 38, we find that:

1. Condensation of hydrocarbons smaller than C_{13} is not a problem, even with a line temperature of 300°F, as long as the concentration is not above 5000 ppm at 300°F, or 130,000 ppm at 400°F. Since the average carbon content for JP-4 or JP-4R is about 14, it would be expected that there should be few condensation problems with either JP-4 or JP-4R at 300°F.

2. A 400°F, C_{26} can be vaporized to about 1300 ppm (or 33,800 ppmC). This would represent about 80 percent of the fuel at a total F/A of .020 or about 20 percent combustion efficiency from hydrocarbons alone. (CO may add some additional inefficiency.) This concentration would never be encountered in an engine exhaust, but might be found in a primary zone. Therefore, it appears that the major components of a fuel even as heavy as Navy distillate would have a good chance to remain in a vapor state at 400°F.

The foregoing analysis was purposely general to include a wide range of fuel gas analysis problems. However, from the results we conclude that JP-4 fuels should not cause a gas sampling line problem if the sampling line and adjacent parts are held in the 300°F range and if the combustion efficiency is reasonable (85 percent or higher).

Reliability of Measurements of NO_x

The nitrogen oxide emissions are of particular interest because of the gradual atmospheric conversion to NO_2, which is an eye, nose, and lung irritant. However, only the formation of NO can be justified from chemical kinetic considerations. The more important reactions are those proposed by Zeldovich in 1946 (Reference 19):

$$O + N_2 \rightleftharpoons NO + N \quad (8)$$

$$N + O_2 \rightleftharpoons NO + O \quad (9)$$

Other reactions proposed by Newhall and Starkman (1968) and Lavoie, et al (1970), include (Reference 19):

$$OH + N \rightleftharpoons NO + H \quad (10)$$

$$N_2 + O_2 \rightleftharpoons N_2O + O \quad (11)$$

$$N_2 + OH \rightleftharpoons N_2O + H \quad (12)$$

$$N_2O + O \rightleftharpoons NO + NO \quad (13)$$

$$N + O + M \rightleftharpoons NO + M \quad (14)$$

$$N_2 + O + M \rightleftharpoons N_2O + M \quad (15)$$

The Zeldovich mechanism is generally sufficient to account for NO formation under conditions present in spark ignition engines. The entire set of equations can be used for NO prediction for any combustion process. The process is limited by the presence of O radical. The usual method of calculation is to assume equilibrium composition of O radical before the NO formation becomes important. At any rate, neither Reference 19 nor References 20-29 indicate any mechanism for the formation of NO_2 in the combustion chamber. A chemical kineticist working on this problem suggested that an investigation of some NO_2 formation possibilities revealed that if O radical was present in relatively large quantities at 1200° to 1400°F, NO_2 could be formed. However, the chemical kinetic probability of large O concentrations is very low. Therefore, in view of the

available evidence, we cannot explain or justify measurable quantities of NO_2 formed in the combustor.

Nevertheless, the literature is replete with gas turbine exhaust data showing appreciable or even large quantities of NO_2. Typical are data from References 27 and 30. In Reference 30, we find that the NO_2/NO_x ratio is as large as 40 percent in an engine test. Data from the U.S. Bureau of Mines (Reference 27) indicate large percentages of NO_2, but the actual value of NO_2 is only in the range of 5 to 10 ppm. Analysis of NO and NO_2 data from Reference 4 shows that there is a wide range of variation of NO_2 measurements. Contrarywise, the NO data all point in the same direction, but not the NO_2. The conclusion reached is that NO_2 can vary between 5 and 20 ppm, and is sometimes a little more, and that it is almost independent of engine configuration or percent power.

The presence of this NO_2 (not theoretically explainable) is a topic for investigation, but not the principal purpose of this report. However, some evidence suggests that the sample probing system may permit conversion of NO to NO_2.

Thus, it is possible that the only reason for measuring NO_x or NO_2, in addition to NO, is that some of the NO may have converted to NO_2 between combustor and detector. Of course, the total of NO and NO_2 is the toxic pollutant of interest. We can see that if the exhaust gas could be analyzed without any "en route" conversion to NO_2, the analysis of NO only should be quite satisfactory from available knowledge of chemical kinetics. So it is only to make sure that we know this converted quality, that NO_2 or NO_x measurement is needed.

The next problem we encounter in our measurement of NO_x is the precision of the measurement. Presently, the methods used for NO_x measurement are:

1. Polarographic for NO_x
2. Nondispersive infrared (NDIR) for NO
3. Nondispersive ultraviolet (NDUV) for NO_x (not used in these tests)
4. Chemiluminescence for NO and NO_x

Good comparison of NDIR, chemiluminescence and polarographic methods was obtained by Shaw in Reference 31, where he reports agreement within 5 percent. In the present work, agreement was within 10 percent for NO measurement, and within 10 to 15 percent for most NO_x measurements. Chase* reports less than 1 percent difference between chemiluminescence and NDIR and nondispersive ultraviolet (NDUV), when calibrated carefully and known corrections are applied. He used special processing to obtain NO gas without NO_2 contamination, and N_2 zero gas without NO.

The initial problem in NO_x measurement precision is the calibration gas itself. Calibration gases can be purchased with a 1 or 2 percent "guaranteed" accuracy. Information from vendors indicates that at least two methods of filling the bottle and analyzing it are used. In one case, the bottle is filled and analyzed quickly, and sent to the customer. In this case, some of the calibration gas (NO) may absorb into the bottle walls over a time period. But, as the gas is used, the absorbed gas is released. The question of the composition versus time is a moot one. In the other method, the gas is allowed to stay in the bottle for a period of time before the analysis is made. It is assumed that the gases are in equilibrium with the bottle at the time of analysis, and normally will hold their composition until the bottle pressure becomes quite low. At this time, the absorbed gas re-emits. Calibrated gases for these tests were analyzed by the second method.

Other problems are the deterioration of the sample in the bottle. Any traces of O_2 will react with NO to form NO_2. The excellent agreement between three methods of measurement at the Bureau of Mines was obtained by careful mixing of calibration gases to remove O_2 from the N_2 and remove NO_2 from the NO.

Storage at low temperature will cause striation of the gases, a result of condensation or partial condensation of the heavier gases in the bottle. This is characteristic of all mixed gas bottles, and a possible cause of poor reference calibrations.

Next are problems of measurement in the specific instruments.

---

*Chase, J. (U.S. Bur. Mines), CORRELATION OF NDIR, NDUV, AND CHEMILUMINESCENCE NO-NO_x DETECTORS, Private Communication, 10 December 1972.

Nondispersive Infrared (NDIR) for NO

The main problem with this instrument is its sensitivity to water vapor. The NO infrared absorption band is so close to the water vapor band, that two precautions are required:

1. A special narrow band-pass filter is used to reduce (but not eliminate) water vapor effects.

2. The sample must be thoroughly dried.

In the process of drying the sample, the efficiency of the drying compound enters into the picture. "Drierite" was used in the present work. There are disagreements among various investigators as to which driers are effective without absorbing the measured component. The consensus appears about 50-50 for "Drierite".

Sensitivity of this instrument is obtained by using a longer optical absorption tube, which adds to the bulk and complexity of the instrument.

Polarographic

This detector was capable of measuring either NO_x or NO_2; however, only NO_x was measured. The problems found with the NO_x detector were:

1. Zero drift, probably caused by aldehyde interference. This was nearly eliminated by using an activated charcoal filter in line with the detector. Because the charcoal absorbs some NO_x, the unit was calibrated with the charcoal in the sample line. It was then assumed that the percentage of NO_x absorbed during calibration was the same as during testing. It was also found that the duration of use of the charcoal affected response. This effect was thought to be caused by saturation of the charcoal.

2. Nonuniformity of response. The NO_x results appeared to be more variable over a period of time than the NDIR or chemiluminescence data.

3. Carbon monoxide interference. This was checked and was found to be appreciable only when CO was present in large quantitites; i.e., percent concentrations, rather than ppm.

Chemiluminescence

This detector was used on one test to check the NDIR and the polarographic detectors. The detection of NO appeared stable and showed agreement with the NDIR and polarographic (NO_x) within about 10 percent. However, the NO_x values were all lower than the NO values, a physical impossibility. Chase indicated that this phenomenon is not unusual, and that it is associated with the converter unit efficiency in the instrument. Chemical equilibrium is established between NO and NO_2, thus:

$$NO_2 \rightleftharpoons NO + O \qquad (16)$$

This reaction is sensitive to temperature and pressure, and the percent of conversion calculated from chemical equilibrium agreed quite well with the measurements. Conclusions reached on NO_x measurements are:

1. NO measurements with NDIR and chemiluminescence instruments are reliable and agree within 5 to 10 ppm normally.

2. NO_2 measurements are not as reliable because of possible water vapor absorption of NO_2, inefficiency of thermal converters, and interferences in polarographic detectors.

3. Calibration gases for NO, NO_2, and zero references may be contributors to measurement errors.

4. The principal concern in measurement of nitrogen oxides is the total NO plus NO_2, or NO_x. If NO_2 formation can be controlled to a negligible amount, then NO measurement only is necessary. Otherwise, a reliable measurement of NO_x is satisfactory. At present, NO measurements appear to be more reliable than NO_x or NO_2 measurements.

5. A solution is suggested in the use of a thermal converter with all NO_x measurements. Its efficiency would be determined by calibration. NO would be the primary measurement. This procedure would be applicable for engine or combustor testing, and obviously, not applicable to atmospheric measurements. With this approach, any formation of NO_2 in the sample system would be of no concern.

DISCUSSION OF DATA AND RESULTS

ANALYSIS OF PRECISION OF THE MEASUREMENTS

Before discussing the test results, an explanation of the precision of our measurements is justified in order to judge the value of the results. Later, comparisons will be made with data from other sources as a further evaluation of our overall methods, procedures, and accuracy.

Precision of results can be divided as follows:

1. Measurement precision of the instruments only
2. Correlation of gas analysis measurement with fuel-air calculations by other means (fuel and airflow measurements)
3. Effect of sampling probe position on the measured average
4. Effect of measurement precision on emission determination
5. Characteristics of tested engines compared with a statistical group

Instrument Precision

Instrument precision specified by the manufacturers is shown in Table IV. The specifications here can be judged to be as close to reality as is possible if the instruments are carefully maintained, calibrated, and checked, and if calibration curves are correct. However, the accuracy propounded by the manufacturer cannot always be maintained. In one case, minor malfunction of the CO analyzer caused error in the CO analysis that was not discovered until some obviously unreasonable data were recorded. After servicing, the unit operated satisfactorily. In another case, the CO_2 calibration curve apparently shifted slightly. Data were recalculated after determining a new calibration curve. The new calibration curve was generated by plotting instrument response for several CO_2 calibration gas concentrations. As a result of these experiences, it would seem more reasonable to expect dependable accuracies of the order of ± 3 to 4 percent of full scale rather than 1 percent. In addition, the guaranteed accuracy of the calibration bottle is ± 2 percent.

TABLE IV. OPTIMUM AND PROBABLE GAS SAMPLE ANALYSIS PRECISION

	Manufacturer's Specification	More Probable Accuracy
Full Scale		
Instrument Accuracy	±1%	±3%
Calibration Bottle Accuracy	±1%*	±2%
Total Full-Scale Accuracy	±2%	±5%
At 30% of Full Scale		
Instrument Accuracy	±3%	±10%
Calibration Bottle	±0.3%**	±1.4%***
Total for 30% of Full Scale	±3.3%	±11.4%

It is assumed here that no error is present from poor calibration curves.

* Calibration bottles are obtainable guaranteed for 1% accuracy.

** Assumes calibration gas for full-scale deflection.

*** Assumes calibration gas for 1/2 of full scale, which is much more likely to occur than when full-scale calibration gas is obtainable.

Considering that precision values are usually specified at full-scale deflection, if the same variation is applied at 30 percent of full scale (where readings are often made), then accuracy is further affected (Table IV). These values of accuracy (Table IV) represent a "best" and a "conservative" view of accuracy of gas analysis. Now let us look at the effect of these error quantities on the emission measurements.

Correlation of F/A (Gas Analysis) with F/A (Measurements)

The correlation of F/A determined by gas analysis from the engine or test rig with F/A from the fuel and air measurement tells us two things: (1) whether the sample is representative of the average gas composition, and (2) whether there are leaks in the system which would dilute the sample. This F/A correlation is, of course, subject to the accuracy of both the gas analysis and the engine or combustor fuel and air measurements.

In the laboratory combustor tests, fuel flow and airflow can be quite precisely measured with calibrated fuel flow meters and precision-made orifice plates for airflow. Calculations of the flows include temperature corrections. Pressure and temperature instruments are calibrated at regular intervals. Estimated accuracy is ± 1 percent for each measurement.

Engine F/A is also determined by measured fuel flow rate, and airflow measurement at a calibrated bellmouth at the engine inlet. The precision of this measurement is not quite as good as in the laboratory test for these reasons:

1. At low power settings, the pressure drop at the bellmouth inlet is low, and accuracy suffers.

2. The precise quantity of air entering the combustor is determined from bellmouth measured airflow and from calculated engine cooling and internal airflow network.

3. Low-power interstage compressor bleed is reproducible within $\pm 2\%$ of the total airflow.

Considering all of the foregoing problems of calibration, accuracy, and precision, we then look at a comparison of the two completely

independent methods of F/A measurement: (1) gas analysis and (2) fuel and air metering. The comparison tells something about both measurements, and also tells whether the gas analysis sample is representative of the overall gas composition. F/A can be taken as a measure of just how representative are the emission concentrations if we can assume that the gases are all mixed in the same proportion and that there is no selective separation of exhaust gas components. These are thought to be reasonable assumptions.

Fuel-air correlation data for combustors and engine are plotted in Figures 39 through 41. Most of the data lie within the 10 percent margin, and all of it well within the ARP-1256 specification of 15 percent. The T53 engine "traverse average" data lie within 3 to 4 percent. Some detailed explanations are:

1. Figure 39 shows the F/A correlation for the T53 and T55 laboratory combustor measurements. Here the "idle" point gas analysis for both T53 and T55 combustors seems to be low, as does the maximum power T55 point. For the idle point, one possible explanation is that a high concentration of fuel exists near the wall at the measuring station caused by fuel vaporizing off the wall in the upstream end of the combustor. As for the maximum power point in the T55 combustor, the explanation lies in damaged sampling probe. This probe is water-cooled (Figure 15) and contains five sample ports across the height of the combustor exit annulus. At some point in the test, the water was turned off. Overheating occurred at the peak of the temperature profile (2/3 of the channel height) where the F/A was maximum. Thus, the probe selectively sampled the leanest part of the flow and gave the low reading shown. The traversing probes taken from the T53 and T55 rigs after the completion of testing are shown in Figure 42.

2. Figure 40 shows F/A correlation data for the T53 engine. "Traverse average" data correlations are exceptionally close. The averaging probe correlations deviate as much as 10

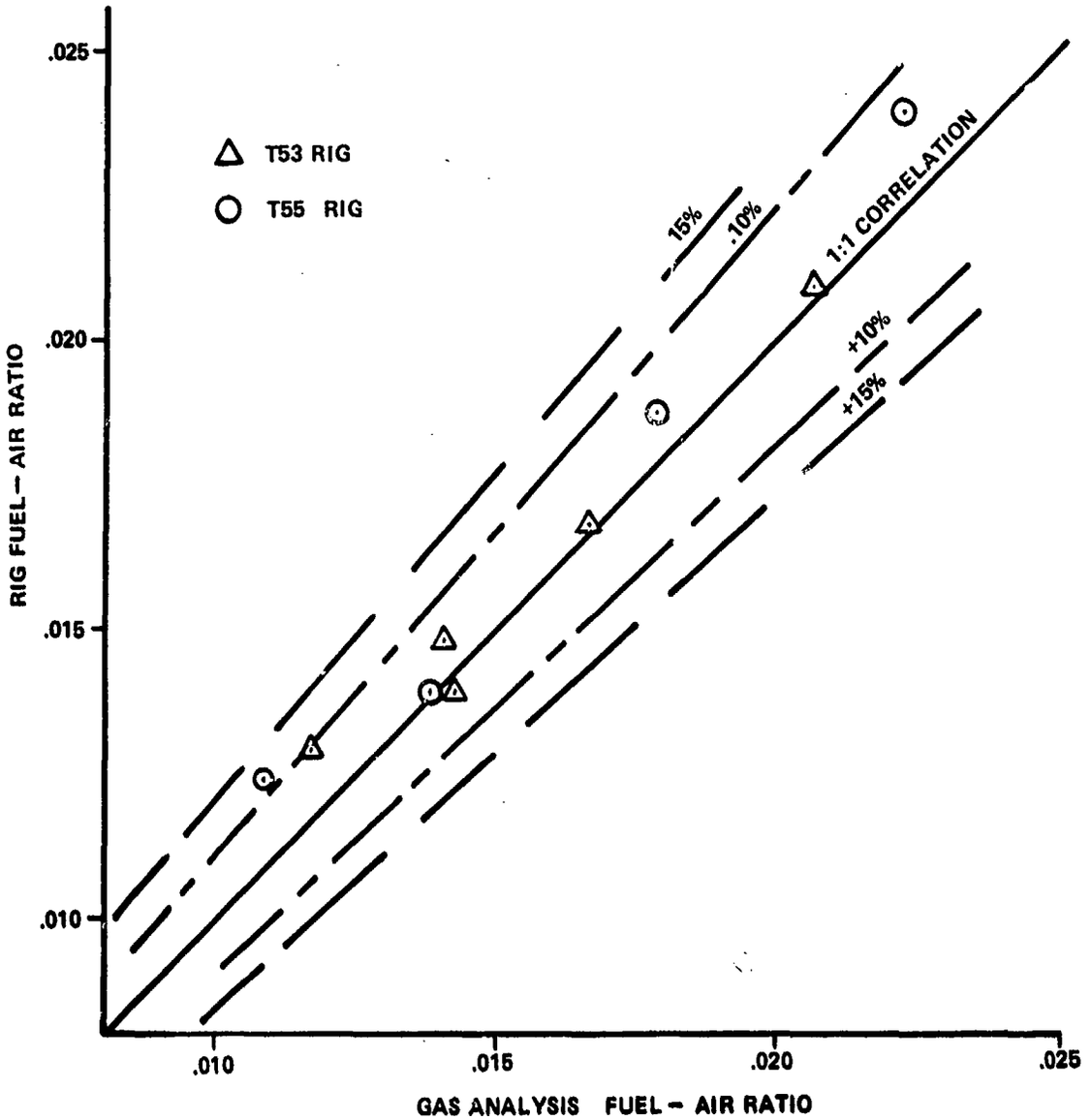

Figure 39. Correlation of Rig Fuel-Air Ratio With Gas Analysis Fuel-Air Ratio for Laboratory T53 and T55 Combustor.

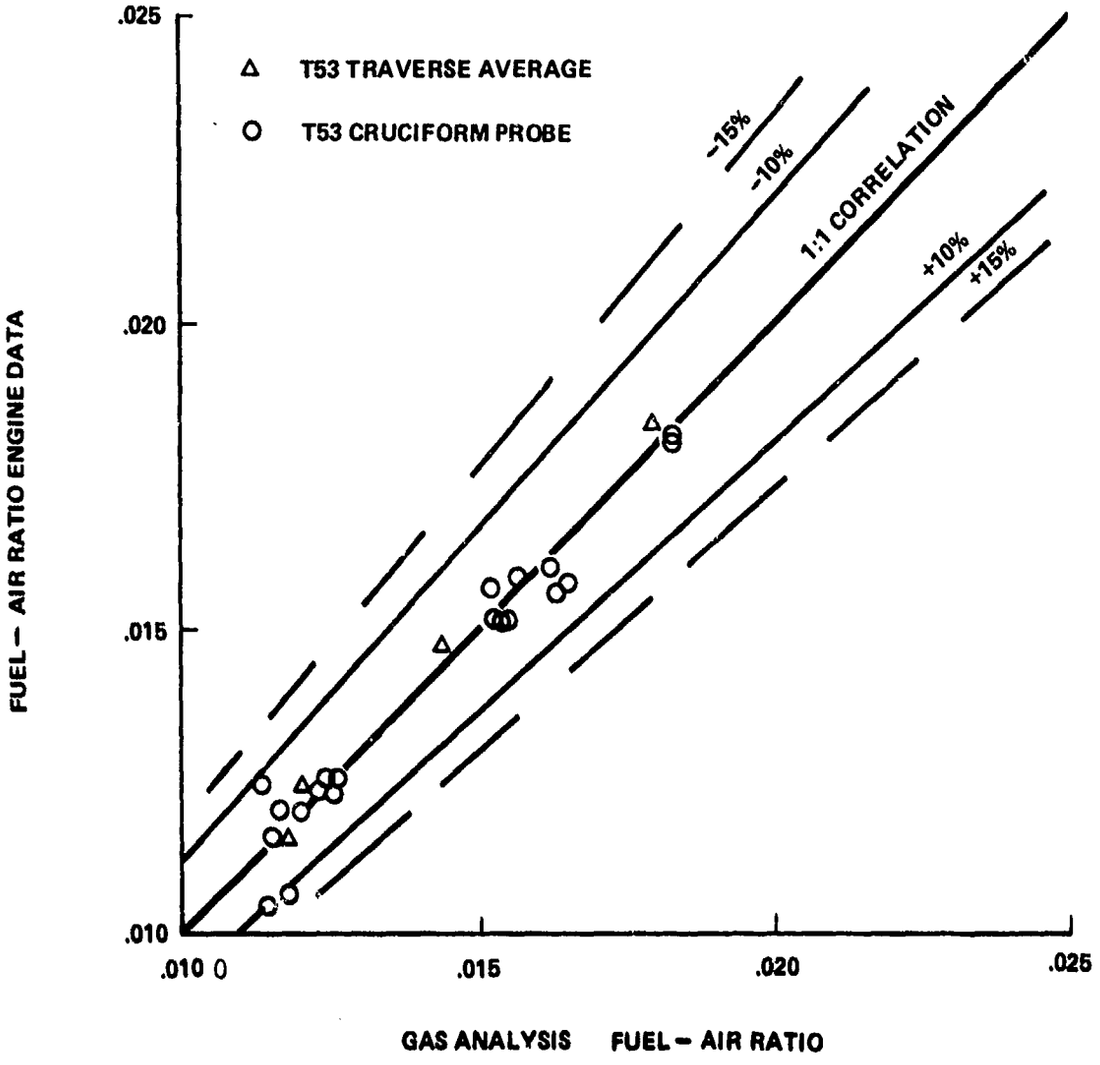

Figure 40. Correlation of T53 Engine Fuel-Air Ratio With Gas Analysis Fuel-Air Ratio for T53 Engine.

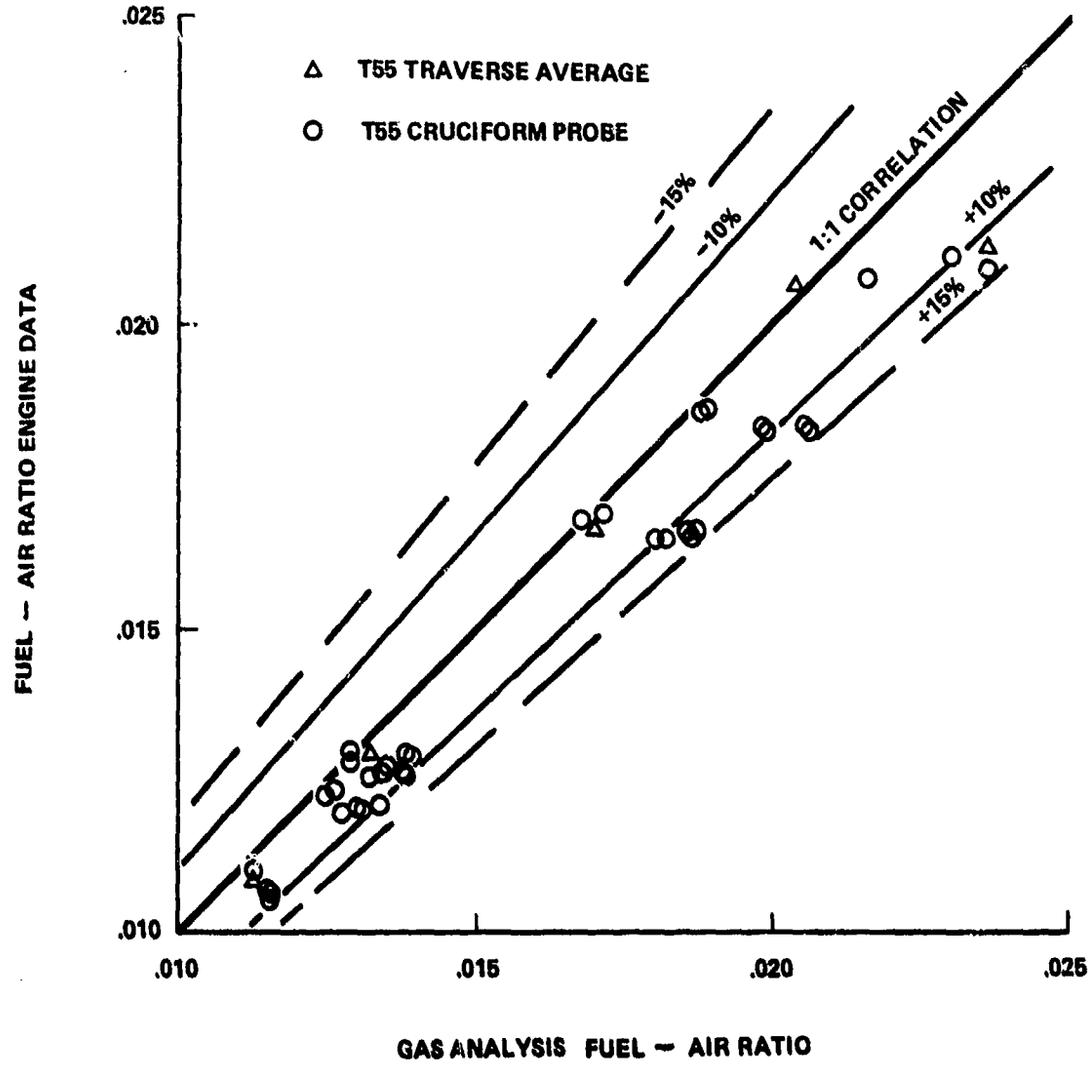

Figure 41. Correlation of T55 Engine Fuel-Air Ratio With Gas Analysis Fuel-Air Ratio.

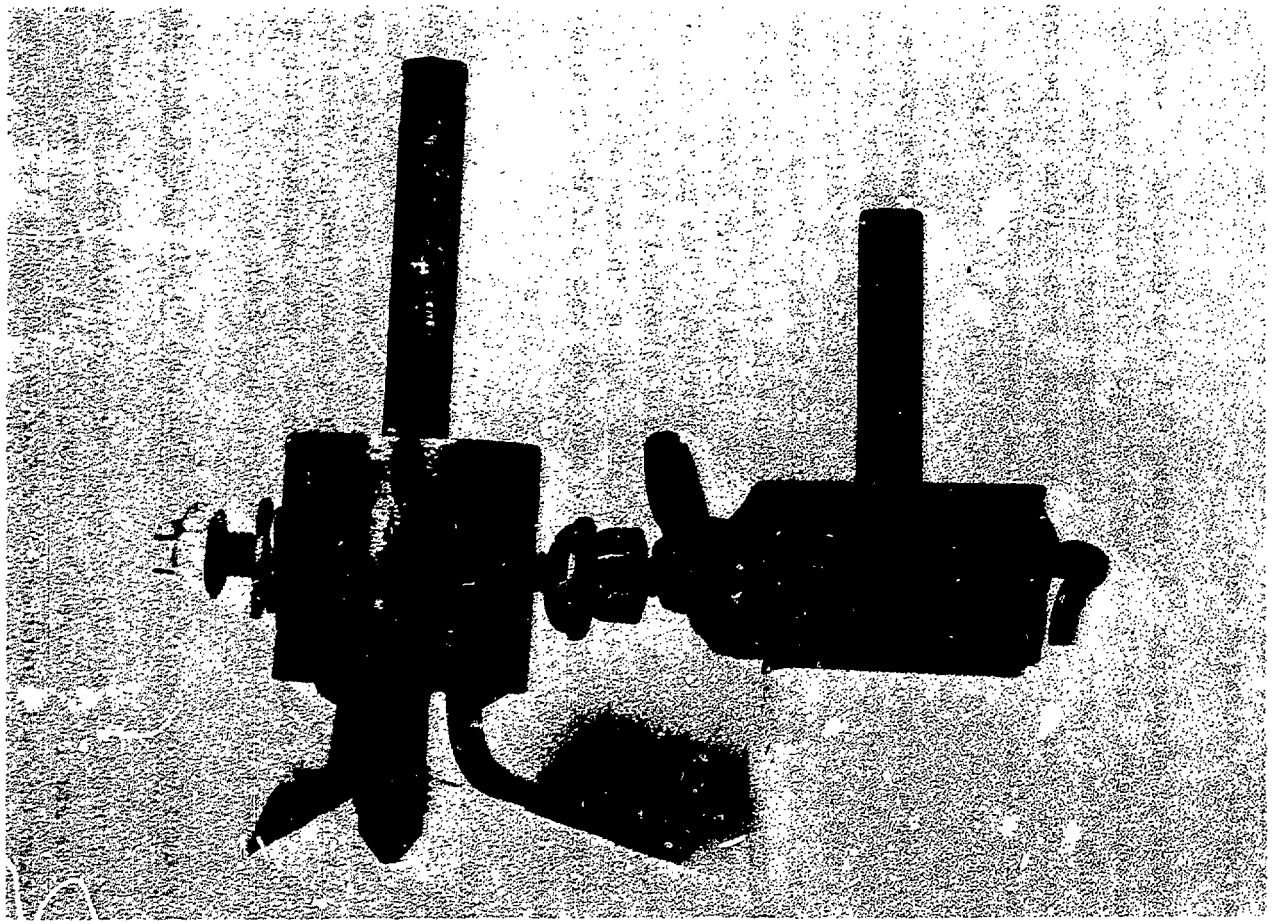

Figure 42. **Water-Cooled Movable Gas Sampling Probes for T53 and T55 Combustor Test After Test Completion. (Overheating of the T55 probe (left) caused damage to the sampling ports.)**

percent. The larger deviations of the fixed probe are caused in part by (1) the probing location, which may not be as representative as the "traverse average", and (2) the short time duration of the measurement, where reading errors cannot be "averaged out".

3. Figure 41 shows the T55 engine F/A correlations. Except for one point, the "traverse average" correlations are within 2 to 3 percent. "Cruciform-probe average" data produce consistently high F/A values, with a 10 to 12 percent band scatter. These high values cannot be explained by the shape of the exhaust concentration profile with respect to the location of points sampled by the cruciform probe. It is likely that the problem results from calibration procedure. Actual CO_2 concentrations for these points lie between 2.6 and 4.5 percent. The data with the largest differences were recorded with 1.6 percent CO_2 calibration gas, whereas the remaining data were recorded with 2.5 percent calibration gas. One "traverse average" point at high power deviated from the 1:1 line by 12 percent. This point represents a 40-point (1/2) traverse performed at a later date to fill in missing emissions data. Again, the use of a 1.6 percent calibration gas is the probable cause of the greater-than-usual deviation.

The variation of concentrations was plotted versus time to provide a graphical illustration of engine variables during a steady-state operation (Figure 43). A method of compensation for this time variable was used in order to compare concentration on a common or "normalized" basis. Variability may be caused by changes in ambient temperature and pressure, small engine control variables, and characteristics of the operator, plus human interpretation of the readings.

Effect of Exhaust Duct Sampling Probe Position on Measured Average

The data taken in this program have provided detailed exhaust traverses for two engines and two laboratory combustor rigs. From the 60-point traverses taken on each combustor or engine, we can select the type of multiport probe to obtain an average emission accuracy within a specified percent. Probe sampling type and probe location, all averages, are compared in Table V.

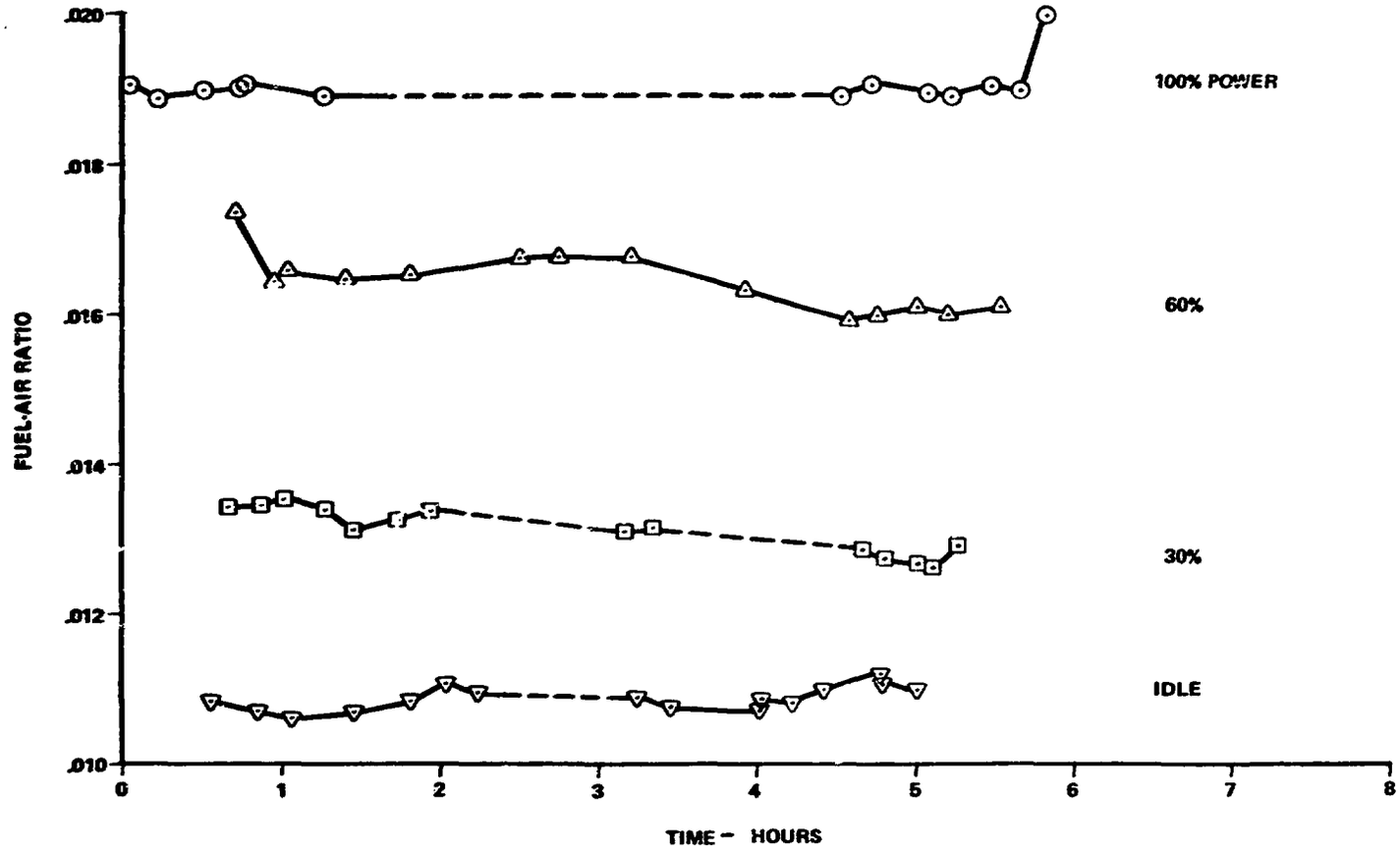

Figure 43. Fuel-Air Ratio from Gas Analysis Versus Time, T55 Center-Point Probe.

TABLE V. COMPARISON OF FUEL-AIR RATIO MEASUREMENTS FROM VARIOUS SAMPLING CONFIGURATIONS WITH COMBUSTOR RIG DATA

POINT	RIG FLOW MEASUREMENT	AVERAGING PROBE	TRAVERSE AVERAGE	INDICATED* AVERAGE PROBE	COMMENT
T55: Idle	.0125	.0116	.0109	(.0109)	40 Point Average
30%	.0139	.0130	.0142	.0138	Uneven CO
60%	.0188	.0181	.0182	.0180	**
100%	.0239	.0226	.0225	.0230	**
T53: Idle	.0131	.0132	.0119	.0127	Blocked Nozzle
30%	.0139	.0149	.0145	.0152	
60%	.0168	.0192	.0173	.0188	
100%	.0208	.0227	.0209	.0224	

* Figure obtained from traverse data using only the four points adjacent to the fixed probe location.

** Inspection of the traversing probe at the conclusion of these tests showed overheating damage which would result in a low reading from the probe.

The traverses in the engine exhaust duct provide both circumferential and radial profiles. However, slight variation in the control of the engine and ambient conditions causes shifts in measured concentrations. The changes in exhaust composition between traverse and cruciform probe tests make a direct comparison of the accuracy of the cruciform probe impractical. Even the variations observed during the course of a single traverse indicate that some of the fluctuations are spatial and some are a function of time. The diametral profiles show some random variations which may be more representative of the time at which the point was taken rather than the position of the probe. At higher power levels, where emissions tend to be steadier, many of the profiles show a clear radial variation which corresponds to the hub to tip temperature profile built into the combustor.

Effect of Precision on Emissions Measurement and Determination

The effect of gas analysis on F/A can be determined from Equations 2, 3, and 4. The predominant effect is the CO_2 concentration, normally one of the most reliable measurements. Errors in F/A are nearly directly proportional to errors in the CO_2 measurement*. The terms "a" and "b" are normally quite small, as is CO and $CH_{m/n}$, compared to CO_2. By using an approximate value of $m/n = 2$ and setting $a = b = \emptyset$, equivalence ratio ($\emptyset$) can be calculated:

$$\emptyset \cong \frac{4.77\ (1.5)}{1/(CO + CO_2 + CH_{m/n}) + m/4n}$$

or

$$\emptyset \cong \frac{7}{1/CO_2 + 0.5} = \frac{7\ CO_2}{1 + .5\ CO_2}$$

It can be seen from this equation that a 10 percent error in CO_2 will have an effect of about 10 percent on $\emptyset$ and F/A. *

*Leak checks were made periodically during the tests by changing the sample line pressure. Any substantial change in concentrations would indicate a change in leak rate, if a leak existed.

With the foregoing considerations of accuracy and precision, we may conclude that ±10 percent is a conservative estimate of accuracy that can be expected for most cases, and with careful work. It is obvious that much better precision than this is possible, and also that 10 percent may be too low when measuring low concentrations. An error analysis is shown in Table IV. Here a small error is a large percentage, and it may be asking too much of any instrument to measure reliably anything closer than ±5 ppm for CO or HC and ±5 to 10 ppm for NO. The principal question is, "How does this relatively easily obtained 10% precision affect the determination of emission measurements?" If we examine the objective of "measuring and reducing pollutants" in perspective, we find that the real objectives are:

1. Determining the quantity of pollutants within a reasonable accuracy

2. Reducing the pollutants by a large amount (Reference 33)

In view of the present EPA proposed requirement of reductions of the order of 90 percent of some pollutants, the ±10 percent in emission measuring accuracy is judged to be "reasonable". It may also be pointed out that in measurements in the exhausts of many engines, as reported in Reference 4, the variations in measurements obtained by different agencies on the same model engine are considerably greater than 10 percent.

Therefore, the specification of EPA (Reference 33) that precision of measurement be set at ±1 to 2 percent appears difficult, and may not be necessary in order to meet measurement objectives. The percentages specified appear to be instrument manufacturer's specifications under ideal conditions, for full-scale deflection only, and for calibration gases with zero error. A more realistic calibration and precision determination should be established by setting standards for calibration and supplying known sample mixtures to users to determine their instrument precision. The efforts of the National Bureau of Standards, or other agencies, would be needed for this procedure.

Comparison of T53 and T55 Test Engine Performance With a Statistical Group Performance

Because this program of emission testing of T53 and T55 engines was

limited to one engine only of each type, it was considered important to analyze the performance of each engine and determine whether it was typical of performance for that engine model.

Test engines used in the exhaust emissions program were chosen from Lycoming's "house engine" resources based on considerations of configuration and availability. A performance analysis was made to establish these engines as representative of a group of engines by comparing their performance with production engine performance available from an extensive data bank. The data bank includes statistical treatment of data to estimate sample population limits on various performance parameters. This comparison is made to ensure that both rig and engine combustor inlet parameters are representative of typical engine operation, particularly as regards possible extraneous combustor bypass airflow caused by overboard leakage, or by nontypical internal cooling and/or seal pressurization flows.

T53-L-13 Engine K-121J

Performance data from T53-L-13A engine K-121J taken during initial checkout and emission testing are shown in Figures 44 and 45 for comparison with performance of over 7400 T53-L-13 engines. "Time since new" (TSN) on this engine prior to test was approximately 140 hours. The tolerance band shown is derived from statistical analysis of this engine population by utilizing computer curve fitting techniques and conventional data reduction practice to normalize data to "standard day" conditions. Available data are limited to the power levels required for production acceptance of the engine; i.e., 75 percent normal rated power to military rated power. The range of the data is sufficient to indicate the K-121J is not untypical of T53 engine performance in the high power (interstage bleed closed regime) with respect to level and slope of the aerothermodynamic parameters. A review of the buildup records of the engine and visual examination of hardware, combined with the measured performance, support a conclusion that engine internal airflows and leakage are within acceptable limits.

Data in the ground and flight idle regime from a sample of 15 T53-L-13 engines are shown in Figures 46 and 47 for comparison with K-121J performance; they indicate typical part-speed interstage bleed-opened operation. Flight idle operation is specified

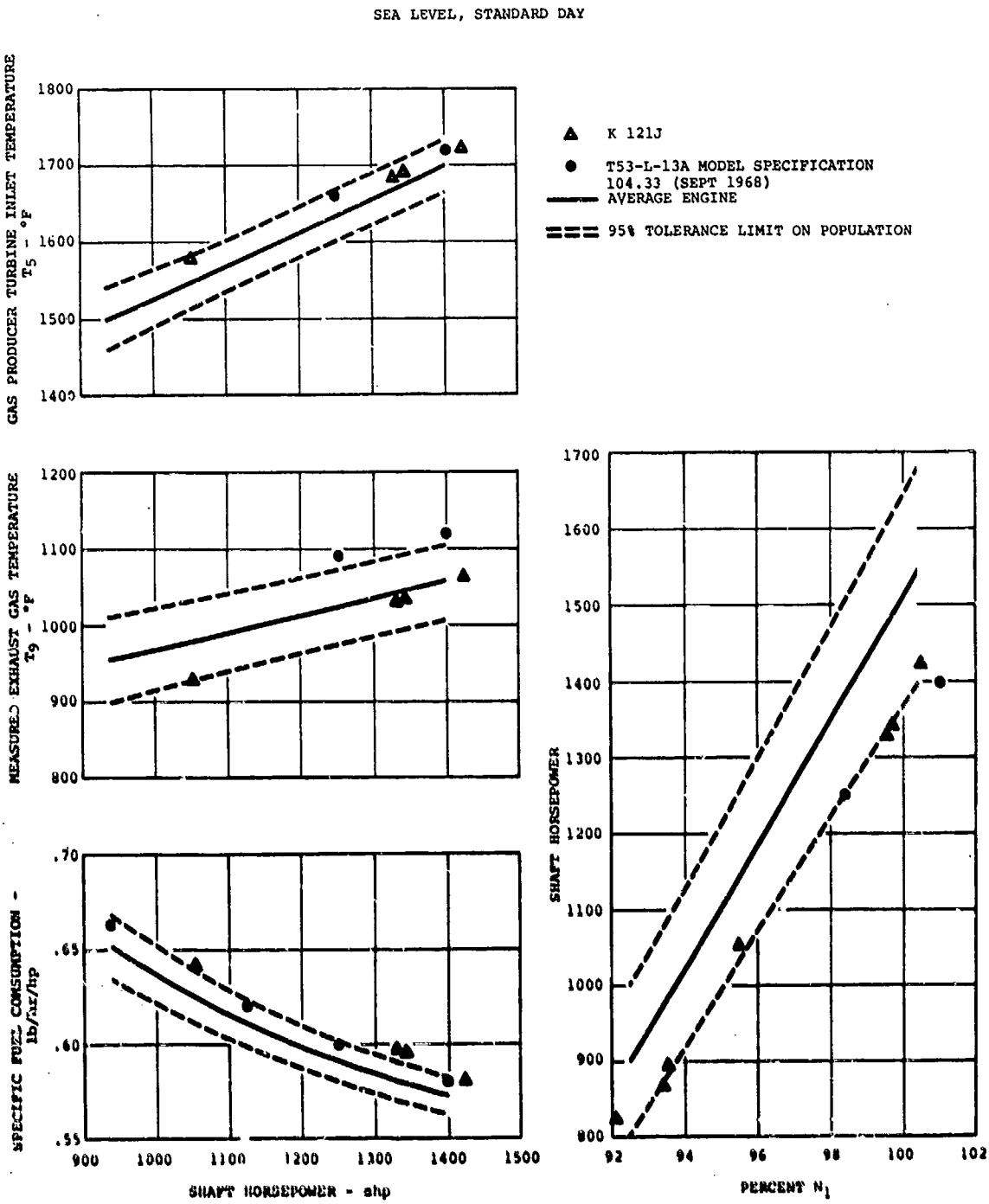

Figure 44. T53-L-13 Engine K-121J Performance Comparison With 7400-Engine Sample.

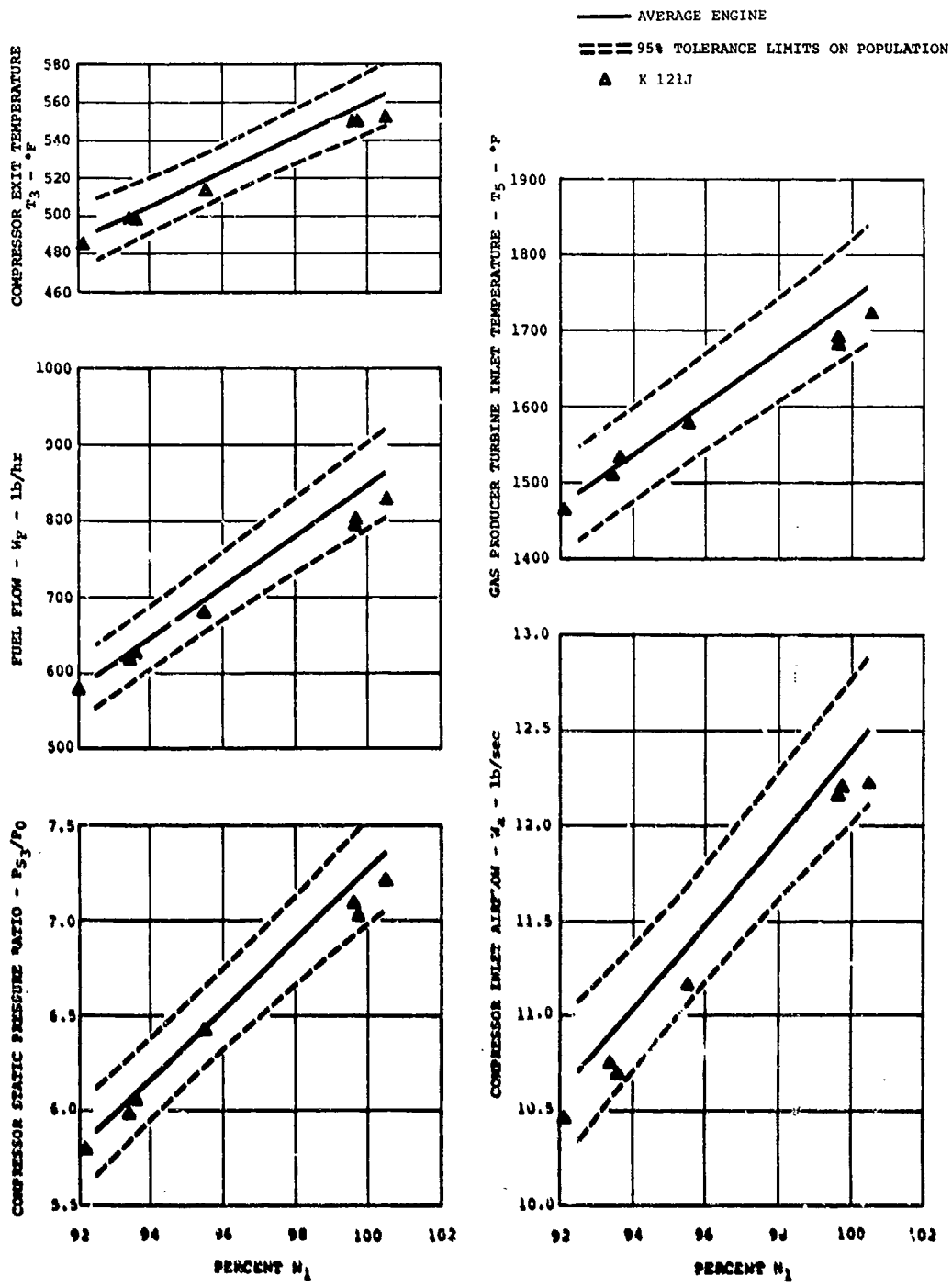

Figure 45. T53-L-13 Engine K-121J Performance Comparison With 7400-Engine Sample

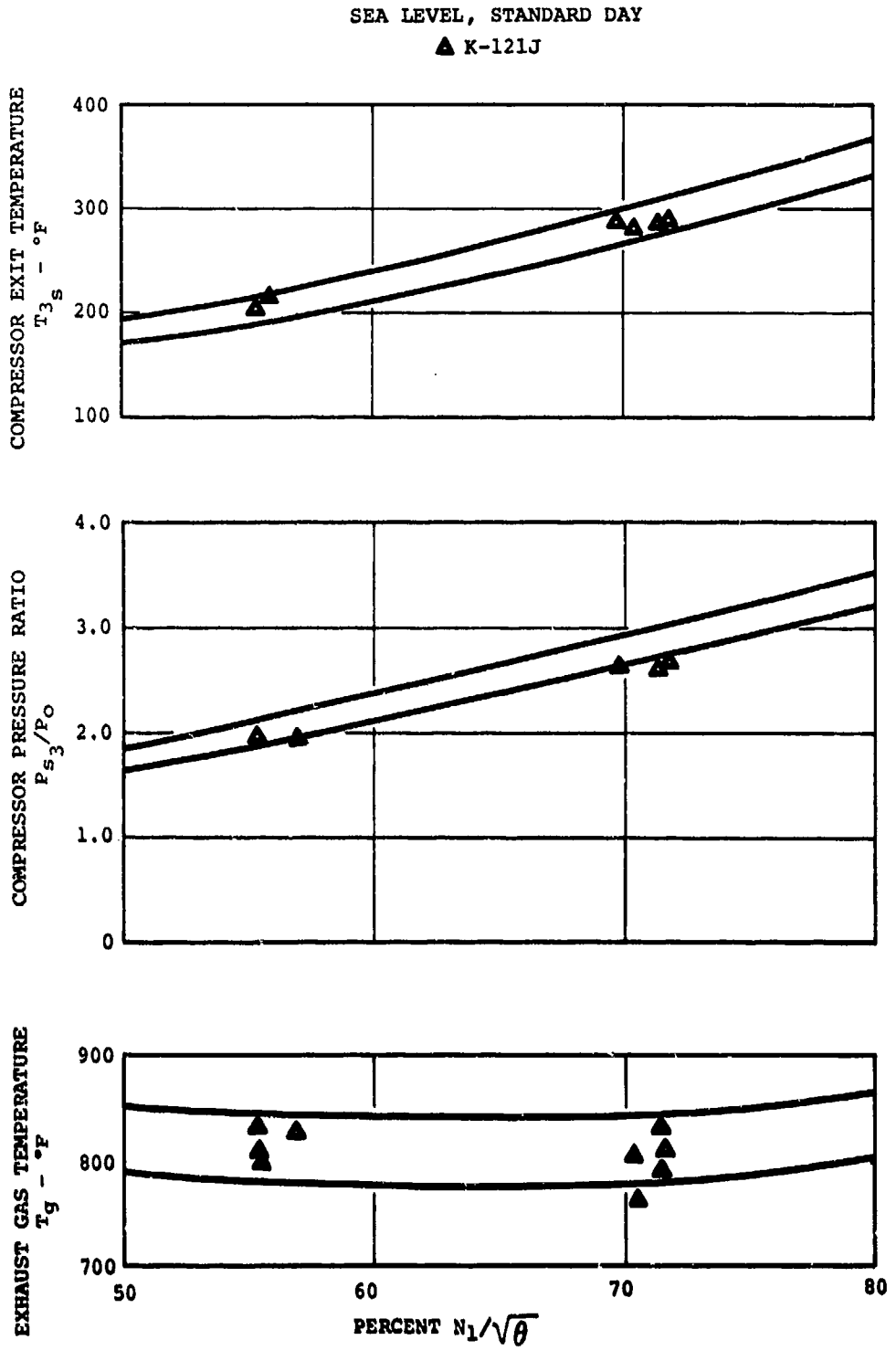

Figure 46. T53-L-13 Engine K-121J Low Power Performance Comparison With 15-Engine Sample.

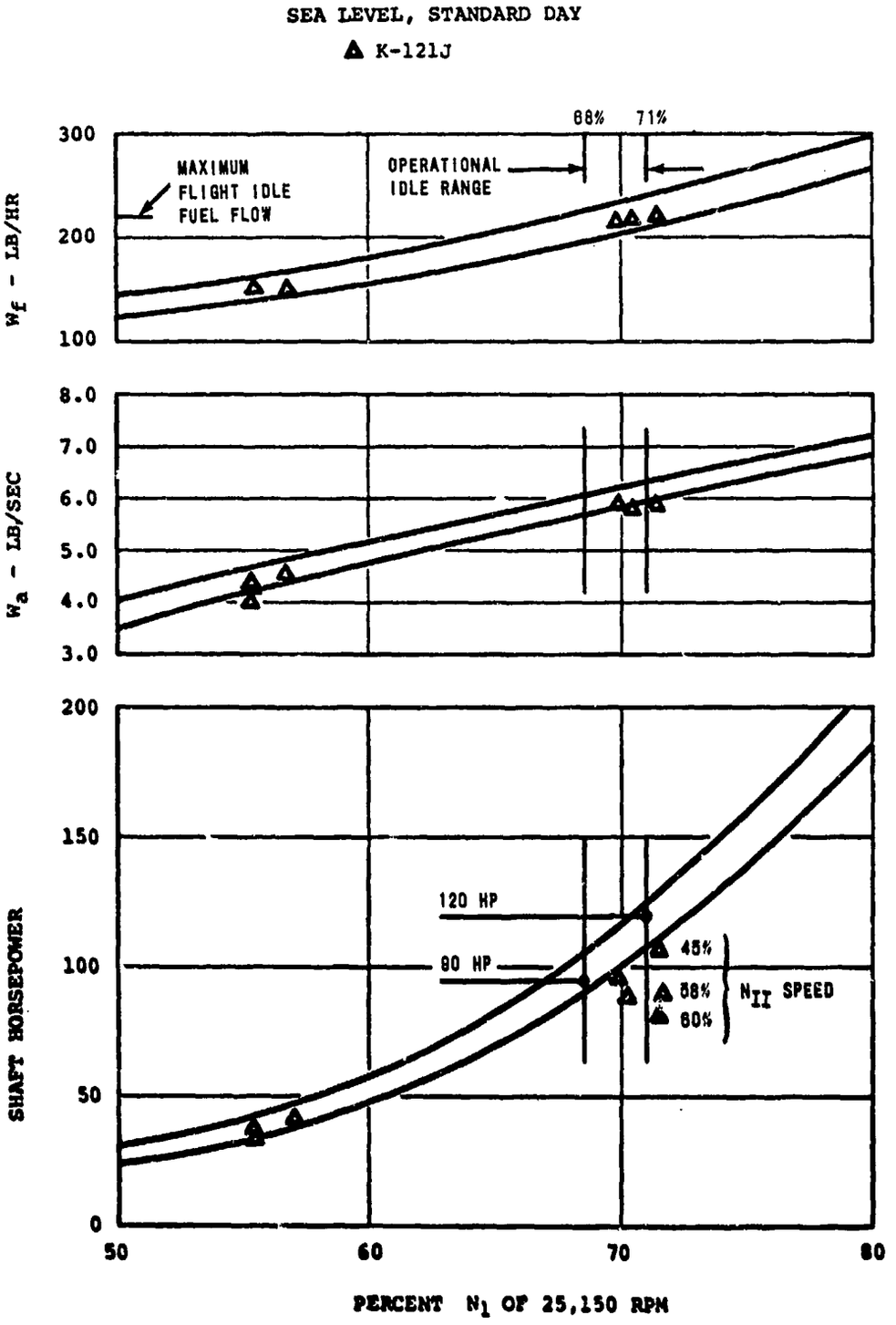

Figure 47. T53-L-13 Engine K-121J Low Power Performance Comparison With 15-Engine Sample.

at a maximum fuel flow of 220 lb/hr, corresponding to a gas producer speed of approximately 71 percent for engine K-121J. Power under this condition may vary from zero, at twice optimum free power turbine speed (approximately 80 percent), to a maximum of approximately 120 horsepower, when the power turbine is running at optimum speed (approximately 40 percent). Based on input from Lycoming's flight test and field service operations, the T53-L-13 engine, as used in the Bell UH-1 aircraft, utilizes the preceding "flight idle" setting as "operational idle" for ground running prior to lift-off. The relationship between free power turbine speed and output power, at constant gas generator speed, is shown in Figure 47, where optimum free turbine speed was maintained for the 15-engine sample.

T55-L-11A Engine B-19Q

Data from T55-L-11A engine B-19Q are compared with T55-L-11 production engine population limits in Figures 48 and 49, and indicate acceptable limits of performance, with all aerothermodynamic parameters within normal values. The engine had acquired approximately 235 hours TSN. The T55-L-11A engine incorporates modifications to the hot-end; this resulted in minor changes to the T55-L-11 model specification as indicated by the acceptance limits per MCR 2108, dated 21 September 1972.

Low-speed, interstage bleed-open data from a sample of T55-L-11A engines (Figures 50 and 51), when compared with B-19Q performance, indicate that bleed and turbine cooling airflows are within acceptable limits. Flight idle operation is specified at a maximum fuel flow of 505 lb/hr for the T53-L-11A, which would correspond to a gas generator speed of approximately 70 percent compressor speed for engine B-19Q. Power turbine speed was set close to optimum values for this test series, as can be seen in Figure 51.

"Operational idle" as applied to the Vertol CH-47C is set at approximately 82 percent compressor speed (slightly above the interstage bleed steady-state closure point). Data from B-19Q at this condition are shown in Figures 50 and 51. This compressor speed meets the engine-airframe systems integration requirements.

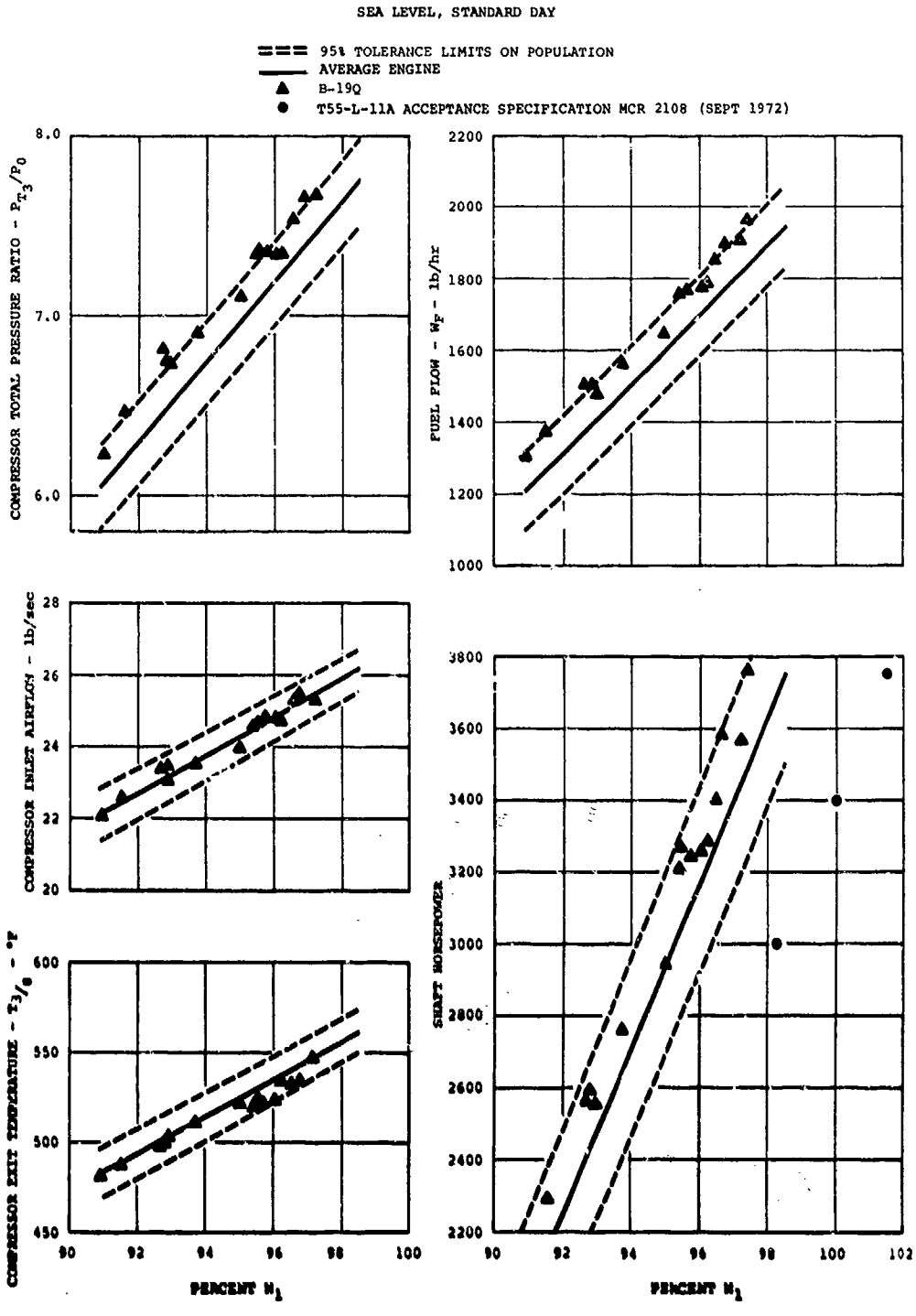

Figure 48. T55-L-11A Engine B-19Q Performance Comparison With 493-Engine Sample.

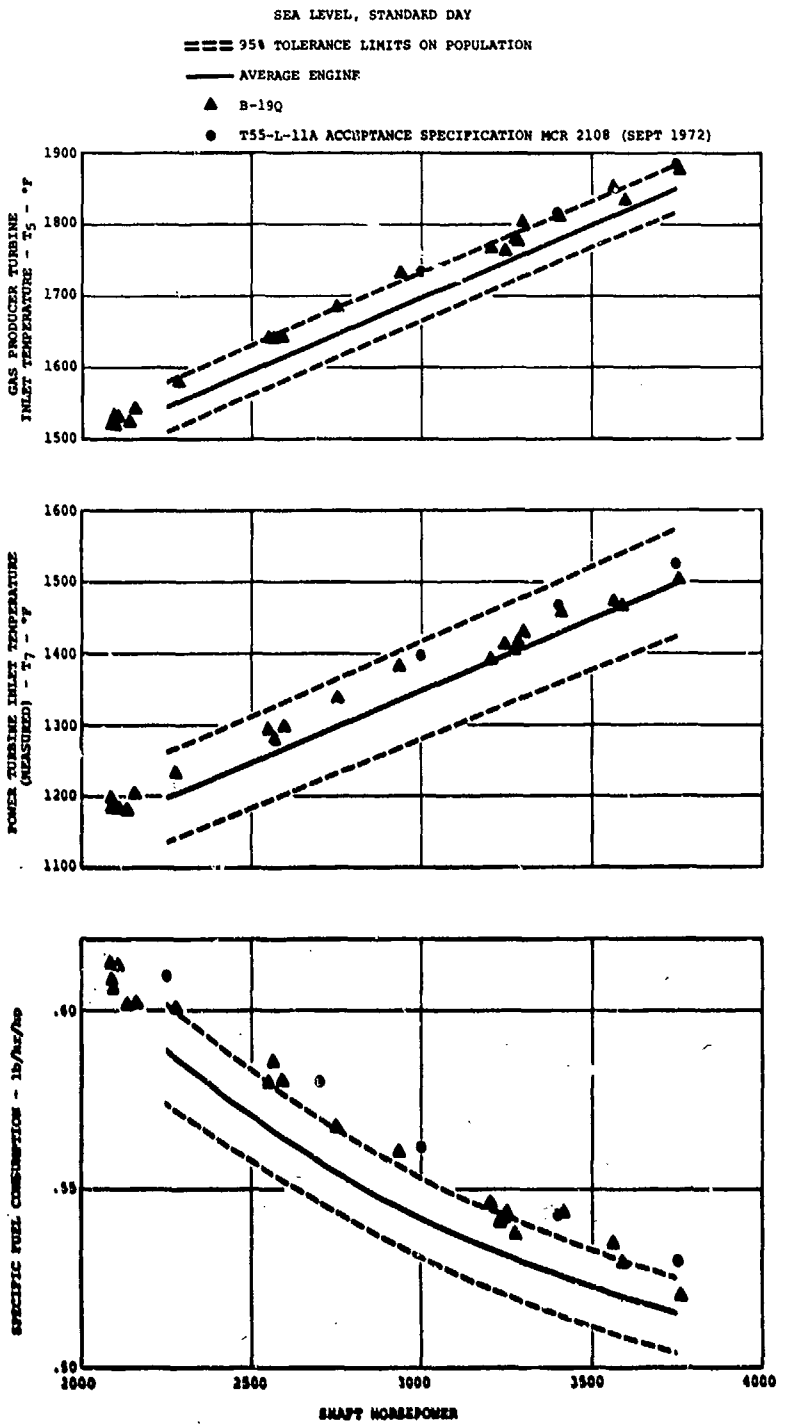

Figure 49. T55-L-11A Engine B-19Q Performance Comparison With 493-Engine Sample.

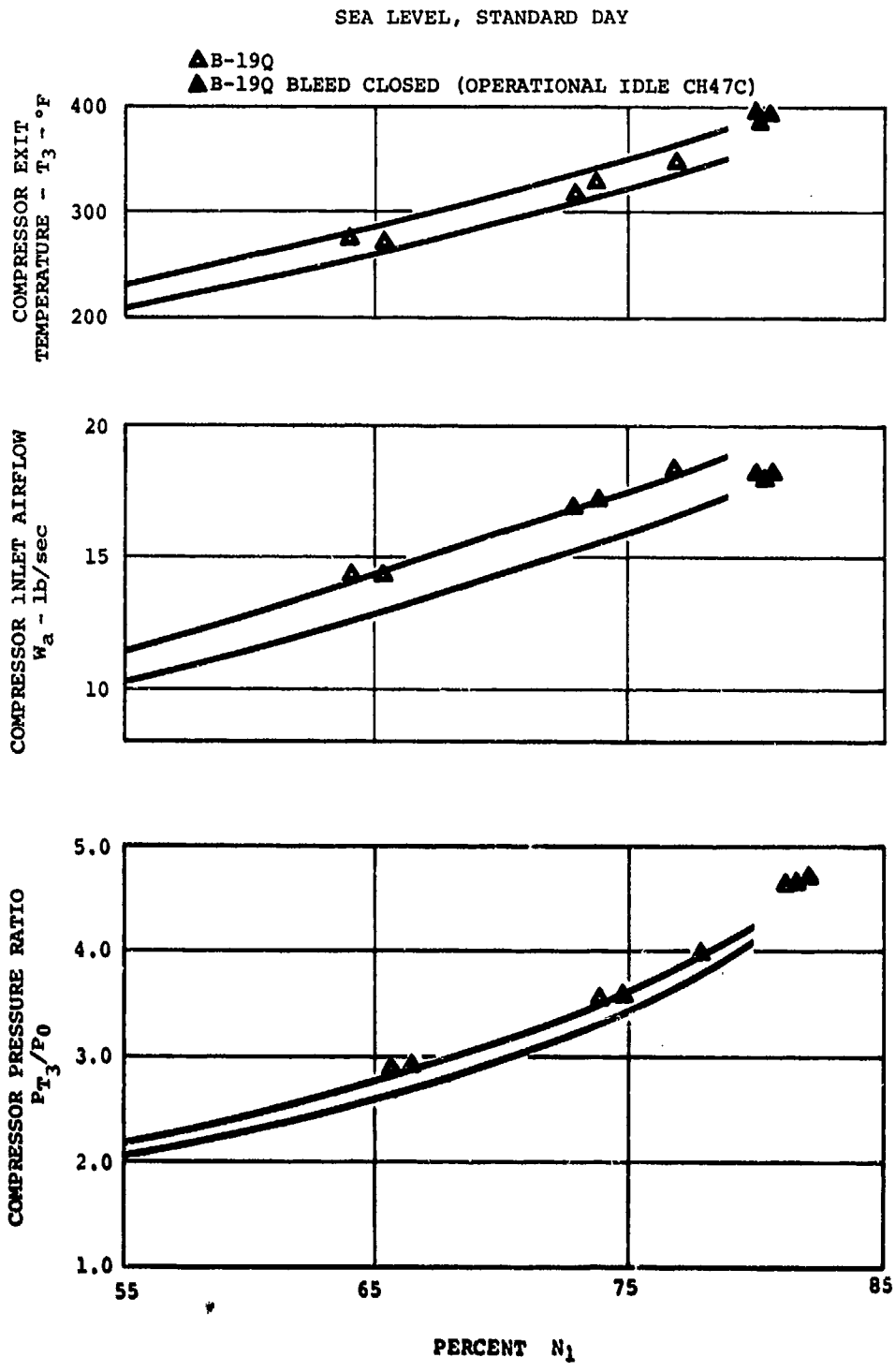

Figure 50. T55-L-11A Engine B-19A Performance Comparison With 5-Engine Sample.

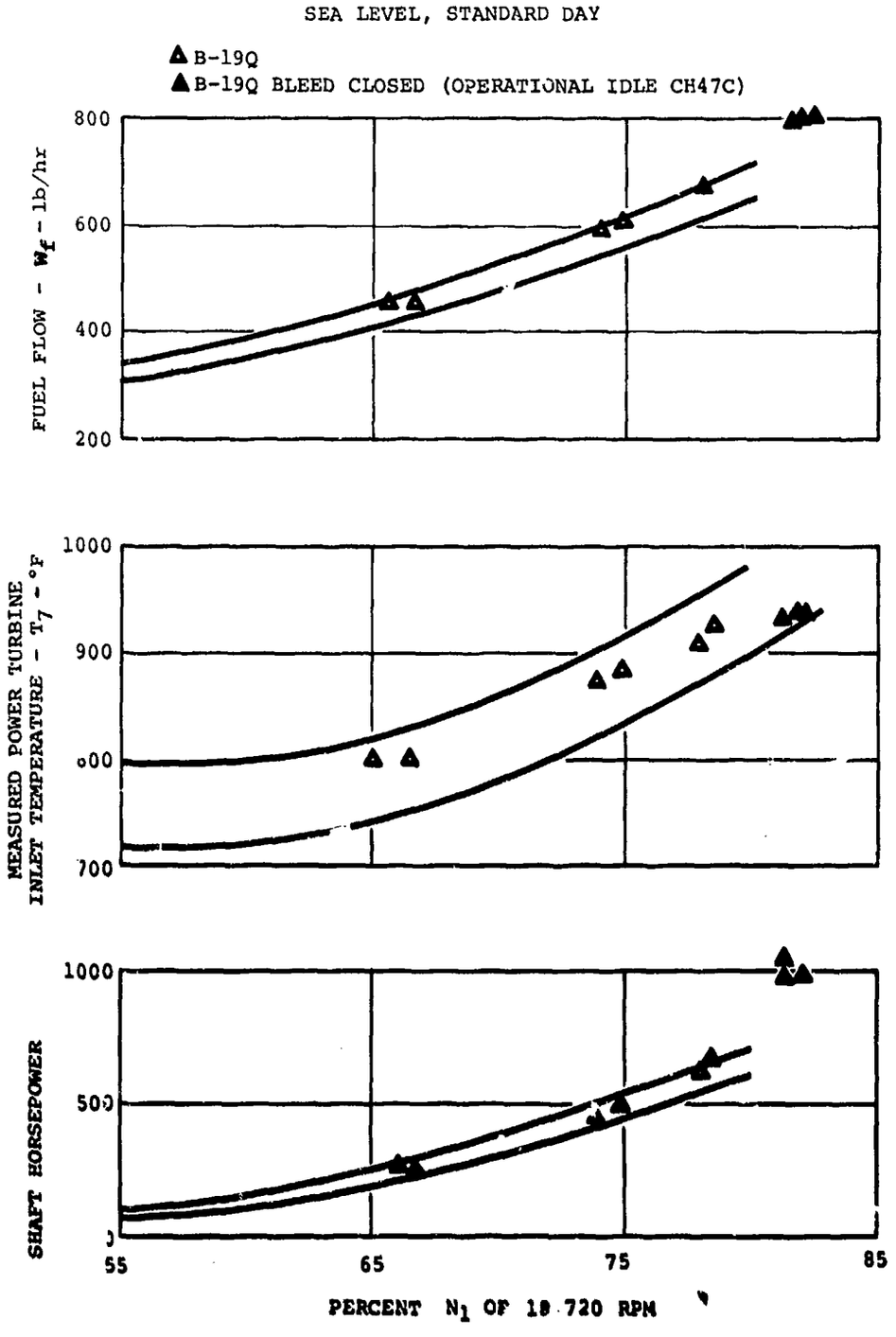

Figure 51. T55-L-11A Engine B-19A Performance Comparison With 5-Engine Sample.

Conclusion

Both engines selected for these emission tests meet their specific performance requirements. "Operational idle" used in the aircraft application should be the idle used for reporting emissions. The power used to describe this condition should be assumed to be optimum N_{II} rather than the measured power resulting from real N_{II} used in the aircraft. Combustor operating conditions are the same in both cases.

TEST RESULTS

The data will be discussed in groupings to better correlate the results, in this order for each engine:

1. Combustor results
2. Engine results
3. A comparison of combustor and engine data
4. Comparison of Lycoming and Navy data
5. Other comparisons

T53 Combustor Results

The combustor tests were performed to simulate engine operating conditions as closely as possible, but, obviously, there are limitations. Known differences between engine and laboratory combustor operation are:

1. Turbulence level and velocity profiles that enter the combustor from the compressor
2. Pressure level in cases where combustor pressure was not exactly duplicated
3. Effect of the first turbine nozzle
4. Compressor interstage bleed and turbine cooling air bypass, which was allowed for in setting the test point.

The bleed air quantities were included in calculations. Turbulence factors, however, were not included, but are not known to be of significance. Pressure level effects were found to be negligible. The effect of the first turbine nozzle was not determined.

In some cases, the engine combustor operating pressure could not be reached in the laboratory combustor because of facility limitations.

The T53 combustor data consist of:

1. Combustor test rig operating data (fuel, air, etc.)
2. Averaging probe gas sample data
3. Traversing probe gas sample data

The combustor was operated at conditions simulating idle to full power as shown on Table I. During the 60-point probe traversing operations, averaging probe data were recorded after each 10 or 15 points. The gaseous components output was converted to ppm and Emission Index (EI, lb/1000 lb fuel). A plot of CO, hydrocarbons (HC), NO, and NO_x as a function of F/A is shown in Figure 52. Some observations from these data are:

1. Trends of HC and CO are as expected, with large decreases as simulation of high power is approached.

2. NO and NO_x increases as expected as simulated power increases

3. The difference in idle F/A seen by the traverse average and the four-point averaging probes can be traced directly to the location of the four averaging probes. By selectively averaging traverse probe data for locations identical to the fixed probes only, identical F/A's were obtained.

Concurrent with the 60-point gas analysis profiles in the combustor exit (6-degree rotation angle interval), temperature profiles were recorded with 5 thermocouples, spaced as shown in Figure 9. If we assume that combustion efficiency is constant around the combustor, then average thermocouple temperature at a point on the combustor circumference should be proportional to average fuel-air ratio from the gas analysis. This is exactly what happens. Results of tests at simulated idle, 30, 60, and 100 percent of full power are shown in Figures 53 through 56, respectively. The significance of the close correlation between the two plots is that two entirely different types of measurement produce very similar results. The absolute thermocouple temperature measurement is low because of radiation and conduction losses, but the perturbations of temperature in traversing the circuit are valid.

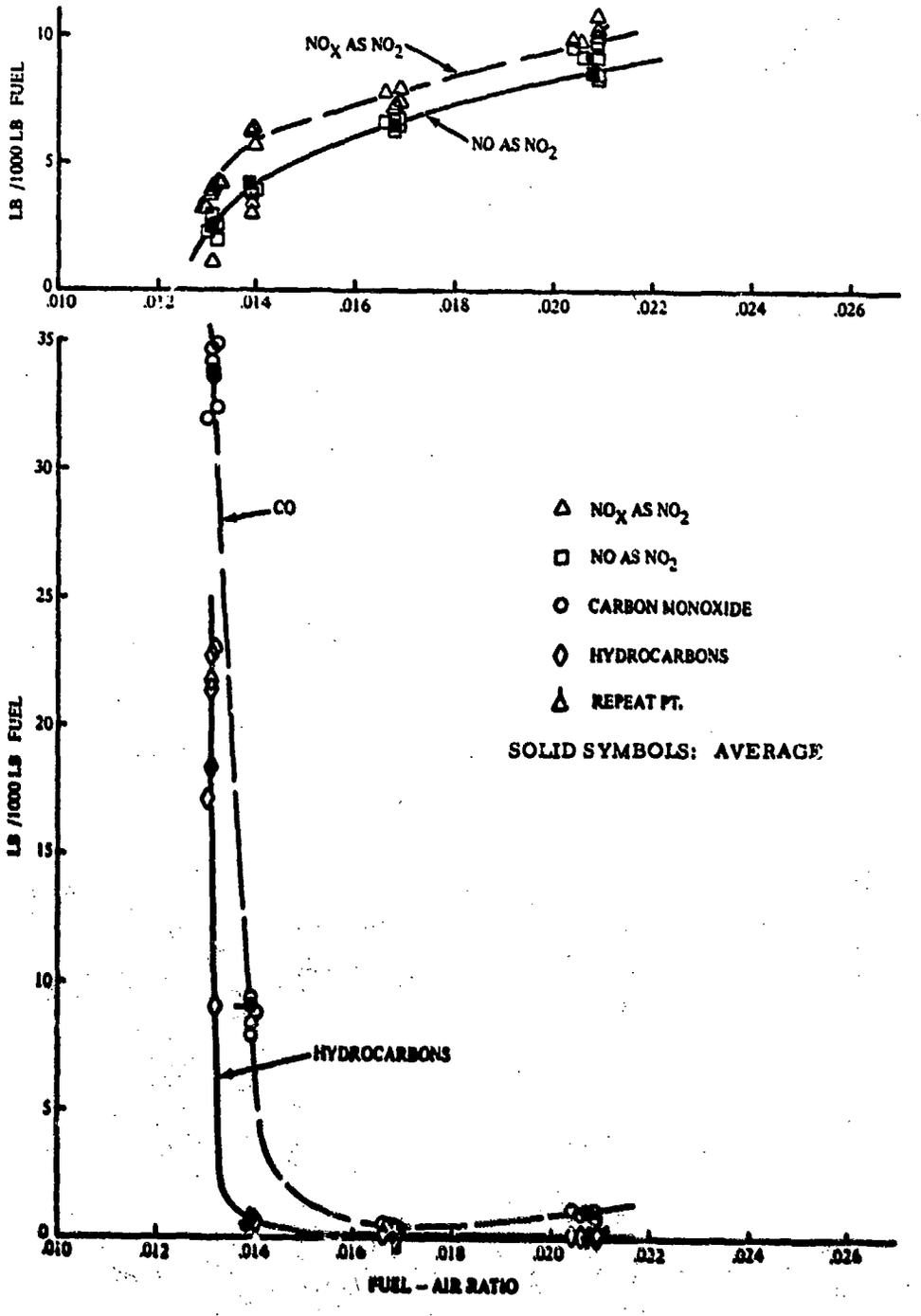

Figure 52. T53 Combustor Rig Emissions Versus Fuel-Air Ratio (Cruciform Probe).

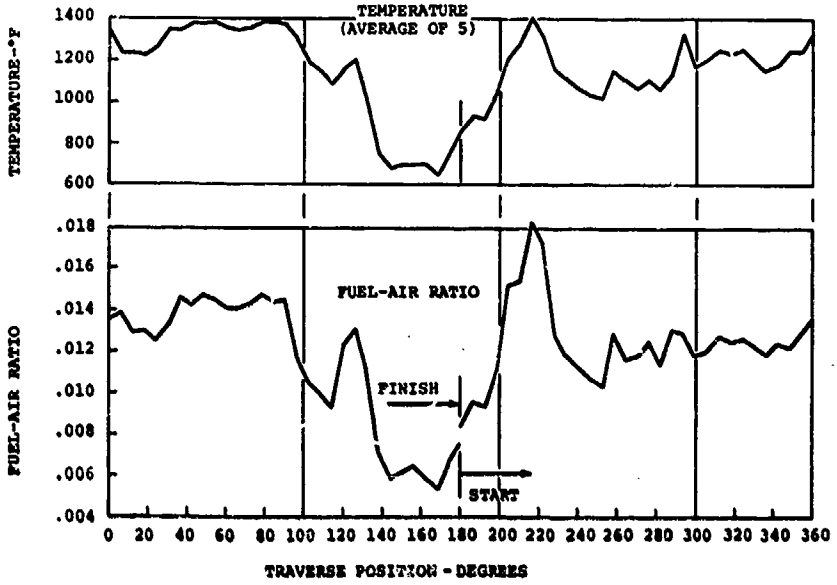

Figure 53. Comparison of Average Traverse Temperature and Fuel-Air Ratio From Gas Analysis - T53-L-13 Rig Simulation of Idle.

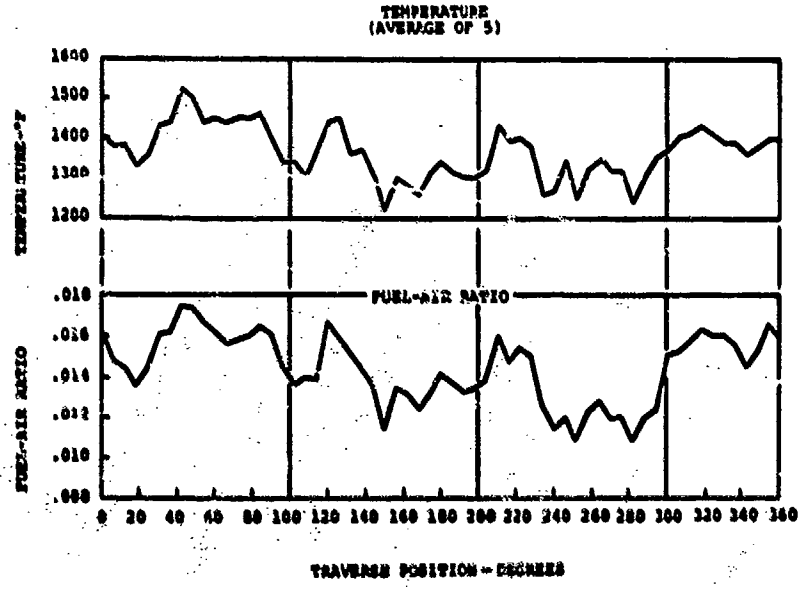

Figure 54. Comparison of Average Traverse Temperature and Fuel-Air Ratio for Gas Analysis - T53-L-13 Rig Simulation of 30 Percent Power.

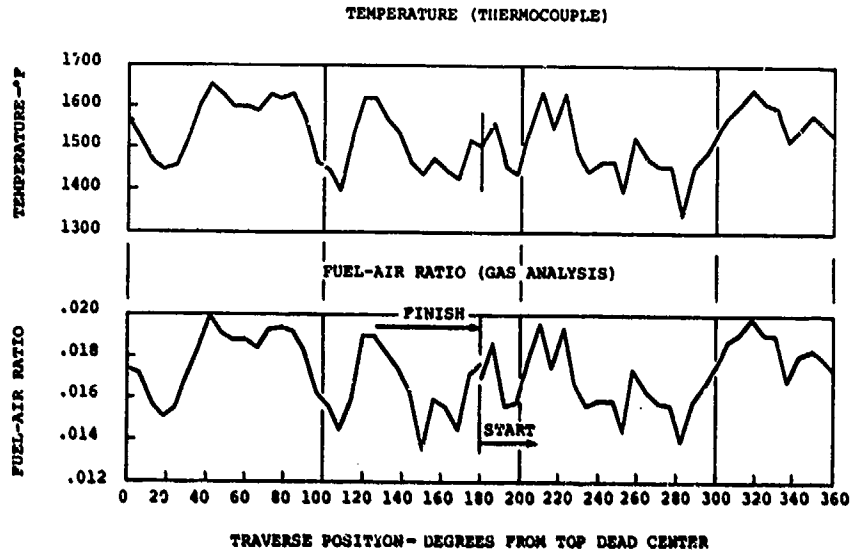

Figure 55. T53-L-13 Rig Simulation of 60 Percent Power.

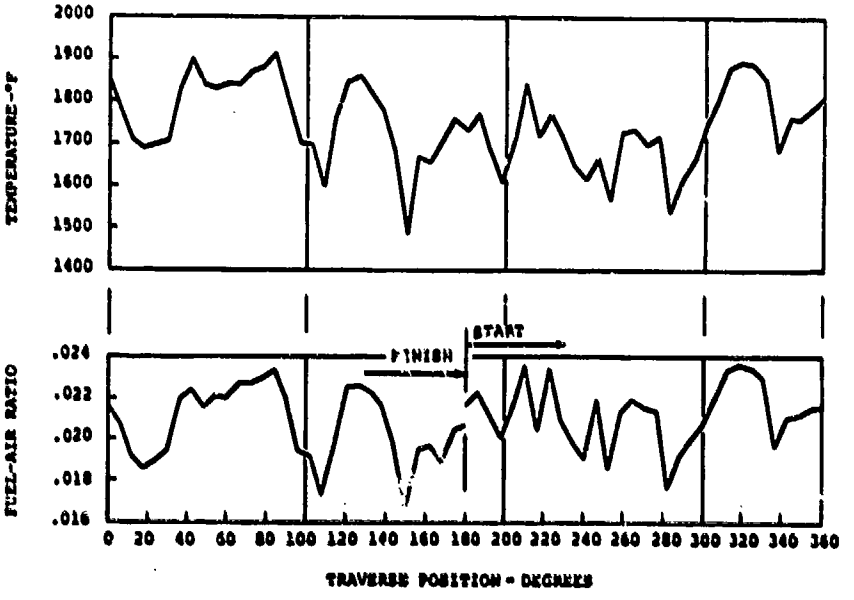

Figure 56. T53-L-13 Rig Simulation of 100 Percent Power.

The "cold" spot in the combustor exit for "idle" power (Figure 53) was found to correlate precisely with a lack of fuel in that area. This was later found to be caused by malfunctioning fuel nozzles.

The level of concentrations of each pollutant has been measured in the T53 combustor with good precision and repeatability.

A complete set of detailed concentration plots of the T53 laboratory rig traverse data recorded at 6-degree intervals is presented in Appendix II. The preceding comparison in this report shows the close correspondence between the F/A profile and the temperature profile.

Other aspects of the traverse data from Appendix II which can be utilized for improvement of combustor design are:

1. If one compares the F/A traces of the T53 with those of the T55 (Appendix IV), a significant difference appears. At idle, both show large random variations due to the poor mixing which is characteristic of low-pressure operation. At the three higher power settings, the T53 traverses show larger variations than the T55, and these variations are of larger spatial extent. The T55 profile is characterized by sharp, short fluctuations that diminish as the simulated power level increases, while the large, smooth variations of the T53 do not vanish at high power. This indicates that the large scale (or circumferential) stirring of the T55 is superior to the T53.

2. A comparison of the T53 F/A traverse at the 30, 60, and 100 percent power levels shows that most of the characteristics of the traverse carry through from one simulated power setting to the next. This is also true of the NO and NO_x profiles. At the higher power settings, the incompletely reacted species (CO and HC) tend to vanish, and the profiles lose meaning. Hence, the only similarity that carries through is for the CO between 30 and 60 percent.

3. Comparative study of the EI and ppm plots for CO, HC, NO, and NO_x will show that the EI plots are considerably smoother than ppm. Since the EI is the ratio of pollutant to fuel-air ratio, this smoothing means that each of these

pollutants is partially proportional to fuel-air ratio. One would expect this for NO_x, but the fact that it is also true for HC and CO must mean that the primary zone is on the rich side and that the richer regions tend to be quenched before combustion is completed.

4. The correspondence in detail of the NO_x profile to the F/A profile is so strong that one could infer the shape of the NO_x profile from a simple temperature traverse. While there is some coupling between the HC and CO and the F/A, the relative magnitude of the fluctuations is very different and the form of the profile could not be determined from a temperature traverse. However, there is a correspondence between CO and HC. As combustion efficiency increases, both CO and HC decrease, with CO decreasing at a slower rate than HC. The trends are similar to those shown in Reference 8, and the ratio of CO/HC is a function of combustion efficiency and combustor style.

T53 Engine Data and Results

T53 engine data consist of:

1. Engine operating performance data (fuel flow, airflow, etc.)

2. Cruciform (averaging) probe exhaust measurements for gas composition and smoke

3. Single-point traversing probe measurements for gas composition

Engine operation performance data were recorded for each data point where the engine power was changed, as in a performance power test. For the long-term steady-state tests, during which time the single-point gas analysis probe was traversed, engine data were recorded at 15-minute intervals in order to establish that operations were steady. Engine data are listed in Reference 5.

Cruciform probe data included average CO, NO, NO_x, and hydrocarbon pollutant data, shown plotted versus percent power in Figure 57. A discontinuity is shown between "bleed open" and "bleed closed" to denote the bleed closure. The changes in pollutant concentrations are as expected. CO and hydrocarbons rise steeply at low power; NO_x

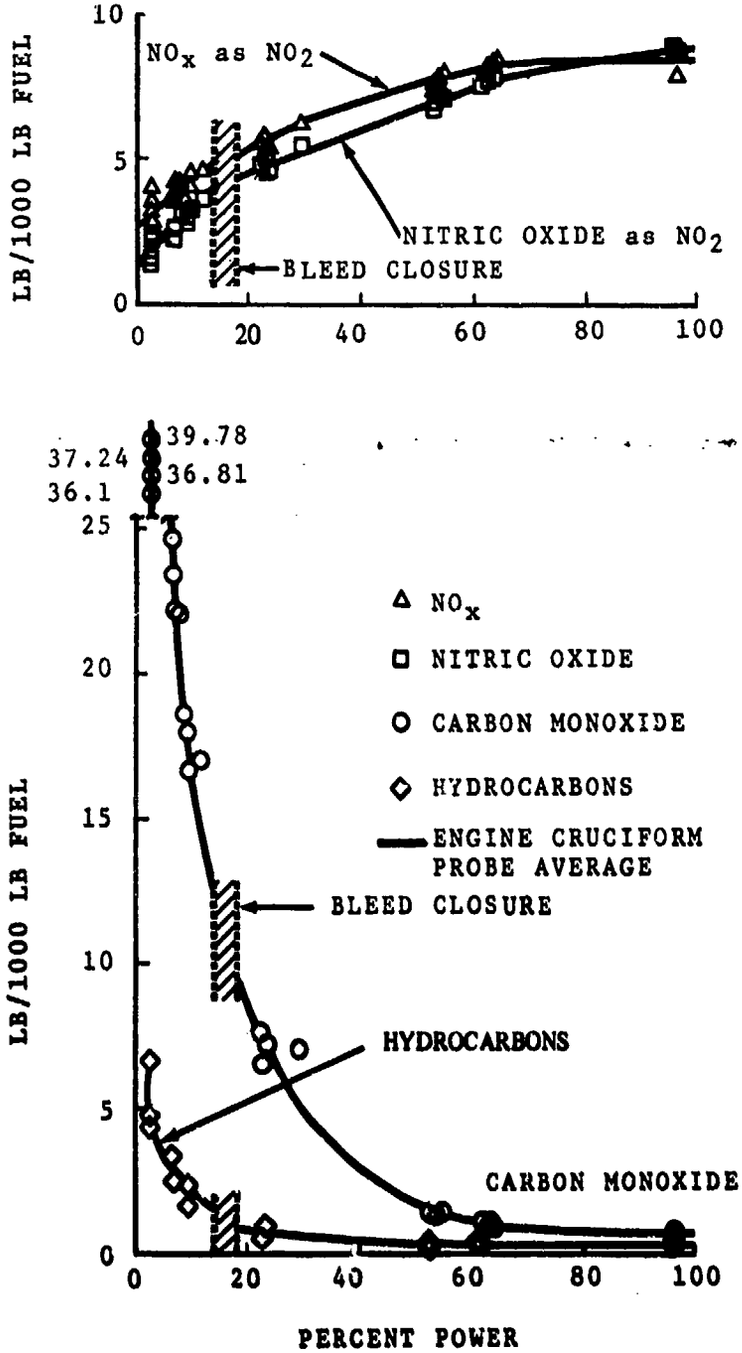

Figure 57. T53-L-13 Engine Emissions Versus Power (Cruciform Probe).

increases with increasing power. Carbon monoxide concentrations at low power are high, and are shown as a discontinuity on the upper part of the CO plot.

Single-point probe data were recorded for 73 data points (61 positions) for determining the exhaust gas profiles and correlating the results with cruciform probe data. Data were recorded at idle, 30, 60, and 100 percent of full power. The average of the single-point concentrations and the cruciform probe data are compared in Figure 58.

The single-point probe data were used to plot the concentration gradients on three diameters for NO_x, NO, CO, HC, and F/A for the four test conditions: idle, 30%, 60%, and full power. These are shown on Figures 59 through 62. The general trend is an increase in the gradient of each component as the absolute concentration increases. We note also that somewhat higher concentrations of hydrocarbons, and CO to some extent, exist near the tailpipe walls at low power, although the F/A does not show a particular wall increase. At high power and high F/A, the NO and NO_x gradients tend to correspond to that of F/A, with higher values near the wall.

Some irregularities and discontinuities are noted on the diametral profile data. In many cases, these are a result of slight variation in operation. The test time covered a period of about 3 hours. During this time, the ambient air pressure, temperature, wind velocity, and direction could change. To determine the extent of these effects, plus those associated with changes in engine airflow, fuel flow, etc., the center point was used as a reference level and was sampled on each diameter sweep of the probe. The time average center point concentrations were used to correct or "normalize" the surrounding data point position concentrations. The results have been plotted in Appendix II for the four power settings and components CO, HC, NO, NO_x. In addition, combustion efficiency and F/A were plotted. For most of these plots, the exhaust gas is quite uniform. Nonuniformities that were measured in the combustor exhaust in the laboratory combustor are not pronounced in the engine exhaust. The large gradients of concentration reported in the exhaust of large fan jet engines (JT9D) (Reference 34) are not observed in the T53 exhaust. There are noticeable similarities between F/A profile gradients and NO (or NO_x) gradients for the higher power points, as might be expected.

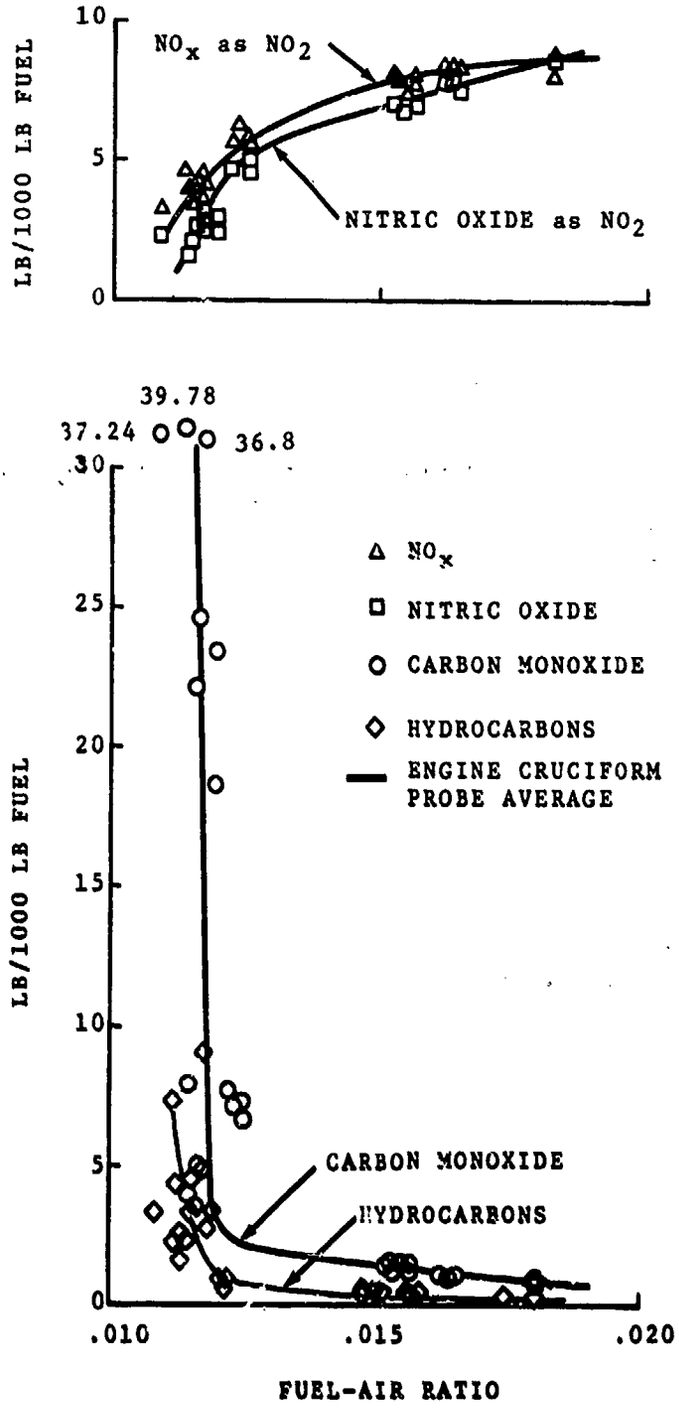

Figure 58. T53 Engine Emissions Versus Fuel-Air Ratio.

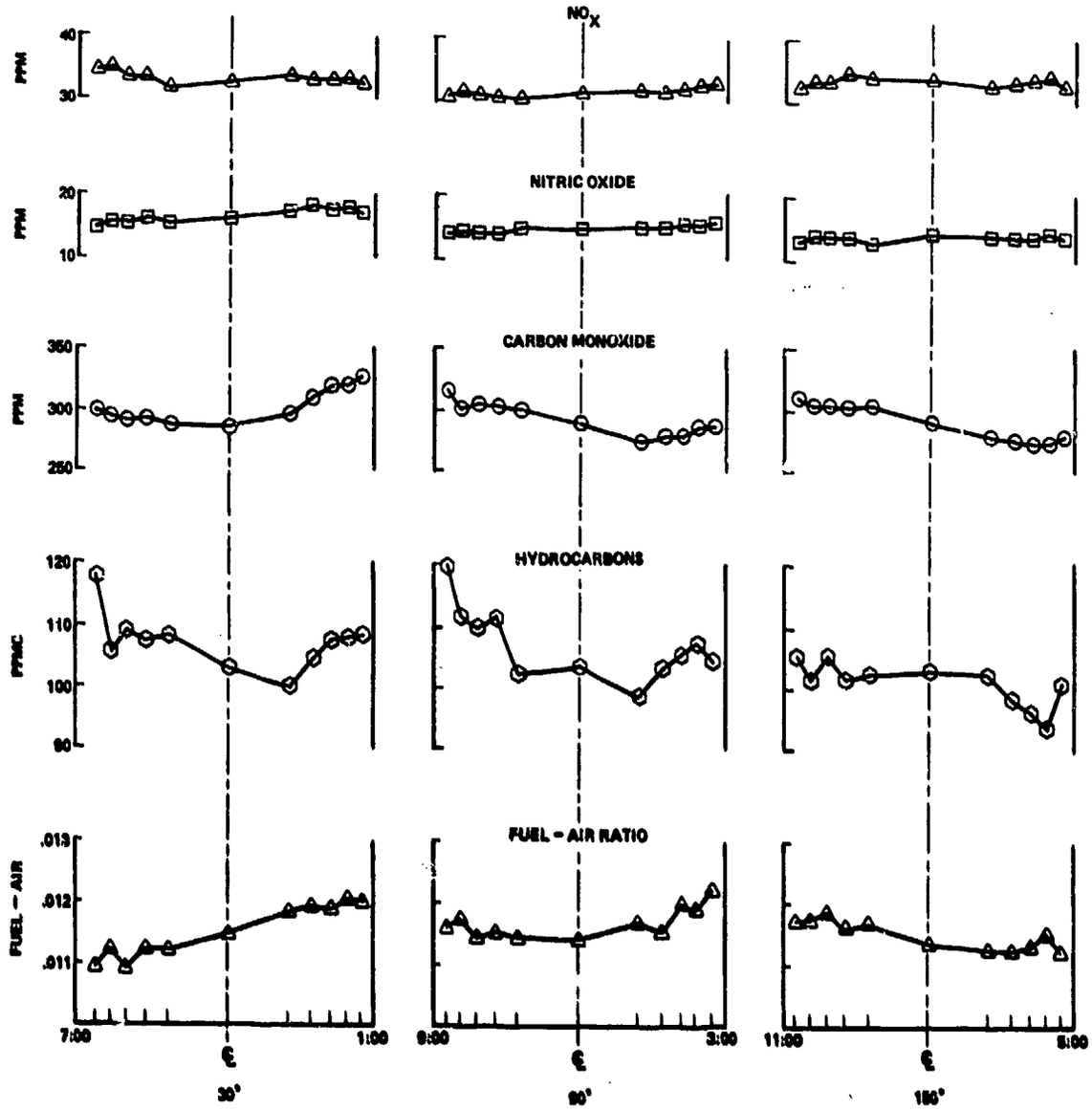

Figure 59. T53 Engine Idle Diametral Profiles.

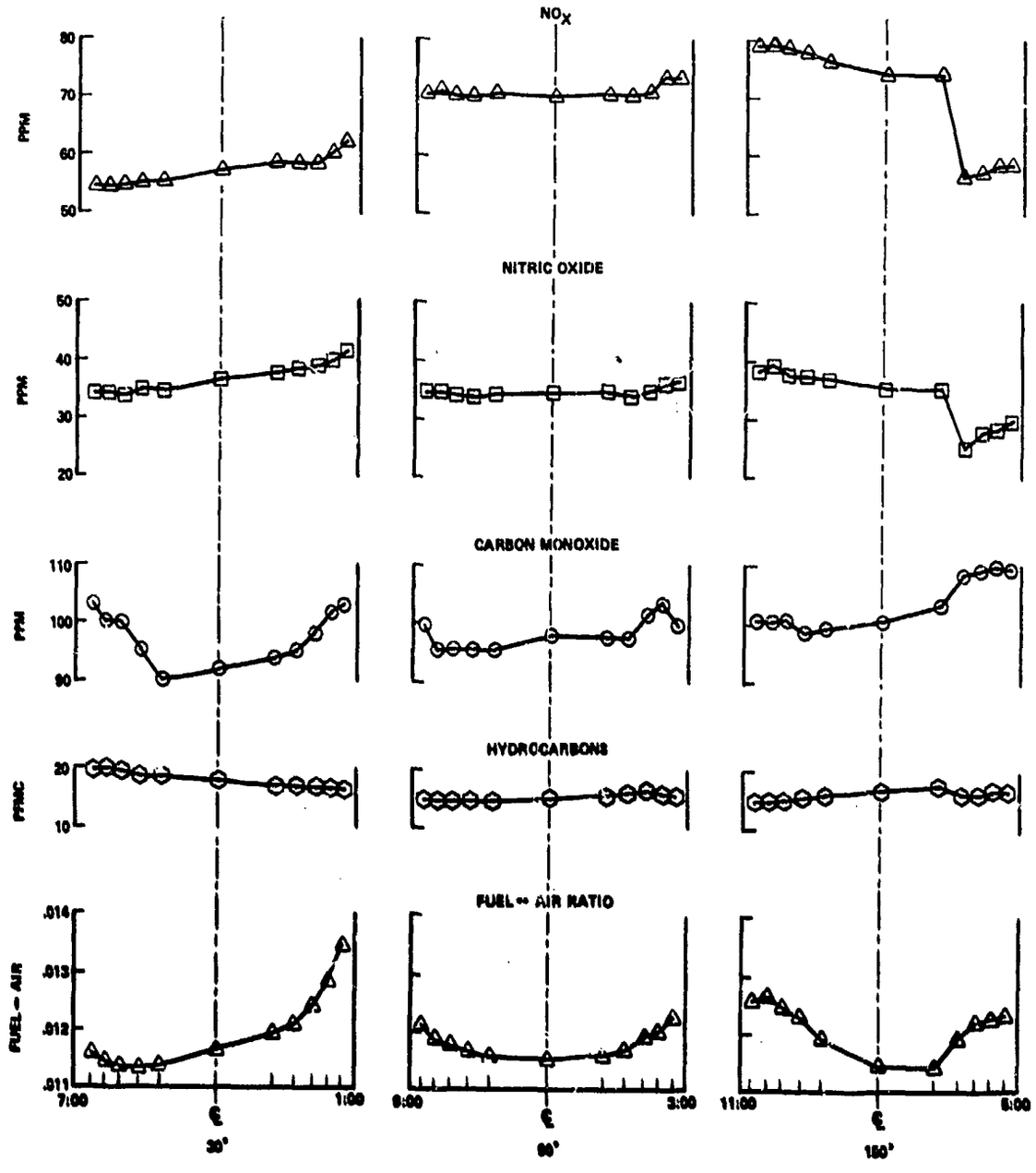

Figure 60. T53 Engine 30-Percent Power Diametral Profiles.

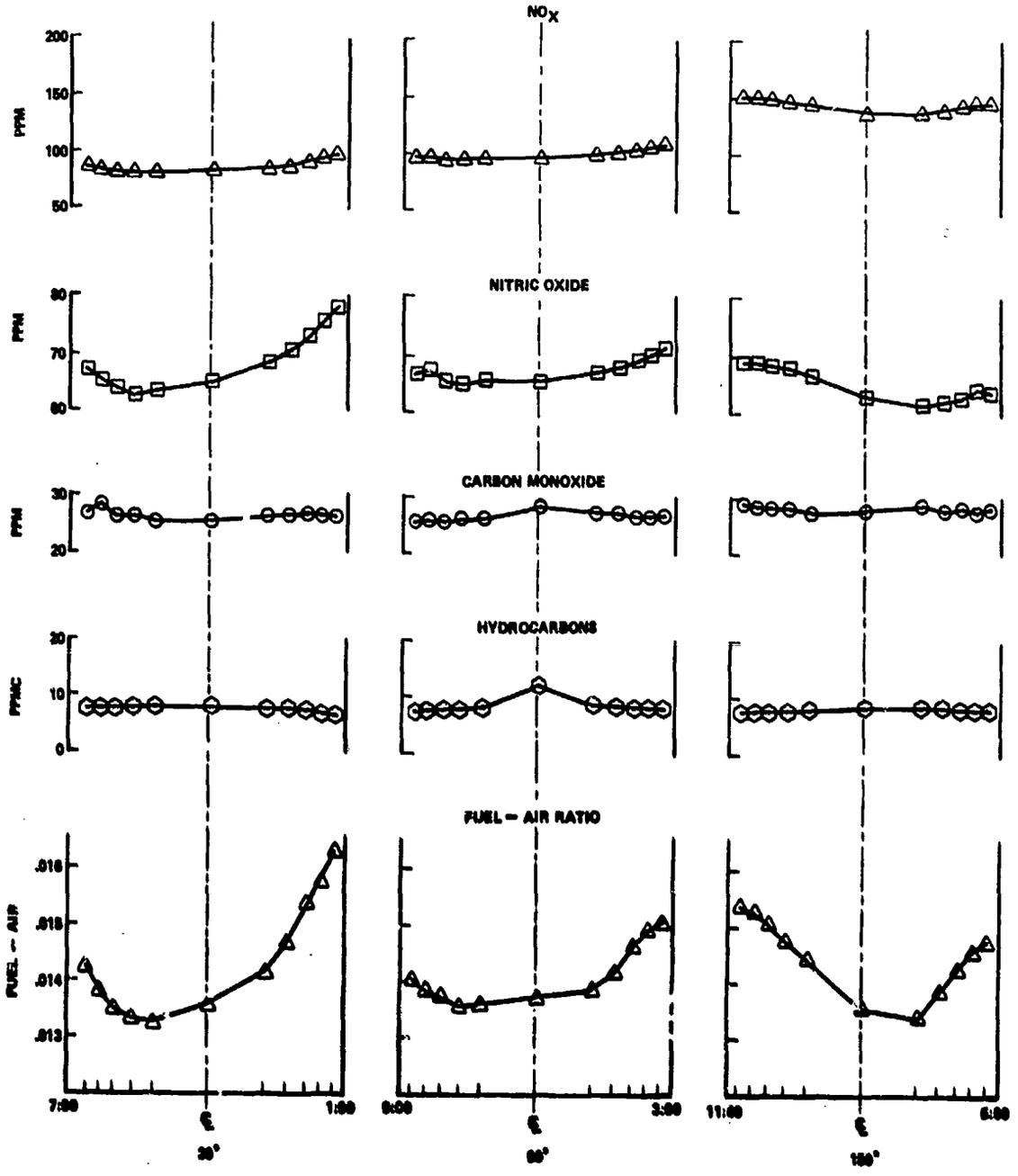

Figure 61. T53 Engine 60-Percent Power Diametral Profiles.

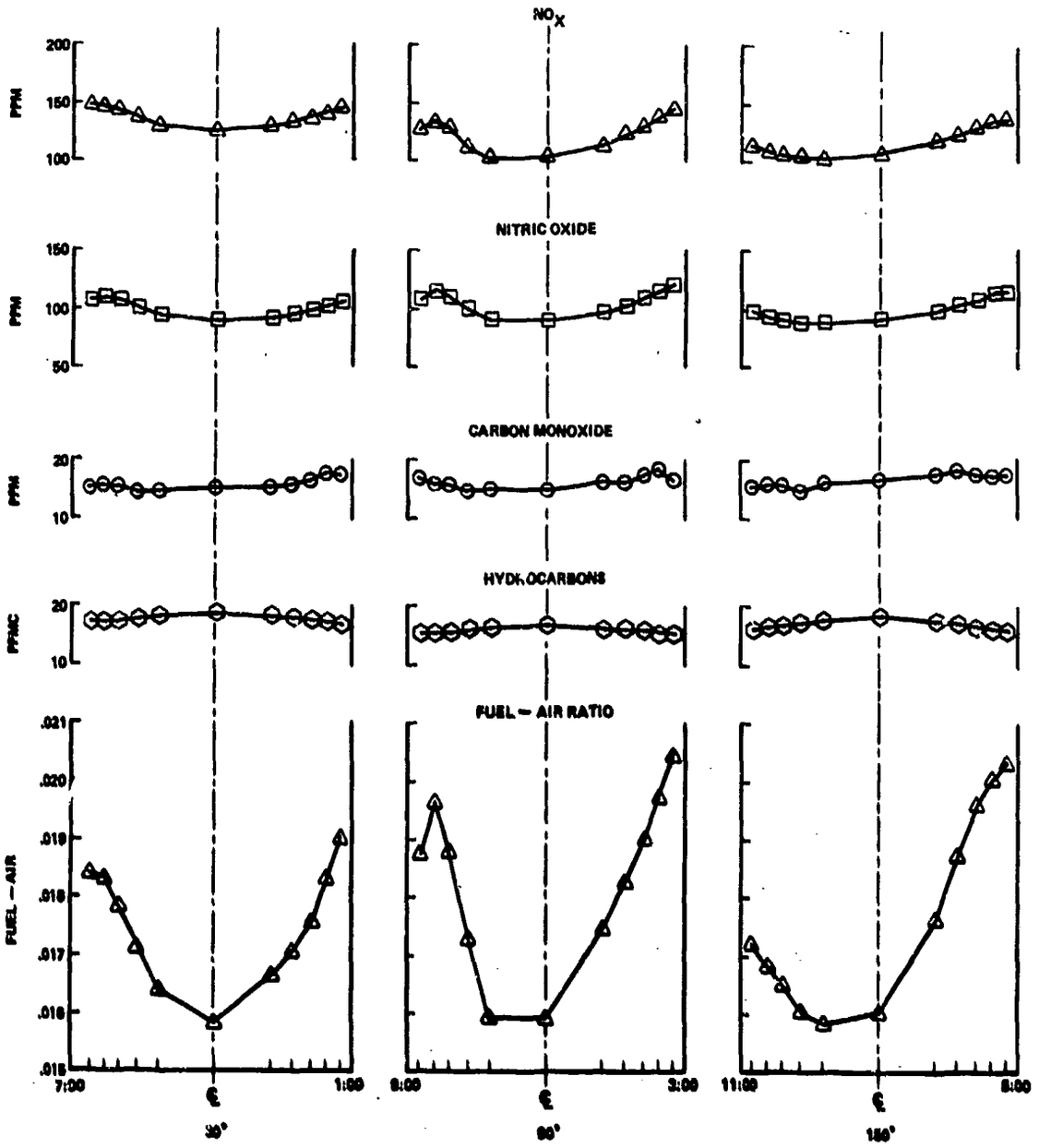

Figure 62. T53 Engine Maximum Power Diametral Profiles.

In addition to the contour plots of combustion efficiency at each power rating, a plot was made of combustion efficiency versus percent rated power (Figure 63). Both of the two ascending and descending power tests are plotted. Divergence and data scatter at the low power end is as much as ± .5 percent at 98 percent. At high power, scatter is of the order of 0.05 percent or ± .025 percent. An interesting aspect of these "up and down" performance tests is that there appears to be some hysteresis on the return. Those data will be compared in a later section of this report with respect to NO formation

These data lead to the following conclusions regarding the design of average sampling probes for Lycoming engines:

1. Probes should be designed for a systematic variation in the radial direction; i.e., the equal area design concept is correct.

2. The maximum number of major circumferential variations observed indicates that the cruciform probe with four radial bars is adequate to obtain a representative sample. If one uses the isopleth plots to calculate the value that a cruciform probe would read, they agree, in all cases, within about 3 percent of the traverse average.

3. The random spatial variations are probably no larger than the time variations; this means that the cruciform probe with a sample time of 2 minutes is preferable to the traverse that takes several hours.

Smoke measurements, recorded concurrently with the gas analysis, were converted to AIA smoke number per Reference 6. The results are plotted versus power in Figure 64. The peak smoke number measured is 15, which is well below the visible limit of 30 to 35.

Comparison of T53 Combustor and Engine Emissions

Data from the T53 combustor and engine were examined to learn whether laboratory combustor exhaust gas data could be used to correlate with the engine exhaust gas profiles. The laboratory combustor

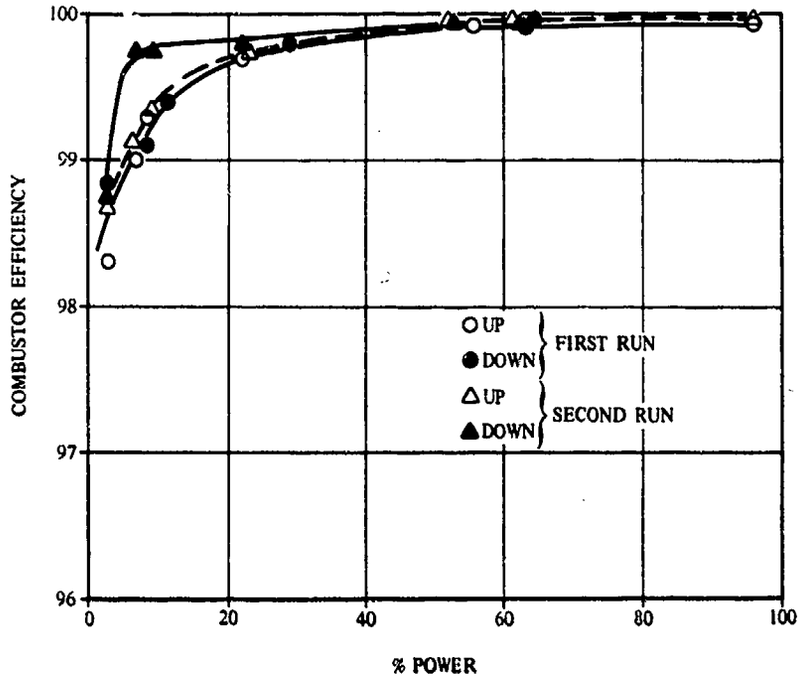

Figure 63. T53-L-13 Engine Combustion Efficiency Versus Percent Power.

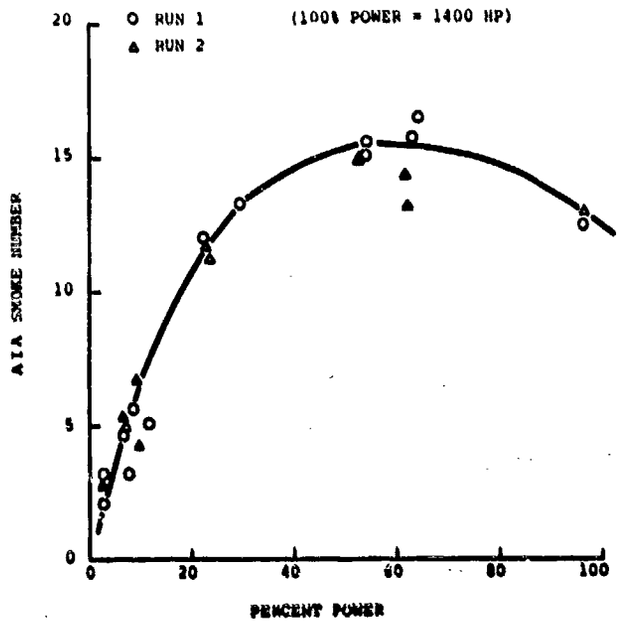

Figure 64. T53-L-13 Engine AIA Smoke Number Versus Percent Power.

probe contains 5 ports (Figure 13) which ingest the gas and arrive at an average mixture for a sector of the exhaust. This composition was compared with an engine traverse of gas composition along a radial circumference that corresponds to the geometric centroid. The two are plotted in Figure 65. An examination of the two profiles reveals no similarities, although the average F/A values are similar, as would be expected. The conclusions are:

1. Any small circumferential concentration profile that is present at the combustor exit is essentially wiped out by mixing in the turbines and exhaust ducting.

2. Aerodynamic flow in the laboratory test may be different enough from the engine flow so that a comparison of profile detail may be meaningless.

Emission level from the combustor test was compared with emissions from the engine. Because the engine F/A is not the combustor F/A, comparison of the two requires adjustments. Engine horsepower was plotted against both engine F/A and combustor F/A (Figure 66). The airflow adjustments included compressor bleed and cooling air for the turbine, as discussed previously in this report. With this correction applied to the engine data, a plot was made of pollutants versus combustor F/A (Figure 67). Agreement between cruciform (averaging) probe, engine traverse average, and laboratory traverse average is excellent for nearly all components. (The NO_x values from the engine traverse average are higher than the other two values.)

The good agreement between the three measurements in the laboratory and on the engine demonstrates that:

1. **The measurements in the laboratory can be used to predict engine emissions.**

2. **Conditions of test in the laboratory closely approximate engine operation from an emissions point of view.**

3. **The precision of the measurements is obviously satisfactory and reproducible over a period of several weeks and under varied testing conditions.**

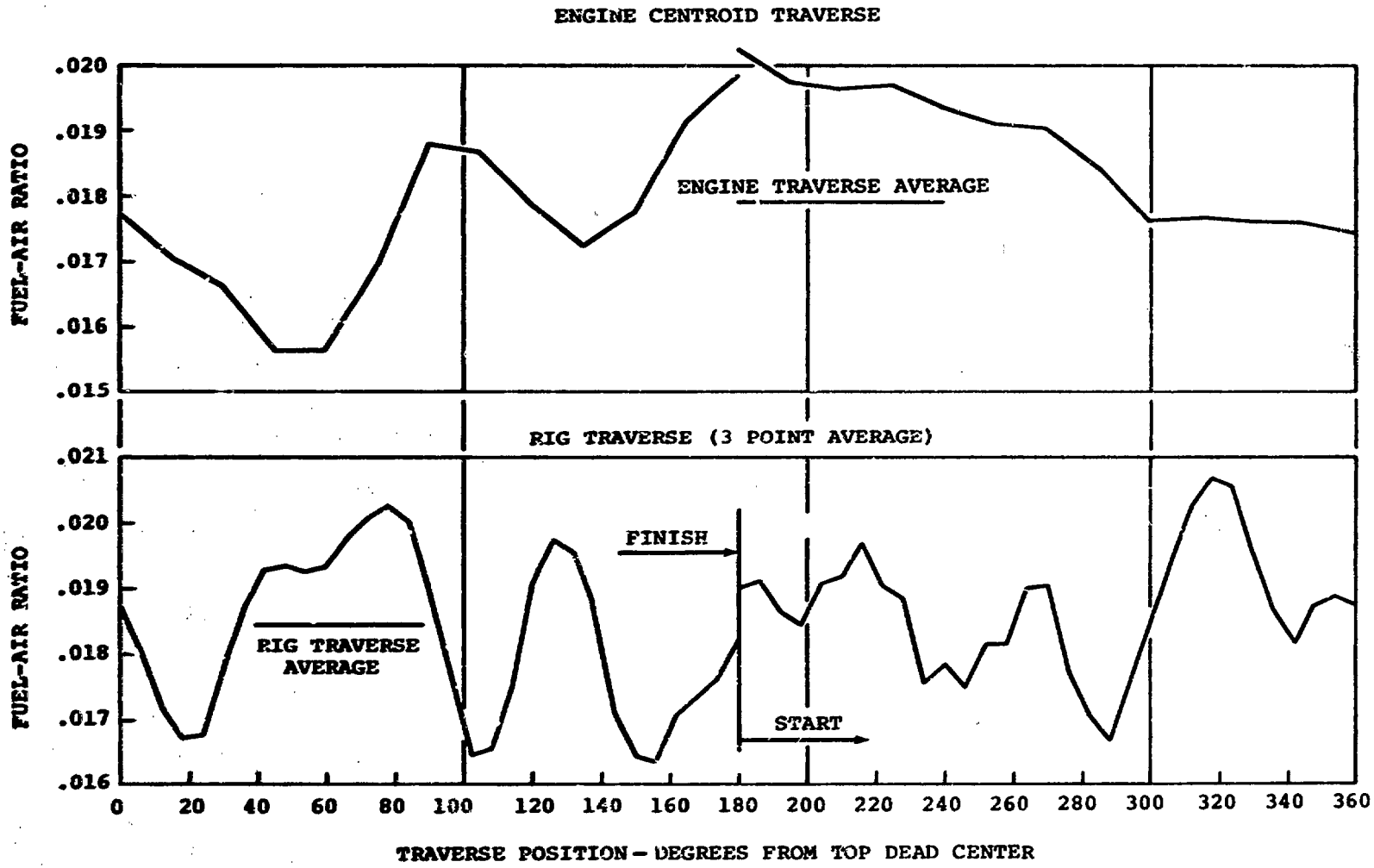

Figure 65. Fuel-Air Ratio Versus Probe Angular Position for T53 Engine and Combustor at Maximum Power.

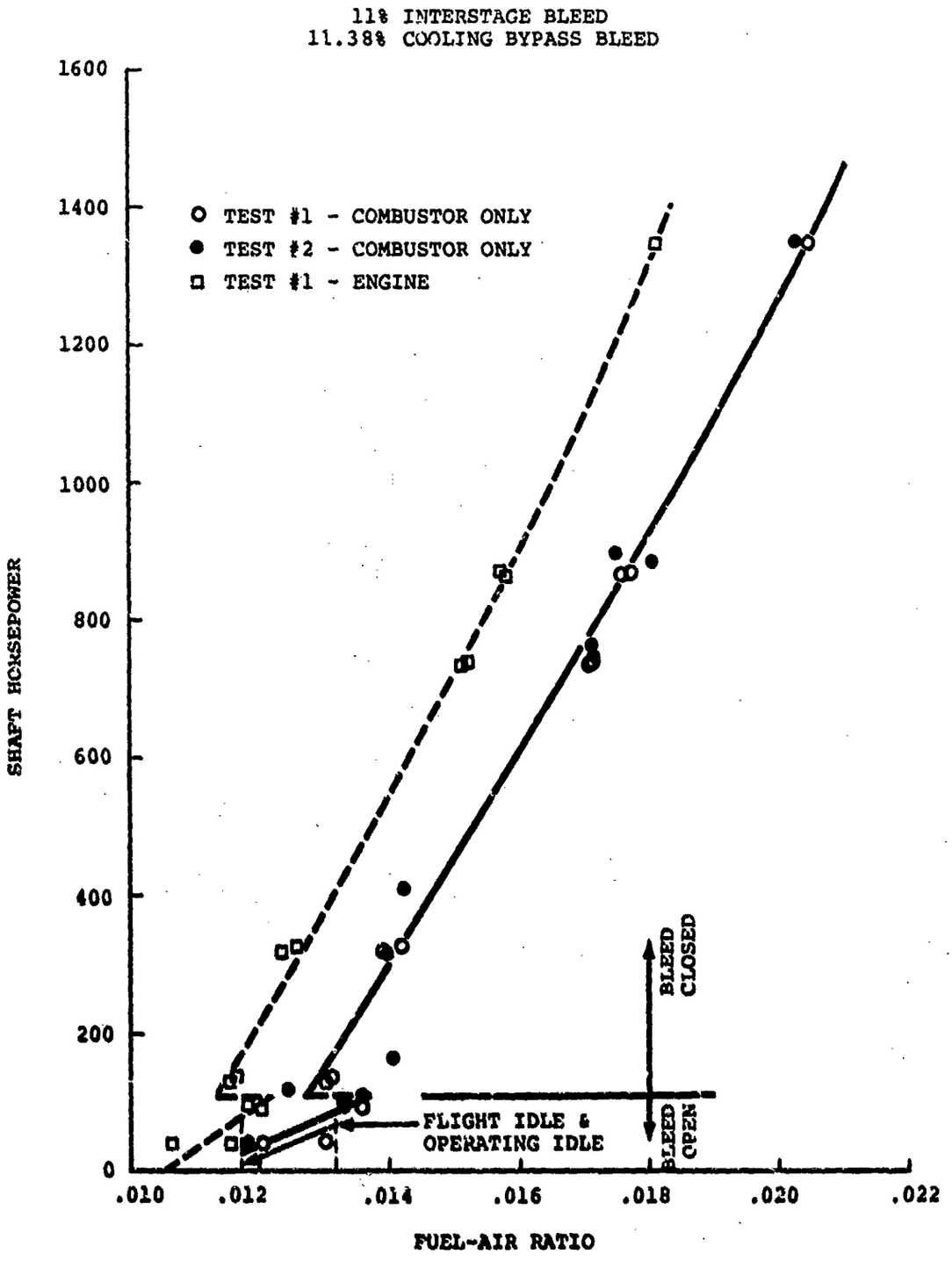

Figure 66. Fuel-Air Ratio Versus Shaft Horsepower for T53 Engine and Combustor.

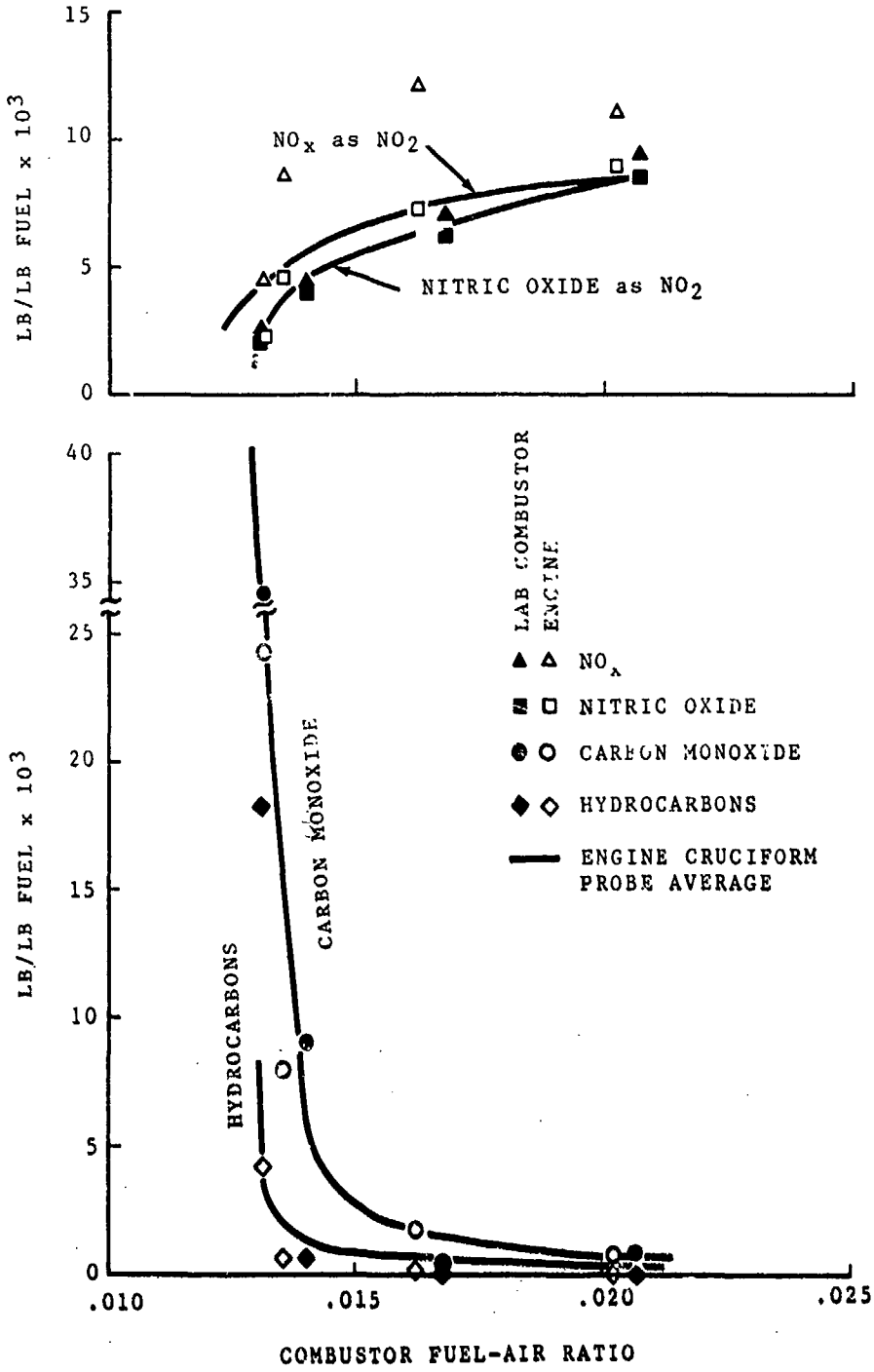

Figure 67. Comparison of T53-L-13 Emissions From Engine and Laboratory Combustor Tests.

4. The preponderance of evidence from the three measurements provides solid ground for a statement on emission level for this engine.

T55 Combustor Data and Results

As with the T53 combustor, the T55 data consist of combustor test rig operating data, averaging probe data, and traversing probe data.

The combustor was operated at conditions simulating engine idle to full power (Table I). Maximum power and 60 percent power conditions were simulated with temperature, but not with pressure, because of compressor facility limitations. During 60-point traverses, averaging probe data were recorded for each 15 data points. This served the purpose of checking the combustor operation for possible variations as time progressed, and for obtaining averaging probe data. Gaseous component output was converted to ppm and to Emission Index (EI).

A plot of emittants CO, HC, NO, and NO_x is shown in Figure 68 as a function of F/A. Observations from these plots show that:

1. Trends of CO and HC are similar to those from the T53 combustor; there are large reductions in concentration as power is increased from simulated idle to full.

2. Increases in NO and NO_x occur, as expected, as simulated power increases.

3. The "traverse average" compares closely to the value read by the four averaging probes. Differences can be traced to the location of the four probes with respect to the shape of the emission profiles; i. e., the four probes were not at representative locations in the traverse.

As with the T53, the T55 temperature profiles were recorded with a 5-thermocouple rotating probe (Figures 12 and 13) while the gas sample traverse was being made, and similar results were obtained. Temperature peaks and valleys correspond almost exactly with F/A peaks and valleys at all flow test conditions (idle, 30, 60, and 100 percent power) (Figures 69 through 72). These results again substantiate the correlation between thermocouple gas measurement and gas analysis.

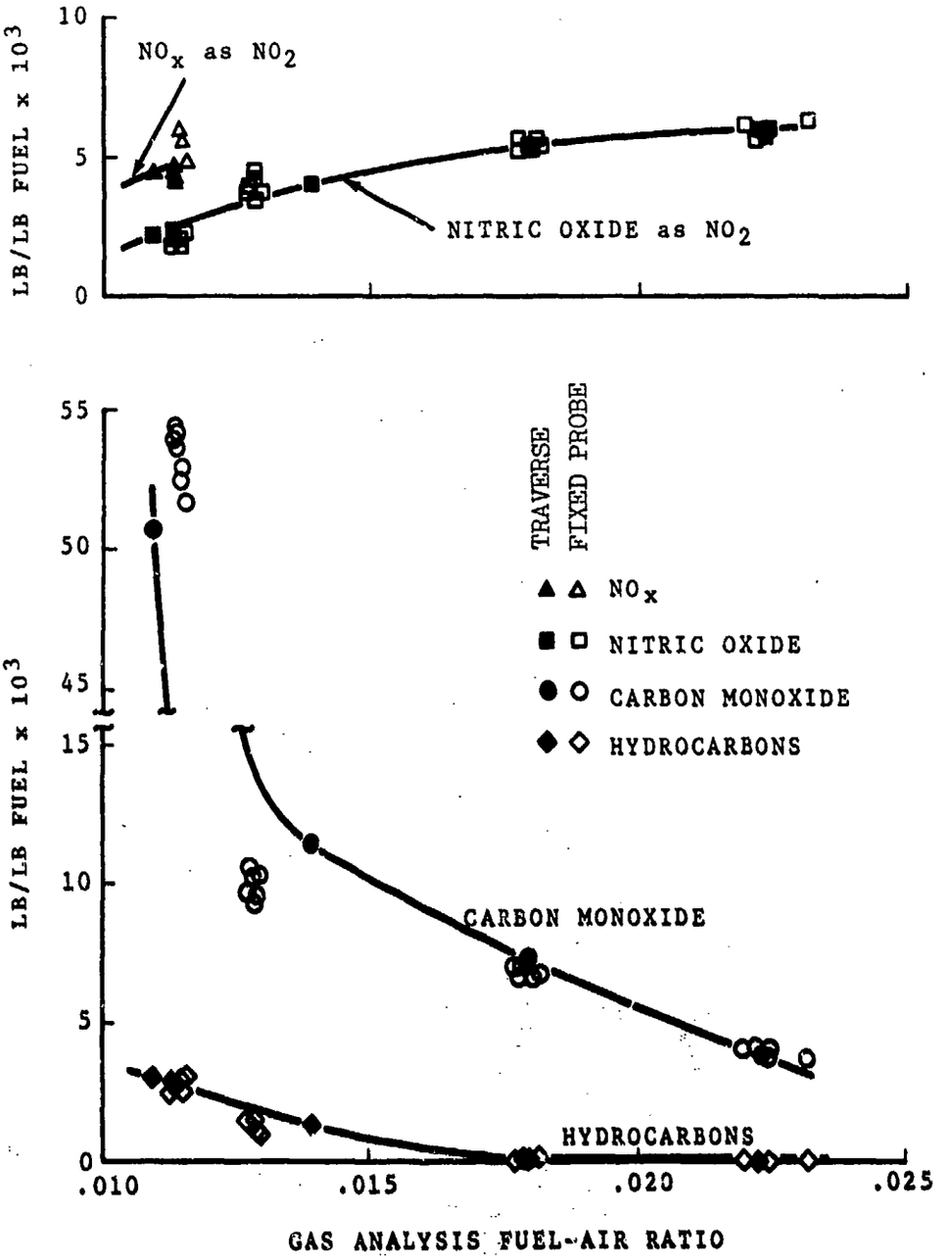

Figure 68. T55 Laboratory Combustor Emissions Versus Fuel-Air Ratio.

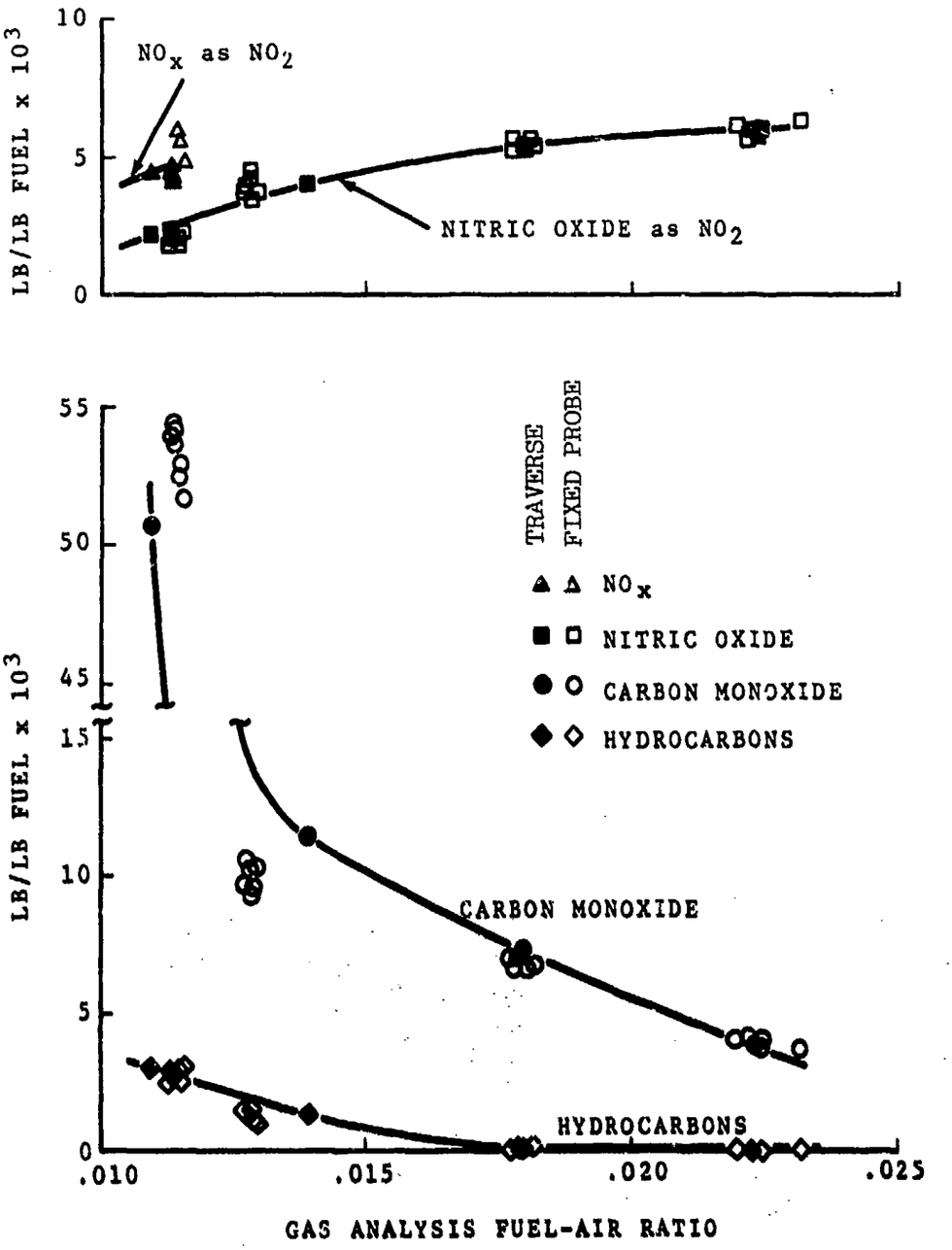

Figure 68. T55 Laboratory Combustor Emissions Versus Fuel-Air Ratio.

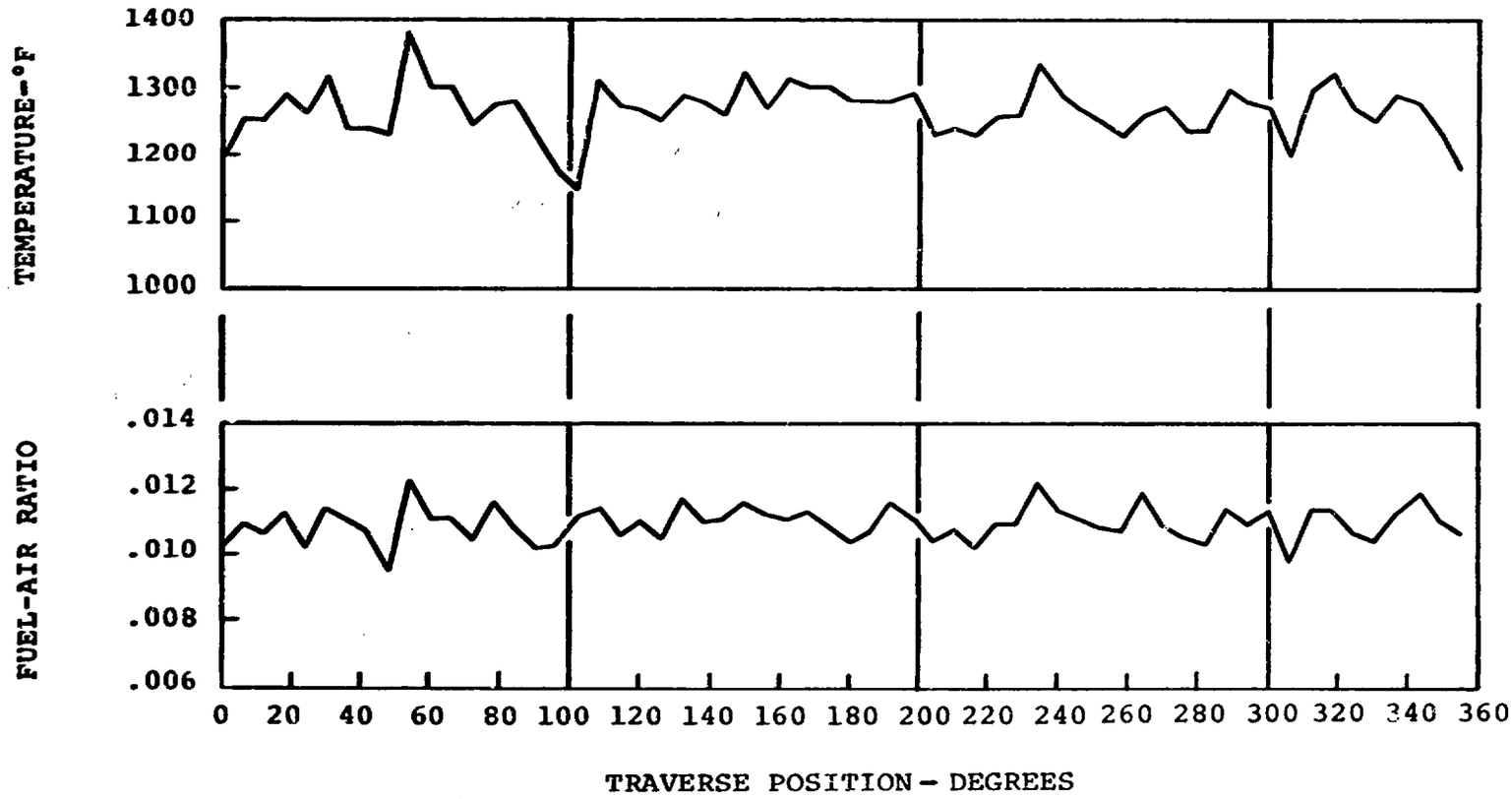

Figure 69. T55-L-11 Rig Simulation of Idle.

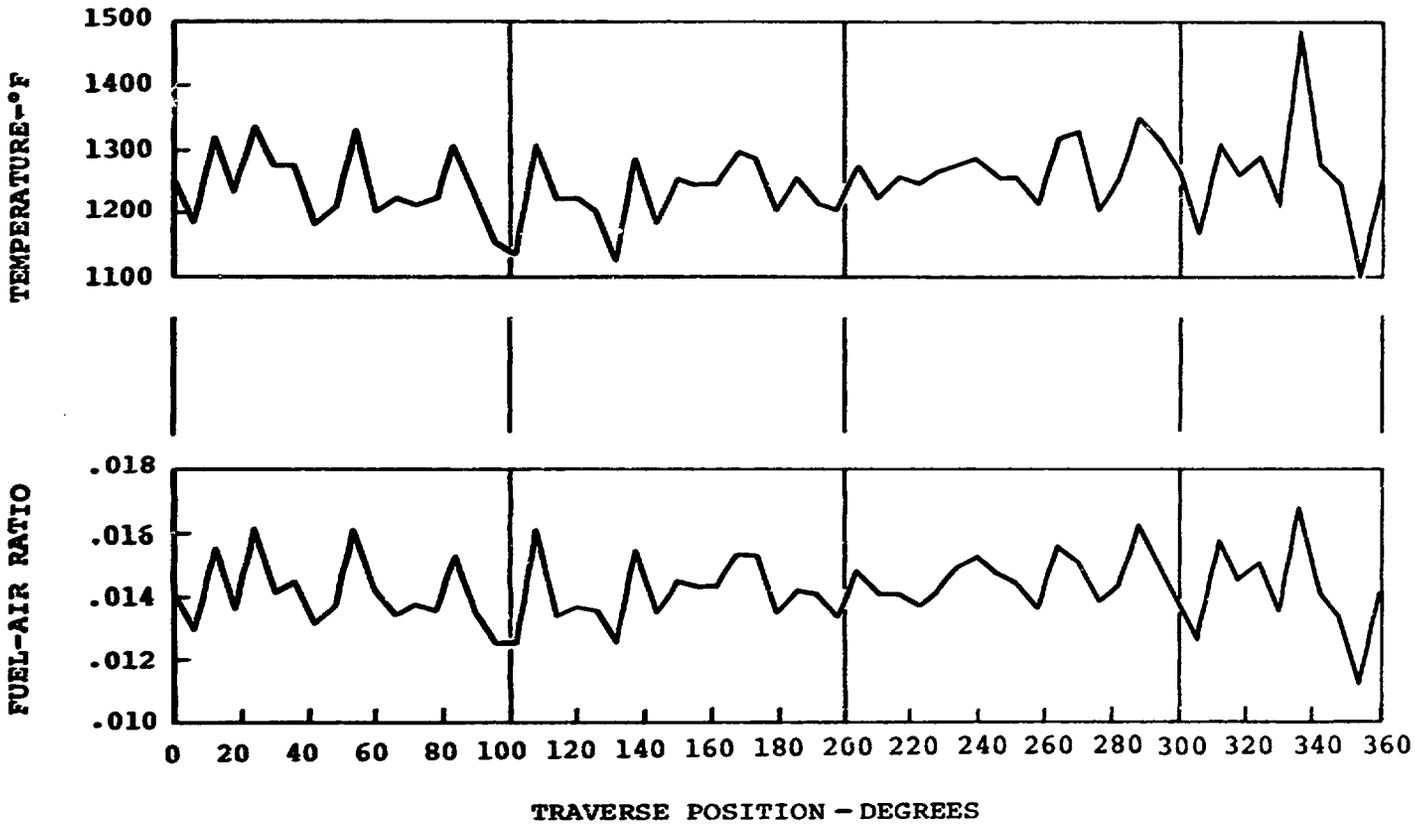

Figure 70. T55-L-11 Rig Simulation of 30 Percent Power.

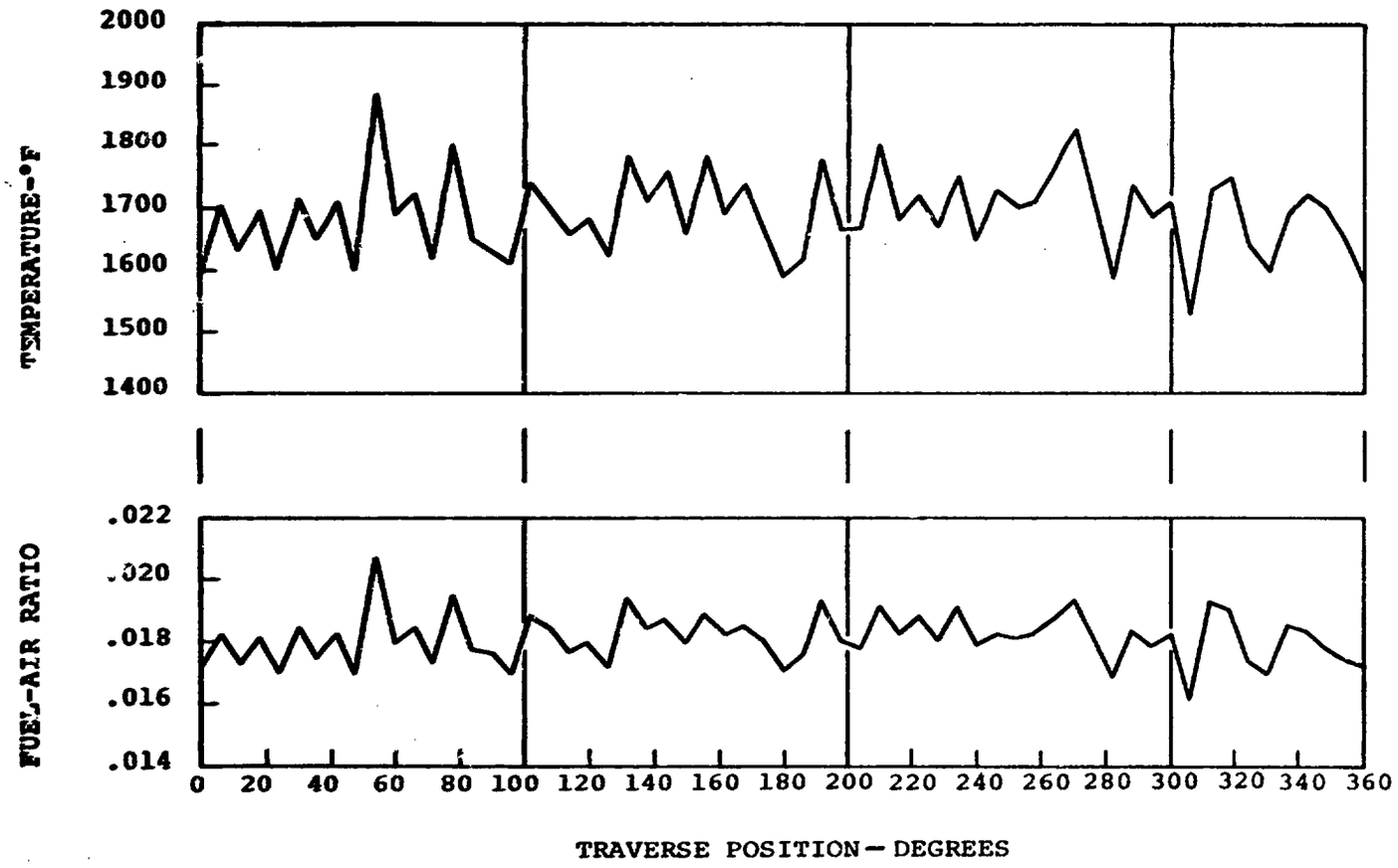

Figure 71. T55-L-11 Rig Simulation of 60 Percent Power.

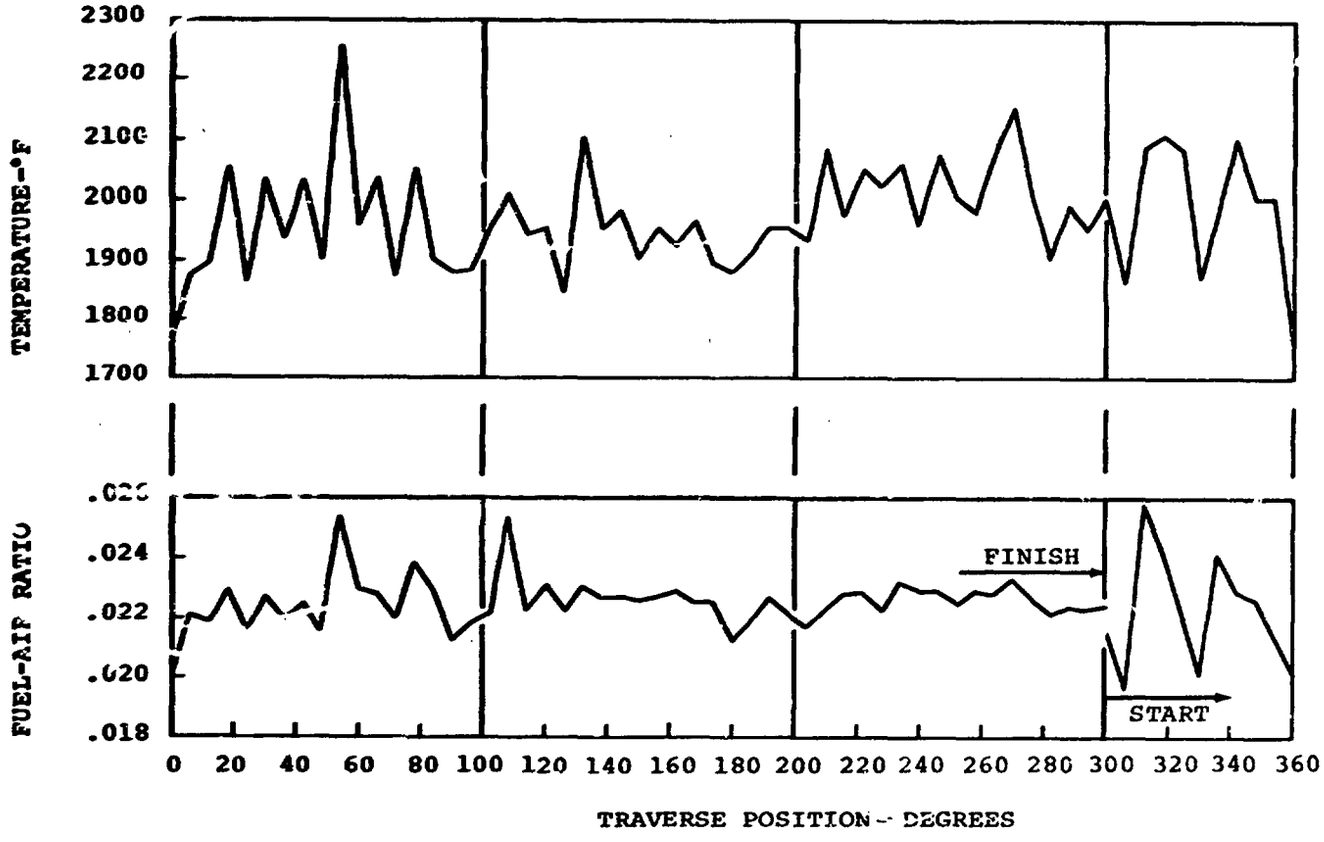

Figure 72. Comparison of Temperature and Fuel-Air Ratio for T55-L-11 Rig Simulation of 100% Power.

Complete plots of the T55 rig traverse gas composition data are presented in Appendix III. The T55 F/A traverses show variations over short distances which diminish to a steady value at higher simulated power. From a combustor design viewpoint, this indicates good circumferential mixing. As with the T53, the characteristics of the traverses tend to recur at each successive power setting. This holds for all the pollutants, as well as F/A, except at high power simulation where HC becomes minute, and traverse detail vanishes.

During the T55 "idle" traverse, a valve was left open in the sample line for the central one-third of the traverse; this resulted in sample dilution with ambient air. As one may estimate from the F/A profile, this resulted in roughly 1.5 parts of air to each part of exhaust gas. This dilution does not affect the calculated value of EI or combustor efficiency because these are evaluated from a ratio of exhaust gas component concentrations rather than an absolute value. Notice that the EI's for CO, HC and NO are not significantly shifted in this section of the traverse. Such is not the case for NO_x, which shifts downward to just above the level of NO. Apparently the disturbing effects of the other exhaust components were eliminated by the heavy dilution. This effect may be an instrument phenomenon, because the NO level does not change as it would if NO_x were being created in the sample line.

When one compares the plots of EI with those of ppm, the NO and NO_x are substantially smoother for the EI traverse, which once again demonstrates the substantial relationship between NO_x and F/A. For the T55, a similar conclusion cannot be drawn for the CO and HC as it was for the T53. Here the amount of unburned species is quite independent of the local F/A. Apparently the mixing is good, and the primary zone is lean enough so that the richest zones of the combustor have no more tendency to leave unburned components than do the leaner zones.

The correspondence of the NO_x and F/A profiles is sufficiently good to permit the shape, but not the level, of the NO_x profile to be estimated from a simple temperature traverse. CO and HC show no detailed coupling to the F/A, but are coupled to each other up to the point where the HC reaches a negligible concentration at or below 60 percent power. The ratio, CO/HC, is once again a reasonably consistent function of efficiency, although it is not the same dependence observed for the T53 data.

T55 Engine Data and Results

T55 engine data, similar to the T53 data, consist of:

1. Engine operating performance

2. Exhaust gas measurements from the cruciform (averaging) probe

3. Exhaust gas measurements from the single-point probe

As with the T53, both engine data and gas analysis data were recorded at each power setting as the engine operation was increased from idle to full power and down again. For the steady-state operation required for single-point probe traversing, engine operation data were recorded at 15-minute intervals. Engine data are tabulated in Reference 5.

The T55 engine emission levels from cruciform probe "performance" tests are shown in Figure 73 for idle through full power. The discontinuity at bleed closure is obvious. NO, NO_x, and HC emissions repeat within the experimental error for two tests. For CO, two levels of concentration result from two tests. The reason for the CO level difference is not obvious. Agreement of concentrations of other constituents for the two tests is within the experimental error. Trends of NO, NO_x, HC, and CO are similar to those from the T53 engine, as expected. Comparisons of values with other engines will be made later in this report.

Data from the single-point probe were used to plot the concentration gradients for NO, NO_x, CO, HC, and F/A for four test conditions idle, 30 percent, 60 percent, and full power. These are shown in Figures 74 through 77 as profiles at three diameters across the exhaust. General trends of the profiles are similar to those of the T53. Again, some discontinuity is noted for two halves of the traverse, a function of slight changes in operation and ambient conditions. NO_x measurements exhibit more variability than the others, and, in general, indicate 10 to 20 ppm more than NO. These characteristics will be discussed in more detail later in this report. Some erratic behavior is displayed by the CO measurement at 30 percent power, and the level of CO appears to be low. It is suspected that the detector may have been somewhat out of adjustment during this test.

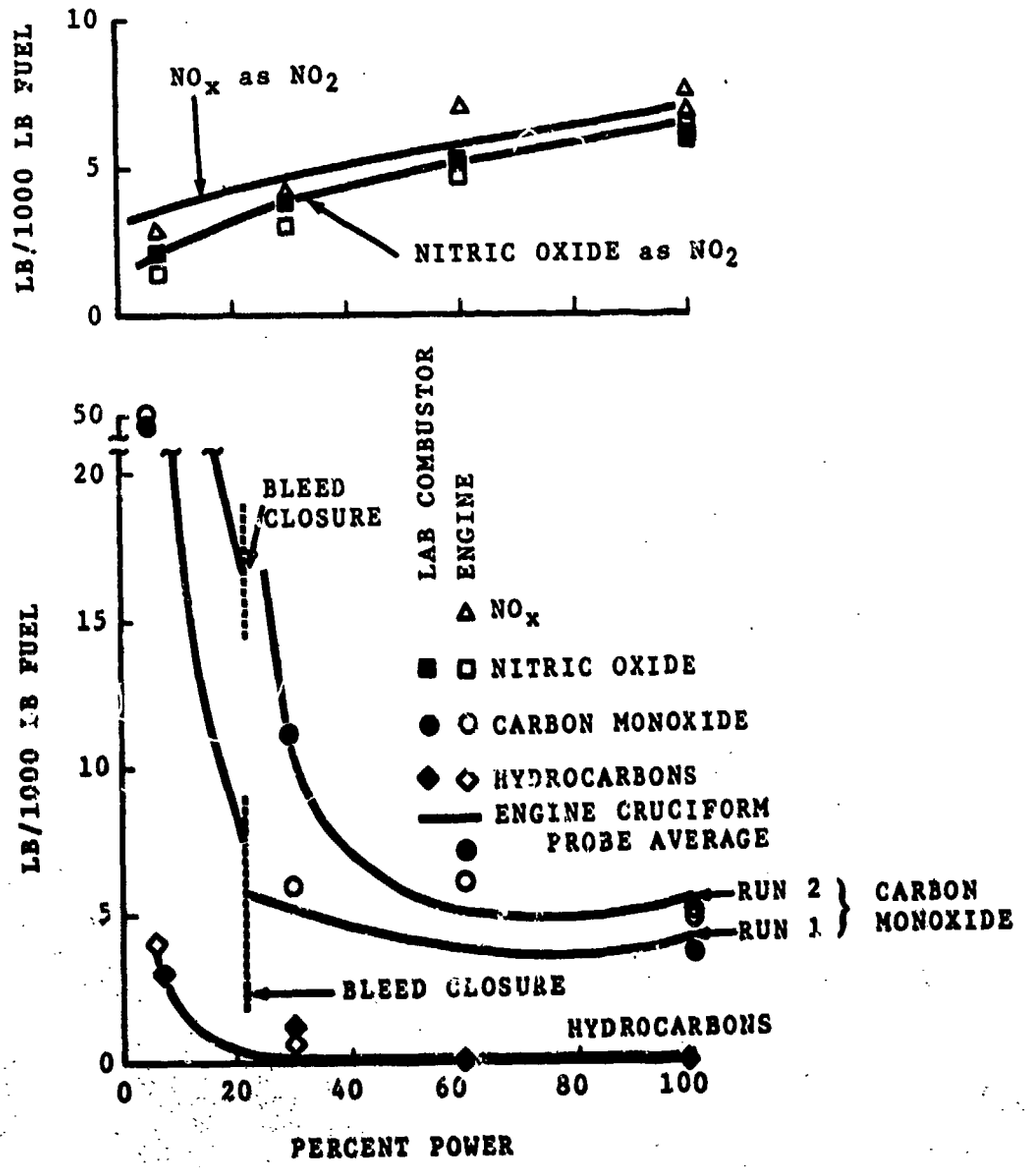

Figure 73. T55-L-11 Engine Emissions Versus Percent Power (Cruciform Probe).

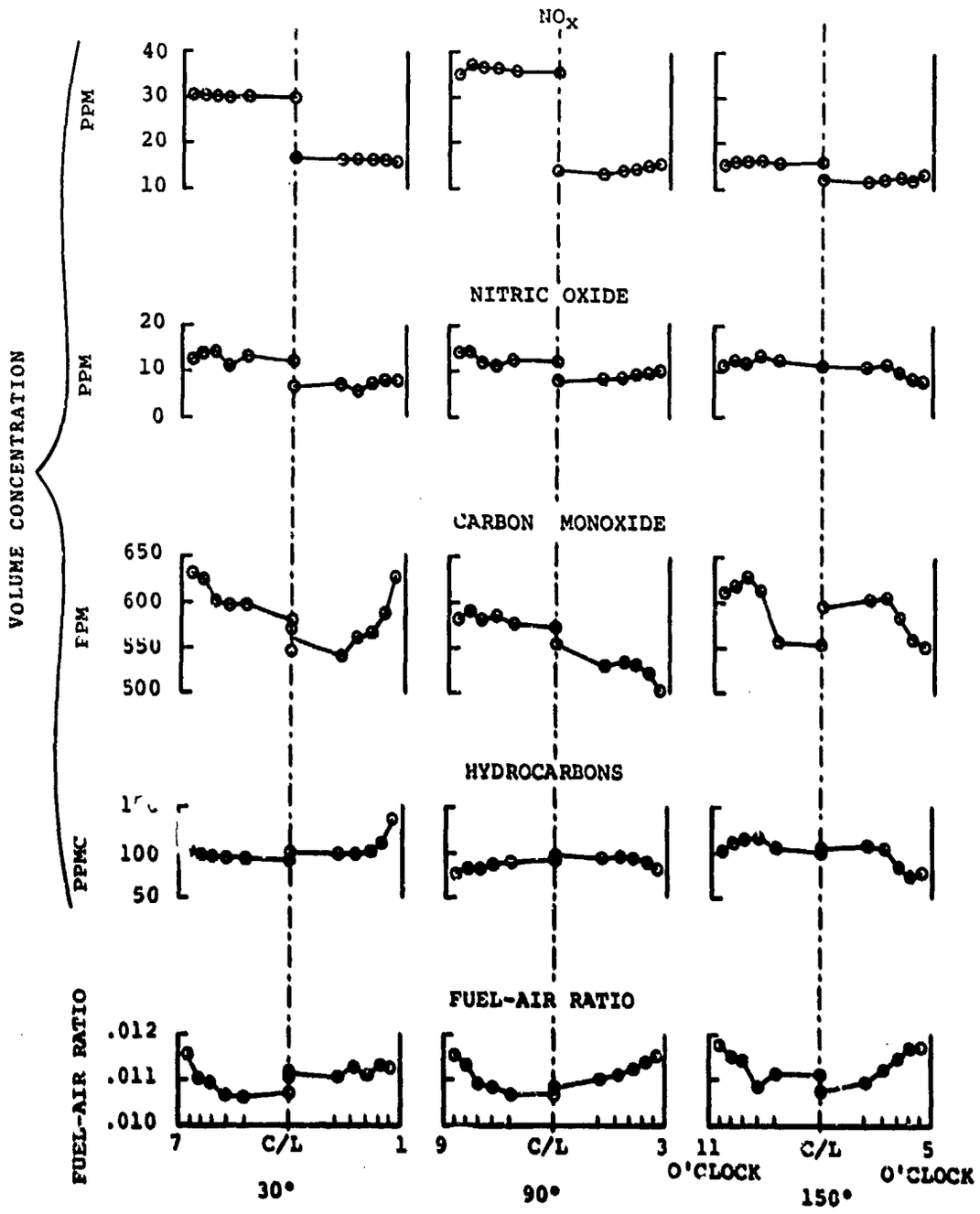

Figure 74. T55-L-11A Engine 470 Lb/Hr Idle Diametral Profiles.

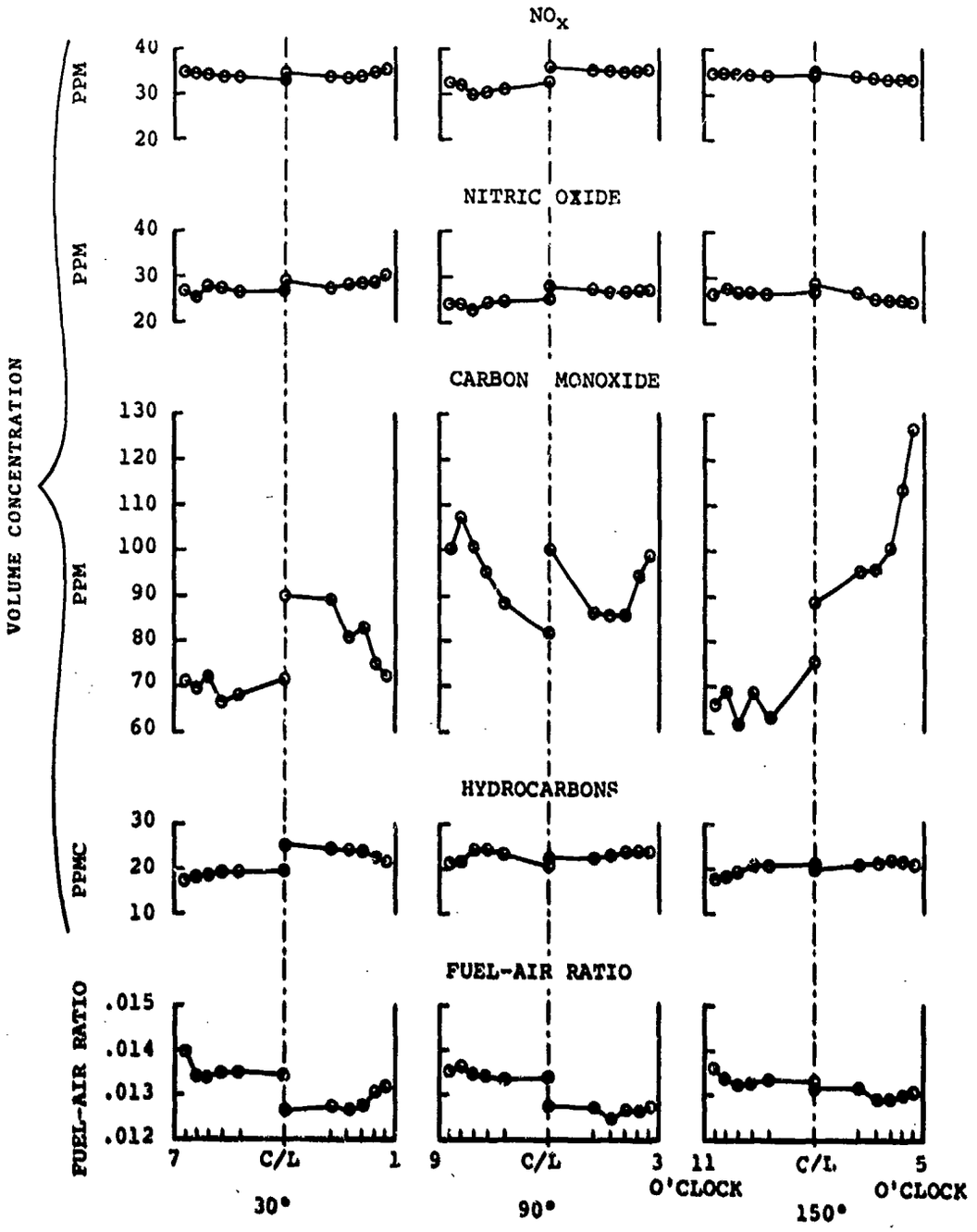

Figure 75. T55-L-11A Engine 30% Power Diametral Profiles.

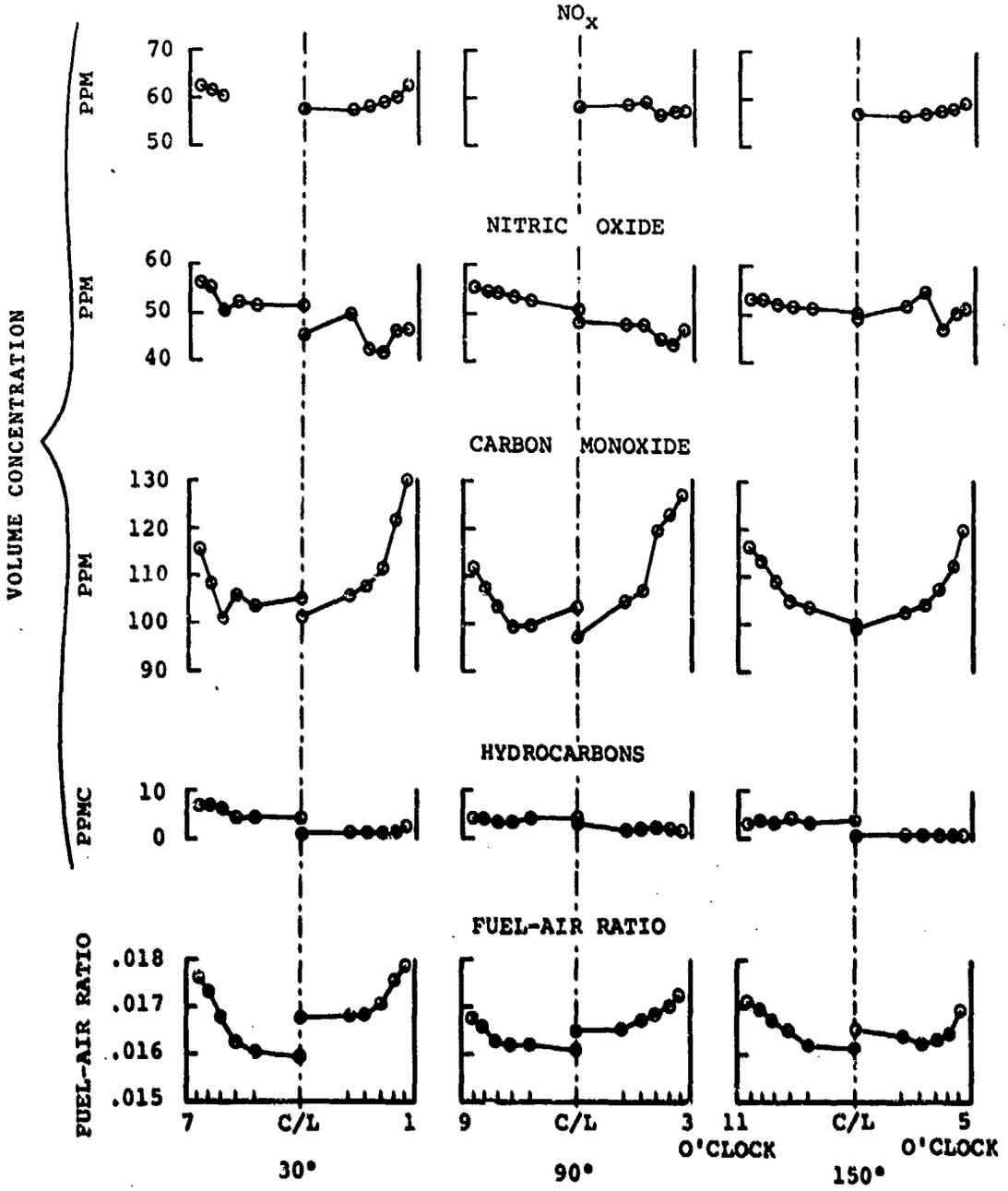

Figure 76. T55-L-11 Engine 60% Power Diametral Profiles.

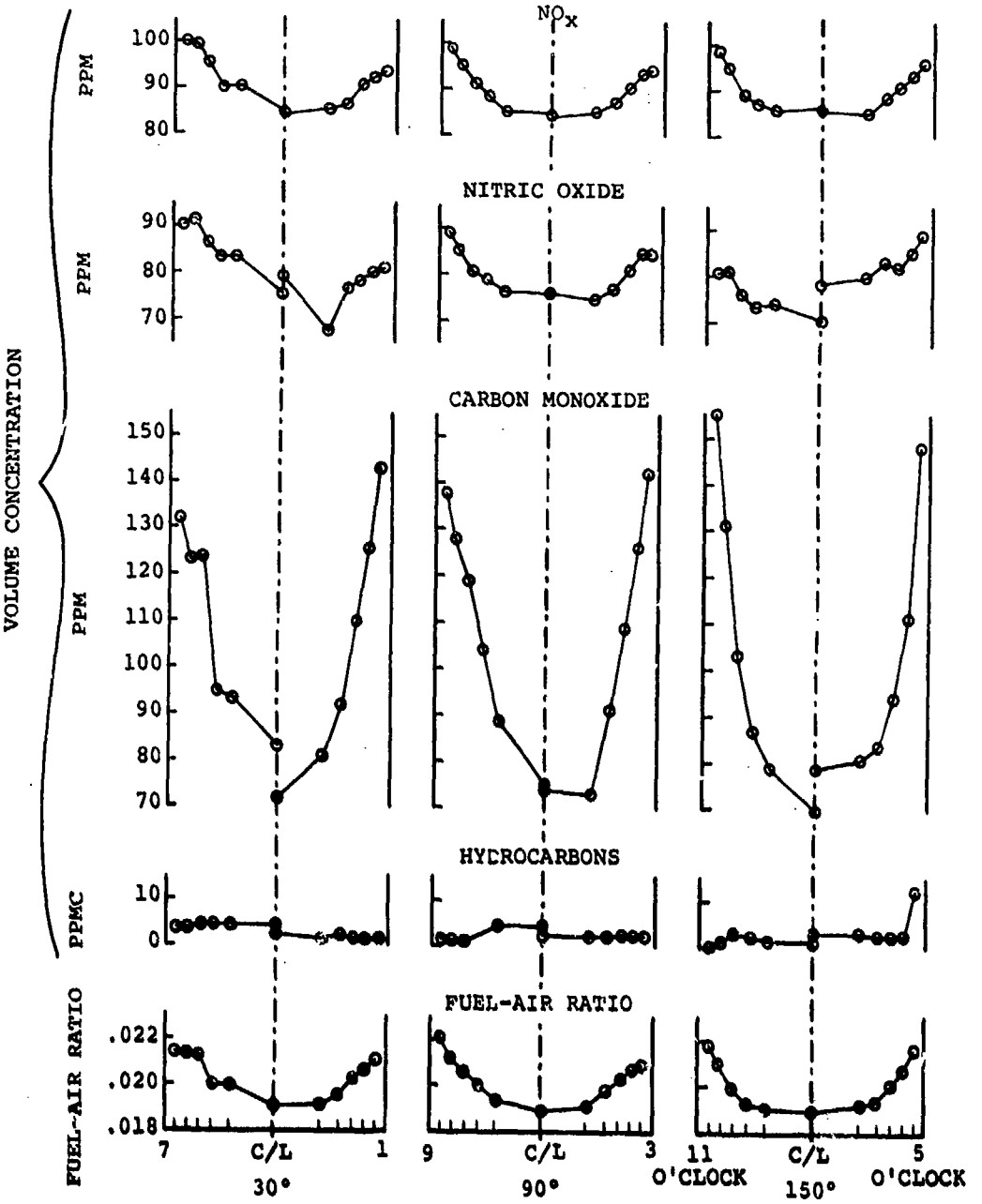

Figure 77. T55-L-11A Engine Diametral Profiles of Emittants and Fuel-Air Ratio at Full Power.

As with the T53, the center-point gas composition in the T55 exhaust was used as a reference level to correct other point samples to the "normalized" level. Contour plots of concentrations could then be made, as shown in Appendix IV. The profiles for the most part indicate nearly complete combustion at high power, and relatively flat profiles, indicating good mixing.

After one test at 60 percent power, it was found that the engine oil seals had deteriorated (Reference 5).* This test was rerun. To compare the effect of oil seal leakage, the data were plotted (Figure 79) and compared with a similar test when the seals had been replaced (Figure 78). A marked increase in hydrocarbons is shown for the oil leakage case. The amount of leakage measured on a short test the next day was 2 quarts per hour ±15 percent. If uniform leakage can be assumed, this would amount to 88 ppmC, as compared with the measured value of 30 to 40 ppmC. The difference between these two values can be explained if we assume that the leaking oil was not distributed uniformly in the airstream, and that some of it made its exit by other means. There was no indication of hydrocarbon saturation or chromatographic effects in the sampling lines from high concentrations of heavy hydrocarbons. "Normal" oil consumption has been measured at 0.25 quart per hour.

A plot of HC concentration versus point sequence (or time) at 60 percent power shows HC increasing, as time progressed and the oil seal deteriorated (Figure 80). Also shown is the small HC concentration when the test was rerun after the seal was repaired. The reduction in HC with the new seal is dramatic.

Combustion efficiency was calculated from gas analysis and plotted as a function of engine combustor F/A in Figure 81. Three tests were made, operating the engine from idle to full power and back. (Two tests were made on one day and one on the second day.) The significance of the three tests is that the combustion efficiency calculations are very close, even overlapping, indicating repeatable results from run-to-run and day-to-day. An examination of Figure 81 for hysteresis shows only a hint of this type of nonreproducibility, and nothing conclusive.

*Smoke was visible in the engine exhaust during the seal failure. No smoke measurements were made during this period.

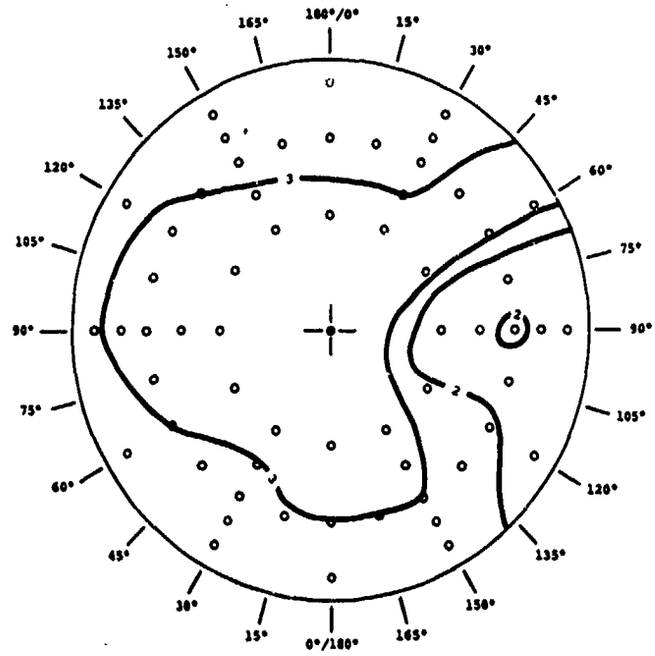

Figure 78. T55 Engine Isopleth of HC (ppmC) at 60 Percent Power.

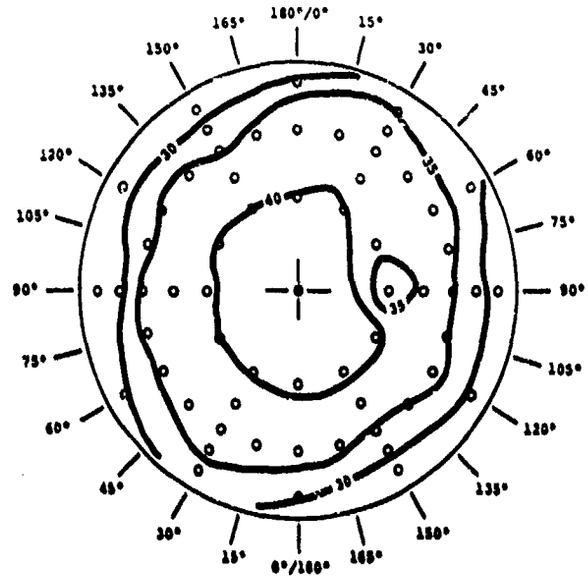

Figure 79. T55 Engine Isopleth of HC (ppmC) at 60 Percent Power During an Oil Seal Failure.

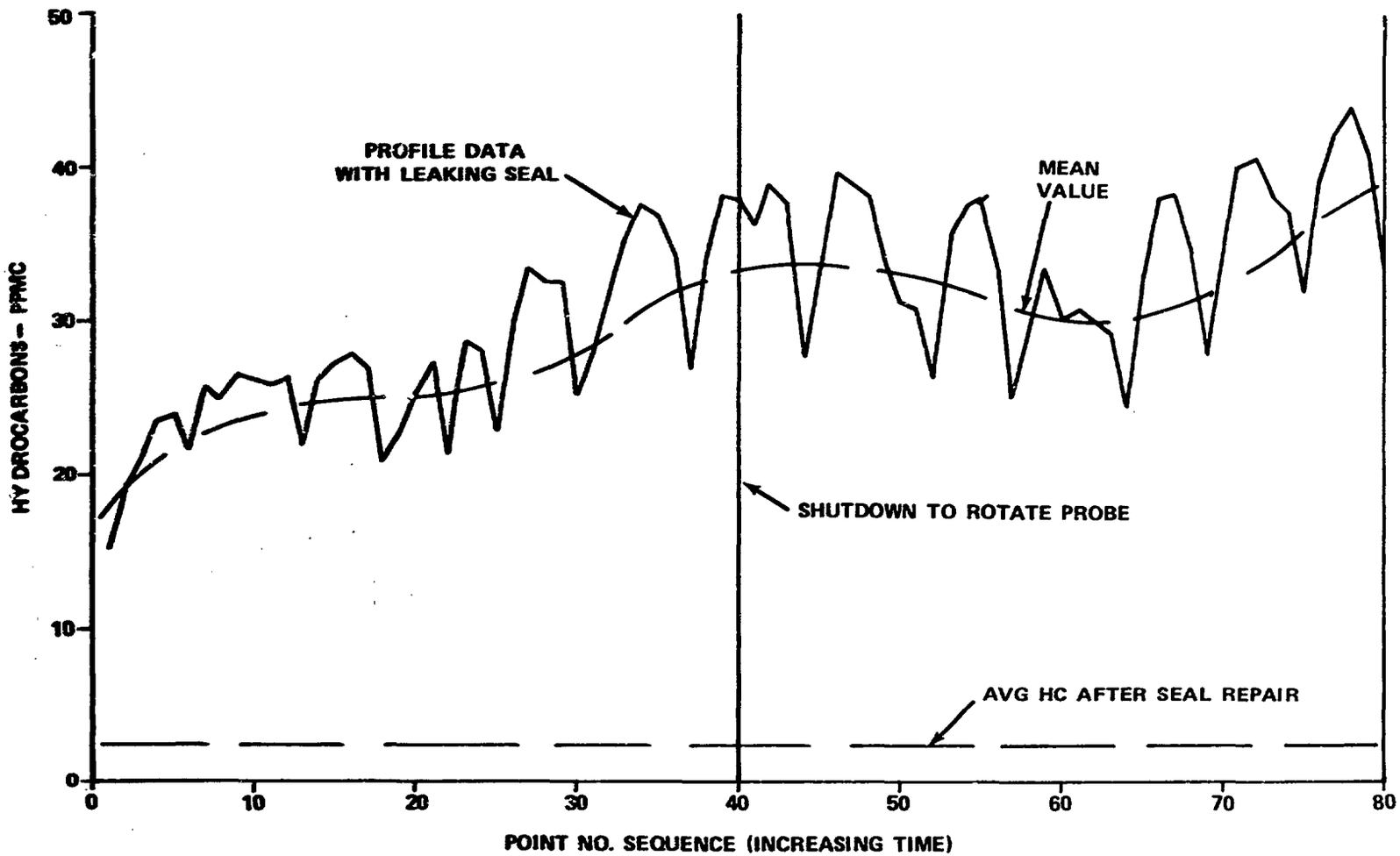

Figure 80. T55 Engine Exhaust Hydrocarbon Concentration With and Without Oil Seal Leakage.

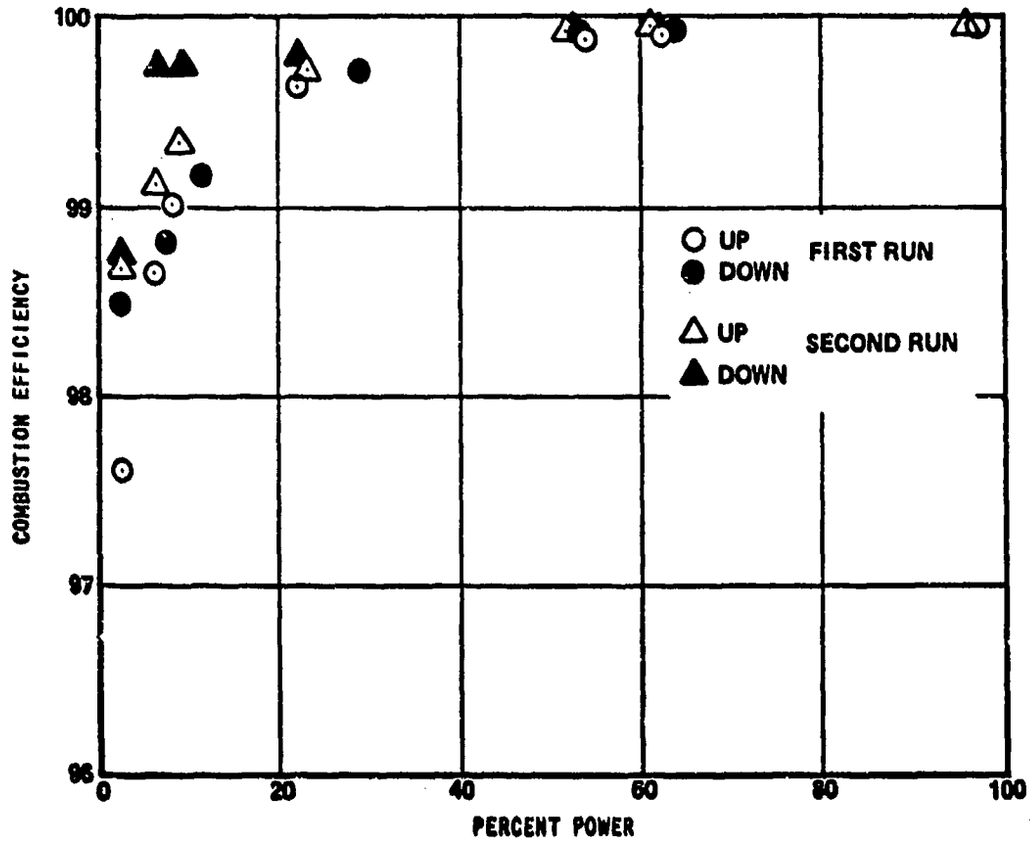

Figure 81. T55-L-11A Engine Combustion Efficiency Versus Percent Power.

Smoke emission data for the T55 engine are shown on Figure 82. Two tests were made, and the agreement between them is excellent in light of the AIA smoke number accuracy specification of ±3 (Reference 6). A marked increase in smoke concentration is shown as power increases, with a full power reading of slightly greater than 45. Smoke was not visible in this engine exhaust except when there was an oil seal failure. There was no known oil leakage during the testing portrayed in Figure 82.

Comparison of T55 Combustor and Engine Emissions

Similar comparisons of "combustor exit F/A" and "engine exit F/A" profile were made for T55 data, as was done for T53 data. A typical example is shown in Figure 83. Combustor sample data were taken at 6 degree rotation intervals with the 5-port averaging probe. Engine data were those from a single-point probe sampling path with the radius at the centroid position. Again, no similarities in the profiles were found. The conclusion reached is that the engine exhaust gas composition profile cannot be predicted from combustor exit composition profile.

To further evaluate the engine exhaust as compared with the combustor exhaust data, we performed a similar procedure as for the T53 engine. A plot of engine horsepower versus F/A of the engine and of the combustor was made from engine performance data (Figure 84). Compressor bypass bleed and turbine cooling air were included in calculating F/A. By using this information, pollutants for both combustor and engine could be plotted as a function of combustor F/A as shown in Figure 85. With three measurements, cruciform probe in the engine, engine traverse average, and laboratory traverse average, we find agreement close to within the experimental error of any one of these measurements. Since these tests were recorded over several test periods and with two separate pieces of equipment (laboratory rig and engine), the agreement is very good. The large spread in CO data appears to repeat for the three measurements--an indication that it is not fortuitous, even though the reason is not perceived.

Again, the good agreement between laboratory and engine measurements demonstrates that:

1. Laboratory measurements can be used to predict engine emissions.

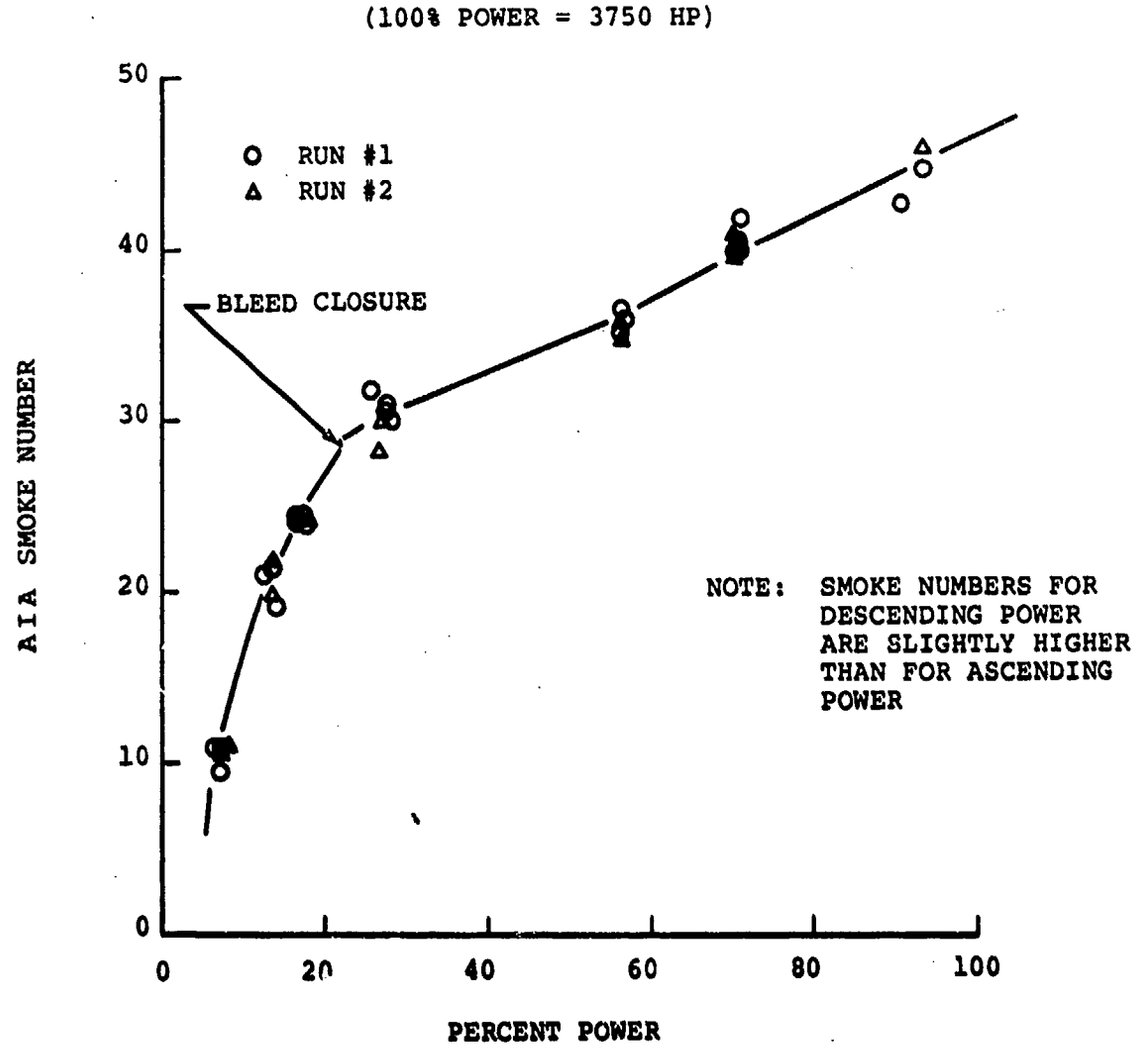

Figure 82. T55-L-11A Engine AIA Smoke Number Versus Percent Power.

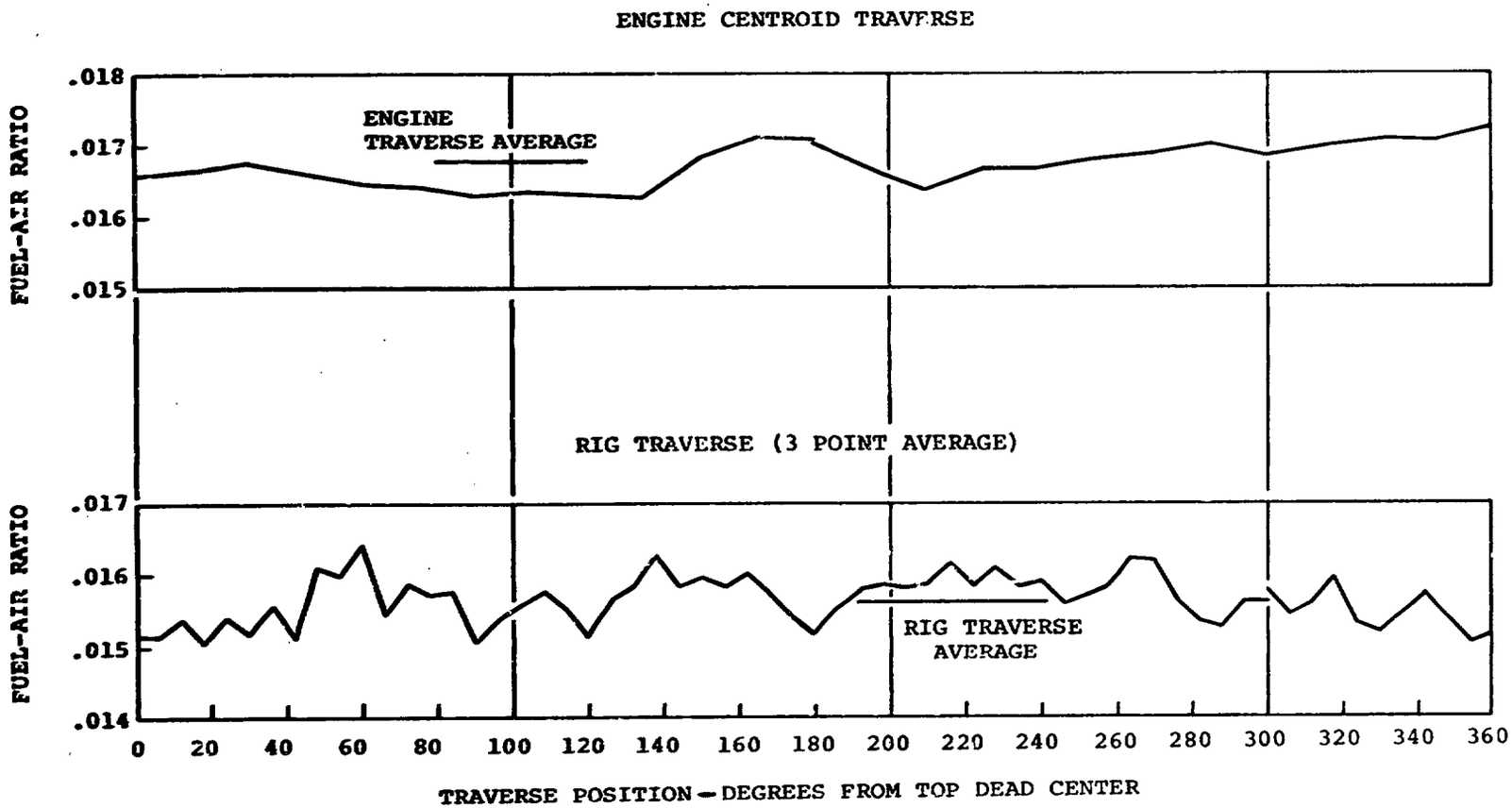

Figure 83. Fuel-Air Ratio Versus Probe Angular Position for T55 Engine and Combustor at 60 Percent Power.

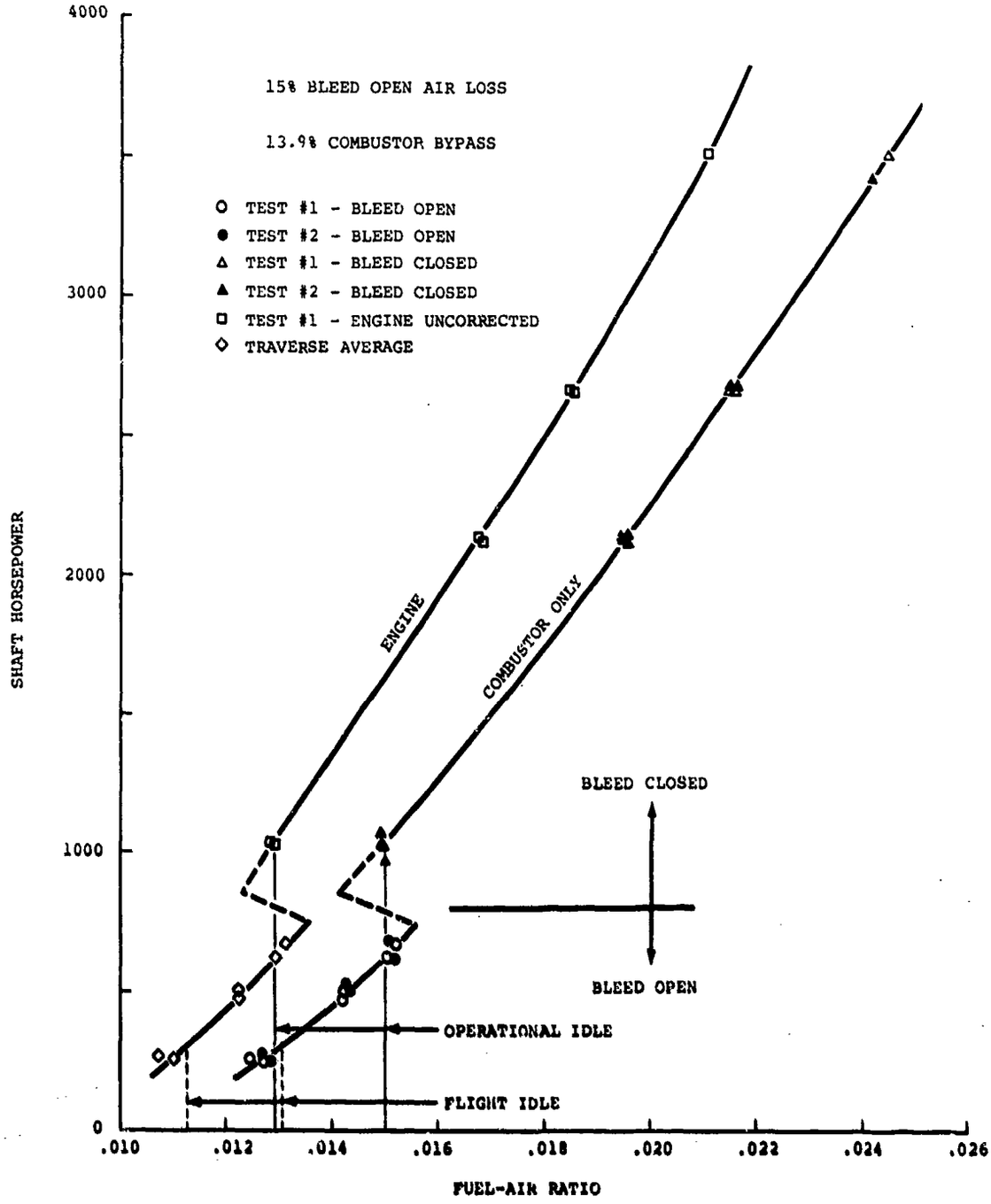

Figure 84. Fuel-Air Ratio Versus Shaft Horsepower for T55 Engine and Combustor.

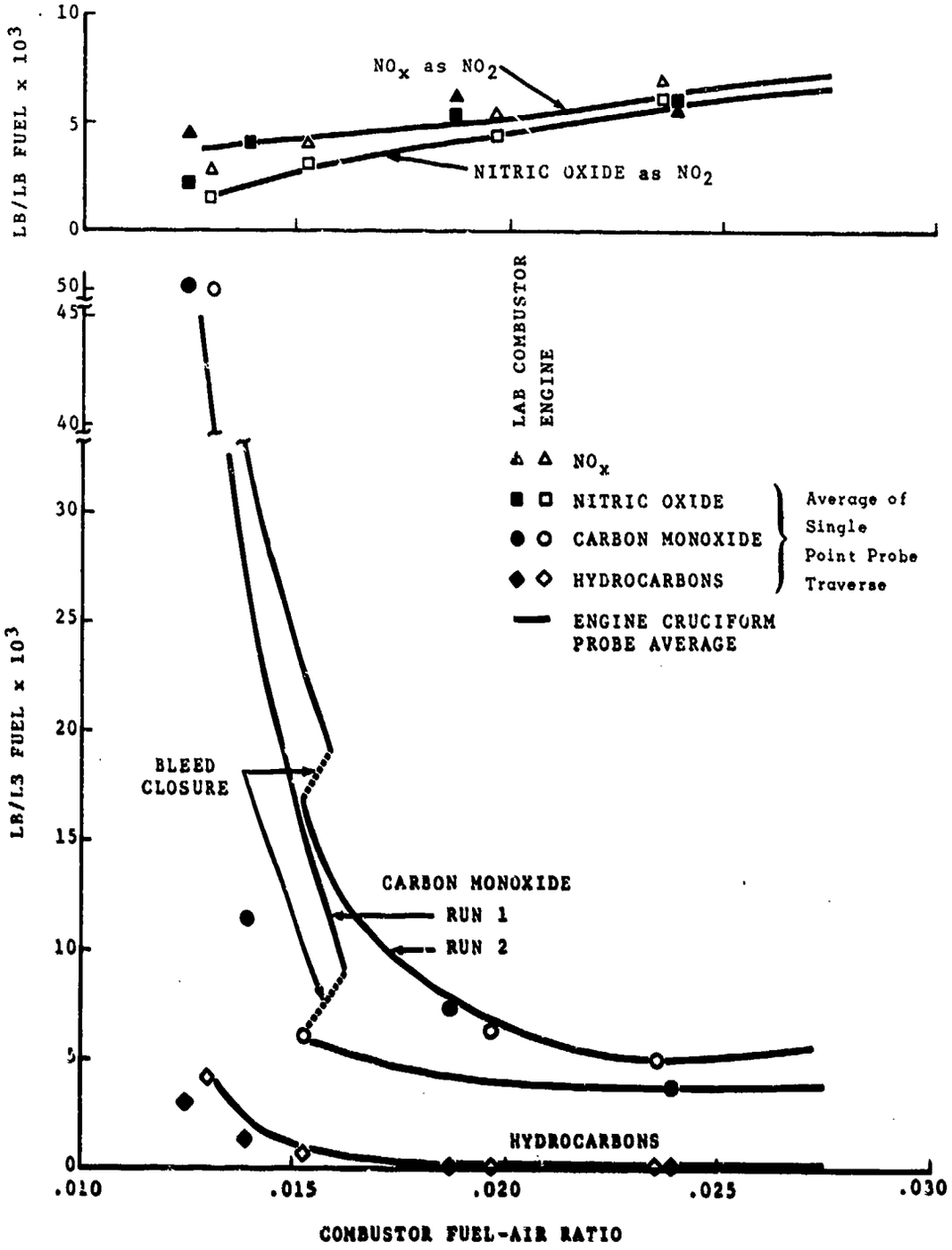

Figure 85. T55-L-11A Emissions Comparison of Engine to Laboratory Combustor Emissions.

2. Laboratory test conditions producing emissions closely approximate engine operation, even though the pressure cannot be exactly reproduced.

3. Tests produced over a period of time can reproduce similar results.

4. A good basis for engine emissions levels has been established.

CORRELATIONS

Correlations of T53 and T55 NO_x Data

The scatter of some of the T53 NO_x data was analyzed by investigating the possibility of hysteresis in the combustor performance with increasing or decreasing power. This was first found in T53 combustion efficiency, as shown on Figure 63. Two tests were made on successive days with an inlet ambient temperature change of about 10°F. The higher combustion efficiency occurred at the higher inlet air temperature, as might be expected. The major point is that after a "warming-up" period, combustion improves somewhat. Likewise, NO_x products increase. The effect of this NO_x increase in the T53 engine is shown in Figure 86 for the same tests. There appears to be some correlation between combustion efficiency and NO produced.

It is interesting to note that the engine exhaust "traverse average" data points (Figure 86) of four tests on different days over a period of 12 days all lie in and around the data from the engine "up and down" performance test run. Ambient temperature during this period was 40° to 50°F, and specific humidity varied from .0034 to .0044 pound of water per pound of air.

A similar plot of combustion efficiency (Figure 81) and an analysis of T55-L-11 nitric oxide data were made (Figure 87). The data scatter is not quite so pronounced as for the T53 engine. If hysteresis exists, it is hidden by data scatter. The change in concentration between the two test runs is small, of the order of 5 percent (Figure 87). Traverse tests, recorded on 6 different days over a period of 18 days, show scatter of the same order as the scatter from a single performance test.

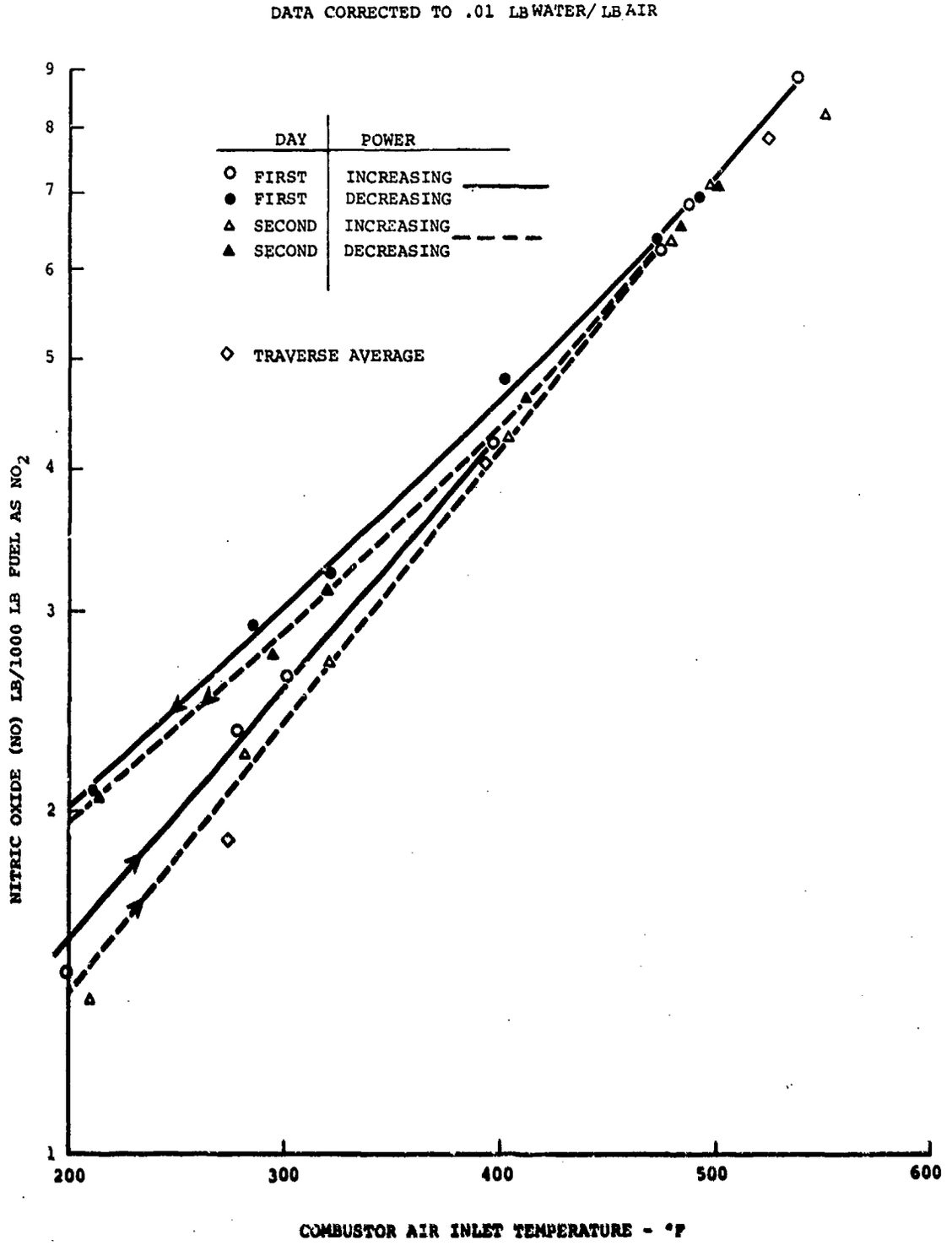

Figure 86. Inlet Air Temperature Versus Nitric Oxide Emitted for T53-L-13 Engine.

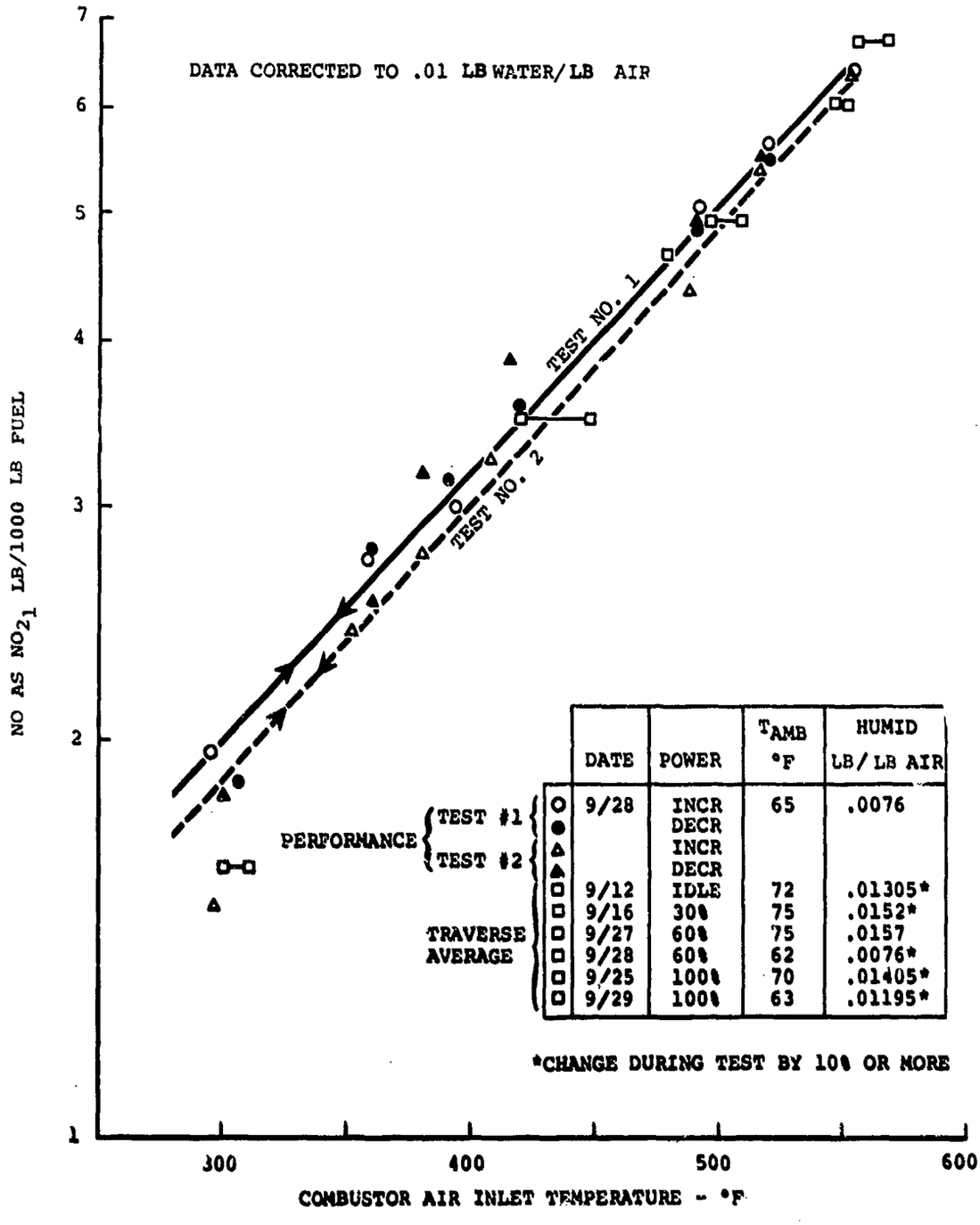

Figure 87. Inlet Air Temperature Versus Nitric Oxide Emitted for T55-L-11 Engine.

The T53 and T55 engine NO_x data were compared with each other and also with a group of engine data from Reference 28. The results are shown in Figure 88. Both T53 and T55 data bands lie mostly within the data band spread of Reference 28. The T55 NO_x is about 30 percent less than that of the T53. The combustor residence time in the T55 is approximately one-half that in the T53. Because NO_x formation is a time function, the difference is reasonable.

Lipfert's compiled data (Reference 28) are for many different gas turbine engines, and obviously, they do not all have the same combustion chamber residence time. Most of the T53 and T55 NO_x data lie within this band. It can be logically assumed that different combustor residence time could account for the major portion of data spread. However, a difference in slope for both T53 and T55 is noted on Figure 88.

Other Correlations and Comparisons

The three measurements, (1) engine cruciform probe, (2) engine traverse average, and (3) laboratory traverse average, were used to calculate combustion efficiency for the T53 and T55 engines. The variation in the calculated combustion efficiency is in nearly all cases less than 0.5 percent (Figures 89 and 90). At the upper power range, agreement is of the order of 0.1 percent for nearly all cases.

This agreement exists in spite of the time, operating conditions, test rig versus engine, and measurement variables. Both exhaust gas composition and measurement precision for both combustor and engine tests were in close agreement.

Another comparison of combustion efficiency in both Lycoming T53 and T55 engines with a group of gas turbine results from Reference 4 is shown in Figure 91. The Lycoming engines are grouped near the upper portion of the combustion efficiency band. Because pollutant CO and HC are directly responsible for loss in combustion efficiency, this infers that these two engines are among the better gas turbines from the standpoint of CO and HC pollution.

Summary of T53 and T55 Gas Analysis

A brief summary of the gaseous emission results from these tests is shown in Table VI. The emission values listed are average numbers to provide the reader with a quick comparison. More precise values and their range must be obtained by closer examination of the data.

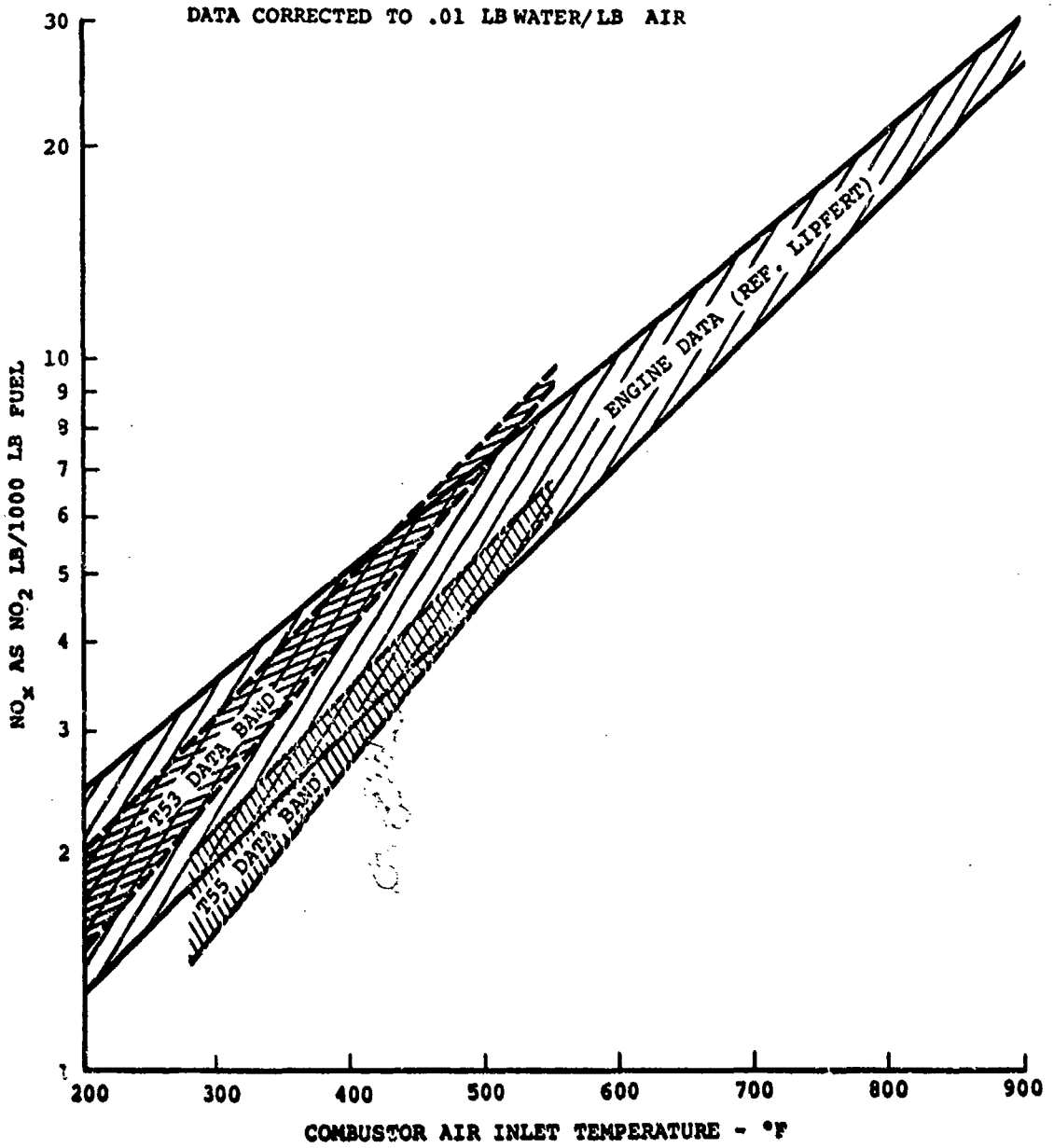

Figure 88. NO_x Versus Inlet Temperature for Several Large and Small Gas Turbines Compared to T53 and T55 Emissions.

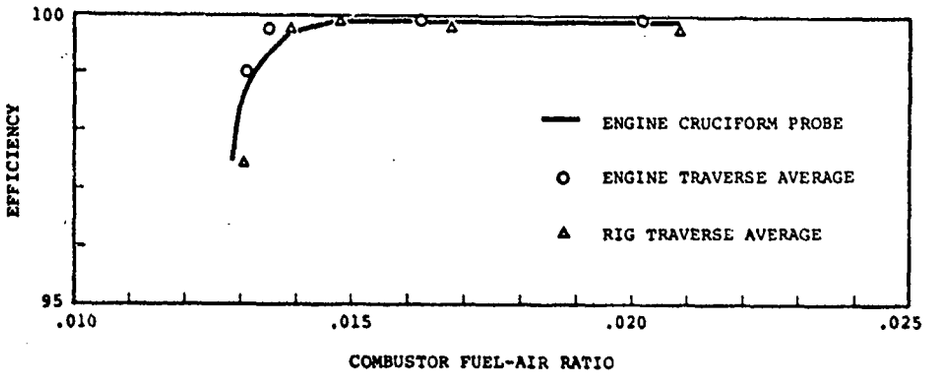

Figure 89. Comparison of T53-L-13 Combustion Efficiency Versus Fuel-Air Ratio for Engine and Laboratory Data.

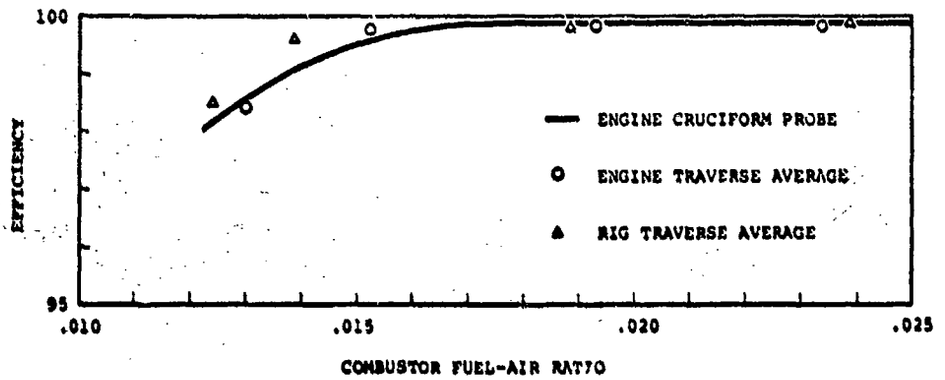

Figure 90. Comparison of T55-L-11A Combustor Combustion Efficiency Versus Fuel-Air Ratio for Engine and Laboratory Data.

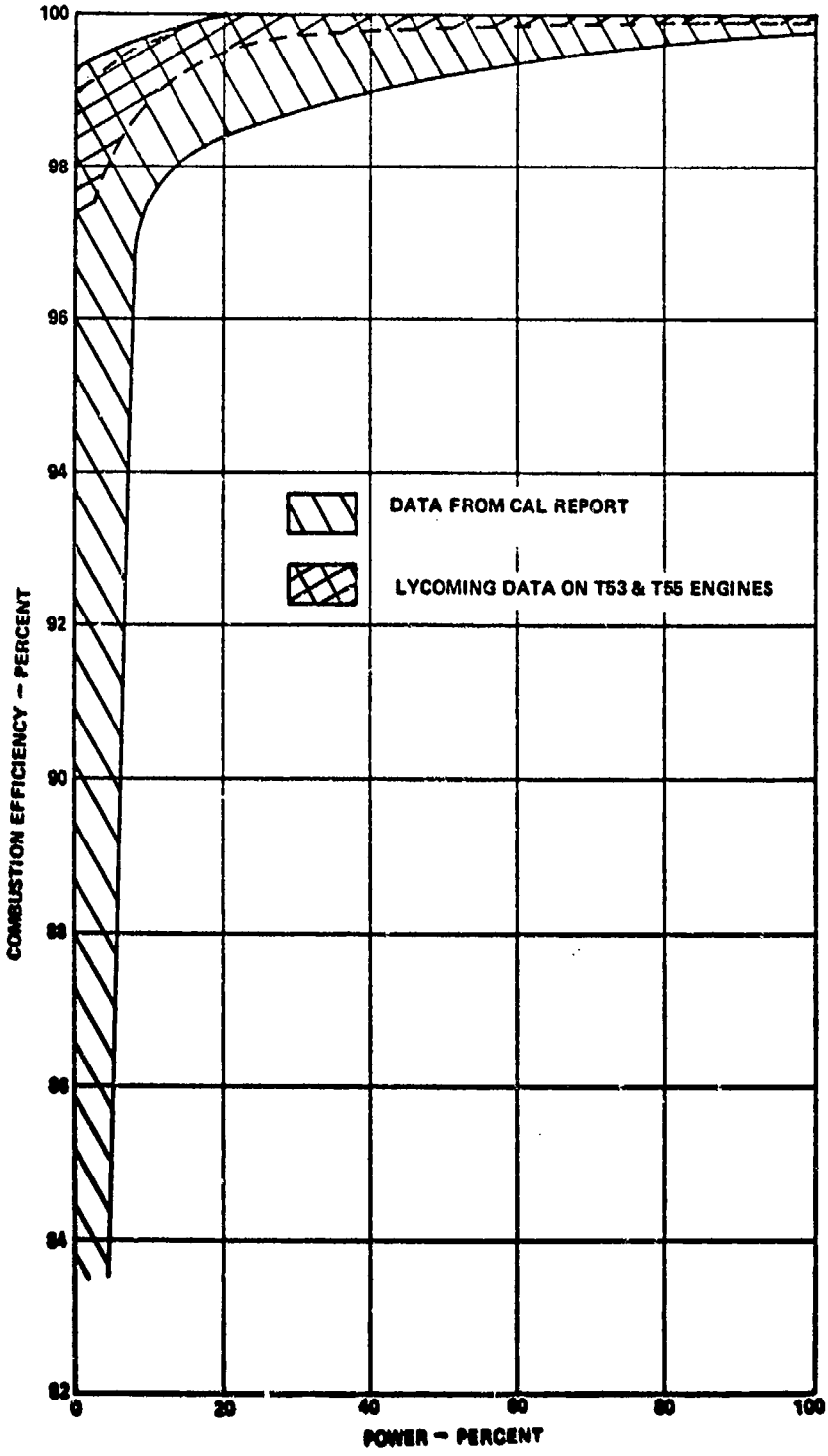

Figure 91. Comparison of Combustion Efficiency Data Variation Versus Power for CAL Report Engines and Lycoming T53 and T55.

TABLE VI. SUMMARY OF EMISSIONS FROM LYCOMING T53-L-13A AND T55-L-11A ENGINES

Engine	Power (%)	Summary of Emissions Data Taken From T53-L-13A Engine K121 J and T55-L-11A Engine B19Q								Average Values For Each Engine Model	
		CO		HC		NO(As NO_2)		NO_x(As NO_2)			
		ppm	EI	ppmC	EI	ppm	EI	ppm	EI	F/A (Gas Analysis)	Comb. Air Inlet Temp. (^{o}F)	Fuel Flow (pph)
T53	Oper. Idle	290	25	75	3.0	18	2.5	26	3.5	.0113	270	205
	30	93	7	17	0.7	38	5.0	45	5.9	.0123	390	360
	60	24	1.5	12	0.4	70	7.4	76	8.0	.0150	455	570
	100	15	0.8	12	0.3	103	9.0	104	9.1	.0180	522	800
T55	Oper. idle	220	21	20	1.1	28	3.1	39	6.4	.0135	400	800
	30	130	10	16	0.6	31	3.7	39	4.5	.0133	430	850
	60	100	5	7	0.2	57	4.9	67	5.8	.0184	500	1320
	100	110	5	7	0.2	98	6.8	109	7.5	.0230	560	1900

Operational Idle: T53-83 HP; T55-1000 HP. T53 Operation Idle is at 68% N_1.
100%: T53-1400 HP; T55-3750 HP.

COMPARISON OF LYCOMING AND NAVY EMISSIONS DATA FROM THE T53 AND T55

GAS ANALYSIS

To further evaluate the results of the emission measurements on the T53 and T55 engines, we considered the results from Navy tests on other units of the same model engine as reported in References 2 and 3, and compared these data with those of the present tests. The emission levels versus power for Navy tests are shown for the two engines in Figures 92 and 93. These data are plotted on the same chart with Lycoming data, shown as bands with a distribution spread (Figures 94 and 95). For the T53 comparison (Figure 94), agreement is quite good for hydrocarbons and CO. There was less spread in the Navy data, mostly because fewer data points were recorded. NO_2 concentration was somewhat higher in Lycoming measured data, and is certainly explainable in terms of expected measurement precision and engine variations.

For the T55, agreement was better for hydrocarbons and NO_2 and for CO at low power. The more pronounced higher concentration of CO from Navy data at the higher power settings is not serious; however, a good explanation is not obvious.

If we construct an "average" curve of concentration of each pollutant for each engine, then comparisons are more obvious (Figures 96 and 97). The confidence level for Lycoming data is high because:

1. Many data points were recorded.
2. Sample validity was checked by constant F/A calculations and compared with the engine input F/A.
3. Frequent checks were made on instrument accuracy.
4. Emission correlation comparisons between engine and combustor rig tests all show agreement within the data band spread (usually 10 percent or less). If we assume that Navy data are equally valid, then the only measurements that appear conflicting are the CO data for the T55 engine.

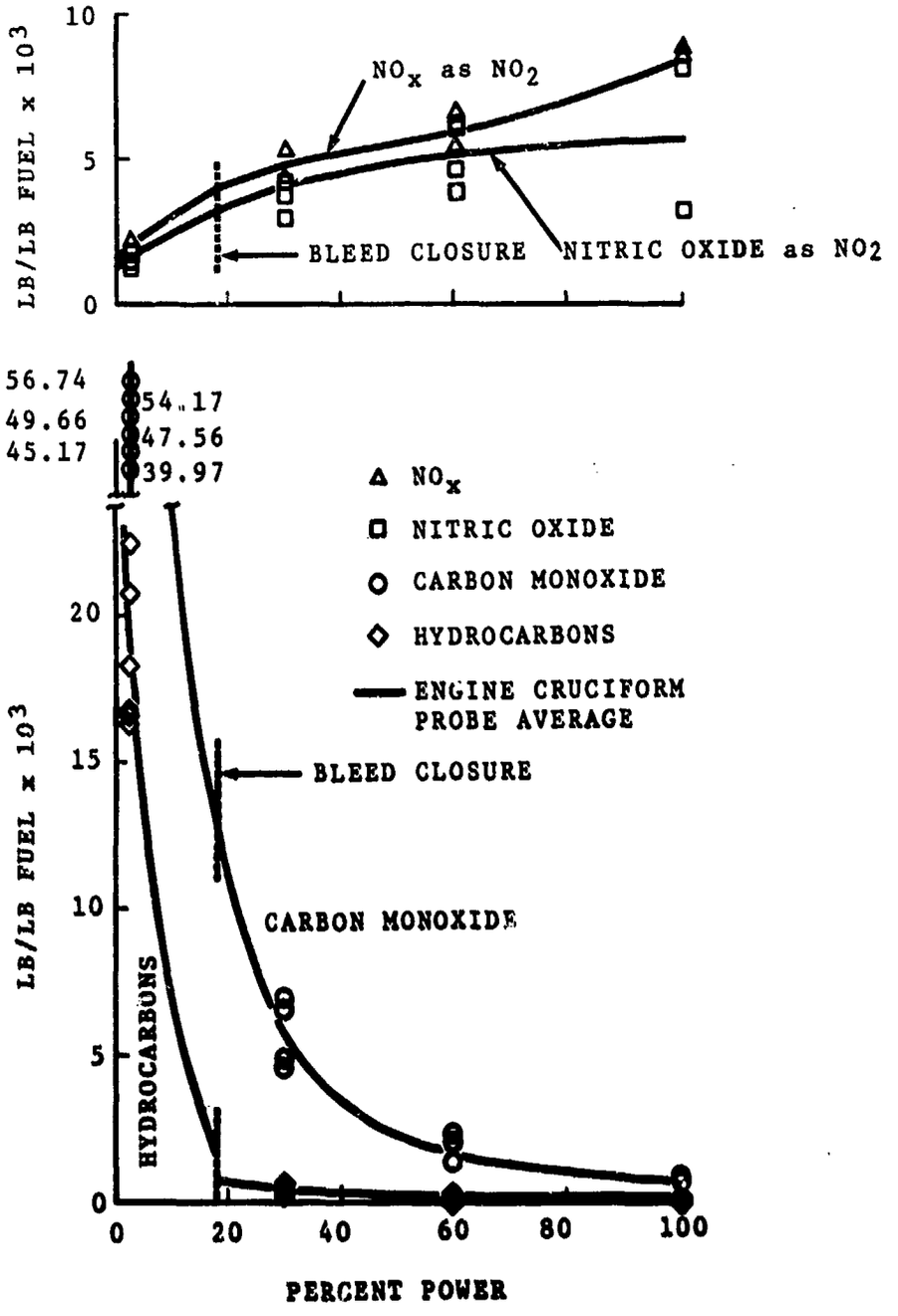

Figure 92. Navy Air Propulsion Test Center T53-L-13A Engine Data.

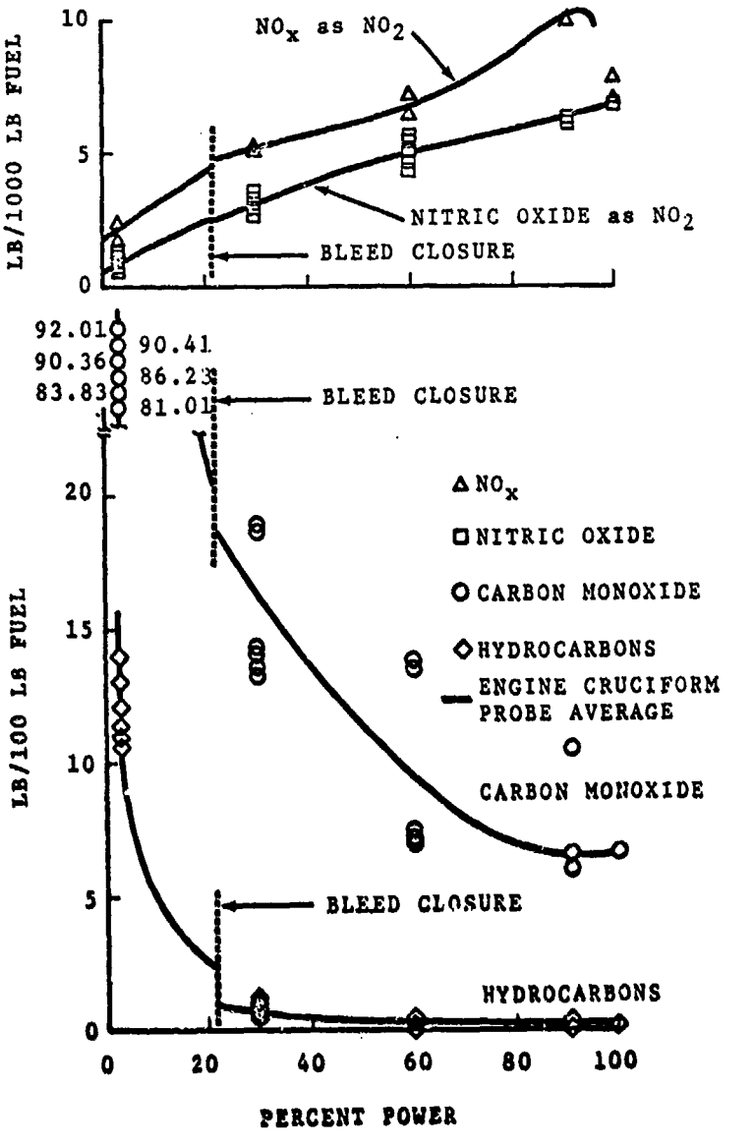

Figure 93. Navy Air Propulsion Test Center T55-L-11A Engine Data.

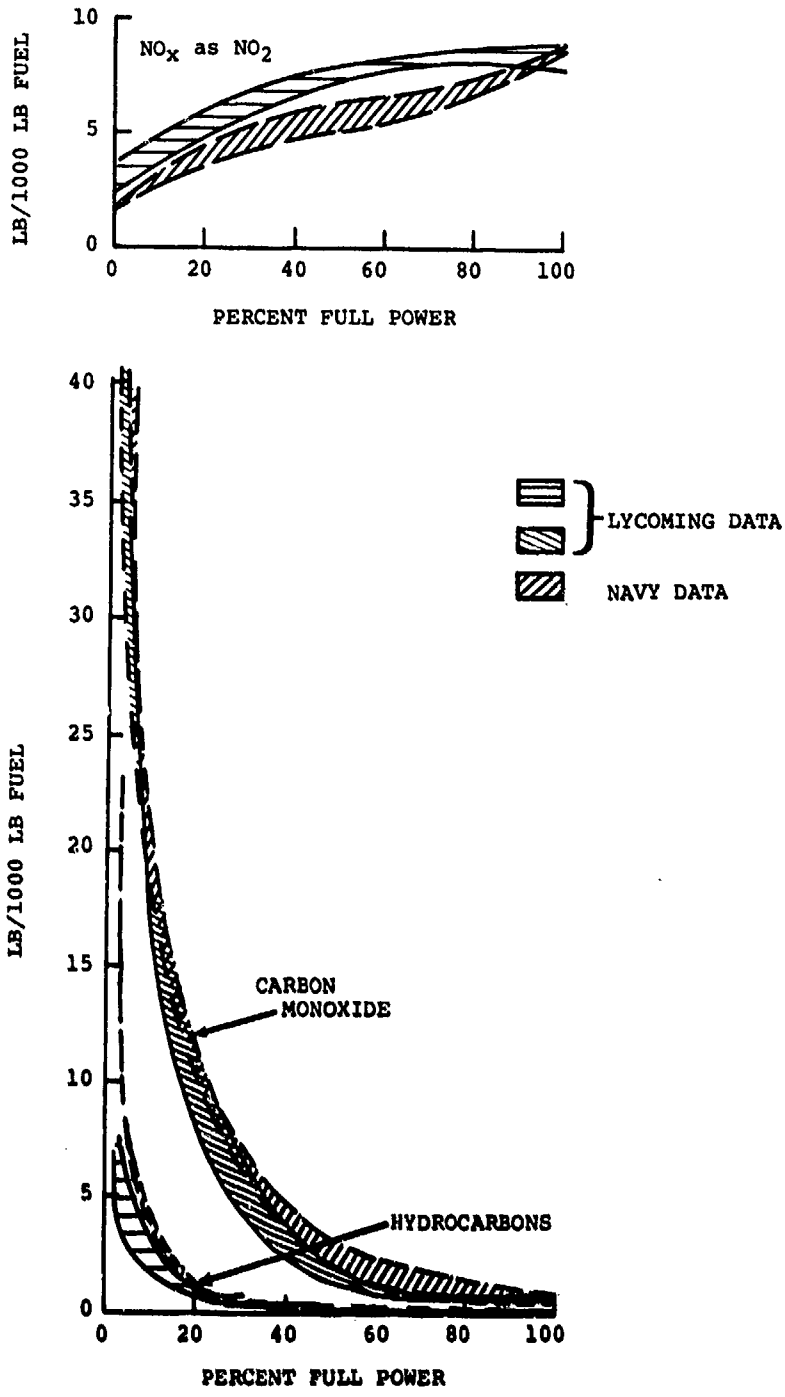

Figure 94. Comparison of T53-L-13A Emission Data Band From Lycoming and Navy Tests.

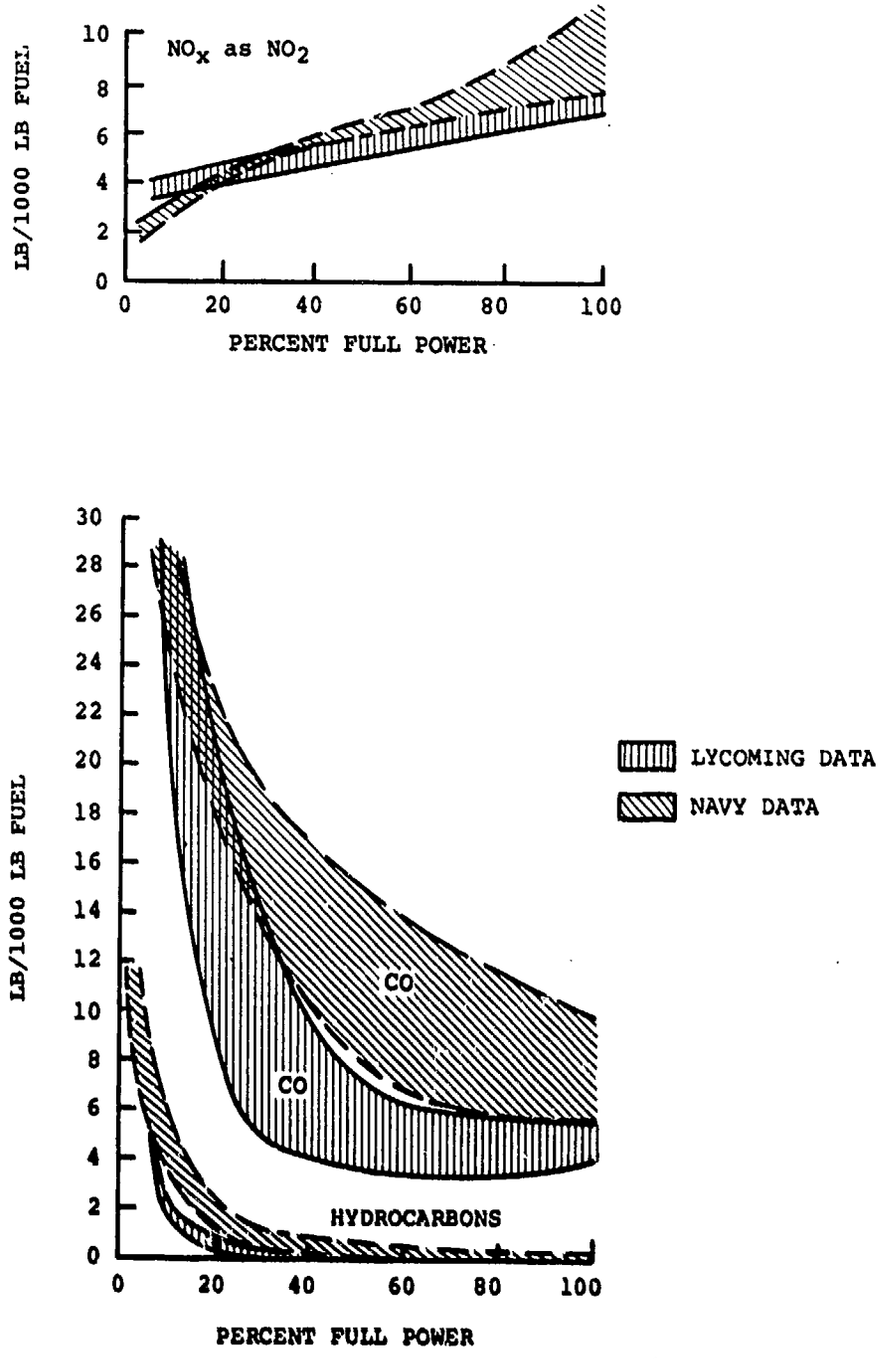

Figure 95. Comparison of T55-L-11A Emission Data Band From Lycoming and Navy Tests.

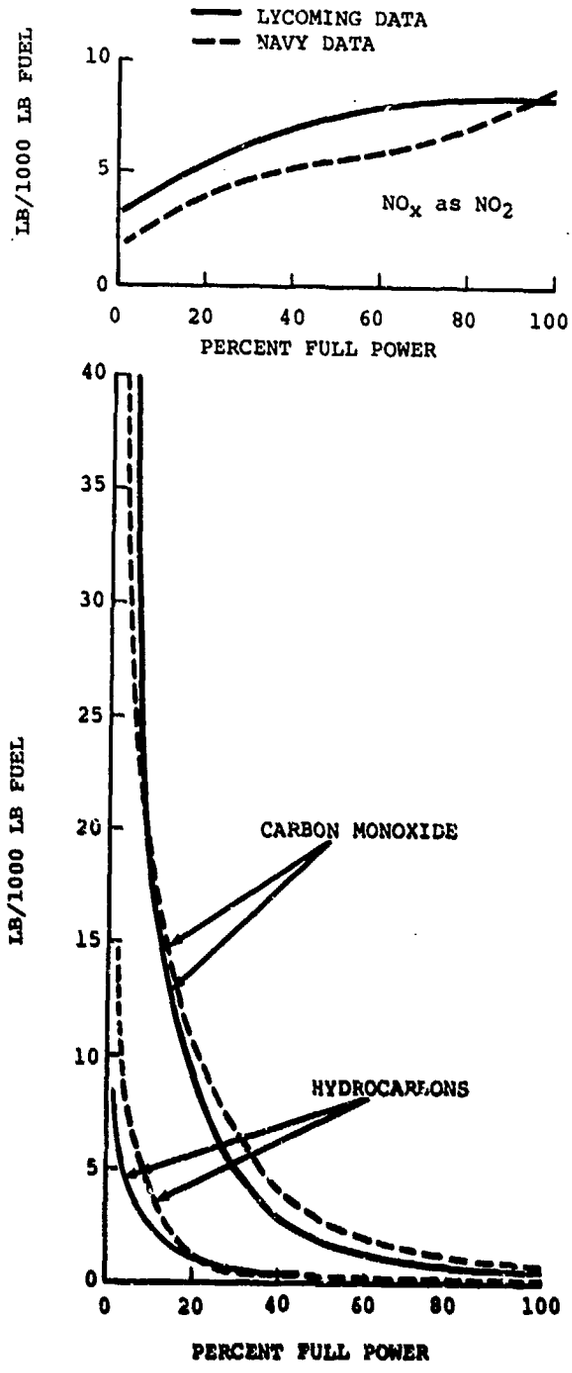

Figure 96. Comparison of T53-L-13 Average Emission Data From Lycoming and Navy Tests.

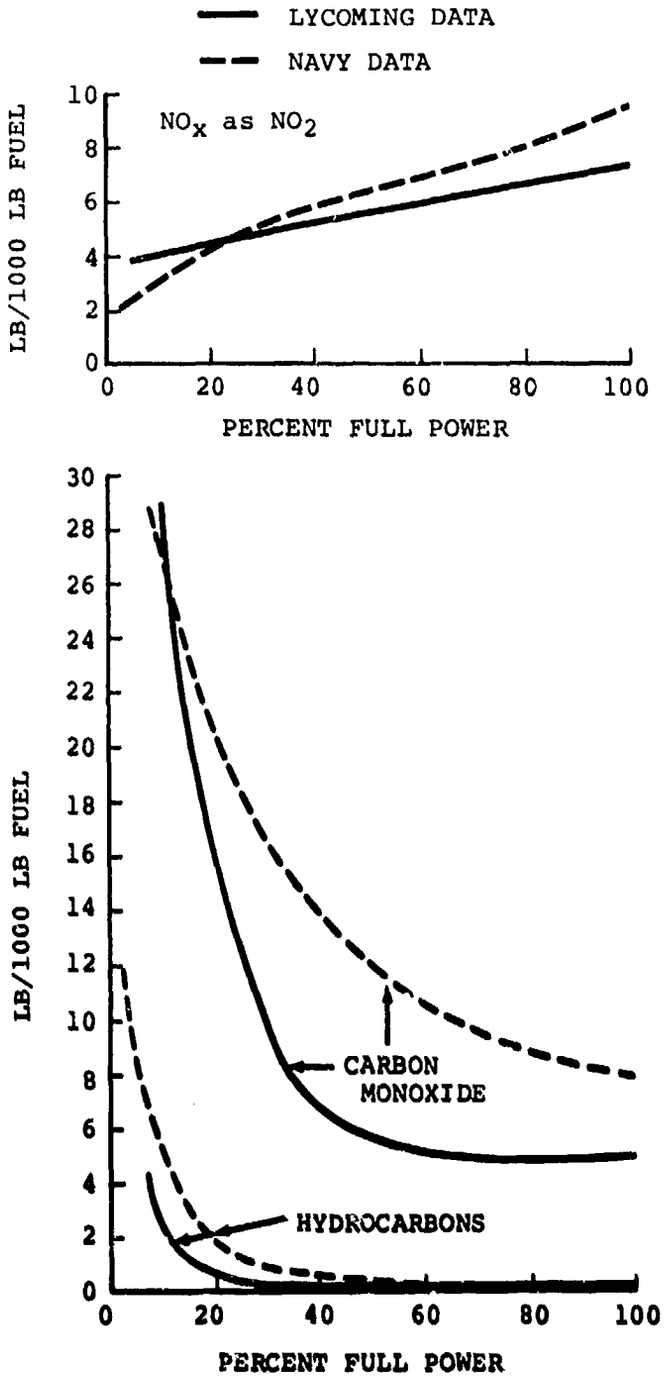

Figure 97. Comparison of T55-L-11A Average Emission Data From Lycoming and Navy Tests.

This being the case, we cannot explain the differences with the Navy test data on the basis of errors in measurement for the T55, since there is good agreement for CO for the T53 engine. Therefore, the difference must be the result of a real difference in gas composition, or a difference in methods or techniques of measurement for the Navy tests.

COMPARISON OF SMOKE DATA FROM LYCOMING AND NAVY TESTS

Smoke data from the Lycoming tests were plotted and compared with smoke data from the Navy tests (References 2 and 3), as shown on Figure 98 for the T53 engine. Although the slopes of the curves are similar, the peak value of the smoke number is about 9 units higher from Navy data. In Reference 2, it is stated the SAE-ARP 1179 was followed in measuring the smoke. The same procedures were followed at Lycoming. If we assume that the numbers obtained are equally valid within $\pm$ 3 smoke numbers, then obviously one of these engines produces more smoke than the other. However, smoke should not be visible in either case.

A similar correlation of curve shape for both Lycoming and Navy data is noted for smoke comparisons in the T55 engine (Figure 99). Again, Navy data show smoke numbers about 10 units higher. The reasons could be the inherent differences between the two engines, the differences in measurement equipment, or both. It is not possible to state which of these effects are present.

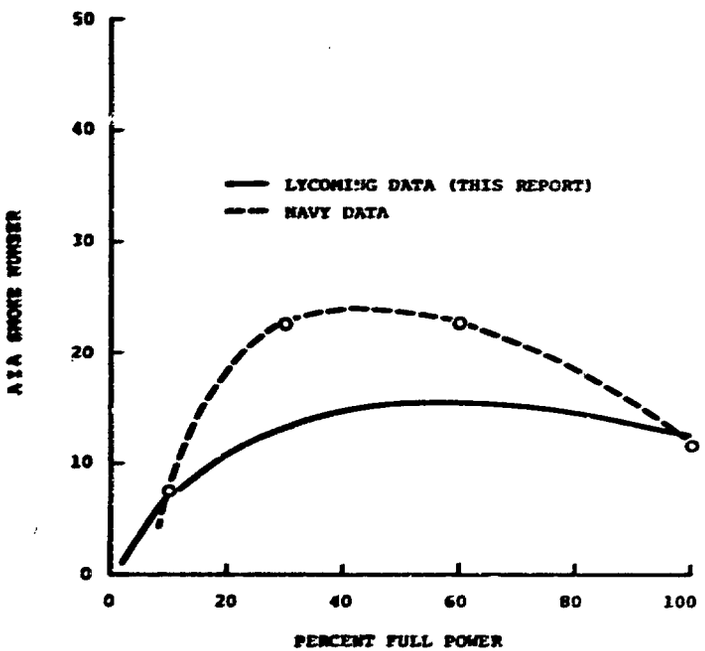

Figure 98. Comparison of T53 Smoke Number Measurements From Lycoming and Navy Data.

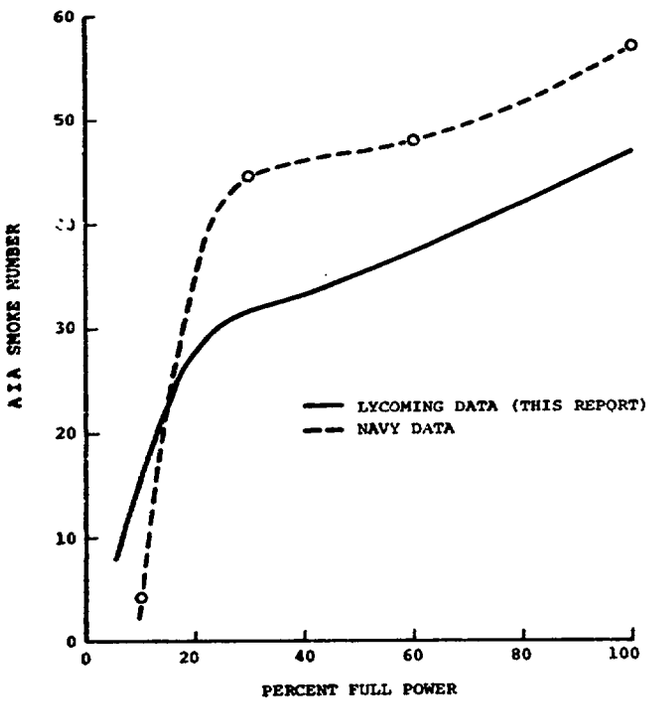

Figure 99. Comparison of T55 Smoke Number Measurements From Lycoming and Navy Data.

CONCLUSIONS AND RECOMMENDATIONS

Conclusions

1. The emissions data obtained in these tests of T53 and T55 engines is in reasonable agreement with previous data taken on these engines.

2. Two engine exhaust gas probe configurations were tested:

   a. Single-point probe used in a traverse of the exhaust

   b. Cruciform or multipoint averaging probe

   Analyzed gas samples from the two measurements agreed within 5 to 10 percent of each other. This establishes the cruciform averaging type of probe as a satisfactory method of sampling the exhaust gas in these engines. The cruciform probe is by far the simplest probe in use.

3. The laboratory combustor tests provided excellent means of measuring gaseous composition and pollutants, and these data could be used to predict engine emissions. This was true even though laboratory rig operating pressure was less than the maximum engine design operating pressure. Temperature simulation was more important and was duplicated in the laboratory tests.

4. The criteria used for determining whether the gas sample is representative of the stream were as recommended by the SAE-ARP 1256. The ARP specifies that engine (or combustor) independent F/A measurement shall agree with the gas analysis calculated F/A within 15 percent. In these tests, agreement was within 5 to 10 percent, or better than required.

5. There was no apparent correlation of the circumferential traverse shape between engine and laboratory, nor was there a significant correlation in either case to the mechanical structure of the rig or engine. However, the engine exhaust profiles of all constituents were smoother than the profiles observed in the combustor rig due to the smoothing action of the turbine and exhaust diffuser.

6. Smoke is invisible in the exhaust of both of these engines at all operating conditions. The one exception occurred when a T55 oil seal failed.

7. NO_x measurements were in nearly all cases approximately 10 to 20 ppm higher than NO measurements.

Recommendations

1. The "Cruciform" or averaging-type probe is recommended as satisfactory for emission measurements on T53 and T55 engines. Further investigations are needed to establish the advisability of using this type of sampling probe on other gas turbine exhausts.

2. Questions of NO_2 formation and measurement need further investigation to improve the reliability of the NO_x measurement.

3. A standard calibration gas checking system should be developed so that all agencies engaged in engine emission analysis have the opportunity to check their analyzer equipment against established gas sample bottles.

LITERATURE CITED

1. Nelson, A. W., EXHAUST EMISSION CHARACTERISTICS OF AIRCRAFT GAS TURBINE ENGINES, ASME Paper 72-GT-75, March 1972.

2. Stumke, F. B., Jr., ARMY MIPR AMRDL 71-6-T53-L-13A ENGINE; RESULTS OF EXHAUST EMISSIONS TESTS ON (Report), AEFL:GS:er, 10340, Ser. 370, Naval Air Propulsion Test Center, 19 July 1972.

3. Stumke, F. B., Jr., ARMY MIPR AMRDL 71-6 - T55-L-11A ENGINE; RESULTS OF EXHAUST EMISSIONS TEST ON (Report), AEL1:GS:er, 10340, Ser. 322, Naval Air Propulsion Test Center, 22 March 1972.

4. McAdams, H. T., ANALYSIS OF AIRCRAFT EXHAUST EMISSION MEASUREMENTS: STATISTICS, Cornell Aero Laboratory, Report NA-5007-K-2, Prepared for Environmental Protection Agency, November 1971.

5. Panas, G., EXHAUST EMISSIONS EVALUATION ON T53-L-13B AND T55-L-11A, B-19Q ENGINES: - ENGINE TEST OPERATIONS AND DATA, Avco Lycoming Report R-0113-902-72 and R-0211-906-72, November 1972.

6. AIRCRAFT GAS TURBINE EXHAUST SMOKE MEASUREMENT, SAE Aerospace Recommended Practice, Report ARP 1179, 4 May 1970.

7. Rubins, P. M., GAS ANALYSIS EVALUATION OF GAS TURBINE ENGINES AND COMBUSTORS, Avco Lycoming Report 4235. 2. 18, May 1972.

8. Toone, B., and Arkless, R., THE APPLICATION OF GAS ANALYSIS TO COMBUSTION CHAMBER DEVELOPMENT, Seventh Symposium (International) on Combustion, Butterworths, London, 1959, pp. 929-937.

9. Perry, J. H., CHEMICAL ENGINEERS HANDBOOK, 4th Ed., McGraw-Hill, New York, 1969.

10. Kolesar, K., CALCULATION METHODS USED IN IBM PROGRAM K110, Avco Lycoming Memo D3-f-026-69, 16 May 1969.

11. Chapier, J., ONE-SPOOL ENGINE BASIC PERFORMANCE DATA, SYSTEM 360/144, Avco Lycoming Memo Program No. E147, 30 January 1970.

12. Doyle, B., GAS ANALYSIS DATA REDUCTIONS SYSTEM 370/155, Avco Lycoming Memo Program No. K-120, 27 July 1972.

13. Cassidy, F., Fresia, J., Tinter, J., and Chantland, R., DS-5 DATA ACQUISITION SYSTEM, OPERATION MANUAL, Avco Lycoming Standard Operating Procedure, Revised 15 April 1967.

14. CALIBRATION SYSTEM REQUIREMENTS, Military Specification MIL-C-45662A, 9 February 1962.

15. C. Glenn, MEASUREMENT AND TEST EQUIPMENT CALIBRATION SYSTEMS, Avco Lycoming Memo IES-1, March 1972.

16. Dick, R., and Hartmann, C.H., CRITICAL EVALUATION OF THE RESPONSE CHARACTERISTICS OF THE HYDROGEN FLAME DETECTOR, Varian Aerograph Tech. Bull. 133-67, 1966.

17. PROCEDURE FOR THE CONTINUOUS SAMPLING AND MEASUREMENT OF GASEOUS EMISSIONS FROM AIRCRAFT TURBINE ENGINES, SAE Aerospace Recommended Practice, ARP 1256, 1 October 1971.

18. T53 AND T55 GAS TURBINE ENGINE EXHAUST EMISSIONS MEASUREMENT, Contract DAAJ02-72-C-0102, U.S. Army Air Mobility Research and Development Laboratory, Ft. Eustis, Virginia, June 1972.

19. Caretto, L.S., Muzio, L.J., Sawyer, R.F., and Starkman, E.S., THE ROLE OF KINETICS IN ENGINE EMISSION OF NITRIC OXIDE, Combustion Science and Technology, Vol. 3, 1971, pp. 53-61.

20. LaMantia, C.R., and Field, E.L., TACKLING THE PROBLEM OF NITROGEN OXIDES, Power, April 1969.

21. Mikus, T., and Heywood, J. B., THE AUTOMOTIVE GAS TURBINE AND NITRIC OXIDE EMISSIONS, Combustion Science and Technology, Vol. 4, 1971, pp. 149-158.

22. Heywood, J. B., Fay, J. A., and Linden, L. H., JET AIRCRAFT AIR POLLUTANT PRODUCTION AND DISPERSION, AIAA Paper 70-115, January 1970.

23. Marteney, P. J., ANALYTICAL STUDY OF THE KINETICS OF FORMATION OF NITROGEN OXIDE IN HYDROGEN AIR COMBUSTION, Combustion Science and Technology, Vol. 1, 1970, pp. 461-469.

24. Westenberg, A. A., KINETICS OF NO AND CO IN LEAN, PREMIXED HYDROCARBON-AIR FLAMES, Combustion Science and Technology, Vol. 4, 1971, pp. 59-64.

25. Hazard, H. R., NO_x EMISSION FROM EXPERIMENTAL COMPACT COMBUSTORS, ASME Paper 72-GT-108, March 1972.

26. Bowman, C. T., KINETICS OF NITRIC OXIDE FORMATION IN COMBUSTION PROCESSES, Paper Presented at 14th Symposium (International) on Combustion, August 1972.

27. Cox, F. W., Penn, F. W., and Chase, J. O., A FIELD SURVEY OF EMISSIONS FROM AIRCRAFT TURBINE ENGINES, U. S. Bur. Mines Report RI-7634 (Dept. of the Interior), 1972.

28. Lipfert, F. W., CORRELATION OF GAS TURBINE EMISSIONS DATA, ASME Paper 72-GT-68, March 1972.

29. Hilt, M. B., and Johnson, R. H., NITRIC OXIDE ABATEMENT IN HEAVY DUTY GAS TURBINE COMBUSTORS BY MEANS OF AERODYNAMICS AND WATER INJECTION, ASME Paper 72-GT-53, March 1972.

30. Klapatch, R. D., and Koblish, T. R., NITROGEN OXIDE CONTROL WITH WATER INJECTION IN GAS TURBINES, ASME Paper 71-WA/GT-9, November-December 1971.

31. Shaw, H., REDUCTION OF NITROGEN OXIDE EMISSIONS FROM A GAS TURBINE COMBUSTOR BY FUEL MODIFICATIONS, ASME Paper to be presented at 1973 Gas Turbine Conference.

32. Keenan, J.H., and Kaye, J., GAS TABLES, Wiley, New York, 1957, pp. 157 ff.

33. AIRCRAFT AND AIRCRAFT ENGINES, PROPOSED STANDARDS FOR CONTROL OF AIR POLLUTION, Environmental Protection Agency, Federal Register, Vol. 37, No. 239, 12 December 1972.

34. Nelson, A.W., Davis, J.C., and Medlin, C.H., PROGRESS IN TECHNIQUES FOR MEASUREMENT OF GAS TURBINE EXHAUST EMISSIONS, AIAA Paper 72-1199, November 1972.

APPENDIX I
T53 LABORATORY COMBUSTOR RIG TRAVERSE DATA

This appendix presents computer "Calcomp" plots (Figures 100 through 111) of all the emission traverse data taken in the T53 combustor test rigs only. Each simulated power condition (idle, 30, 60, and 100 percent) is represented by three separate plots:

1. Performance summary plot showing fuel-air ratio, combustion efficiency, and the separate component contribution to combustion inefficiency

2. Emissions in ppm volume for CO, HC, NO, and NO_x (hydrocarbons are ppmC)

3. Emissions index (EI) in pounds per 1000 pounds of fuel for each component

Scales for the performance summary plot are constant, but the scale for each of the emission plots is computer-selected to attain the largest value on the scale. Traverse position is in degrees from the rig starting point; the T53 rig starts at 180° (bottom center). This is significant in comparing results from the rig with engine data or with rig temperature traverses which start at top dead-center. Symbols on the plots have the following meaning:

* Net combustor efficiency

¤ Fuel-air ratio

C CO (inefficiency, emission index or ppm)

Y HC (inefficiency, emission index, or ppmC)

X NO (emission index or ppm)

Z NO_x (emission index or ppm)

A study of this data will reveal several irregularities that require explanation. The most significant of these are:

1. Traverse data of the T53 combustor during the idle run showed a low fuel-air ratio zone between 300 and 20 degrees.

A posttest examination of the fuel manifold showed several blocked or partially blocked fuel nozzles in the same region.

2. The indicated CO during the first T53 30-percent power point does not appear consistent with previous measurements, although the fluctuations appear to be similar to the fluctuations of other components. Instrument malfunction is suspected. This traverse was repeated. A second set of data shcwn is more reasonable.

3. NO_x data for several runs are not as precise as might be desired. Interference of other gaseous components with the polarographic sensor is a suggested cause.

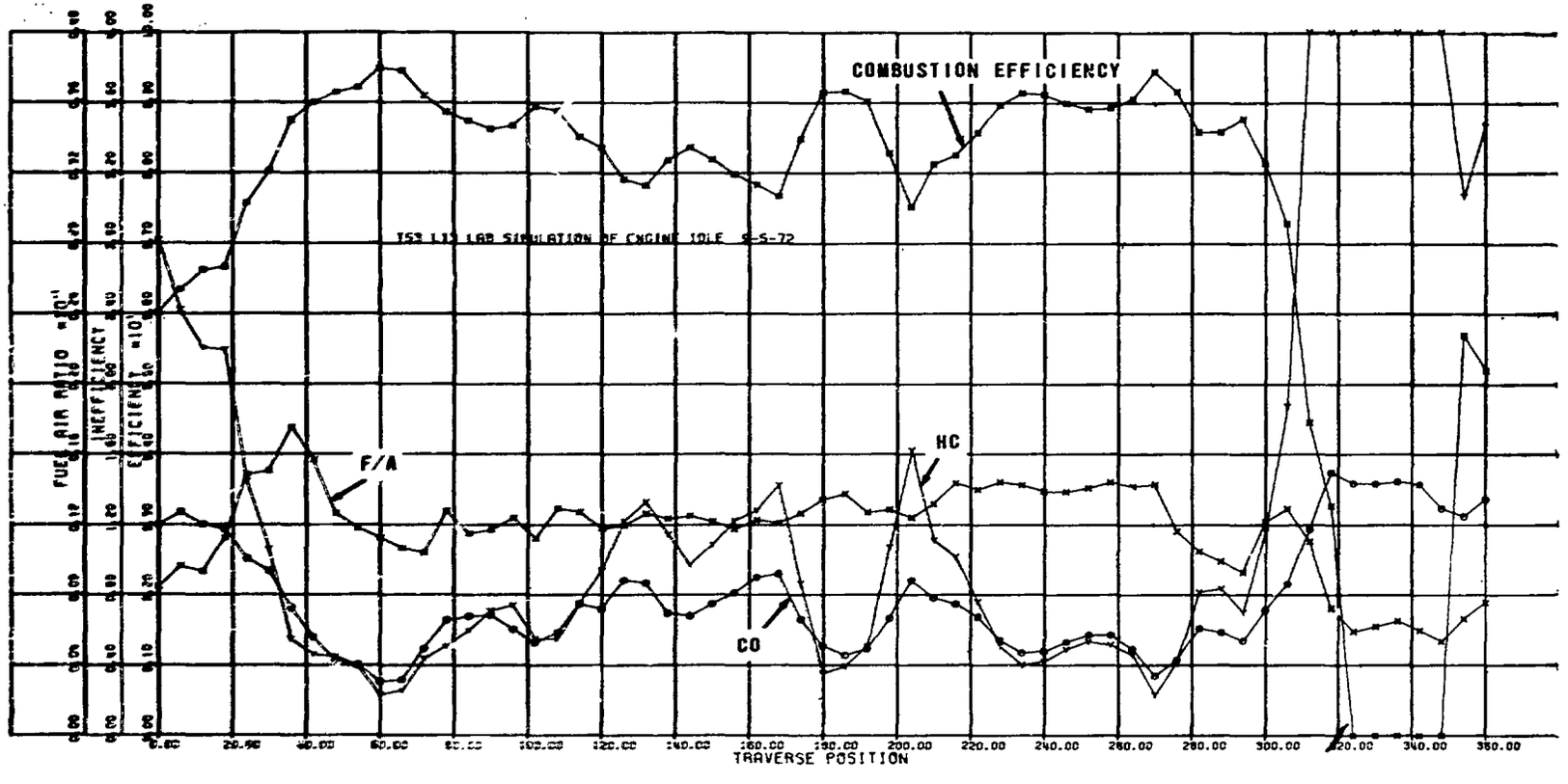

Figure 100. T53 Laboratory Combustor, Fuel-Air Ratio and Efficiency Versus Traverse Angle at Idle.

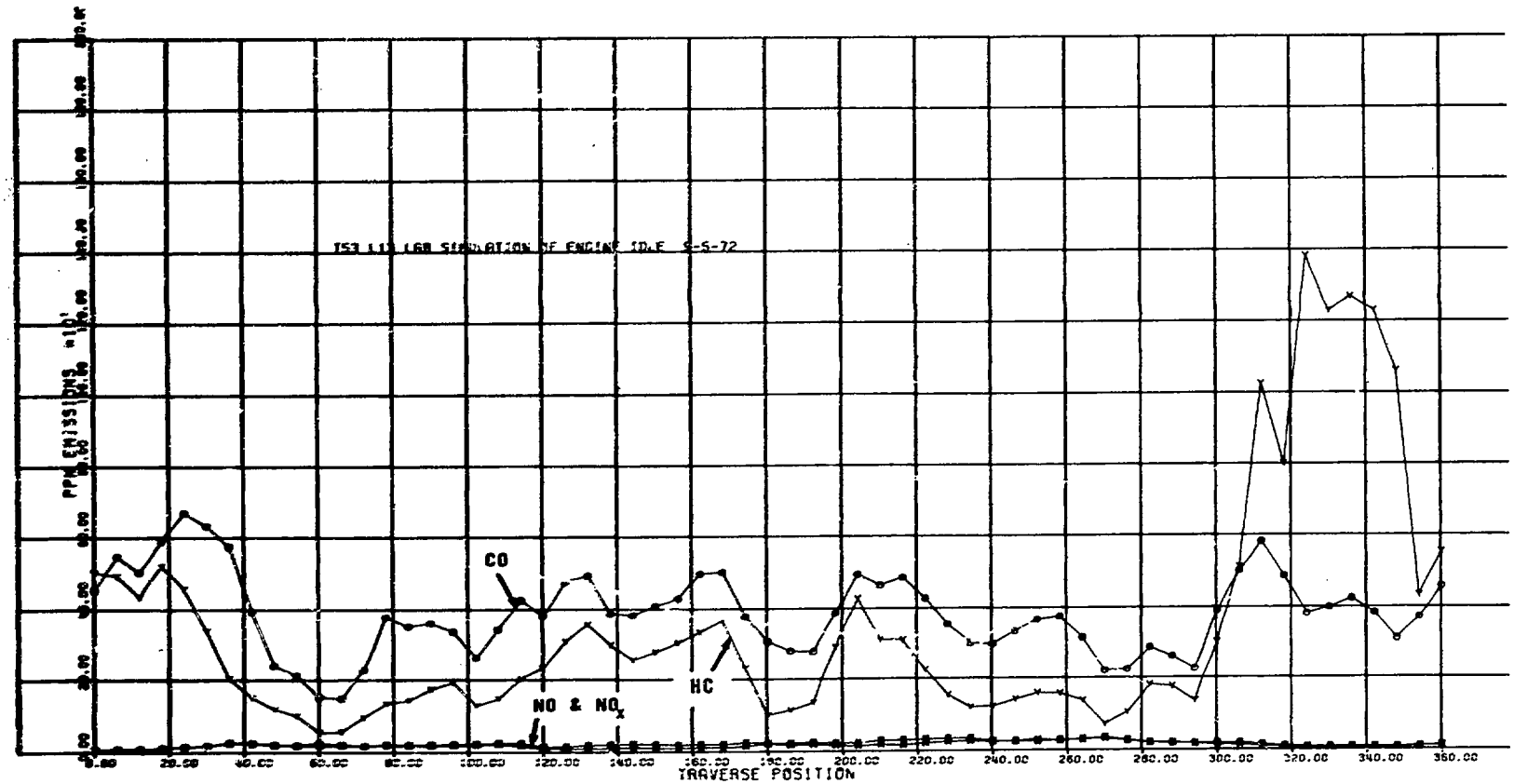

Figure 101. T53 Laboratory Combustor, ppm Emission Versus Traverse Angle at Idle.

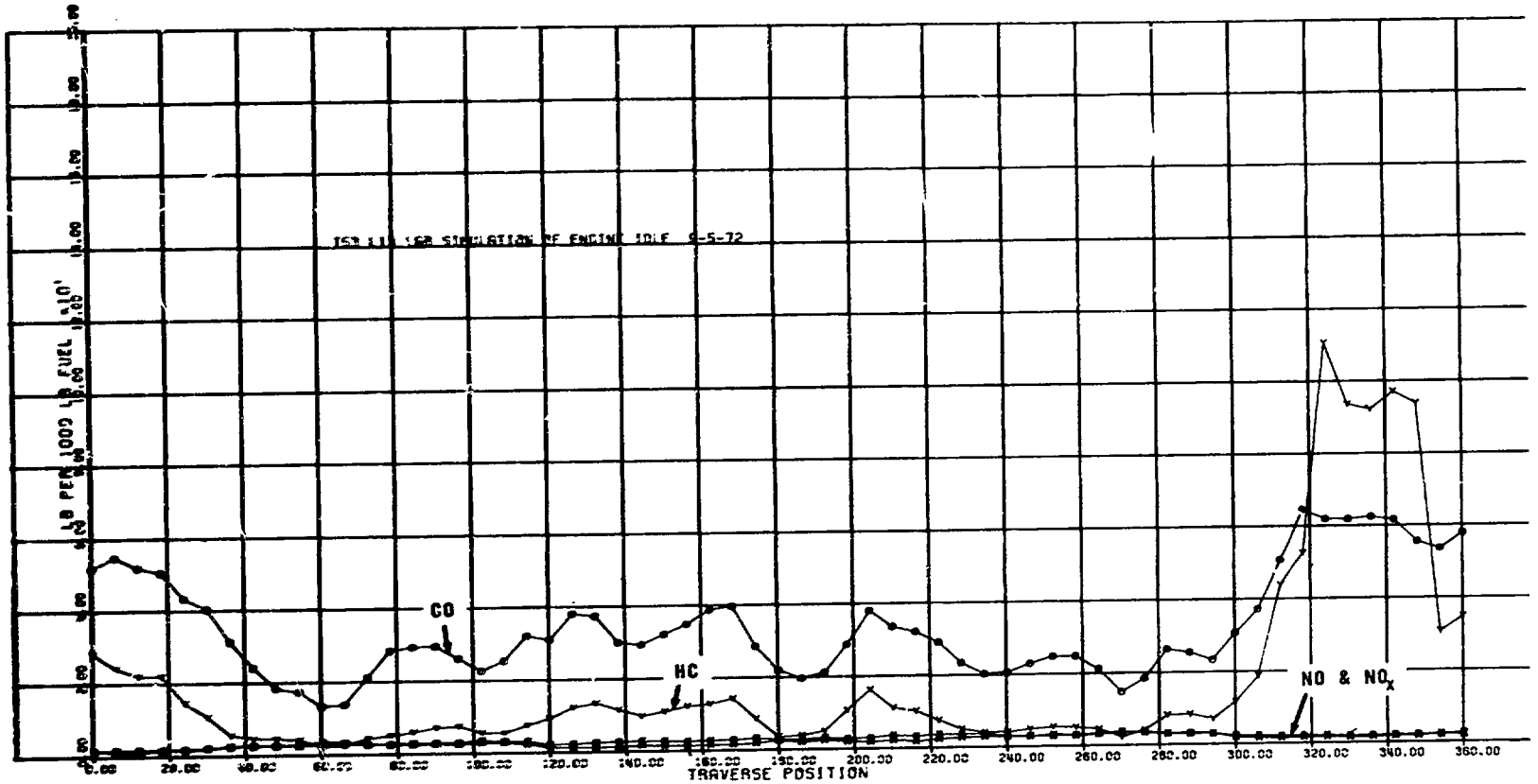

Figure 102. T53 Laboratory Combustor, Emission Index Versus Traverse Angle at Idle.

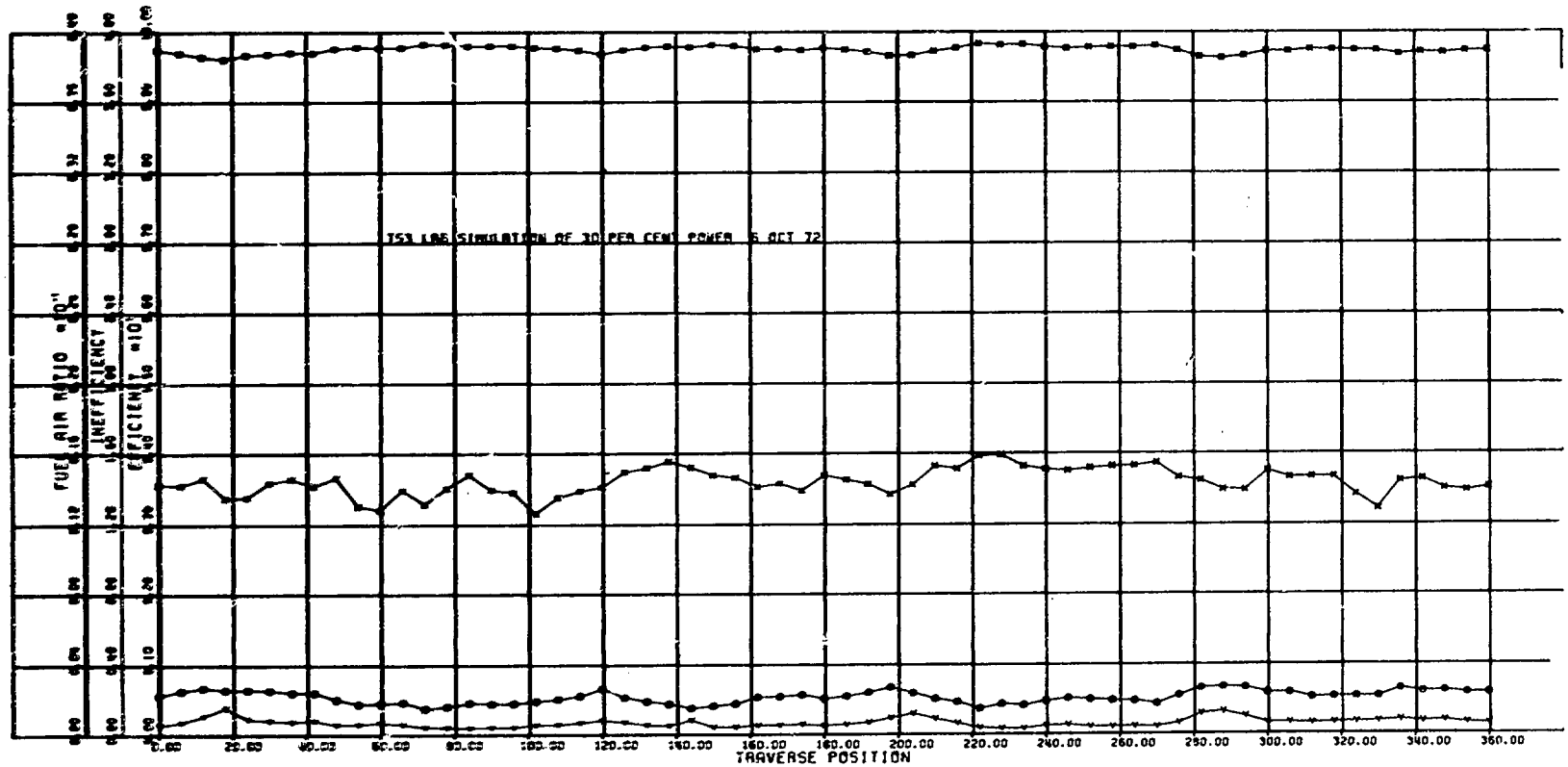

Figure 103. T53 Laboratory Combustor, Fuel-Air Ratio and Combustion Efficiency Versus Traverse Angle at 30% Power.

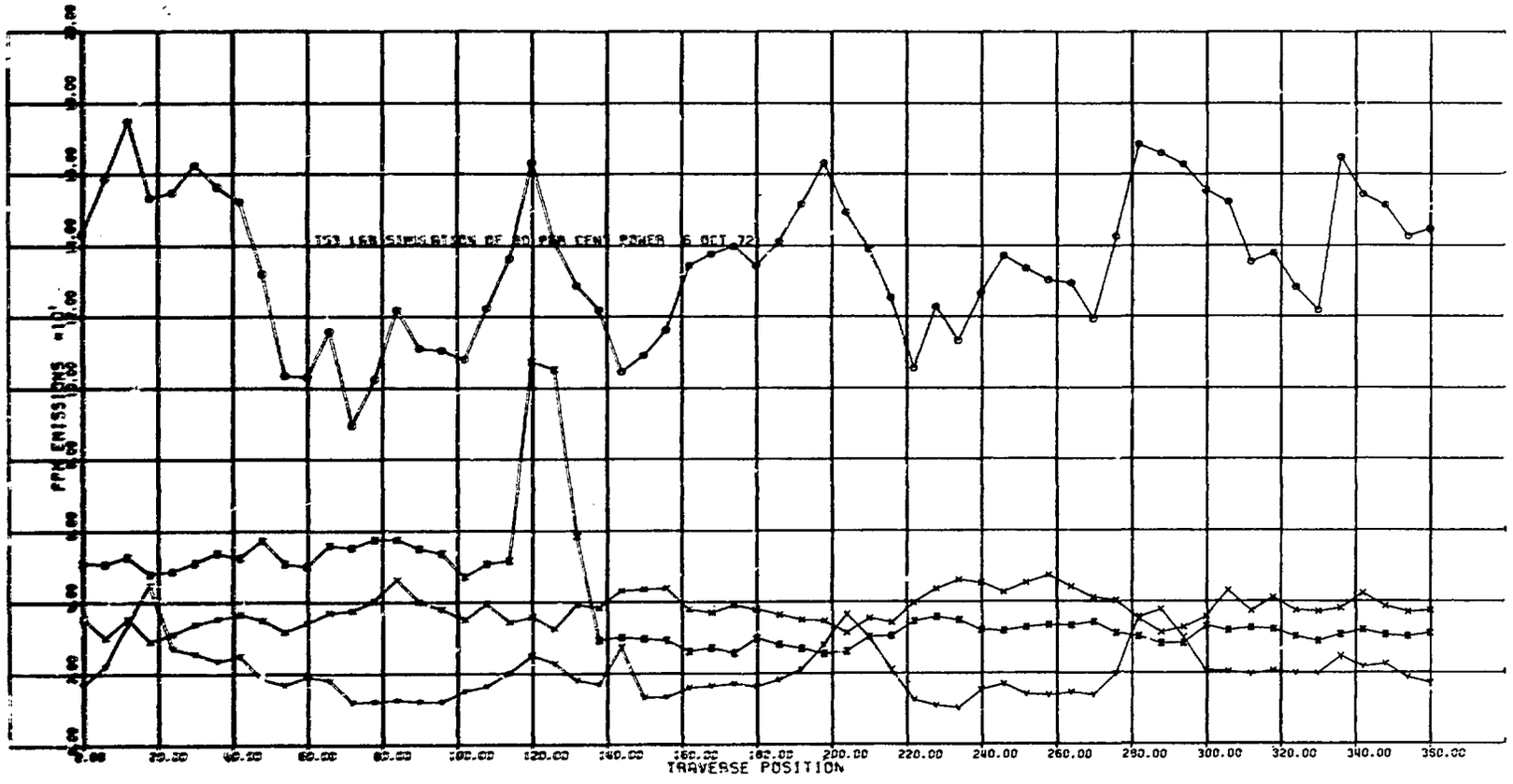

Figure 104. T53 Laboratory Combustor, ppm Emissions Versus Traverse Angle at 30% Power.

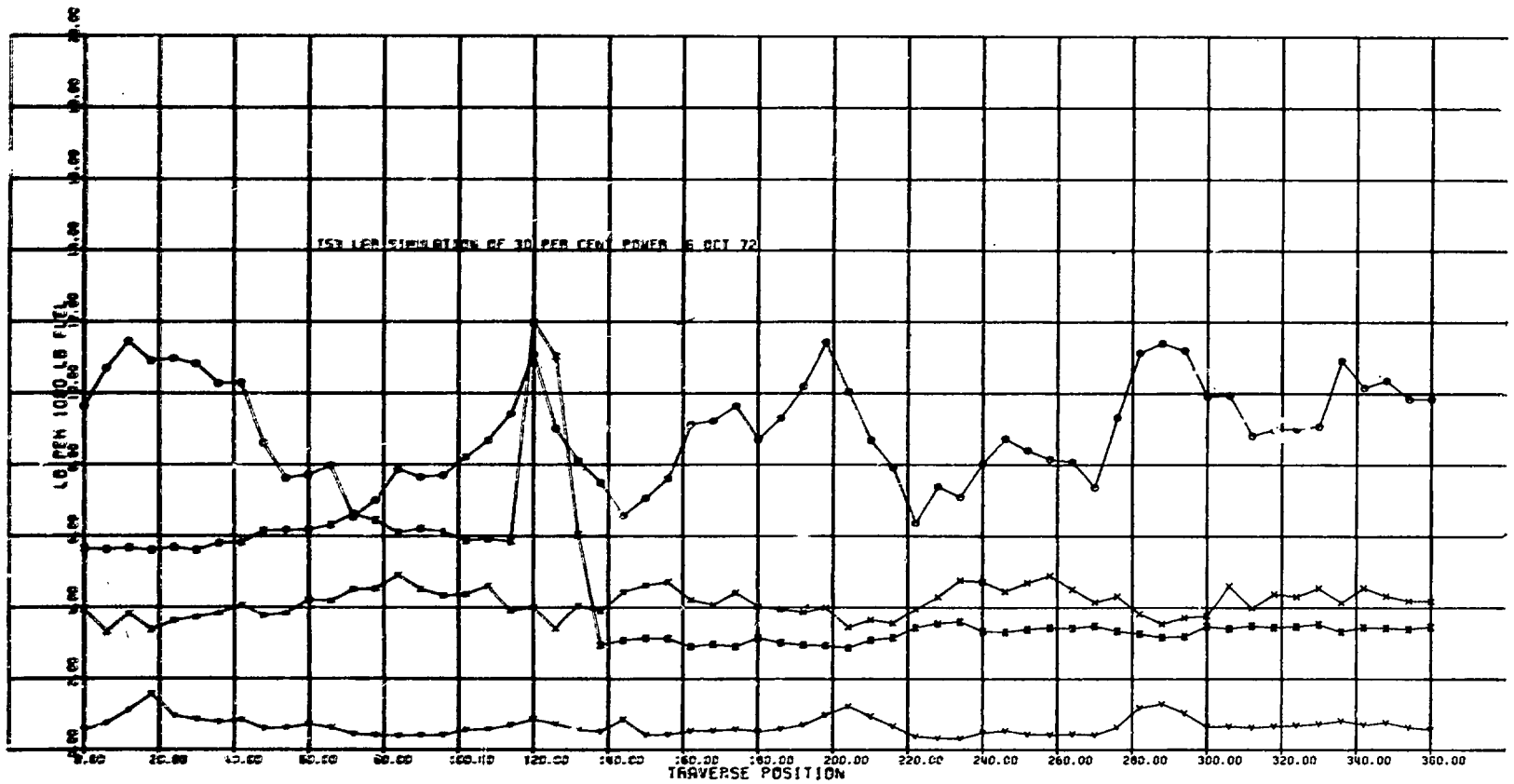

Figure 105. T53 Laboratory Combustor, Emission Index Versus Traverse Angle at 30% Power.

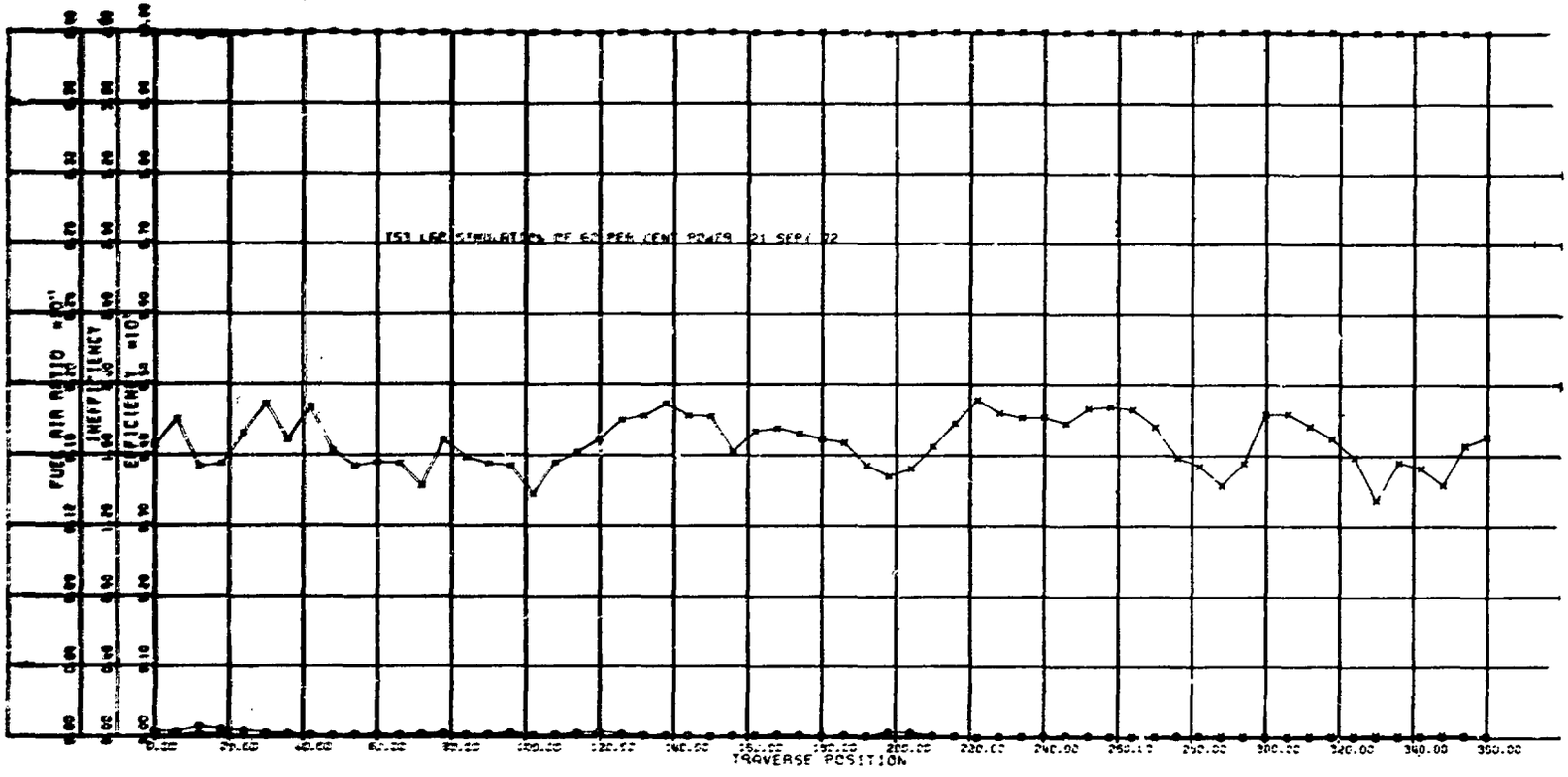

Figure 106. T53 Laboratory Combustor, Fuel-Air Ratio and Combustion Efficiency Versus Traverse Angle at 60% Power.

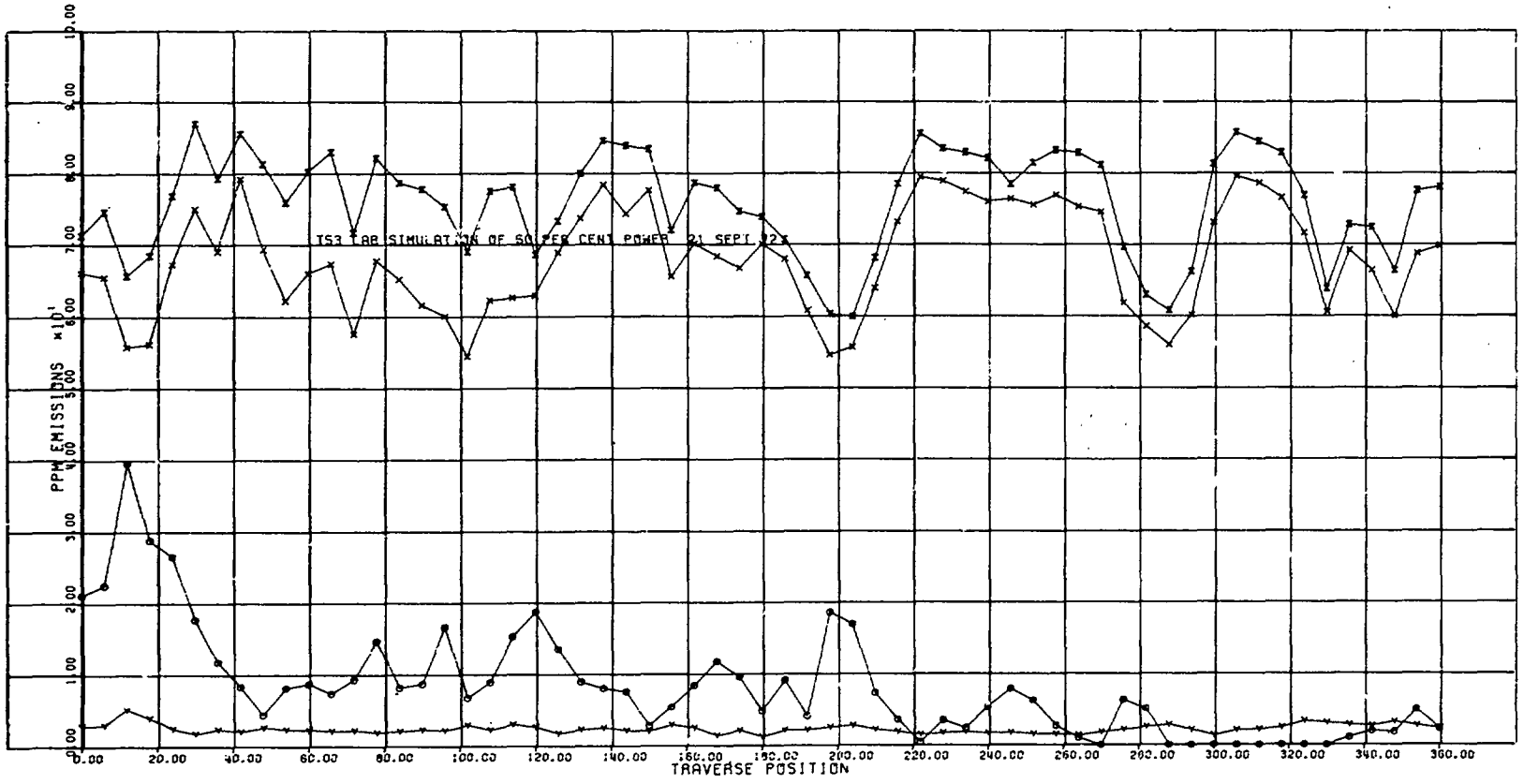

Figure 107. T53 Laboratory Combustor, ppm Emissions Versus Traverse Angle at 60% Power.

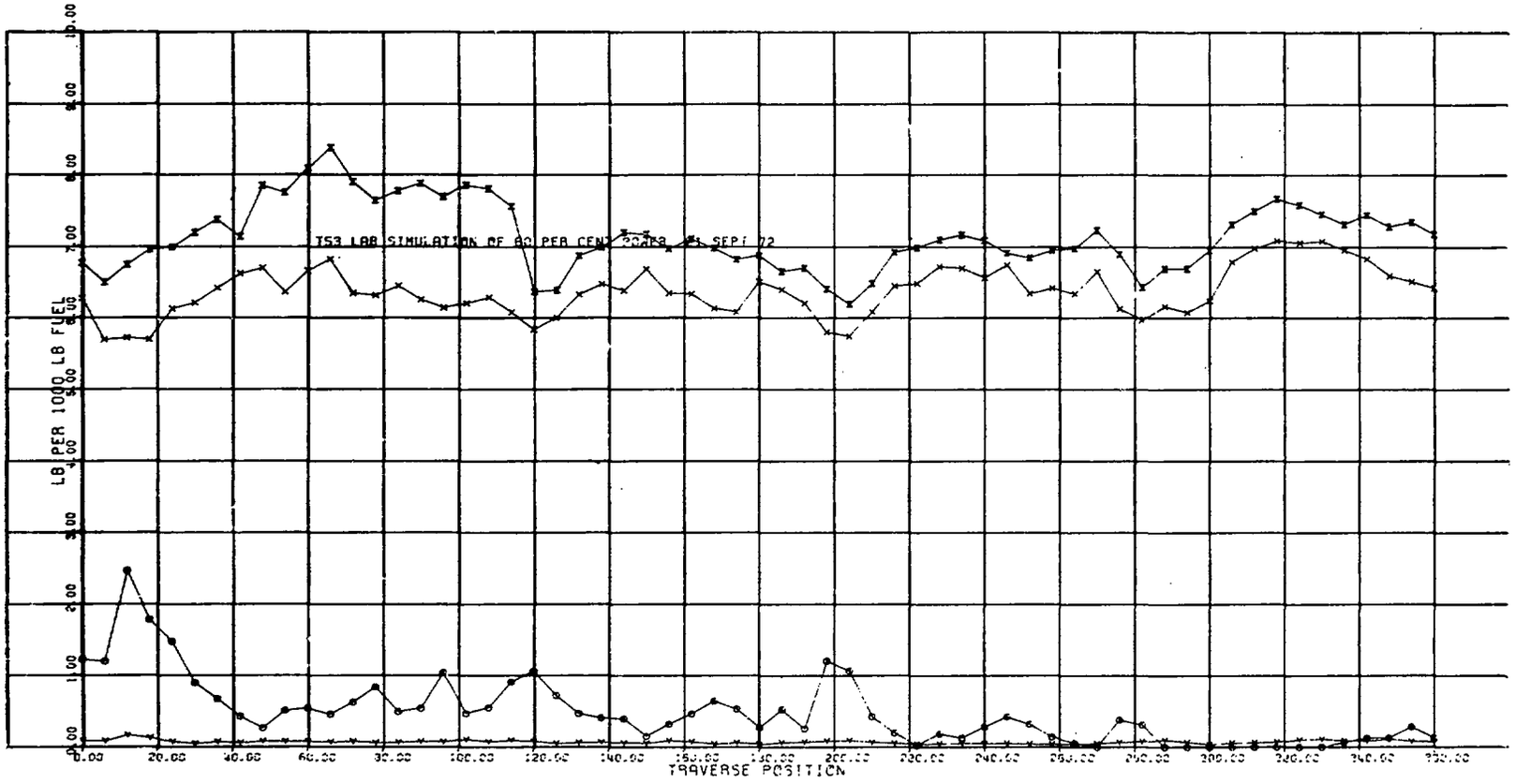

Figure 108. T53 Laboratory Combustor, Emission Index Versus Traverse Angle at 60% Power.

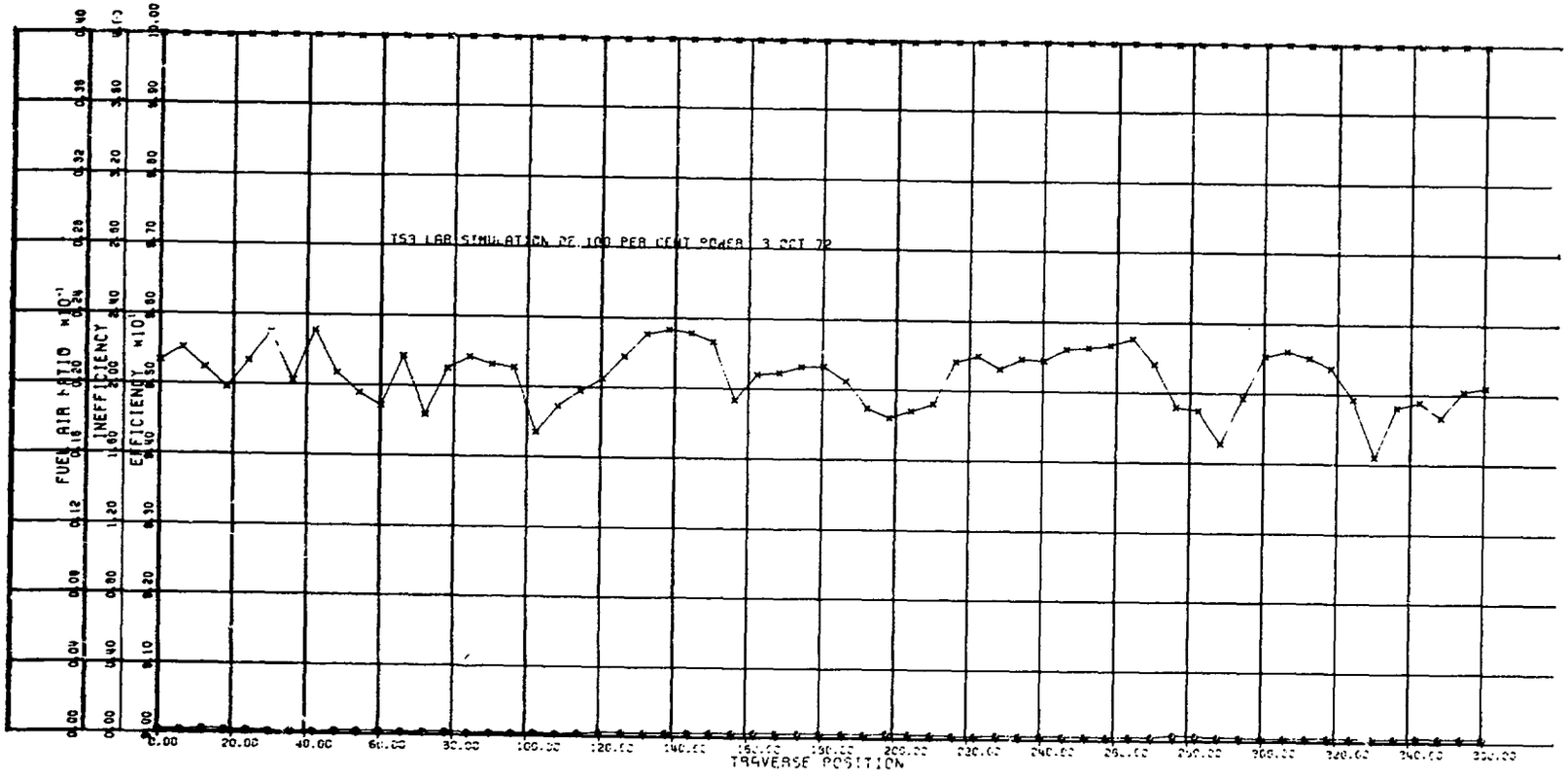

Figure 109. T53 Laboratory Combustor, Fuel-Air Ratio and Combustion Efficiency Versus Traverse Angle at 100% Power.

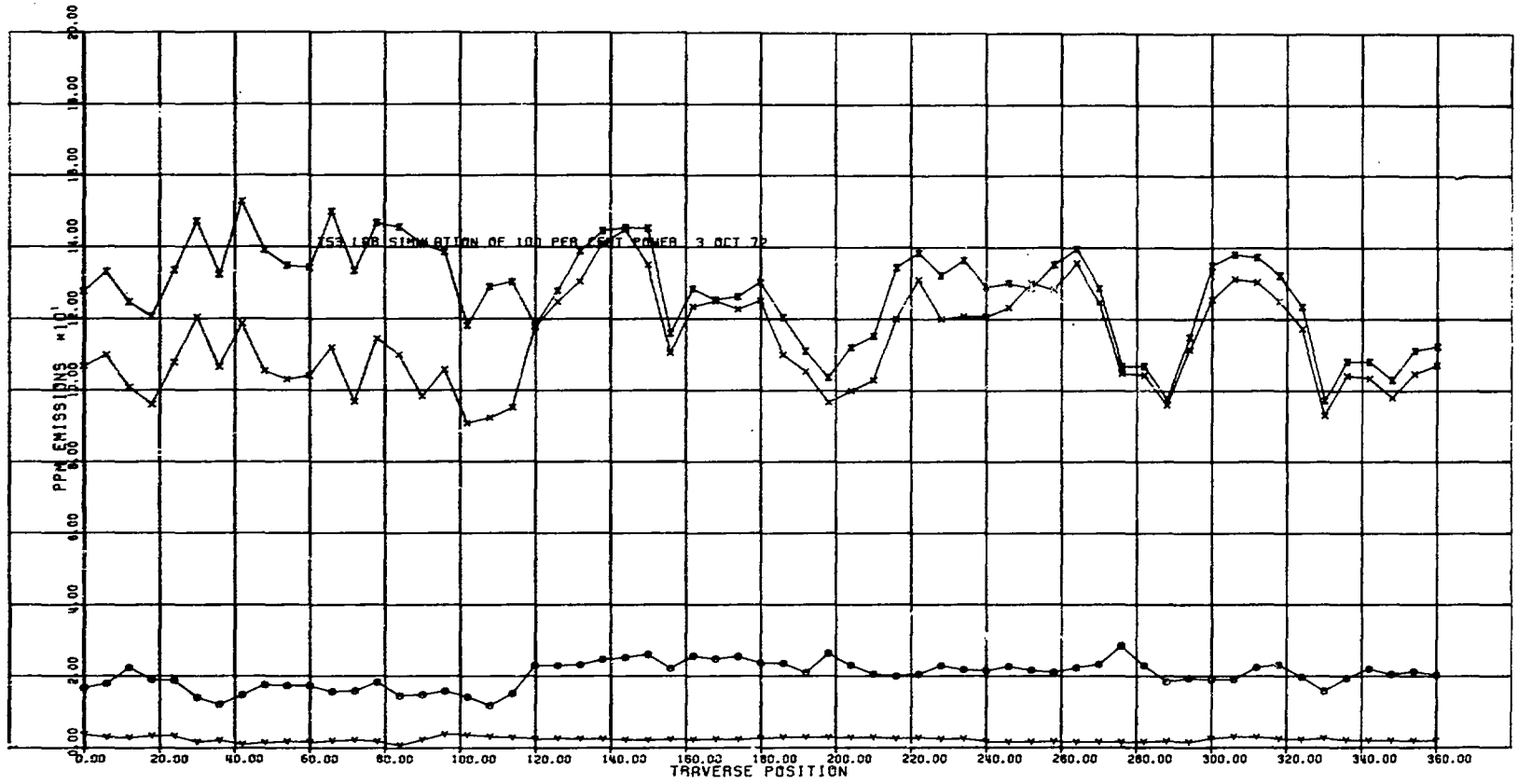

Figure 110. T53 Laboratory Combustor, ppm Emissions Versus Traverse Angle at 100% Power.

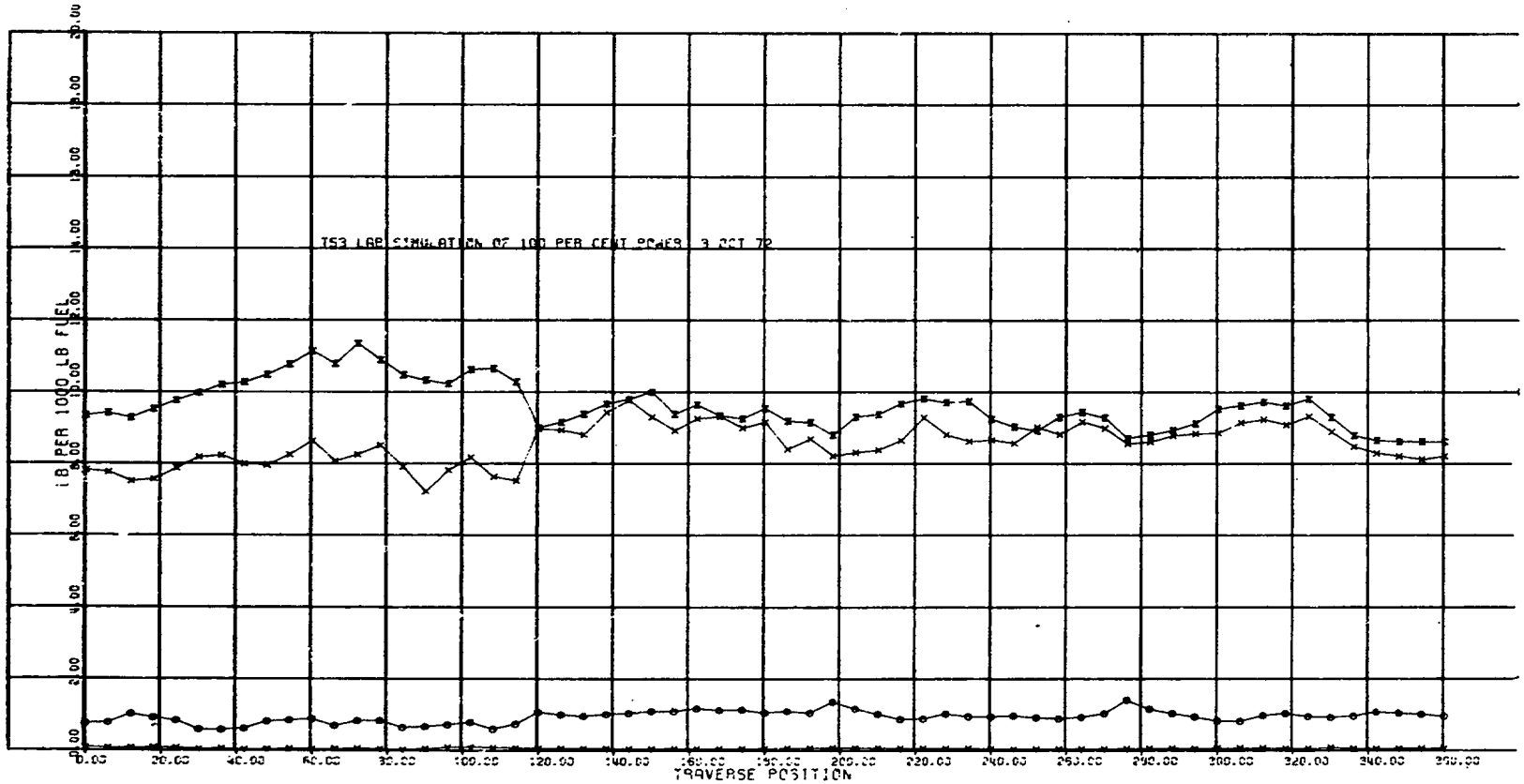

Figure 111. T53 Laboratory Combustor, Emission Index Versus Traverse Angle at 100% Power.

APPENDIX II
T53 ENGINE ISOPLETH EXHAUST CONTOUR PLOTS

The engine exhaust gas sampling traverse was made with the single-point probe to determine CO, HC, CO_2, NO, and NO_x at four power conditions, including idle, 30, 60, and 100 percent of full power. With center-point repetition, 71 data points were recorded. From these data, calculations were made for F/A and combustion efficiency. In order to plot the isopleth concentration (or combustion efficiency) lines, all values were normalized to an average reference value at the duct center. This reduces any time variation of the concentrations to a very small amount. Plotted for each power setting are isopleths for CO, HC, NO, NO_x, fuel-air ratio, and combustion efficiency. See Figures 112 through 135.

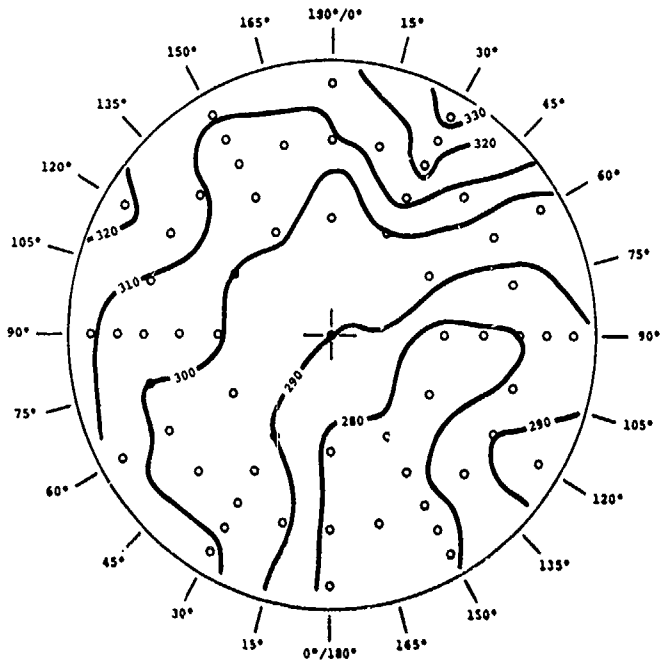

Figure 112. T53 Engine Isopleth of CO (ppm) at Idle Power.

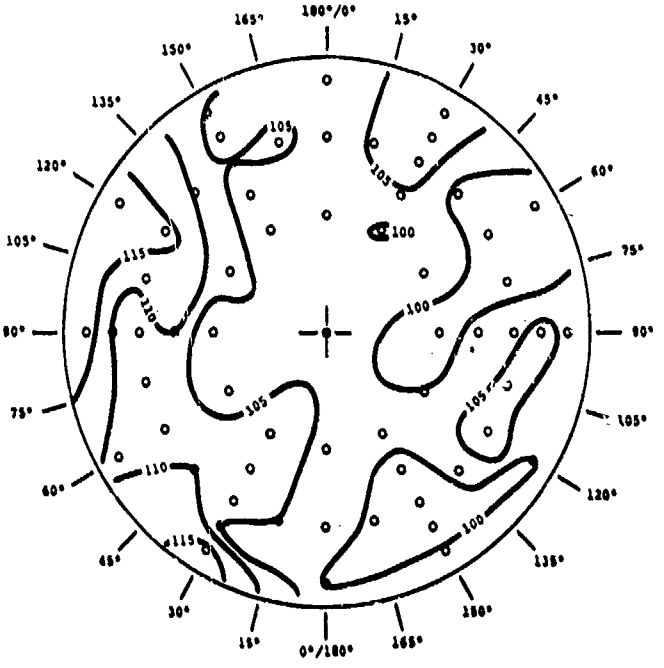

Figure 113. T53 Engine Isopleth of HC (ppmC) at Idle Power.

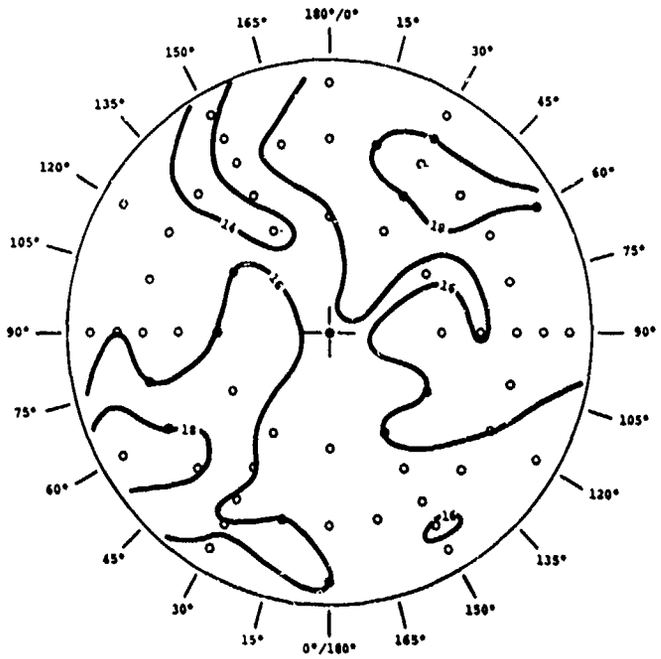

Figure 114. T53 Engine Isopleth of NO (ppm) at Idle Power.

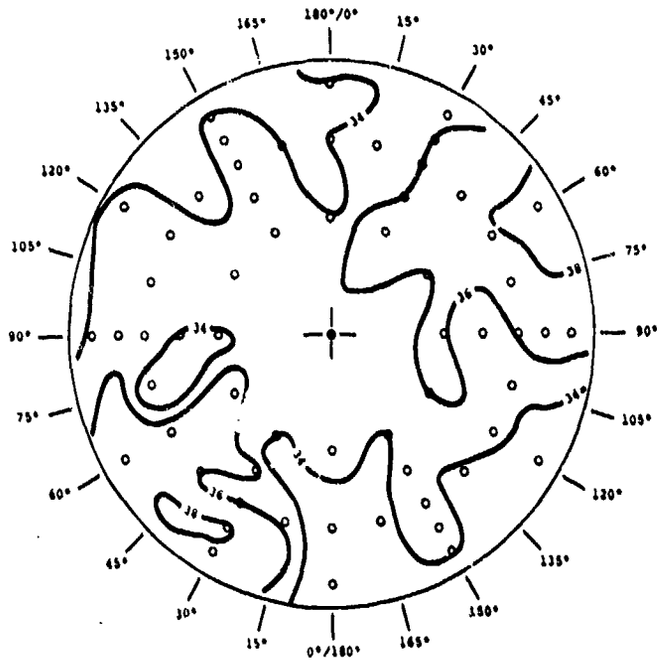

Figure 115. T53 Engine Isopleth of NO_x (ppm) at Idle Power.

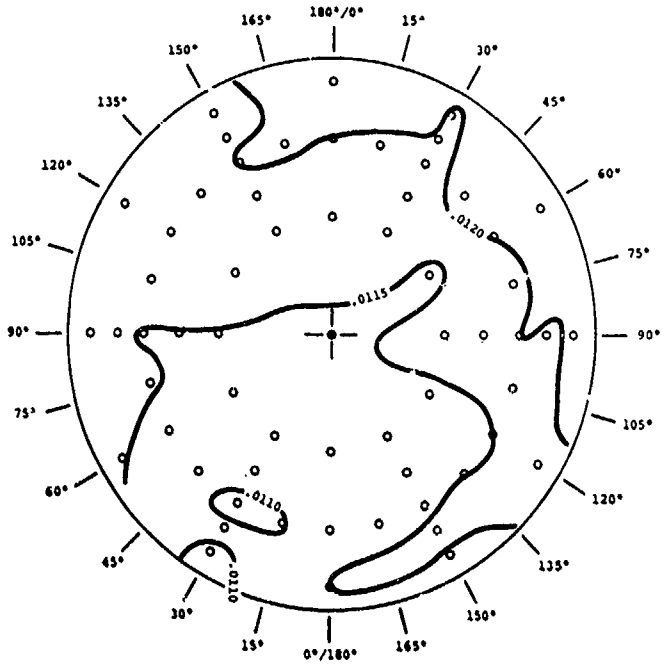

Figure 116. T53 Engine Isopleth of Fuel-Air Ratio at Idle Power.

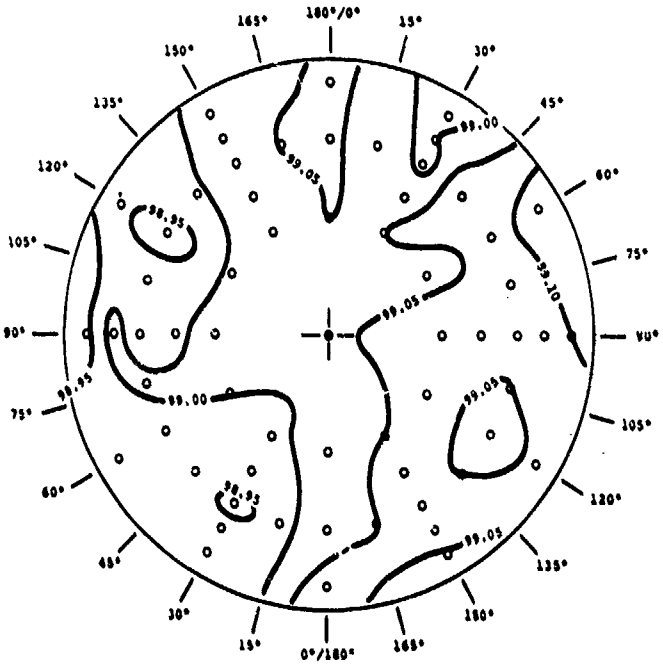

Figure 117. T53 Engine Isopleth of Combustion Efficiency at Idle Power.

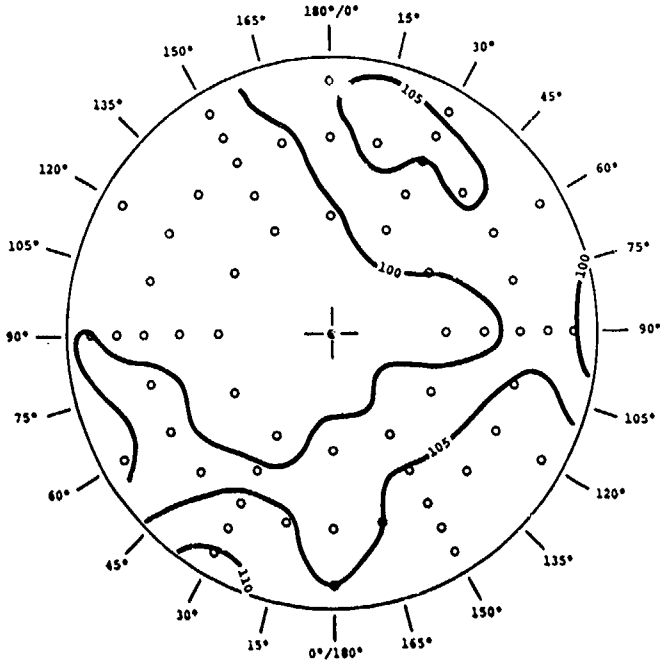

Figure 118. T53 Engine Isopleth of CO (ppm) at 30% Power.

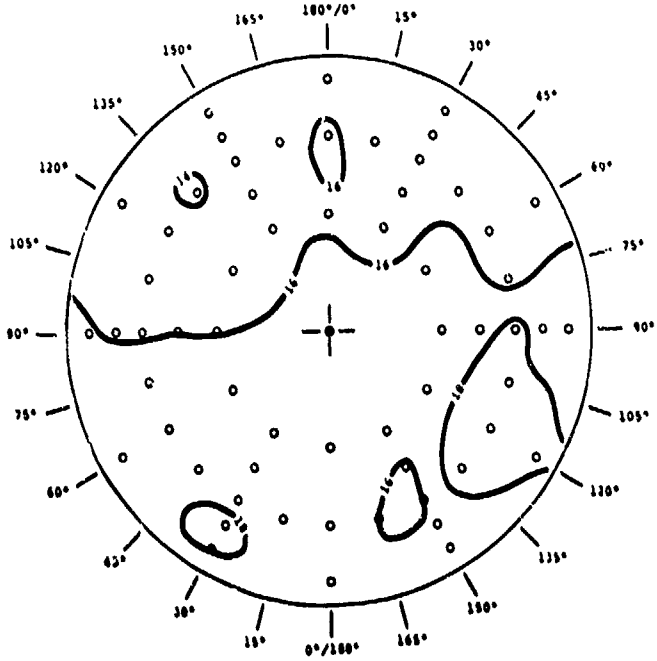

Figure 119. T53 Engine Isopleth of HC (ppmC) at 30% Power.

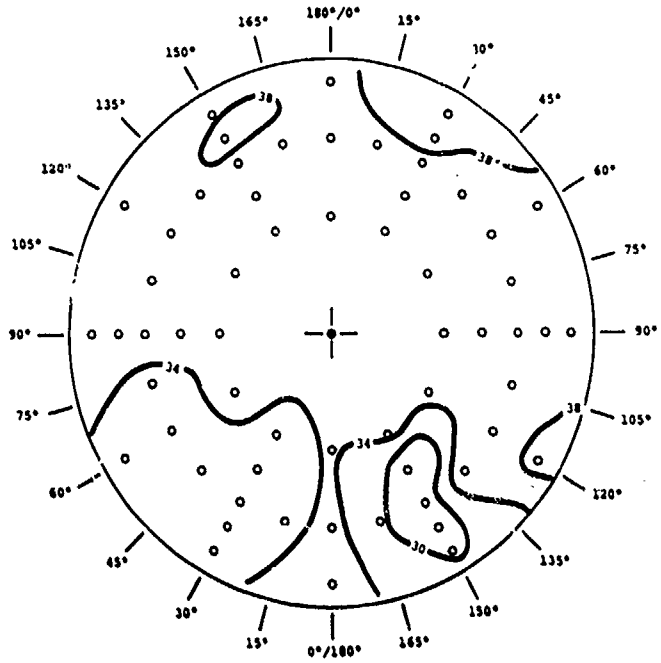

Figure 120. T53 Engine Isopleth of NO (ppm) at 30% Power.

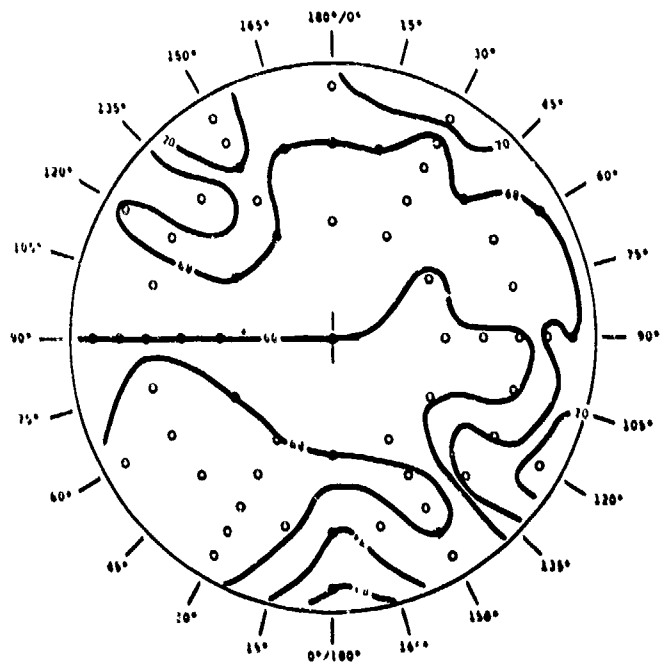

Figure 121. T53 Engine Isopleth of NO_x (ppm) at 30% Power.

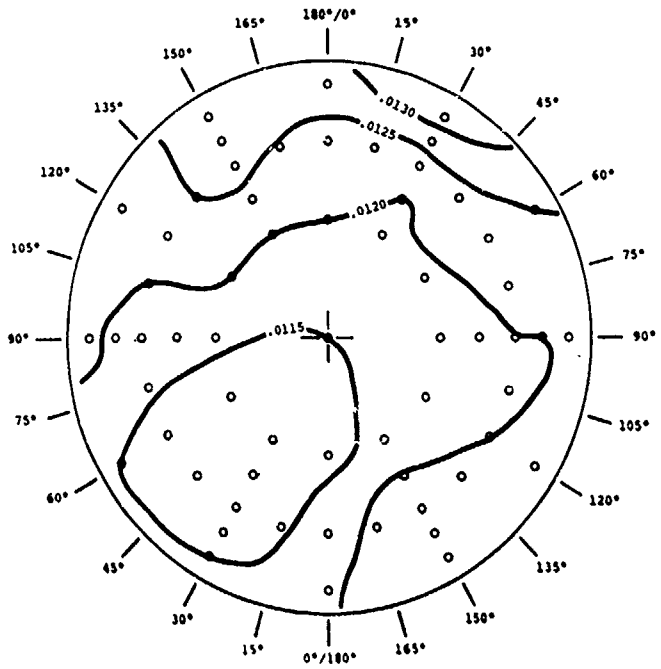

Figure 122. T53 Engine Isopleth of Fuel-Air Ratio at 30% Power.

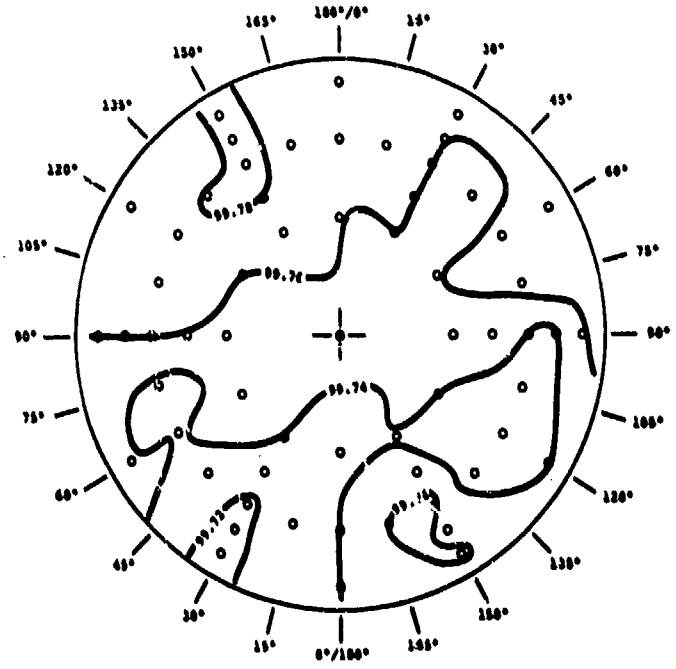

Figure 123. T53 Engine Isopleth of Combustion Efficiency at 30% Power.

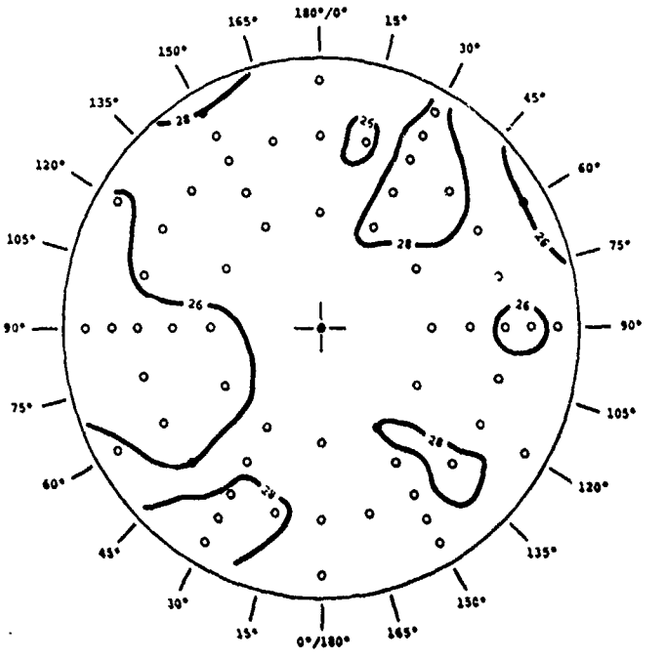

Figure 124. T53 Engine Isopleth of CO (ppm) at 60% Power.

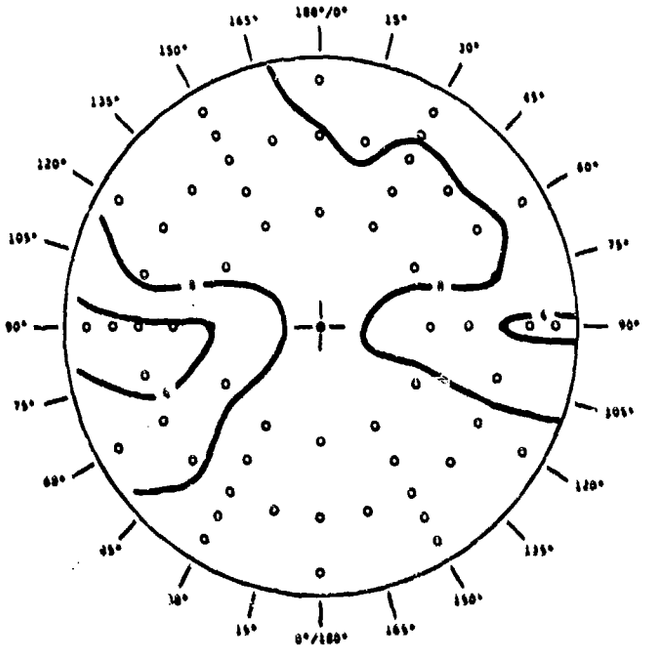

Figure 125. T53 Engine Isopleth of HC (ppmC) at 60% Power.

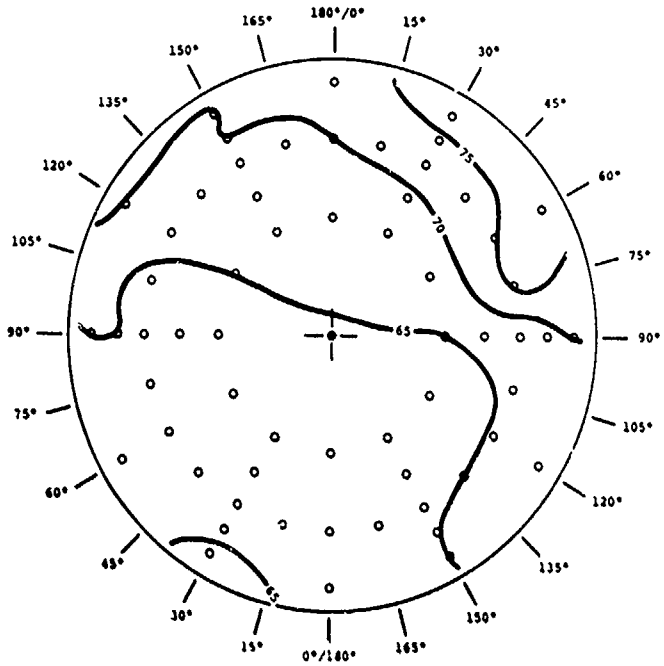

Figure 126. T53 Engine Isopleth of NO (ppm) at 60% Power.

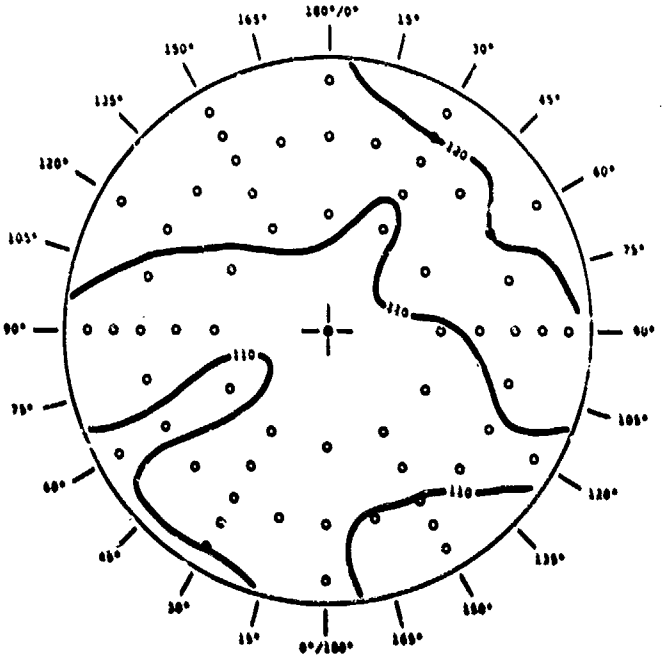

Figure 127. T53 Engine Isopleth of NO_x (ppm) at 60% Power.

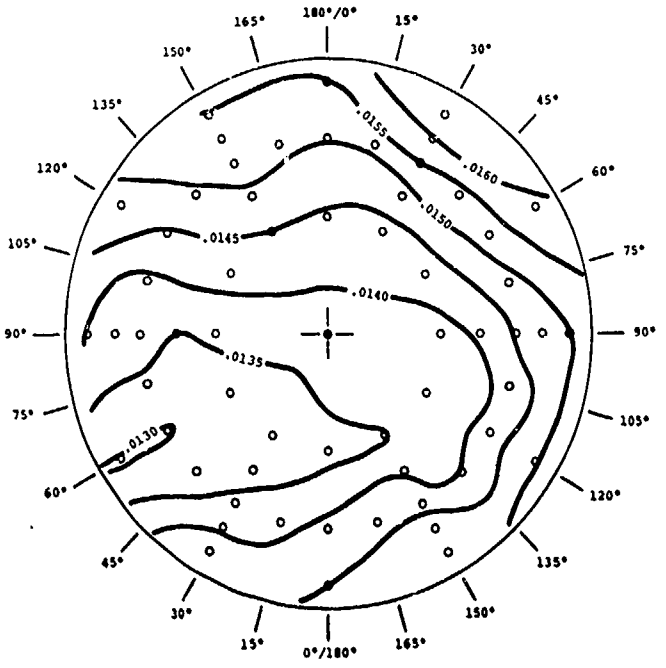

Figure 128. T53 Engine Isopleth of Fuel-Air Ratio at 60% Power.

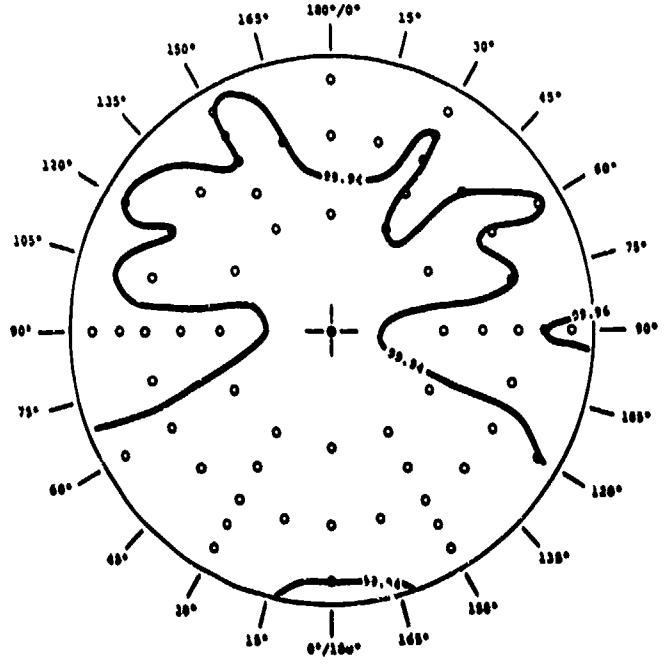

Figure 129. T53 Engine Isopleth of Combustion Efficiency at 60% Power.

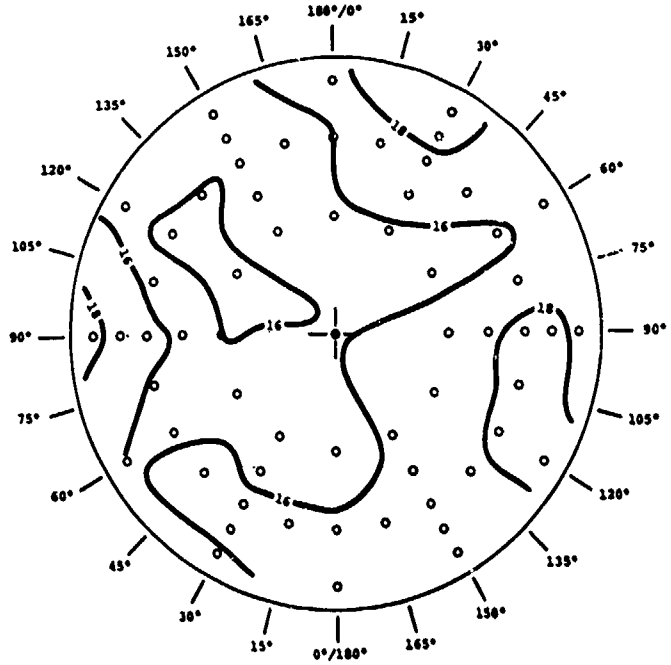

Figure 130. T53 Engine Isopleth of CO (ppm) at 100% Power.

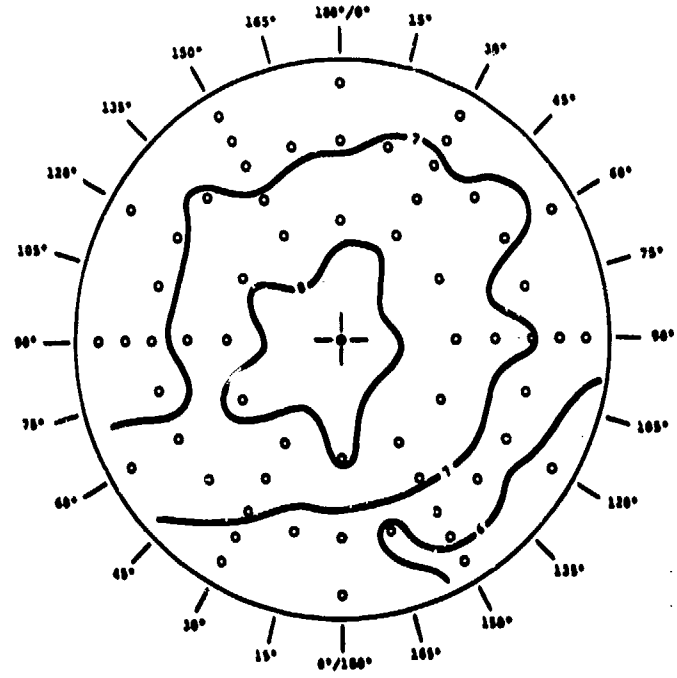

Figure 131. T53 Engine Isopleth of HC (ppmC) at 100% Power.

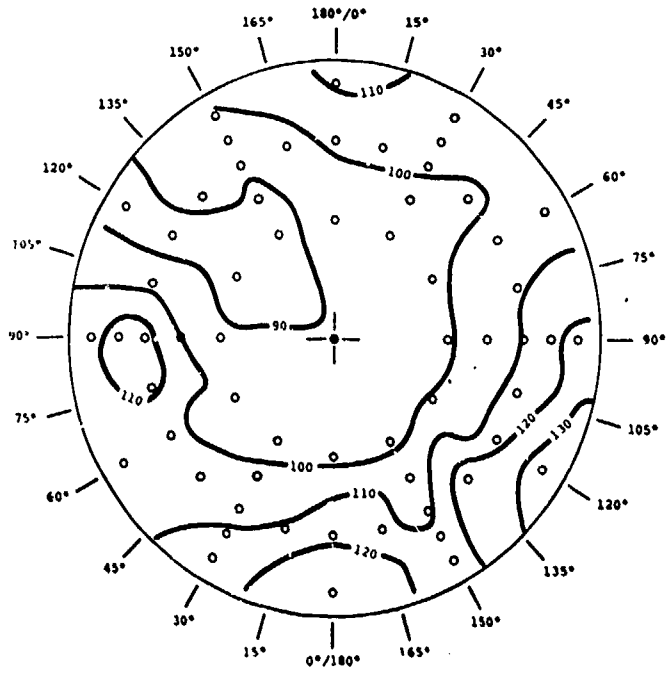

Figure 132. T53 Engine Isopleth of NO (ppm) at 100% Power.

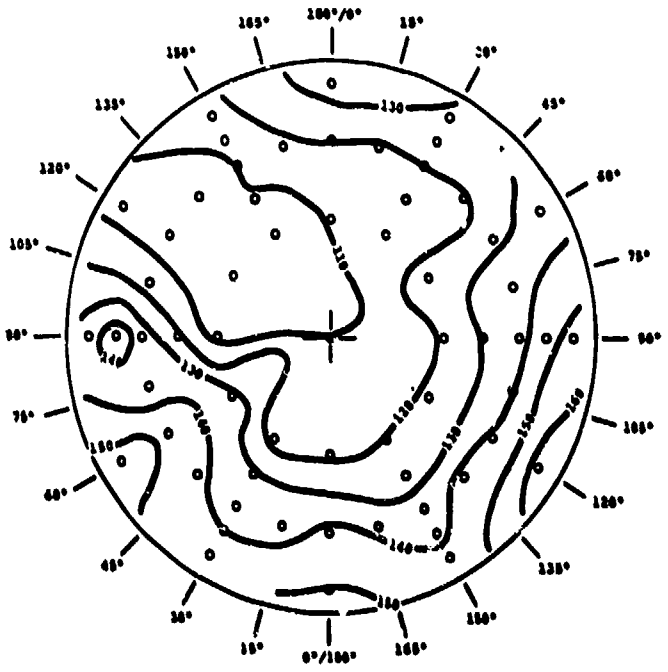

Figure 133. T53 Engine Isopleth of NO_x (ppm) at 100% Power.

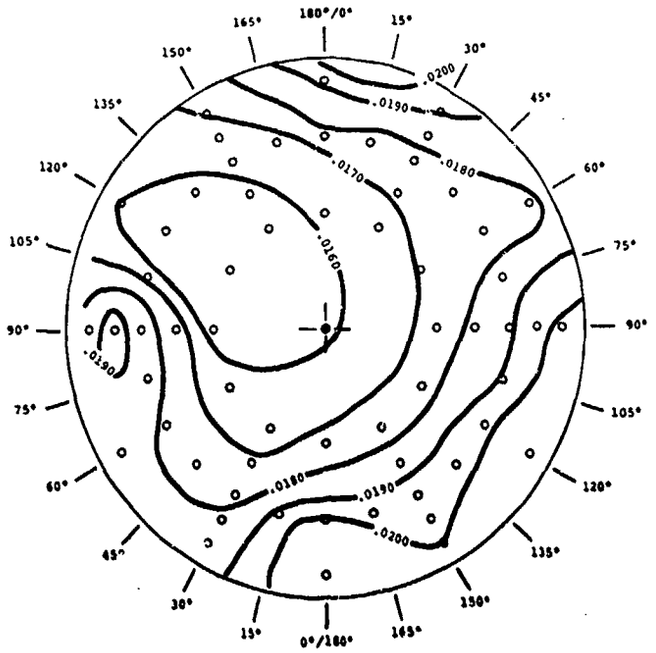

Figure 134. T53 Engine Isopleth of Fuel-Air Ratio at 100% Power.

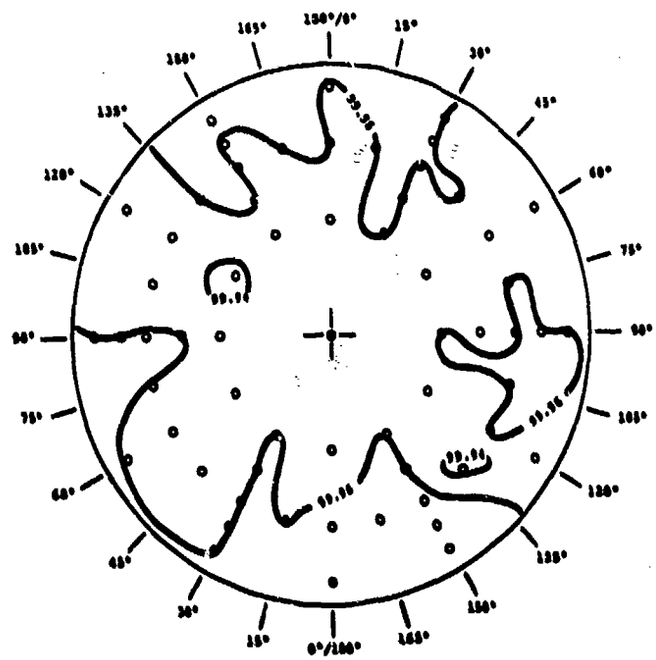

Figure 135. T53 Engine Isopleth of Combustion Efficiency at 100% Power.

APPENDIX III
T55 ENGINE LABORATORY COMBUSTOR RIG TRAVERSE DATA

This appendix presents computer "Calcomp" plots (Figures 136 through 147) of all the emission traverse data taken in the T55 combustor test rigs only. Each simulated power condition (idle, 30, 60 and 100 percent) is represented by three separate plots:

1. Performance summary plot showing fuel-air ratio, combustion efficiency, and the separate component contribution to combustion inefficiency

2. Emissions in ppm volume for CO, HC, NO, and NO_x (hydrocarbons are in ppmC)

3. Emission index, in pounds per 1000 pounds of fuel for each component

Scales for the performance summary plot are constant, but the scale for each of the emission plots is computer-selected to attain the largest value on the scale. Traverse position is in degrees from the rig starting point; the T55 rig starts at 300 degrees. This is significant in comparing results from the rig with engine data or with rig temperature traverses which start at top dead-center. Symbols on the plots have the following meaning:

*	Net combustor efficiency
⌑	Fuel-air ratio
⓪	CO (inefficiency, emission index or ppm)
Y	HC (inefficiency, emission index, or ppmC)
X	NO (emission index or ppm)
⧗	NO_x (emission index or ppm)

A study of this data will reveal several irregularities that require explanation. The most significant of these are:

1. During the T55 idle traverse, a valve in the sample line

was left open for 20 of the 60 traverse points. As a result, the absolute concentrations for the central 1/3 of the traverse are low by approximately 60 percent.

2. During the T55 30-percent traverse, the NO_x instrument malfunctioned, and no data are reported.

3. NO_x data for several runs are not as precise as might be desired. Interference of other gasecus components with the polarographic sensor is a suggested cause.

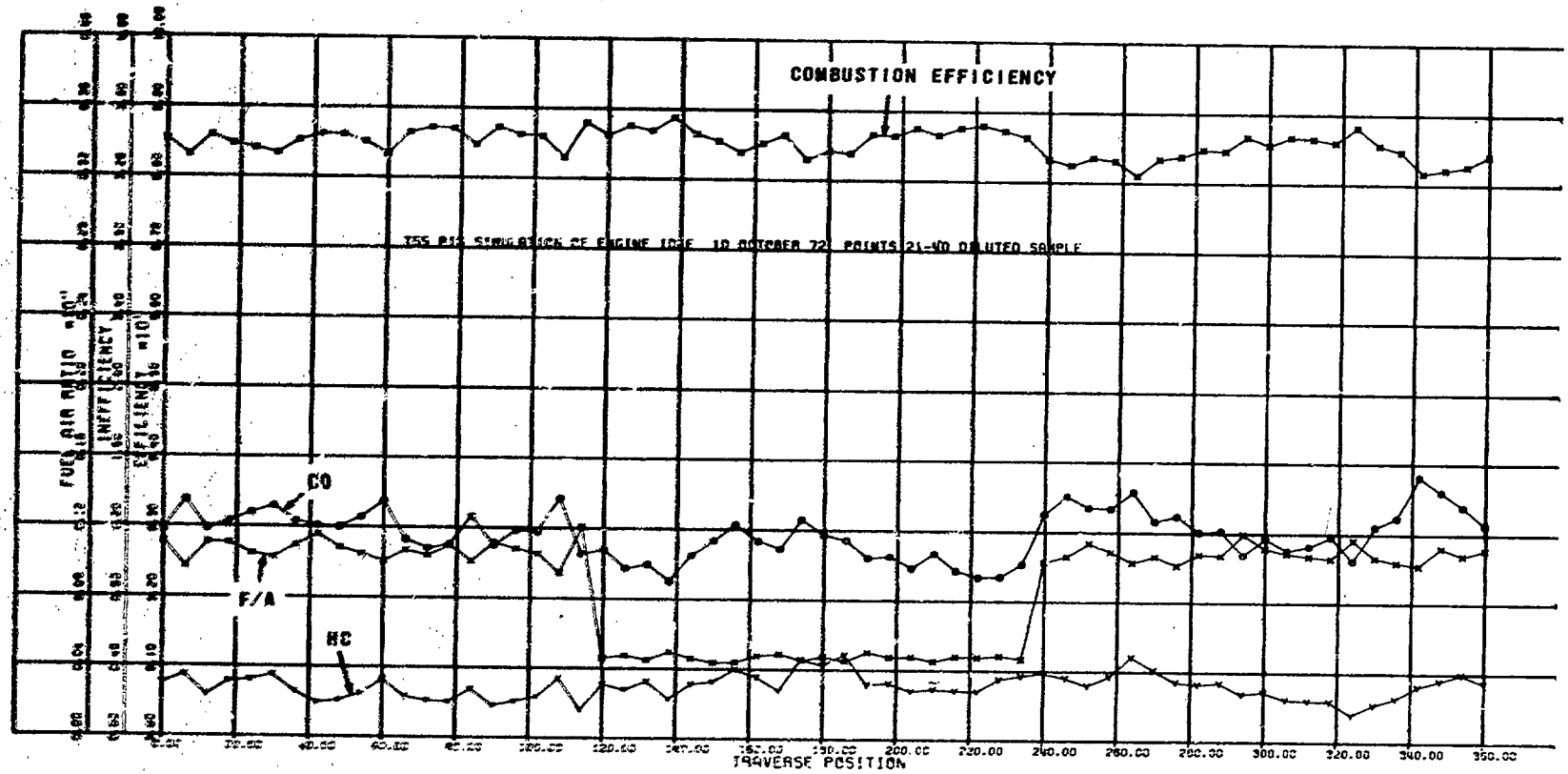

Figure 136. T55 Laboratory Combustor, Fuel-Air Ratio and Combustion Efficiency Versus Traverse Angle at Idle.

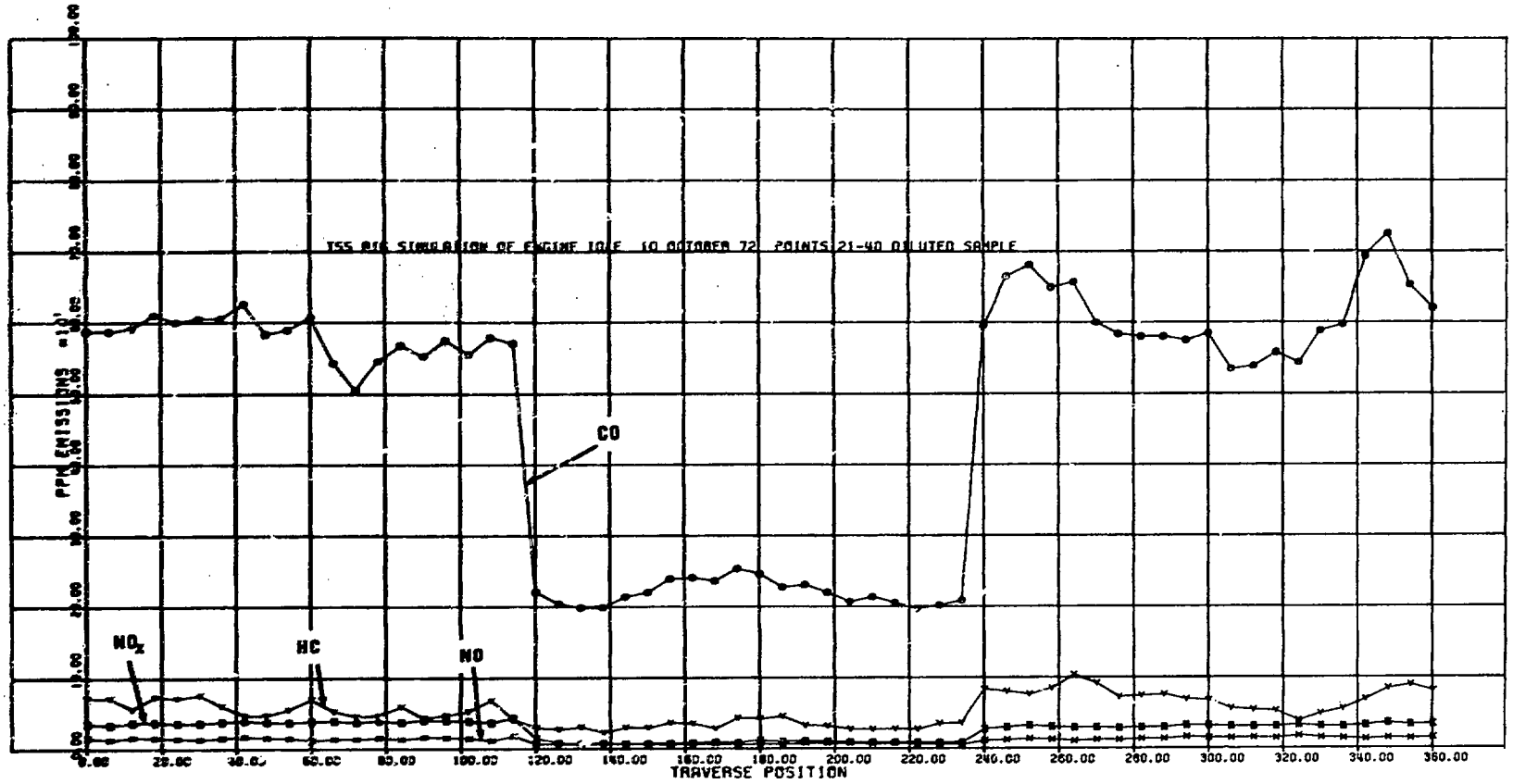

Figure 137. T55 Laboratory Combustor, ppm Emissions Versus Traverse Angle at Idle.

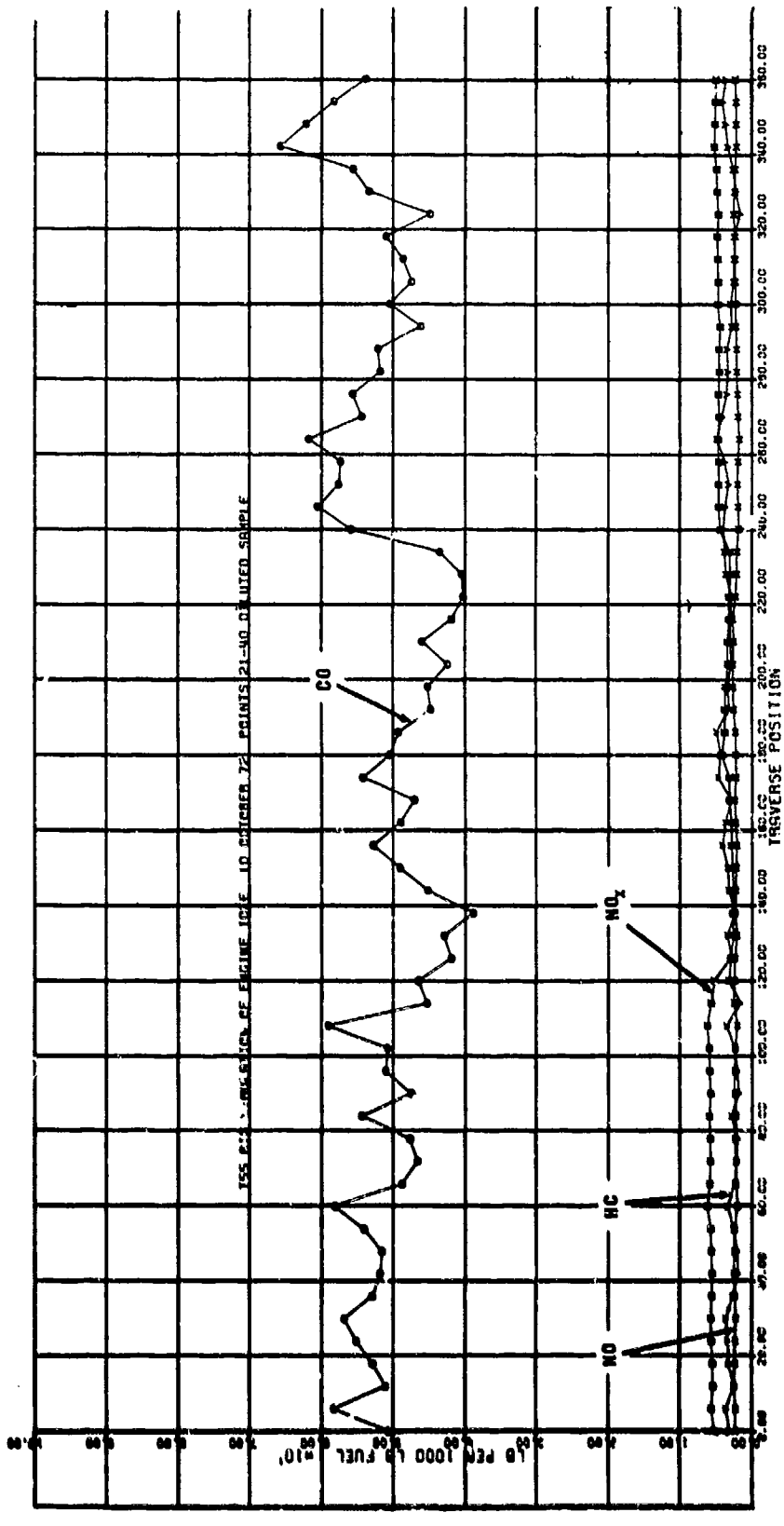

Figure 138. T55 Laboratory Combustor, Emission Index Versus Traverse Angle at Idle.

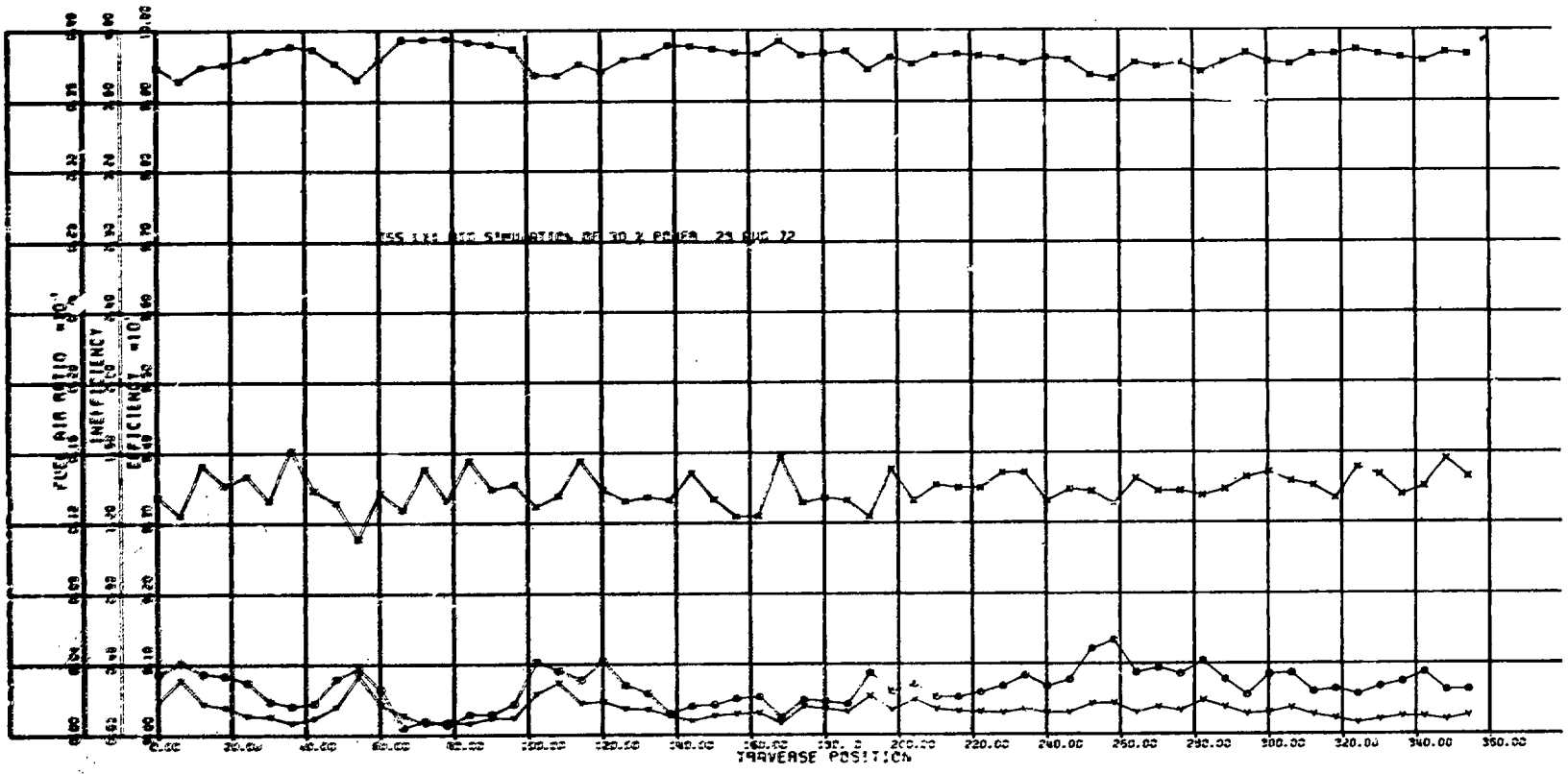

Figure 139. T55 Laboratory Combustor, Fuel-Air Ratio and Combustion Efficiency Versus Traverse Angle at 30% Power.

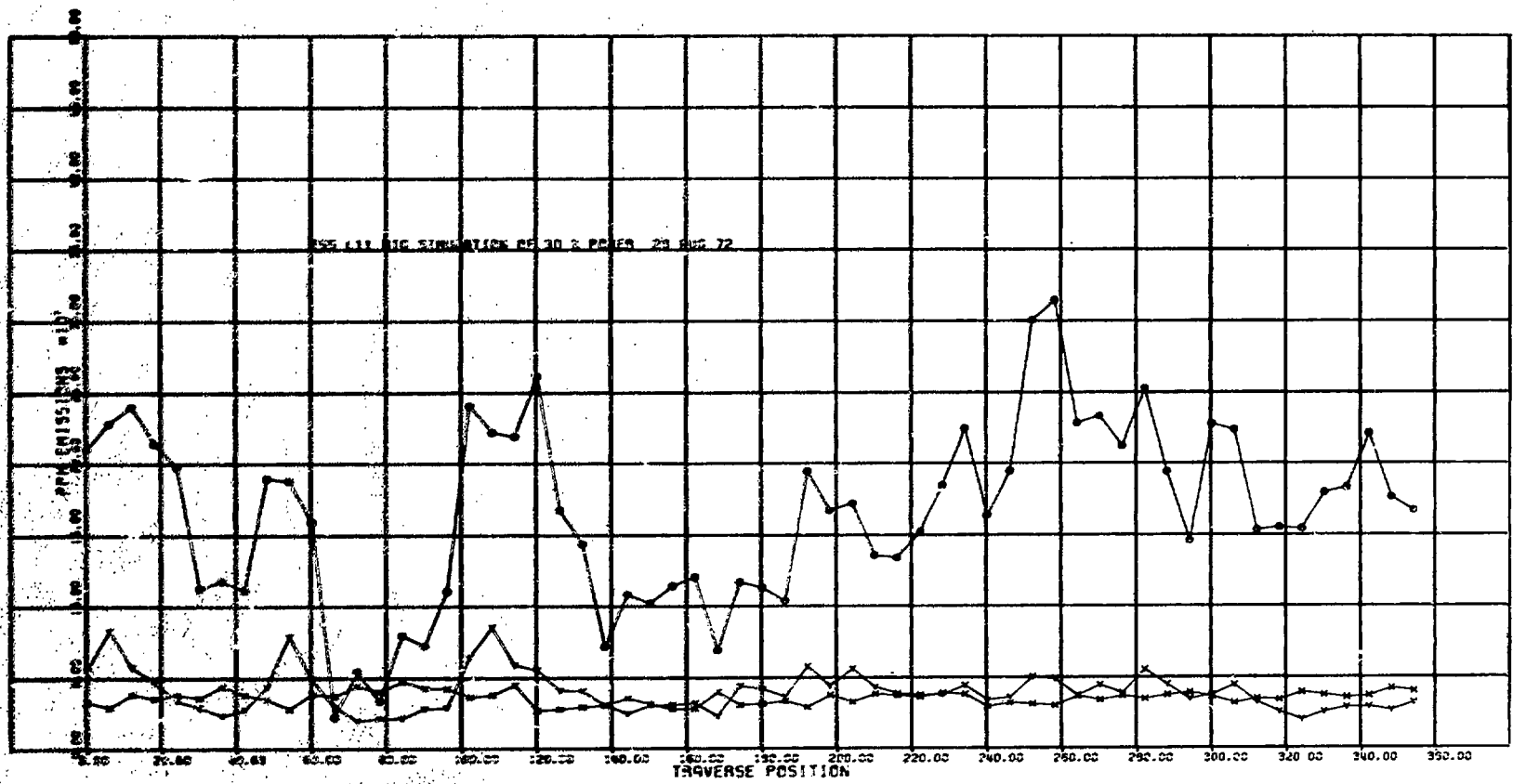

Figure 140. T55 Laboratory Combustor, ppm Emissions Versus Traverse Angle at 30% Power.

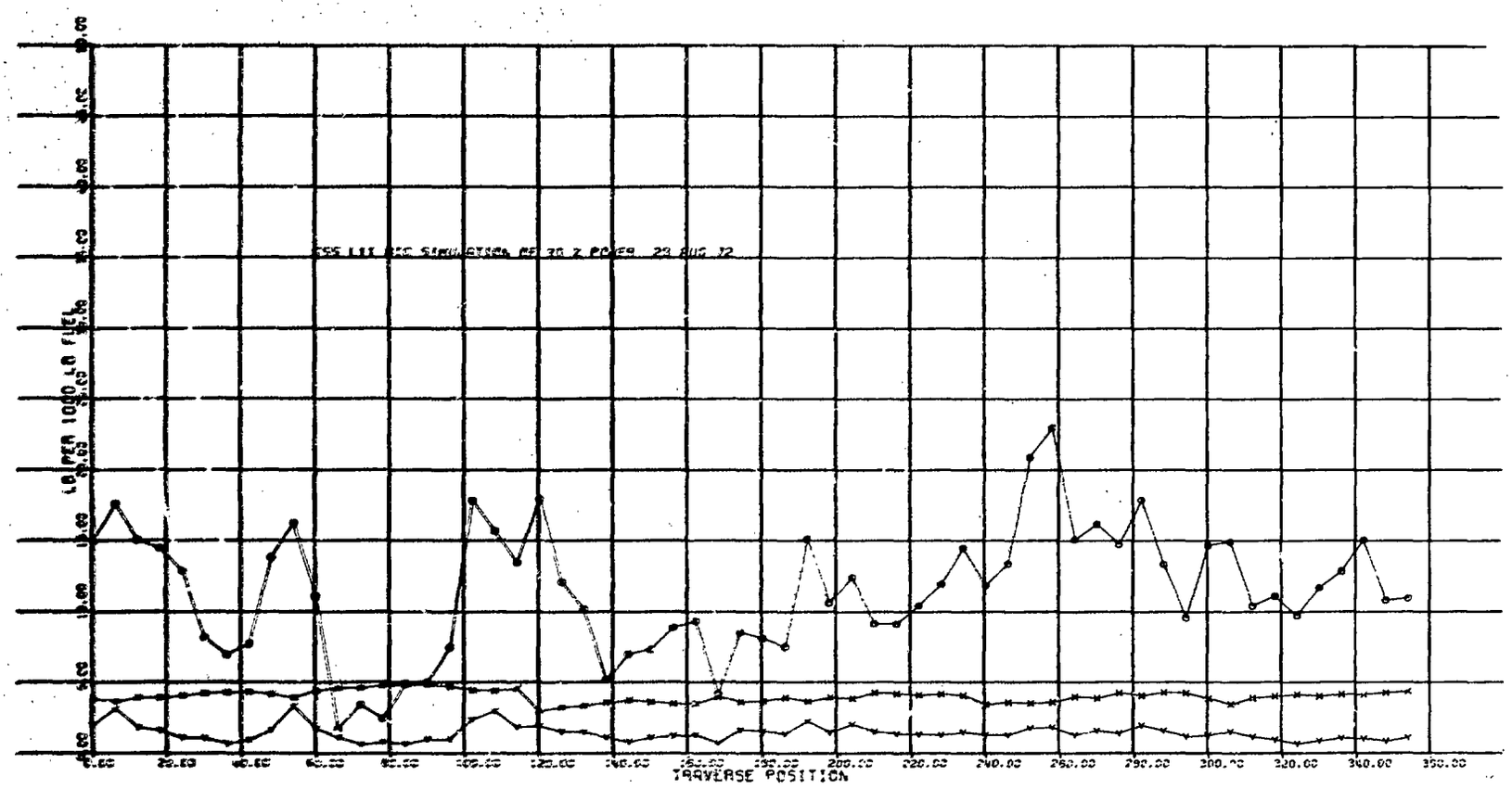

Figure 141. T55 Laboratory Combustor, Emission Index Versus Traverse Angle at 30% Power.

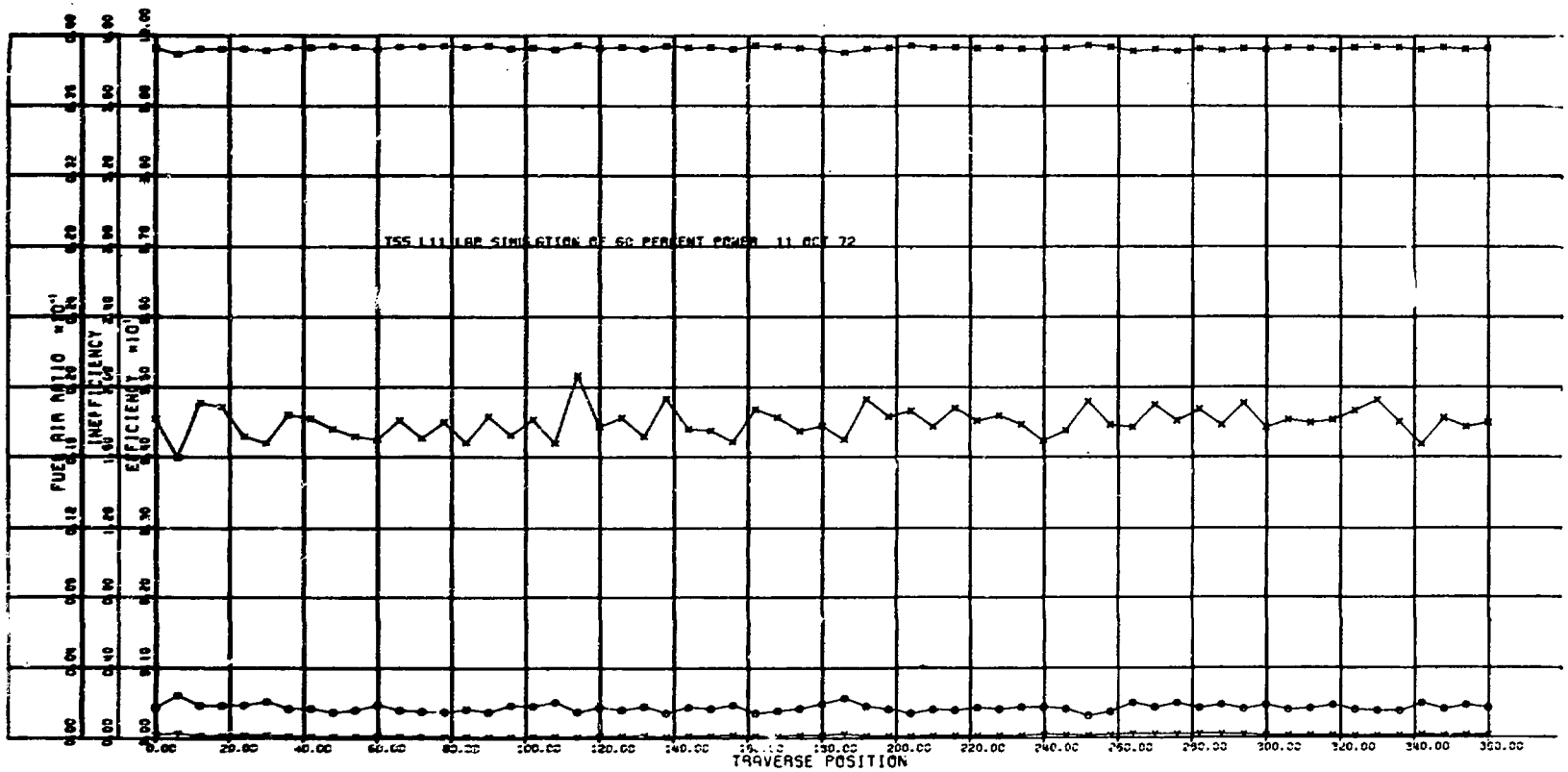

Figure 142. T55 Laboratory Combustor, Fuel-Air Ratio and Combustion Efficiency Versus Traverse Angle at 60% Power.

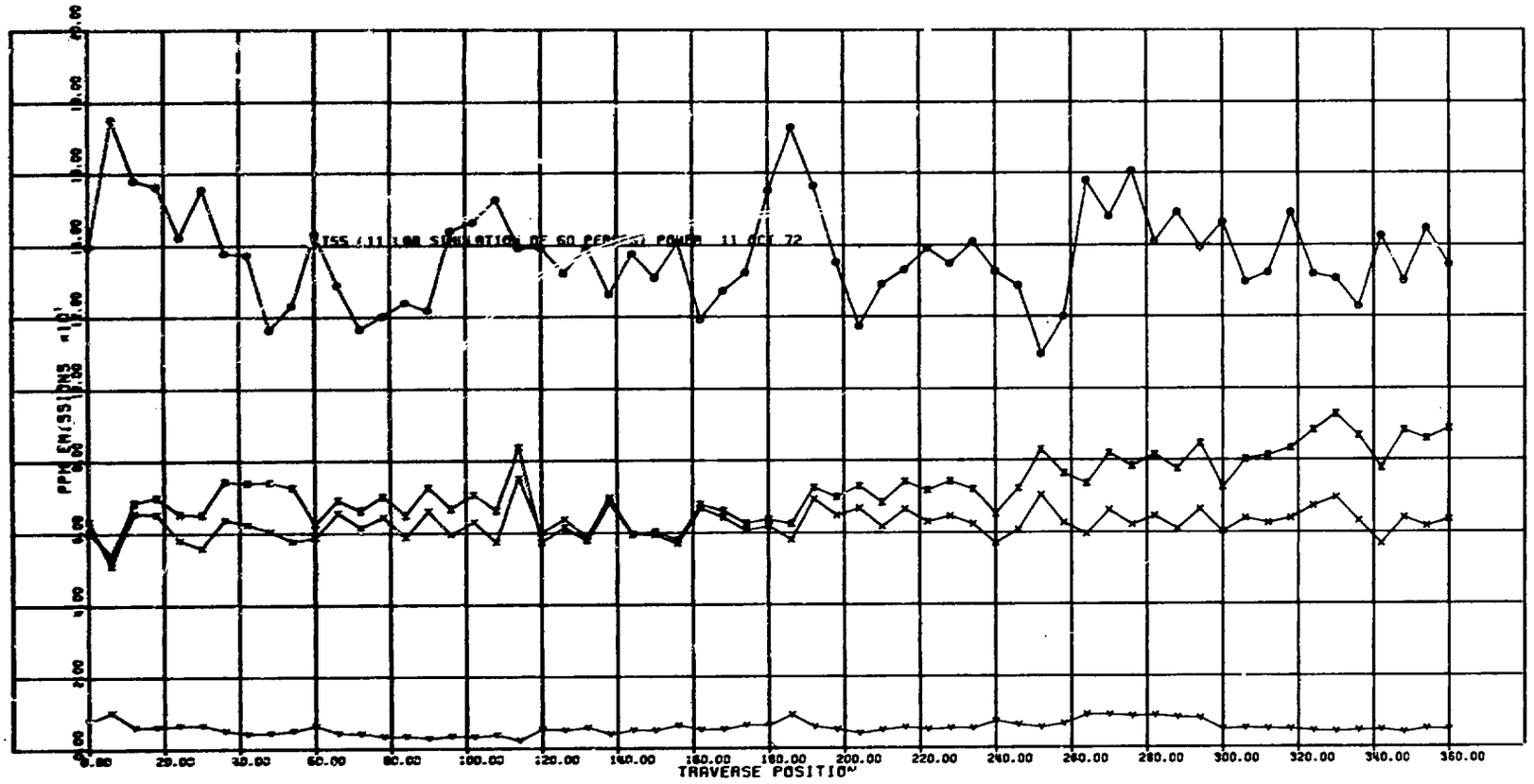

Figure 143. T55 Laboratory Combustor, ppm Emissions Versus Traverse Angle at 60% Power.

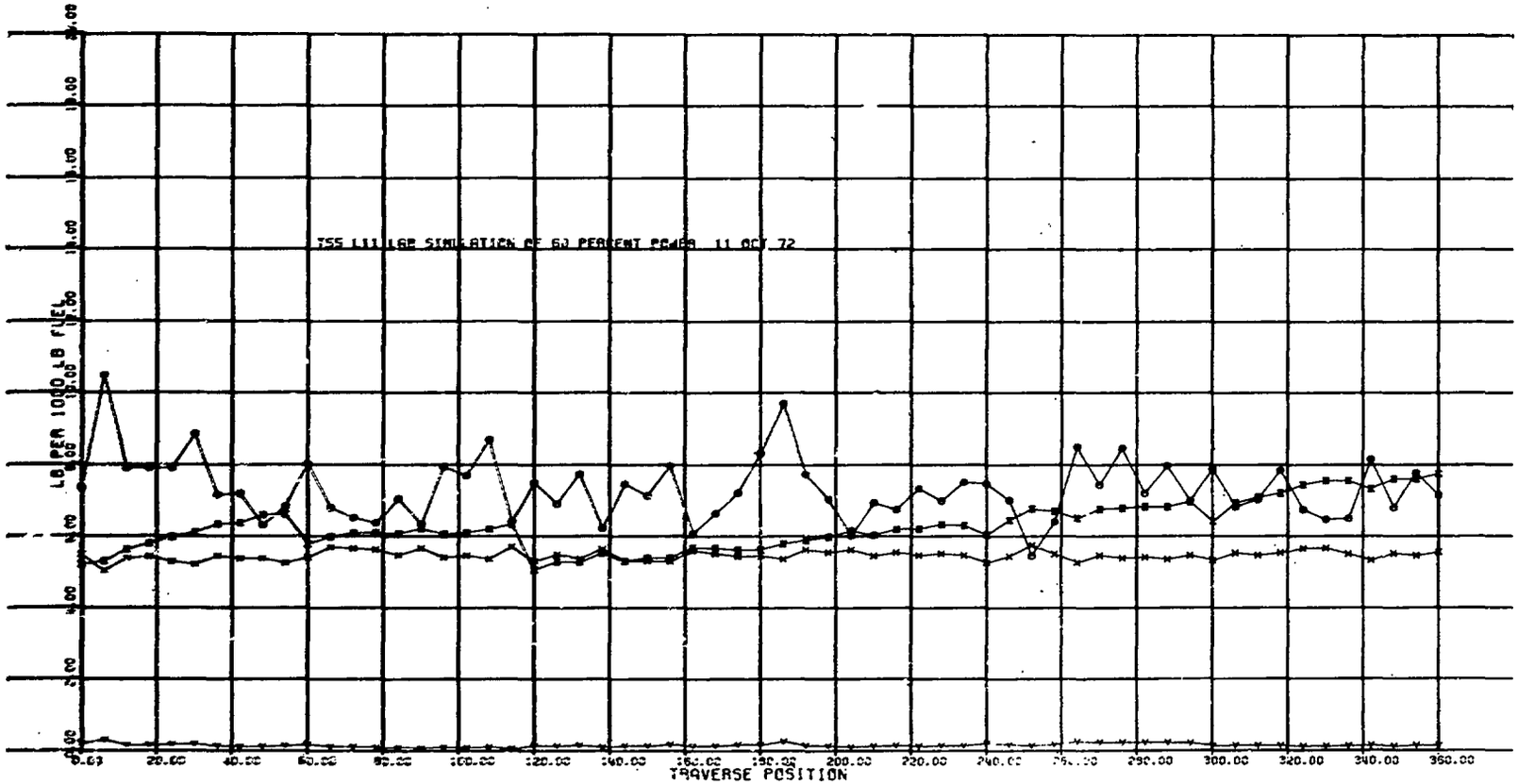

Figure 144. T55 Laboratory Combustor, Emission Index Versus Traverse Angle at 60% Power.

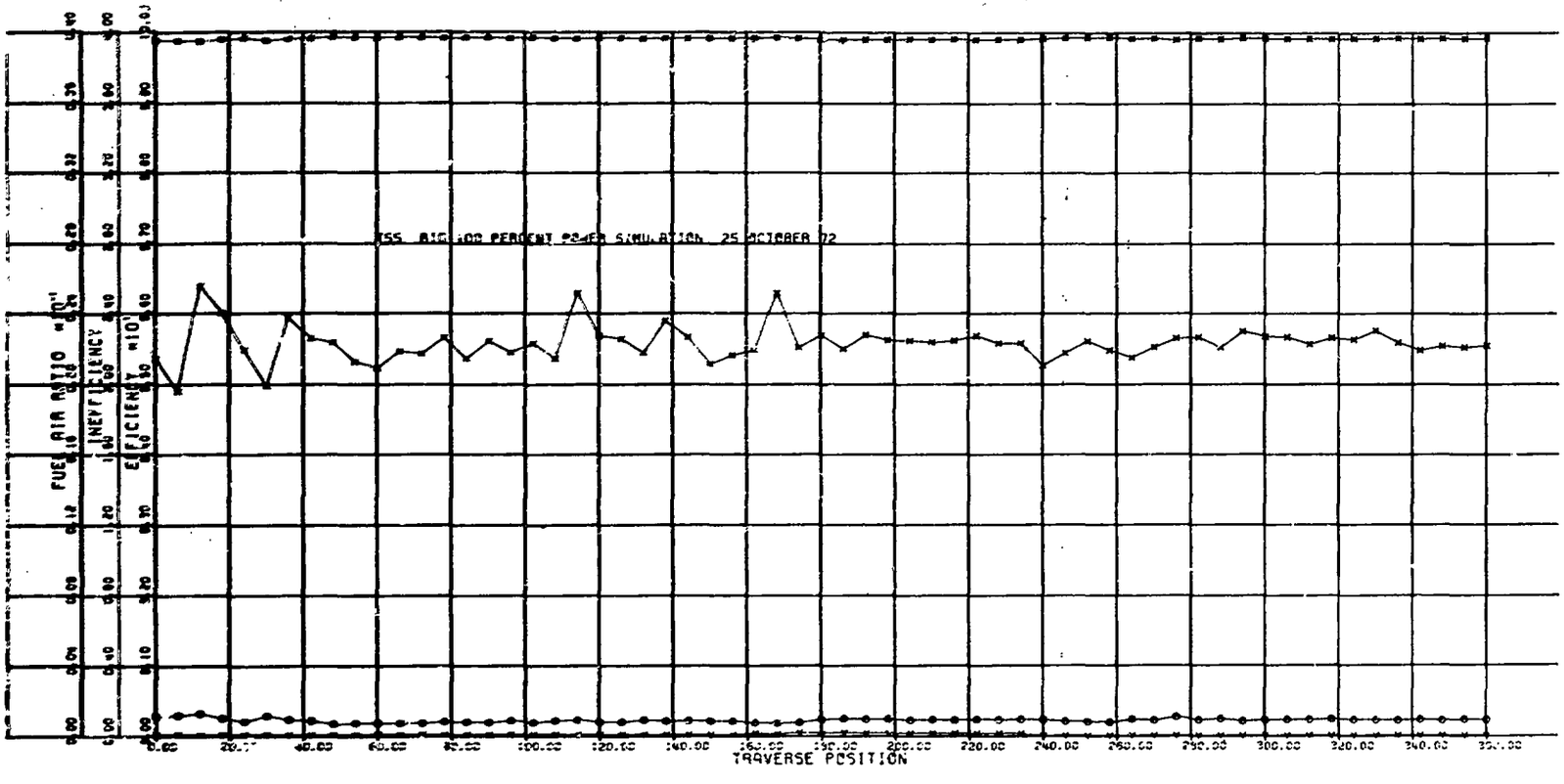

Figure 145. T55 Laboratory Combustor, Fuel-Air Ratio and Combustion Efficiency Versus Traverse Angle at 100% Power.

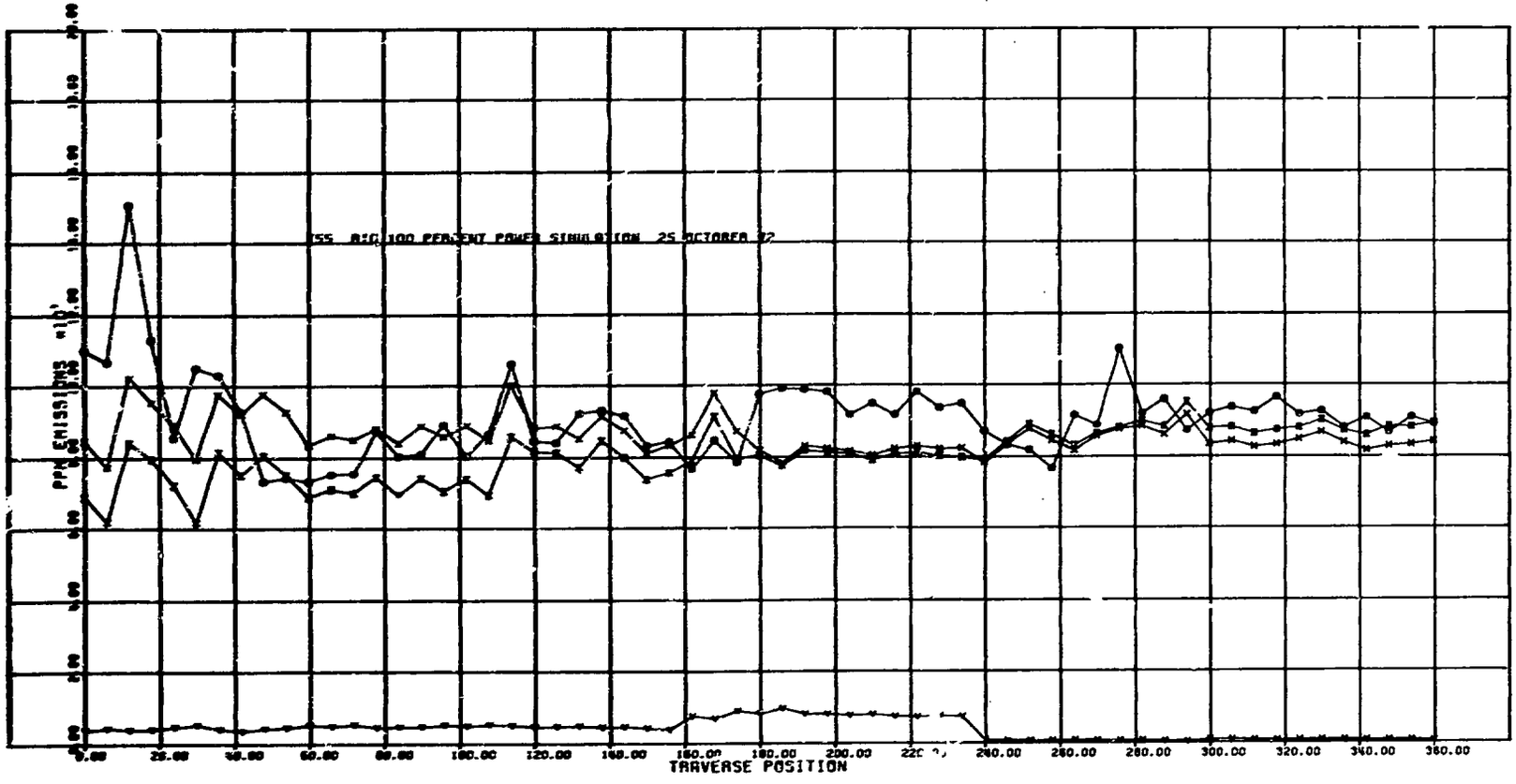

Figure 146. T55 Laboratory Combustor, ppm Emissions Versus Traverse Angle at 100% Power.

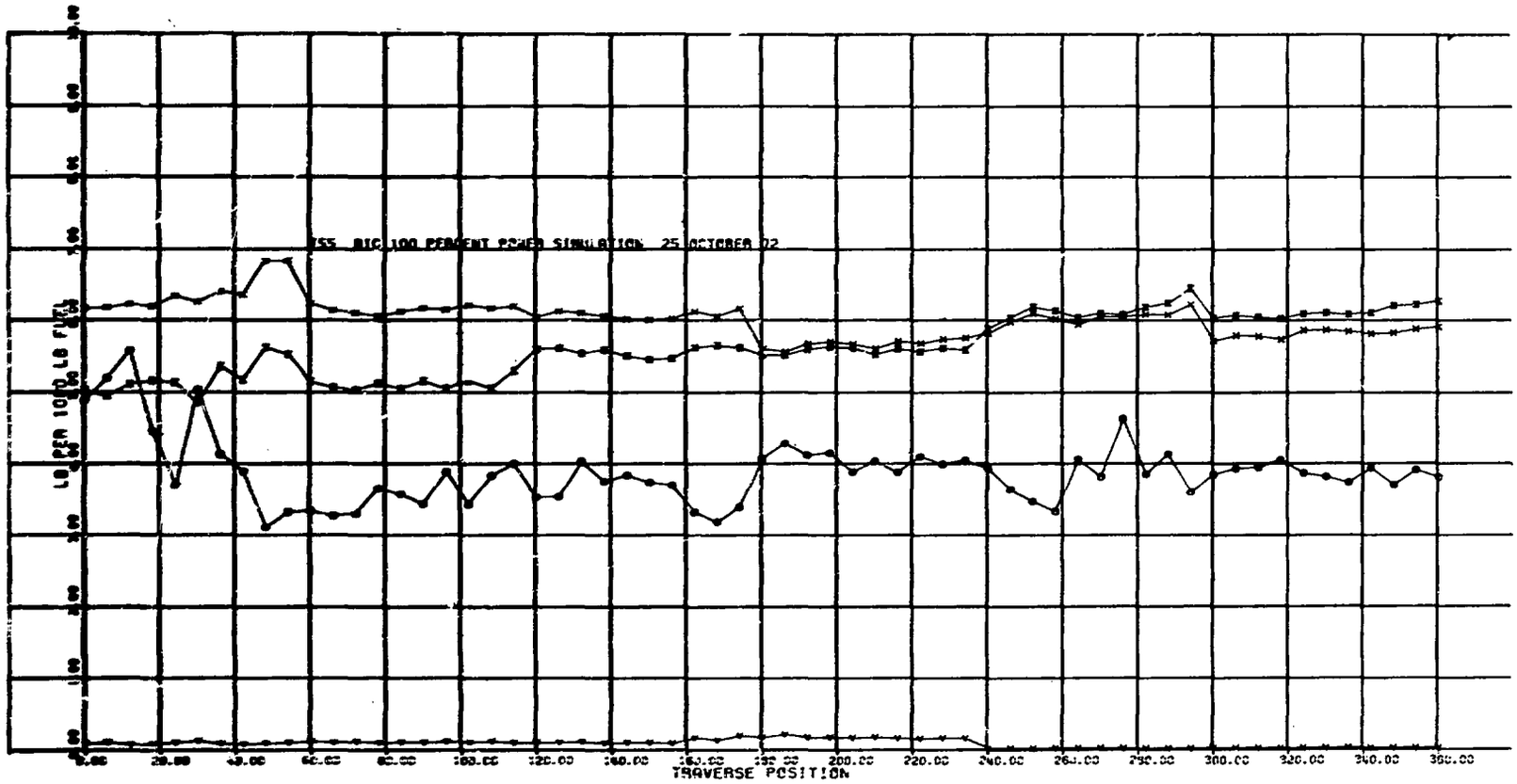

Figure 147. T55 Laboratory Combustor, Emission Index Versus Traverse Angle at 100% Power.

APPENDIX IV
T55 ENGINE ISOPLETH EXHAUST CONTOUR PLOTS

Engine exhaust gas sample traverses were made with the single-point probe to determine CO, HC, CO_2, NO, and NO_x at four power conditions, including idle, 30, 60, and 100 percent of full power. The traverses were completed on one-half of the exhaust, reoriented, and then the second half finished. Including a repeat of the dividing-line diameter between halves and repeats of the centerpoint, 80 data points were recorded per traverse. From these data, calculations were completed for F/A and combustion efficiency, by use of the equations in this report.

In order to plot the isopleth concentration (or combustion efficiency) lines, all values were normalized to an average reference value at the exhaust duct centerpoint. This reduces any time variation of the concentrations to a very small amount. Plotted for each power setting are isopleths for CO, CH, NO, NO_x, fuel-air ratio, and combustion efficiency. See Figures 148 through 171.

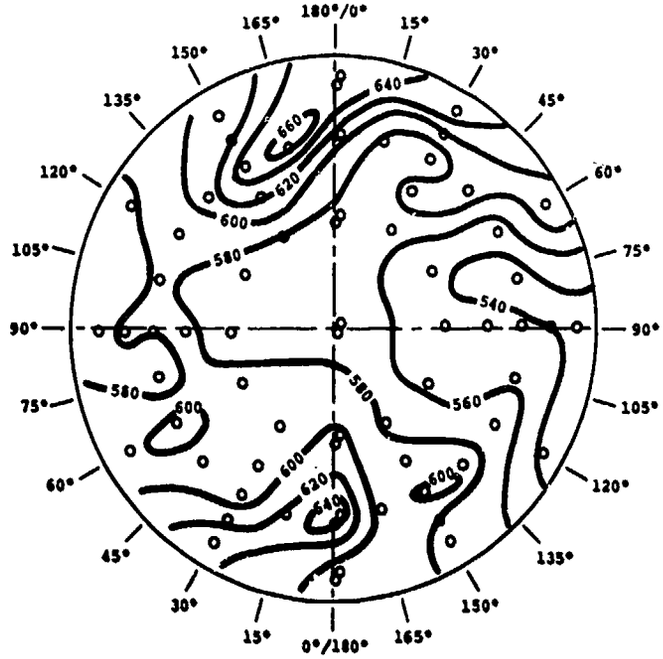

Figure 148. T55 Engine Isopleth of CO (ppm) at Idle Power.

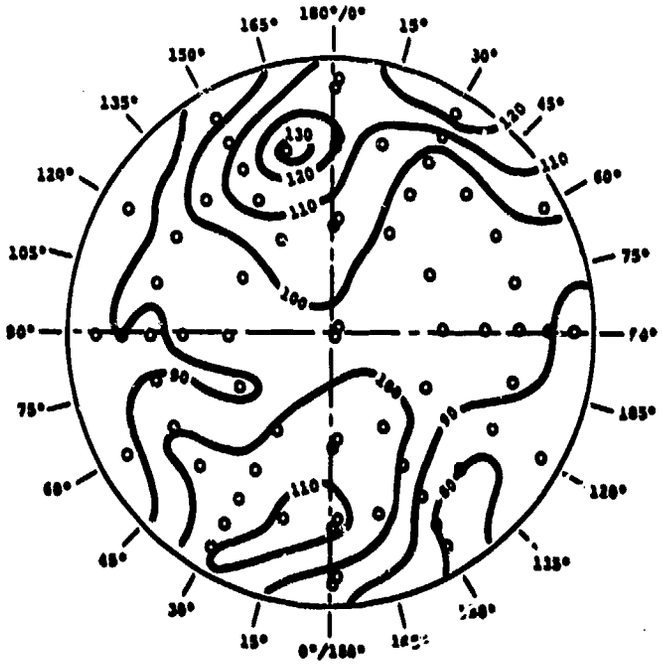

Figure 149. T55 Engine Isopleth of HC (ppmC) at Idle Power.

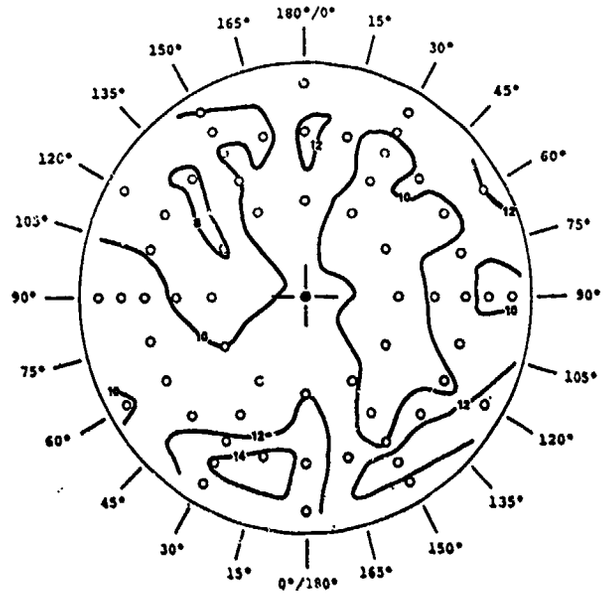

Figure 150. T55 Engine Isopleth of NO (ppm) at Idle Power.

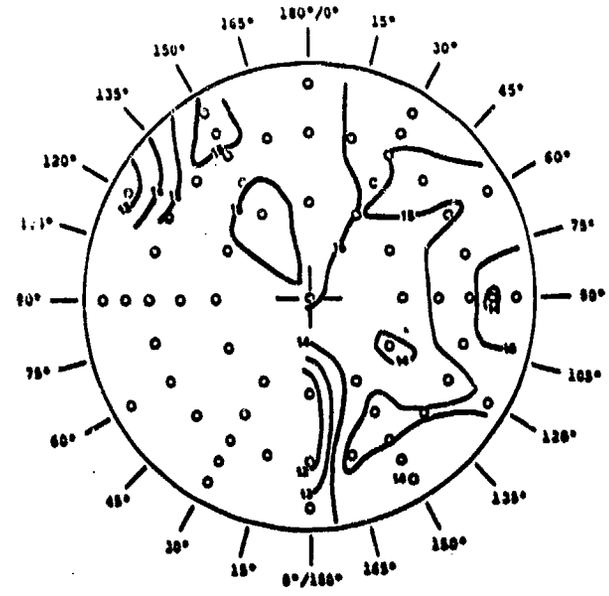

Figure 151. T55 Engine Isopleth of NO_x (ppm) at Idle Power.

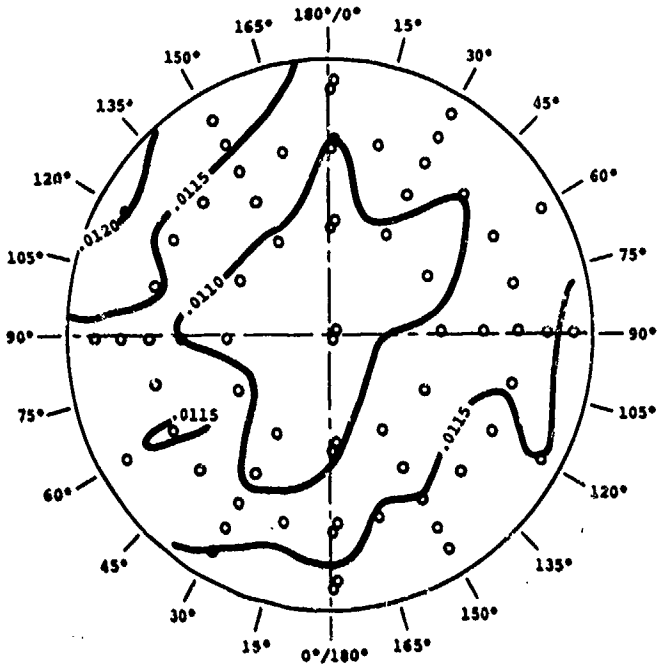

Figure 152. T55 Engine Isopleth of Fuel-Air Ratio at Idle Power.

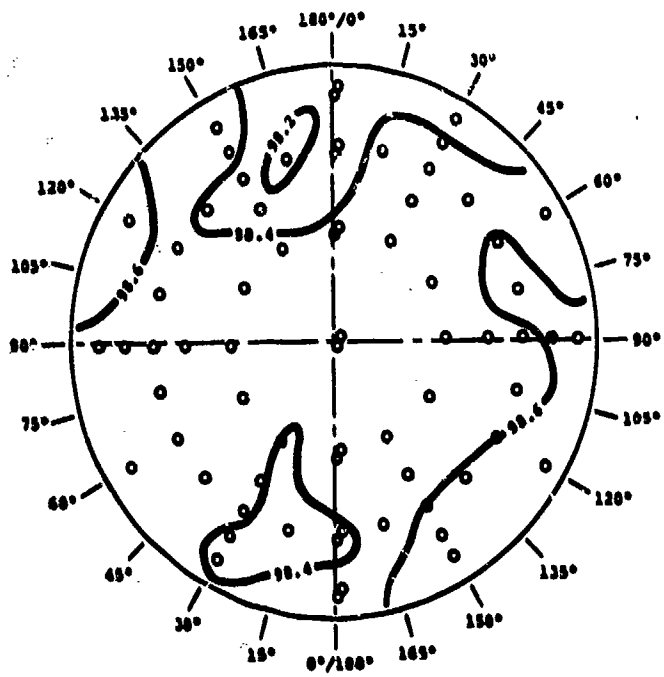

Figure 153. T55 Engine Isopleth of Combustion Efficiency at Idle Power.

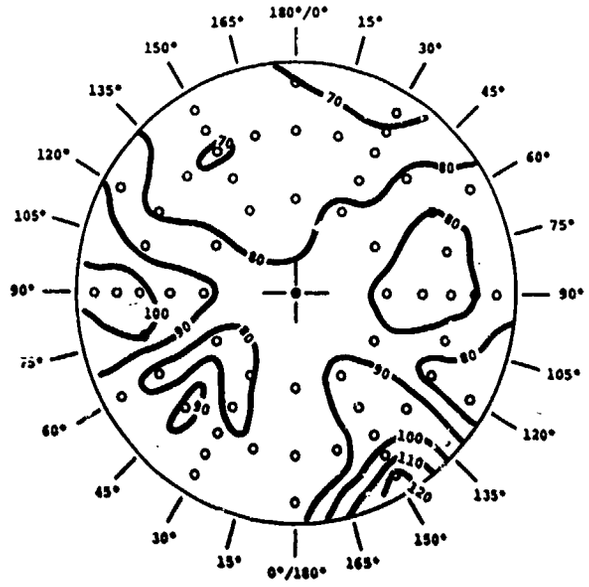

Figure 154. T55 Engine Isopleth of CO (ppm) at 30% Power.

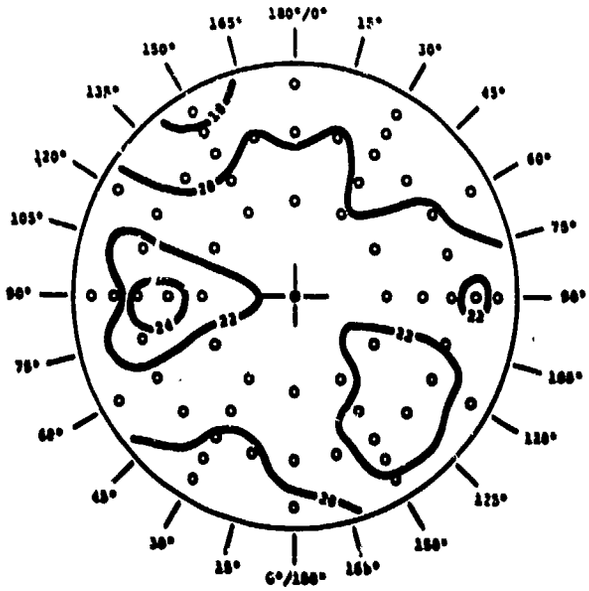

Figure 155. T55 Engine Isopleth of HC (ppmC) at 30% Power.

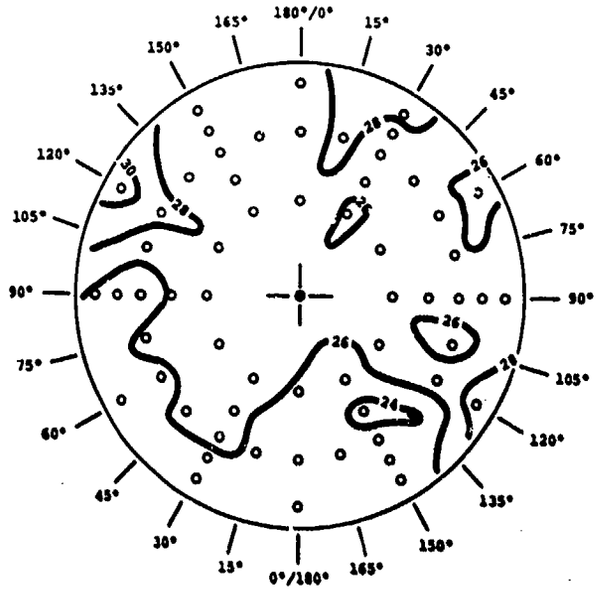

Figure 156. T55 Engine Isopleth of NO (ppm) at 30% Power.

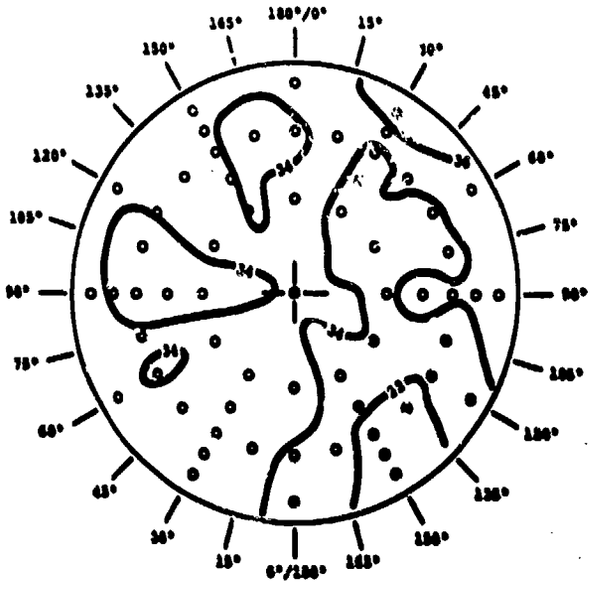

Figure 157. T55 Engine Isopleth of NO_x (ppm) at 30% Power.

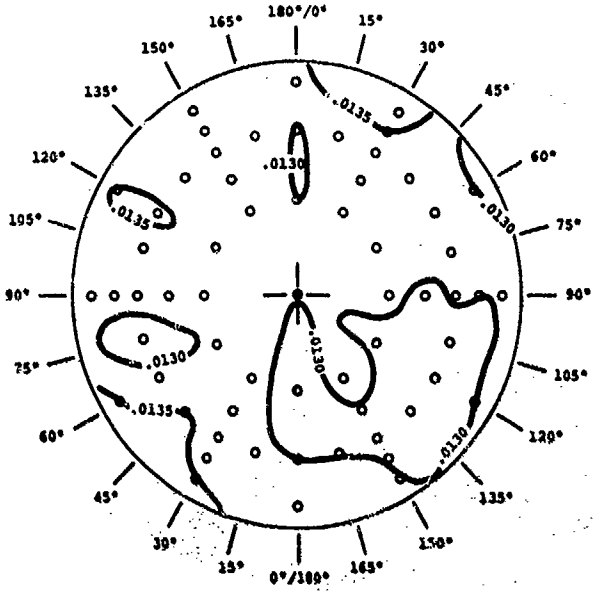

Figure 158. T55 Engine Isopleth of Fuel-Air Ratio at 30% Power.

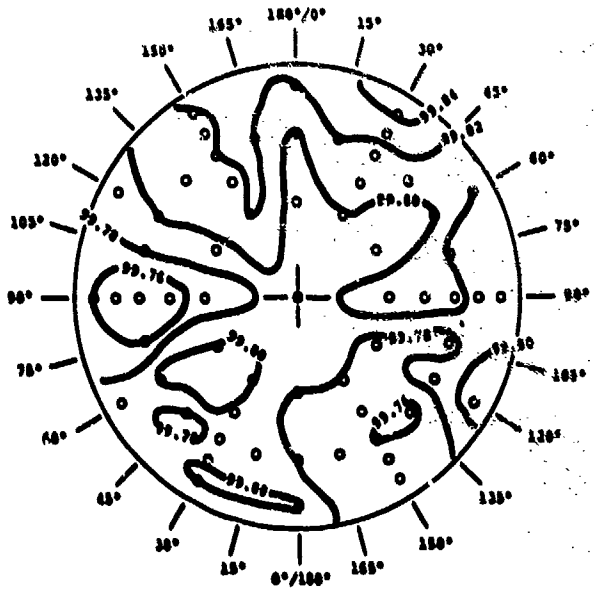

Figure 159. T55 Engine Isopleth of Combustion Efficiency at 30% Power.

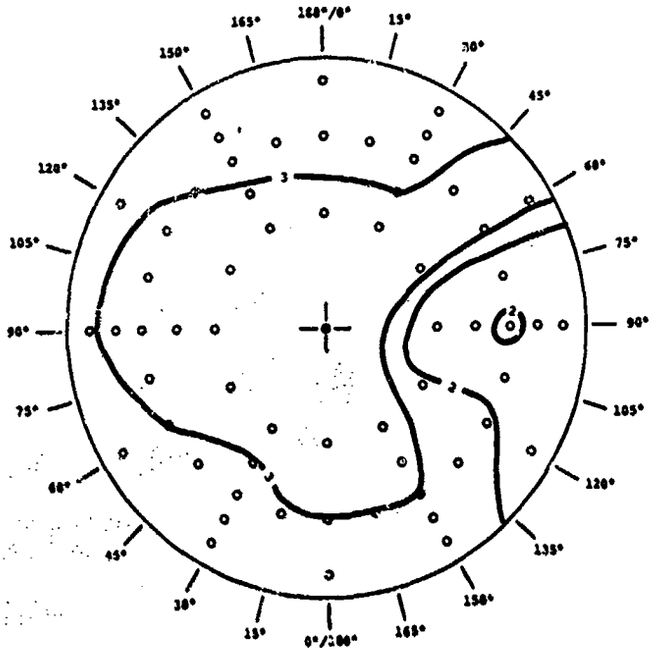

Figure 160. T55 Engine Isopleth of HC (ppmC) at 60% Power.

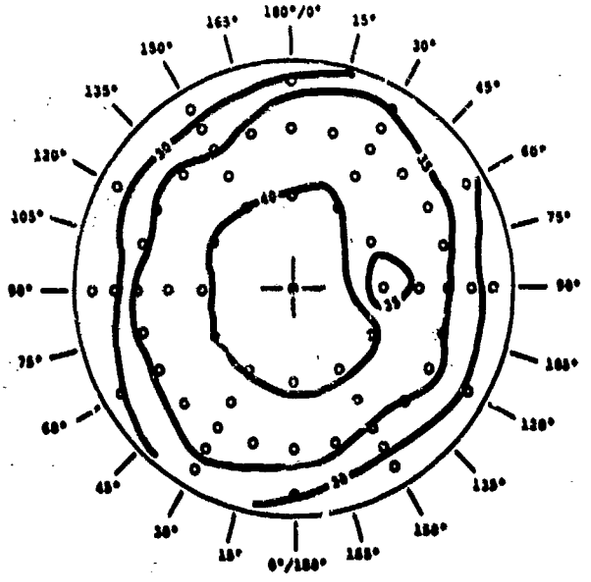

Figure 161. T55 Engine Isopleth of HC (ppmC) at 60% Power During an Oil Seal Failure.

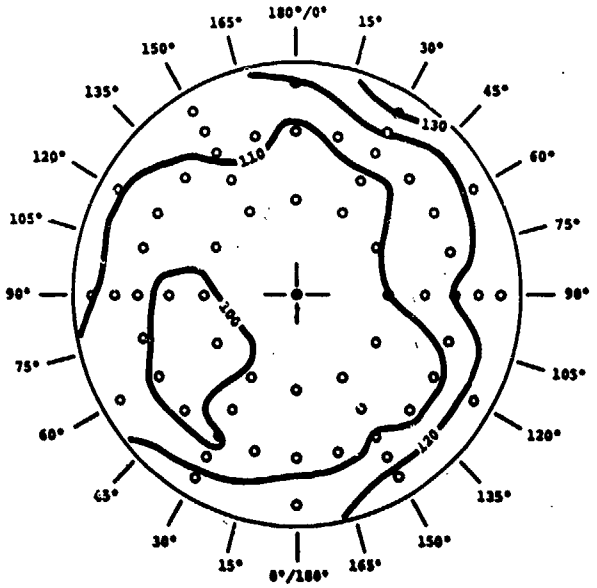

Figure 162. T55 Engine Isopleth of CO (ppm) at 60% Power.

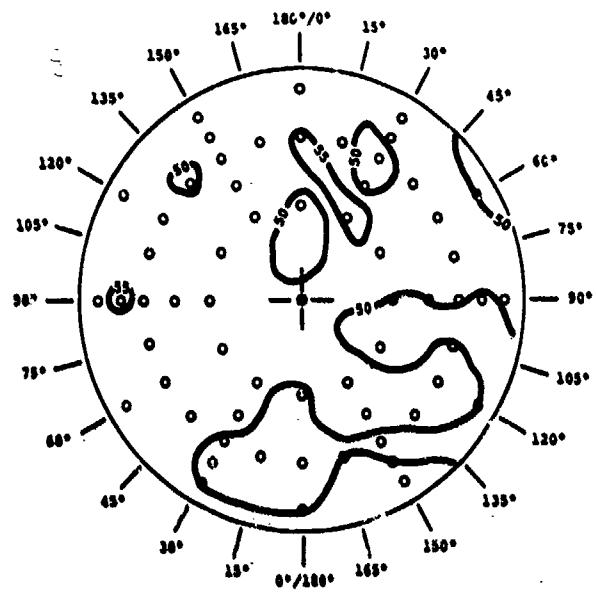

Figure 163. T55 Engine Isopleth of NO (ppm) at 60% Power.

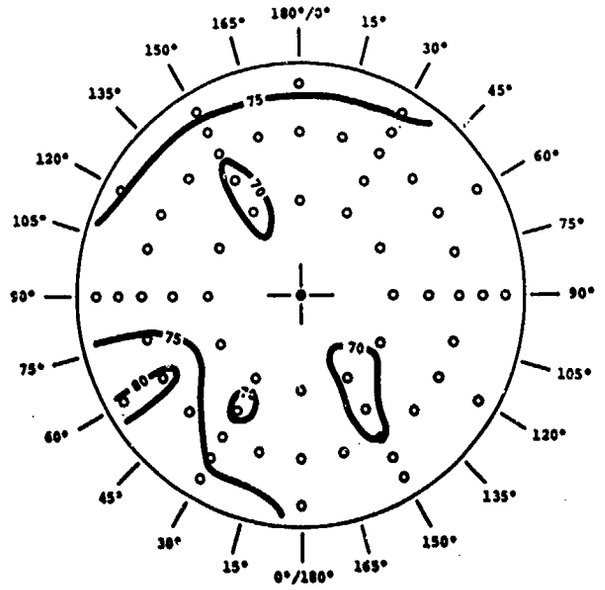

Figure 164. T55 Engine Isopleth of NO_x (ppm) at 60% Power.

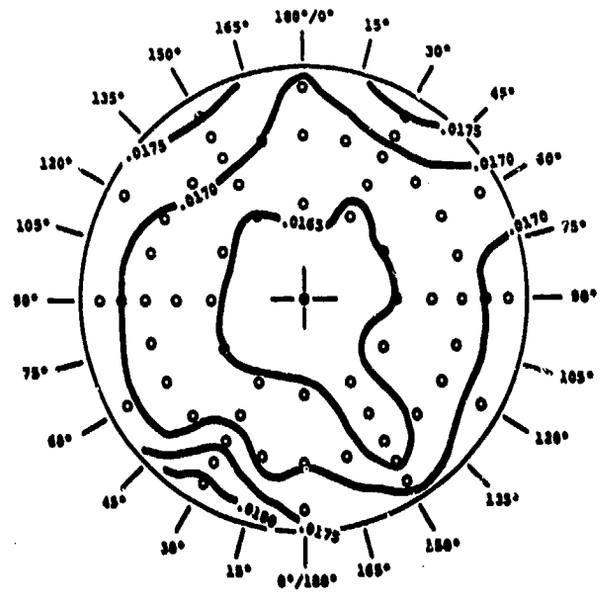

Figure 165. T55 Engine Isopleth of Fuel-Air Ratio at 60% Power.

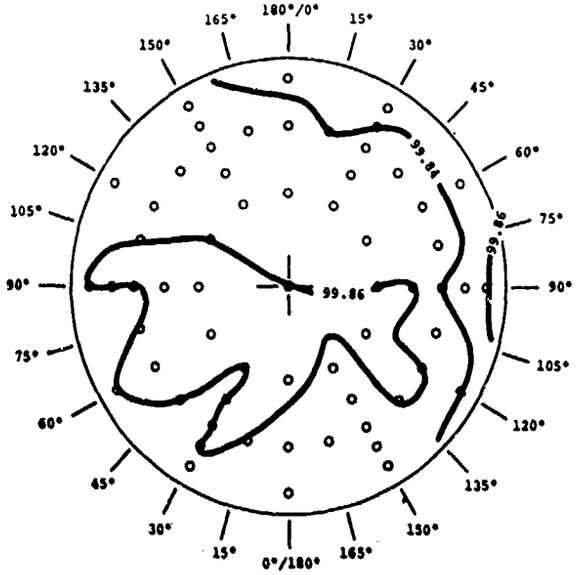

Figure 166. T55 Engine Isopleth of Combustion Efficiency at 60% Power.

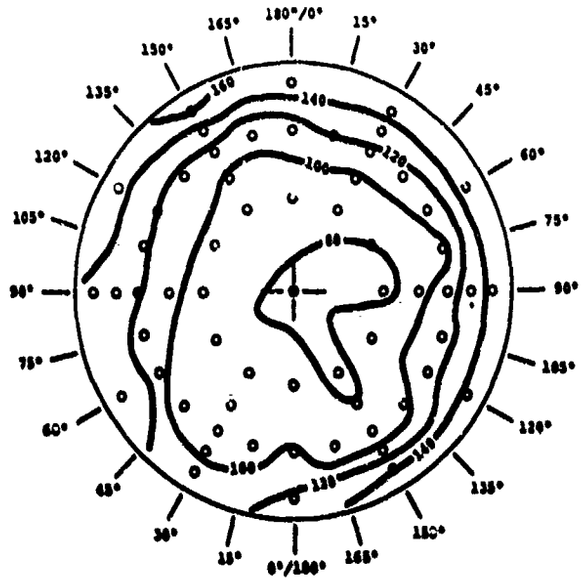

Figure 167. T55 Engine Isopleth of CO (ppm) at 100% Power.

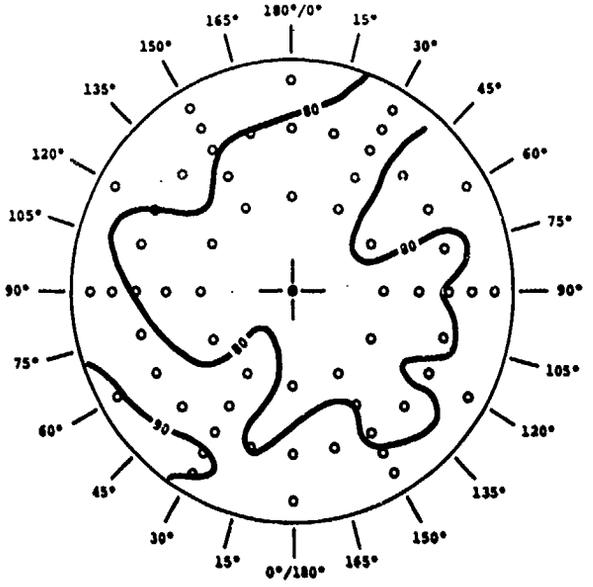

Figure 168. T55 Engine Isopleth of NO (ppm) at 100% Power.

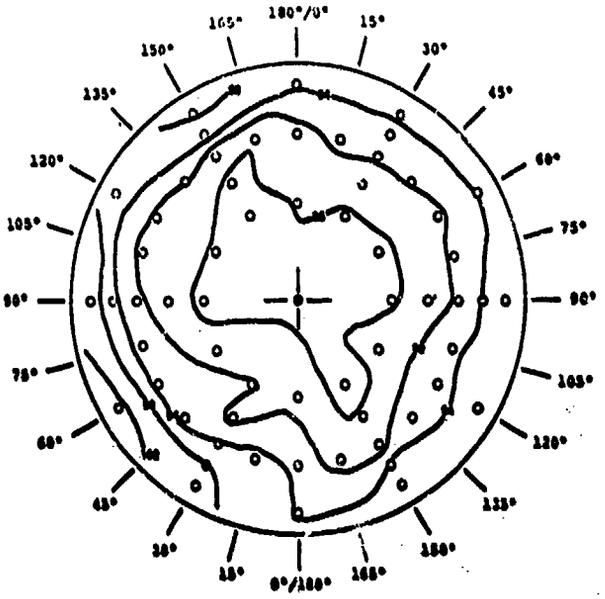

Figure 169. T55 Engine Isopleth of NO_x (ppm) at 100% Power.

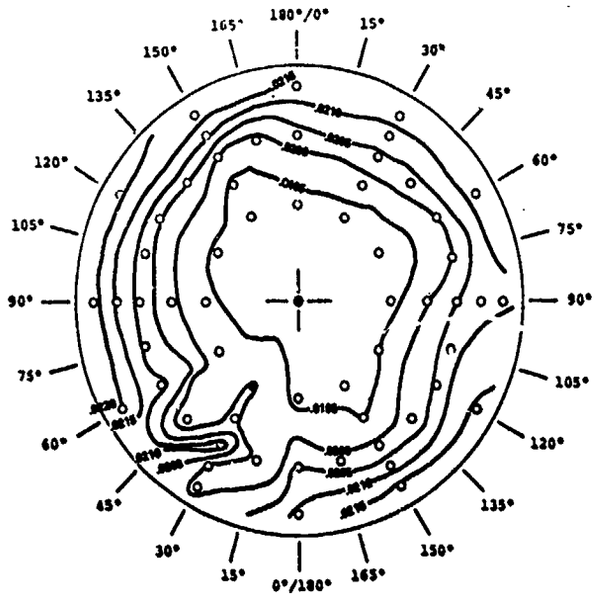

Figure 170. T55 Engine Isopleth of Fuel-Air Ratio at 100% Power.

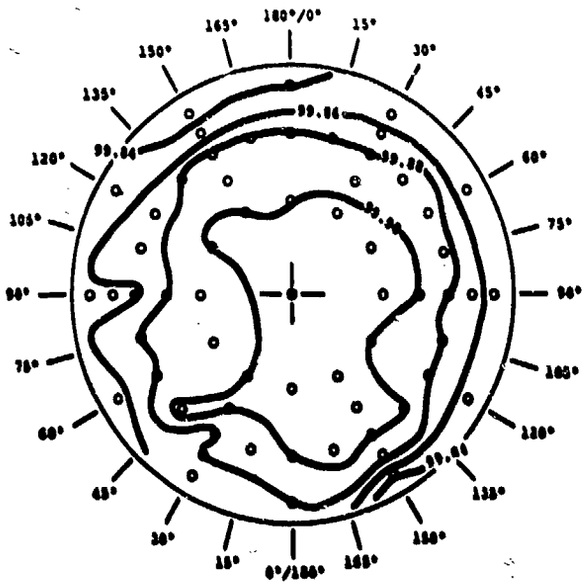

Figure 171. T55 Engine Isopleth of Combustion Efficiency at 100% Power.